The Photophysics and Electrochemistry of Carboranes

RACHEL ABIGAIL HARDER

Durham University, Department of Chemistry

The Photophysics and Electrochemistry of Carboranes

Rachel Abigail Harder

2012
A thesis submitted in part fulfillment of the requirements for the degree of Doctor of Philosophy at Durham University.

Acknowledgements

I would like to thank Mark Fox for his help and guidance in completing this thesis. I truly could not have got this far without his patience, kindness and his knowledge and love of carboranes. Despite the fact that I completely avoided studying computational chemistry as an undergraduate, I am also thankful that he introduced me to calculations and taught me how to use them. Thanks also go to Paul Low, for his words of encouragement. My thanks go to all those who have worked with me offering their friendship, synthetic skills and expertise; Mark Embleton, Silje Nordanger, Vincent Ching, Winnie Man, Kevin Vincent, Andrea Perrin, Axel Tortenson, Pippa Coffer, Dima Yufit, Durham University mass spectrometry and NMR services, Judith Keane, Douglas Carswell, Geri Rosser and Robert Edkins. Thank you also to everyone else who has worked in labs 100 and 134 over the years and all those who have worked in office 111 with me.

My parents and in laws have been so kind and encouraging and have had great belief that could finish this process. I couldn't have done this without the love and support of my husband, Scott, who has helped me keep this PhD in perspective, reminding me constantly that ultimately only the true and trustworthy word of the God who created the world will endure forever.

Contents

Abstract

This thesis describes research carried out on compounds containing icosahedral carborane moieties (*ortho*/*meta*/*para*-$CB_{10}H_{10}C$-), investigating their photophysical and electrochemical properties. The *ortho* carborane cage is shown to play an active role in the fluorescence and electrochemical reduction properties. *Meta* and *para* carborane groups, however, chiefly act as spectators. Chapter one gives an overview of carboranes in the literature, highlighting the syntheses, photophysical and electrochemical studies done previously on C-aryl-carboranes.

Chapter two describes the syntheses of naphthyl carboranes. *Ortho* di-naphthyl carborane displays emission with a large Stokes shift, while the *meta* and *para* isomers emit with a small Stokes shift. *Ortho* monosubstituted naphthyl carborane, by contrast, displays two distinct fluorescent emission bands, with large and small Stokes shifts. TD-DFT calculations reveal that the two emission bands can be attributed to two different S_1 excited states formed on excitation. The low energy band is due to a geometry in which the cage C-C length is elongated. The high energy band is due to a closed cage conformation in which the cage C-C bond length is smaller.

In chapter three the syntheses and fluorescence emission of carboranyl triarylamines are investigated. *Meta* and *para* carboranyl triarylamines are found to emit in DCM solution, giving higher fluorescence quantum yields than the non-cluster triarylamines. Emission of *ortho* carboranyl triarylamine, with a large Stokes shift, is observed in 1:99 THF:H_2O solution, due to aggregation induced emission. The S_1 excited state geometry is calculated to have an extended cage C-C length. Chapter four investigates the syntheses and fluorescence of some bridged *ortho* carborane compounds of the type (1-R-1,2-$C_2B_{10}H_{10}$)$_2$X, where X=1,1'-$(C_6H_4)_2$/C_4SH_2/C_6H_4 or C_6F_4. These compounds are found to give a broad range of emission maxima, from 355 to 763 nm in THF:H_2O solutions.

Chapter five looks at the electrochemistry of some simple carboranes, naphthyl carboranes, carboranyl triarylamines and bridged carboranes. Calculations of the cage C-C bond lengths are shown to be successful at predicting trends in the reduction potentials of simple carboranes. On reduction to a dianion, the cage C-C bond length is elongated as the carborane cage opens up to accommodate the additional electrons. The greater the cage C-C bond length in the ground state, the greater the ease with which the reduction occurs. Di-napthyl *ortho* carborane displays formation of a radical anion before further reduction to the dianion, as reported for di-phenyl *ortho* carborane. Bridged carboranes where X=C_6H_4/C_6F_4/C_4SH_2 display communication between carborane cages and suggest considerable bridge involvement.

Abbreviations

° - degrees

°C – degrees Celsius

A - amps

Å - angstrom

Abs – absorption

AcOEt – ethyl acetate

AIE – aggregation induced emission

ASAP - atmospheric solids analysis probe

Ar – aryl group

BuLi – n-butyllithium

Cb - carborane

cm - centimetres

cm^{-1} – wavenumbers (reciprocal centimetres)

Cp - cyclopentadiene

Cp*- pentamethylcyclopentadienyl

CV – cyclic voltammetry

d – doublet

DBU - 1,8-Diazabicyclo[5.4.0]undec-7-ene

DCM – dichloromethane

DFT – density functional theory

DME - dimethoxyethane

dppe - 1,2-Bis(diphenylphosphino)ethane

DSD – diamond square diamond

EI – electron impact

Em – emission

Et - ethyl

Et_2O - diethylether

EtOH - ethanol

eV - electronvolts

FcH – ferrocene

h - hours

HOMO – highest occupied molecular orbital

HOSO – highest occupied spin orbital

IR – infra-red

LUMO – lowest unoccupied molecular orbital

LUSO – lowest unoccupied spin orbital

m - medium

m – meta

m – multiplet

m/z – mass per unit charge

Me – methyl

MeCN - acetonitrile

MeOH – methanol

mg - milligrams

mins - minutes

ml - millilitres

mmol - millimoles

MO – molecular orbital

Nap – naphthyl

NBu_4PF_6 – tetrabutyl ammonium hexafluorophosphate

NIR – near infra-red

nm – nanometres

NMP - 1-Methyl-2-pyrrolidone

NMR – nuclear magnetic resonance

o – *ortho*

OLED – organic light emitting diode

OTTLE – optically transparent thin layer electrode

Ox – oxidation

p – *para*

Ph – phenyl

PLED – polymer light emitting diode

Py - pyridine

Red – reduction

s - singlet

s - strong

SE – skeletal electrons

$SiMe_3$ – trimethylsilyl group

t – triplet

TBS - *tert*-butyldimethylsilyl

^{t}Bu – tertiary butyl

TD-DFT – time-dependent density functional theory

TFR – triangular face rotation

T_g – glass transition temperature

THF – tetrahydrofuran

TMS - tetramethylsilane

TMSA - trimethylsilylacetylene

Tol – para tolyl, 4-$CH_3C_6H_4$

V - volts

w - weak

δ – chemical shift

ΔE – potential difference

ε – molar extinction coefficient

1 : Literature Review

1.1 Introduction

Carborane clusters contain boron, carbon and hydrogen. There are widely ranging structures possible given this definition, with some examples given in Table 1–1. Typical skeletal shapes of *closo*, *nido* and *arachno* *n*-vertex polyhedra are shown in Figure 1–1. Based on Wade's rules, a carborane with *n* vertices is *closo* if it has 2*n* + 2 skeletal electrons, *nido* if it has 2*n* + 4 and *arachno* if it has 2*n* + 6 skeletal electrons.[16] A twelve vertex *closo* carborane, as the name suggests, is a closed structure. On removing one vertex, a *nido* structure is obtained. Removing another vertex gives the *arachno*.

	x	y	z	References
closo	2	3	5	1
	2	4	6	1
	2	5	7	1
	1	5	7	2
	2	6	8	3
	2	7	9	4
	2	8	10	5
	2	9	11	6
	2	10	12	7
nido	1	5	9	8
	2	4	8	9
	3	3	7	10
	2	3	7	11
arachno	1	4	10	12
	2	6	11	13
	1	8	14	14
	2	7	13	15

Table 1–1: Empirical formulae of a variety of known neutral carboranes of formula $C_xB_yH_z$.

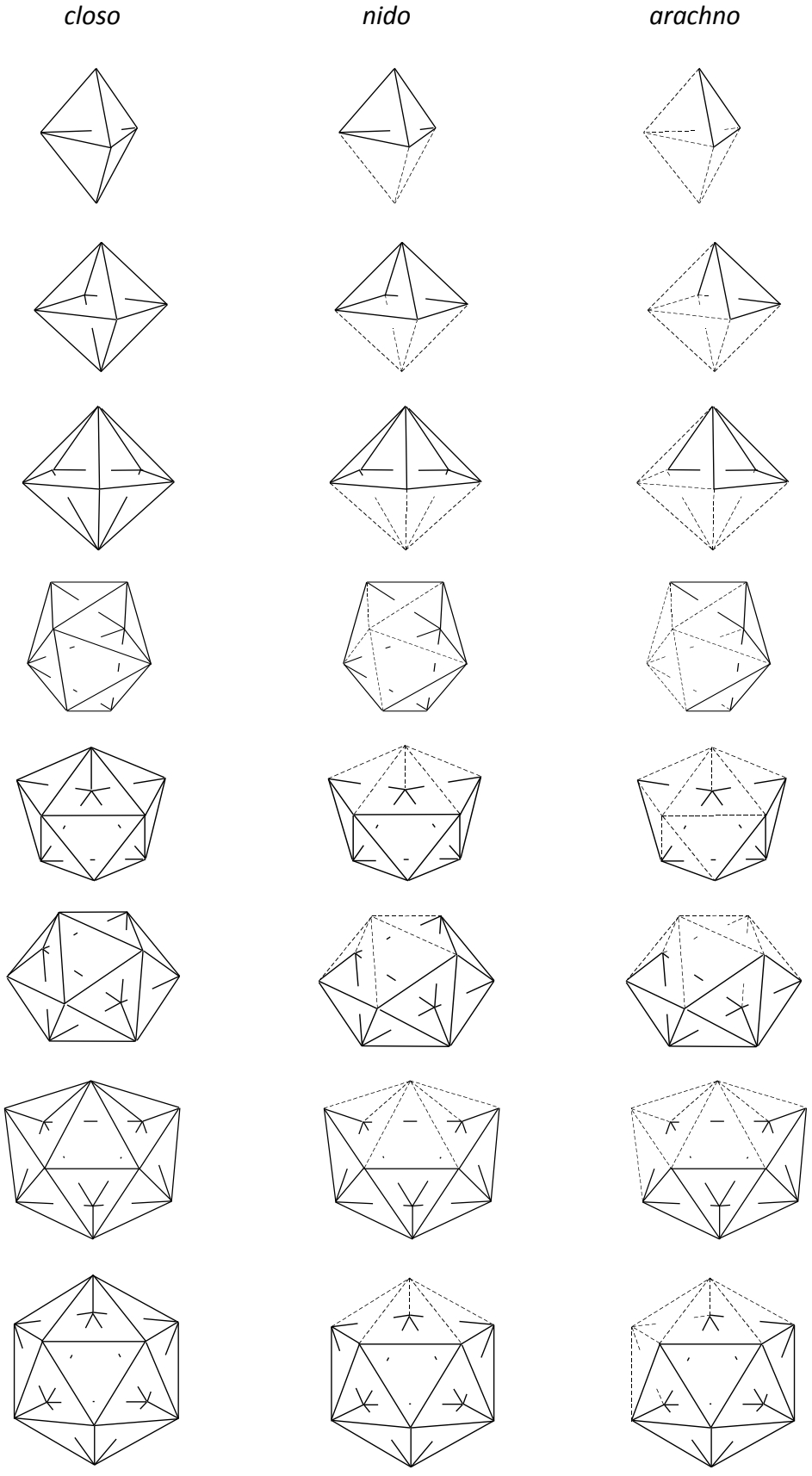

Figure 1–1: Typical skeletal shapes of *closo*, *nido* and *arachno* polyhedra.

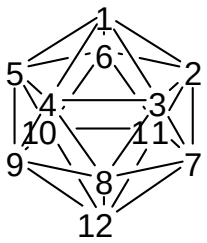

Figure 1–2: Cluster atom numbering in carborane structures based on the twelve vertex icosahedron.

The most widely investigated carborane structures, with the formula $C_2B_{10}H_{12}$, are based on the icosahedron geometry with cluster atom numbering as shown in Figure 1–2. The commercially available compounds have three isomers – *ortho*, *meta* and *para* (Figure 1–3). The *ortho* isomer has the CH vertices at the 1,2 positions, *meta* at 1,7 and *para* at 1,12. The *ortho*, *meta* and *para* isomers are priced at £6, £6 and £60 per gram respectively (2012 prices). Note that in some of the older literature, *ortho* carborane is referred to as barene and *meta* carborane is known as neocarborane.[17] The *ortho* isomer has been the subject of the majority of the research carried out due to the relative cost and ease of synthesis compared to the *para* isomer.[18]

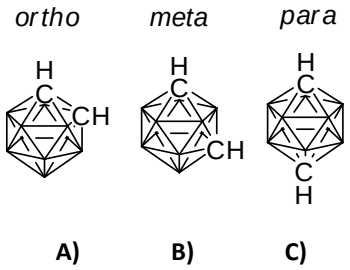

Figure 1–3: Isomers of $C_2B_{10}H_{12}$ (A) *ortho* (B) *meta* (C) *para*. Unlabelled vertices are BH units.

1.2 Possible uses of carboranes

There are many possible applications for carboranes put forward in the literature. For example, the near spherical shape of the molecules suggests that they may find uses as the wheels in nano-cars.[19] Tour *et al.* have synthesised several nanocars using *para* carboranes as the wheels.[20,21,22] Figure 1–4 shows one such molecule which has light-activated unidirectional motion.[20] Light energy will

excite the molecule and break the C-C double bond in the centre of the molecule which will lead to rotation and hence movement.[20]

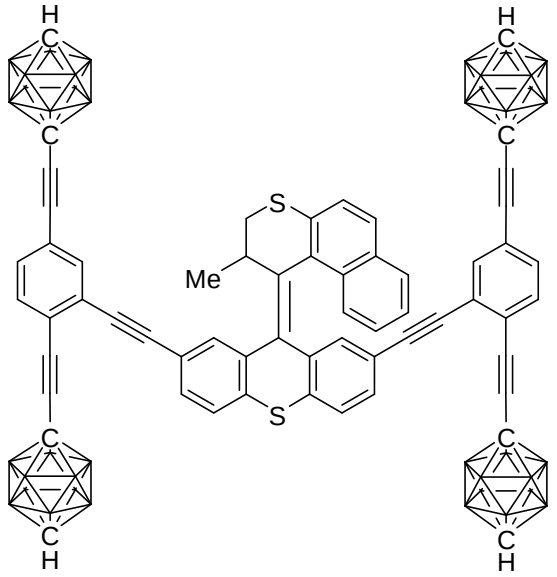

Figure 1–4: Example of a nanocar using para carborane as "wheels".

Carborane derivatives may find use in medicine. Boron neutron capture therapy (BNCT), an experimental form of radiotherapy, uses boron species injected into the patient to destroy cancerous cells. A compound safe for use *in vivo*, which is rich in ^{10}B and functionalised such that it binds preferentially to the target cells whilst not contaminating the healthy tissue is required.[23] ^{10}B has a 19.8 % natural abundance. This isotope undergoes the following reaction on irradiation with neutrons:

$$^{10}_{5}B + ^{1}_{0}n \rightarrow ^{4}_{2}He + ^{7}_{3}Li + 2.79MeV$$

The high energy products of this reaction, when formed *in vivo*., will destroy the targeted tumour cells.[24] The products will only travel approximately 10 μm and as such will not damage adjacent healthy cells, which do not contain the borane species.[24] Practically speaking however, this has not yet been entirely realised. A high ^{10}B content is desirable, higher than the natural abundance, and therefore the synthesis of the carborane is made more complicated.[24] Additionally, finding a

compound that is safe for use in humans presents a major barrier.[24] Carboranes have been incorporated in carbohydrates, porphyrins, intercalators, polyamines, nucleosides and liposomes in attempts to create such a specific, non-toxic and active species.[23] Boron neutron capture synovectomy makes use of the same chemistry.[23] This treatment aims to relieve the symptoms of severe rheumatoid arthritis using the daughters of the boron neutron capture reaction.[23]

Other carborane-based molecules have been designed to be biologically active.[25] Derivatised carboranes have been reported to be active estrogen receptor agonists as the cage acts as a hydrophobic pharmacophore which promotes binding.[26,27] Also, androgen receptor and retinoid X antagonists have been reported.[28,29] However these carborane receptor binding ligands have displayed a low specificity which may lead to unwanted side effects.[25]

The high thermal and chemical stability of the $C_2B_{10}H_{12}$ carboranes make them useful in the synthesis of stable polymers.[24] Polymers involving carboranes as linker groups can be formed which are stable to very high temperatures. The *meta* and *para* isomers are much more useful in this respect as the *ortho* will tend to form cyclic species.[24] The first commercially available carborane products were siloxy *meta* carborane polymers, known as DEXSIL and UCARSIL, used as stationary phases for high temperature gas chromatography.[30,31,18]

Recently the photophysical properties of carborane containing compounds have been investigated, with a view to incorporating such compounds into OLEDs. The stability of carboranes may be a useful asset in devices of this type. This topic is reviewed in greater detail later in this chapter. The first carborane containing compound to be incorporated into such a device is a polymer of polyfluorene and *ortho* carborane.[90]

1.3 Bonding in carboranes

Carborane cages are electron deficient if considered using a 2-centre 2-electron model. This situation arises because each boron atom contributes 4 orbitals but only 3 electrons to the structure. As such, the basic carborane cage, *closo*-$C_2B_{10}H_{12}$, has 50 electrons (each carbon contributes 4 electrons, each boron, 3

electrons and each hydrogen, 1 electron) and 60 orbitals (each carbon and boron contributes 4 orbitals 2s,$2p_x$,$2p_y$,$2p_z$ and each hydrogen, 1 orbital 1s).[32] Therefore in order to explain the bonding in such clusters we cannot use the simple 2-centre 2-electron picture. We will consider the molecular orbital picture of bonding. Figure 1–6 shows the molecular orbital bonding of $B_{12}H_{12}^{2-}$. The BH unit is isolobal to CH^+ leading to a similar picture of bonding for the $C_2B_{10}H_{12}$. A radial sp hybrid orbital bonds the hydrogen atom.[33] There is therefore also an sp hybrid orbital pointing to the inside of the carborane structure.[33] The remaining two p orbitals donated by the carbon and boron atoms are to be found tangential to the surface of the carborane cage, Figure 1–5.[33] As such there are 12 radial sp orbitals and 24 tangential p atomic orbitals.[34] The combination of these atomic orbitals results in 13 bonding and 23 antibonding molecular orbitals. To fill these bonding orbitals 26 electrons are necessary. These are provided by C-H and B-H units which give 3 and 2 electrons per unit respectively.[35] By adding two electrons to this species the structure forms the more open, higher energy, *nido* structure to accommodate the extra electrons in the antibonding orbitals.[35]

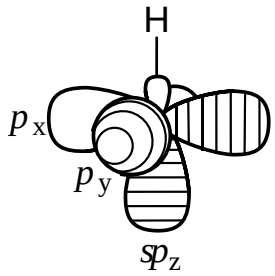

Figure 1–5: Orbitals involved in the skeletal bonding of BH.

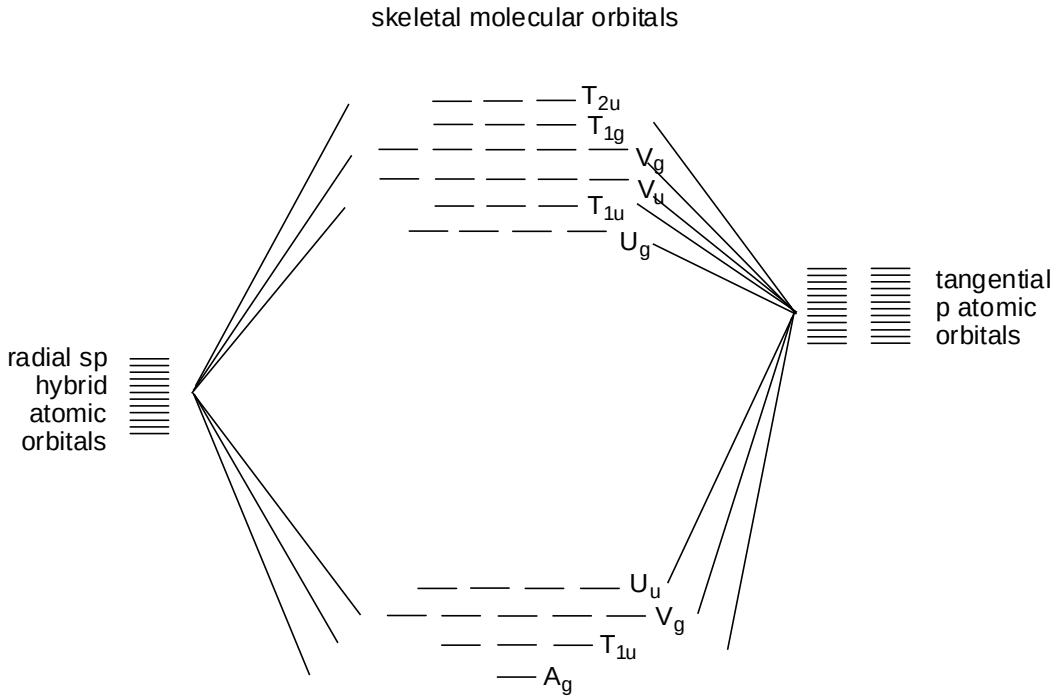

Figure 1–6: Molecular Orbital model of bonding in $B_{12}H_{12}^{2-}$.[34]

1.4 Making carboranes

The reaction of decaborane, *nido*-$B_{10}H_{14}$, with Lewis bases, such as acetonitrile or alkylamines, Figure 1–7, leads to the formation of a compound with a general formula of $B_{10}H_{12}L_2$, which has an *arachno* count, Figure 1–2(c).[18] On reacting this species with acetylene, C_2H_2, *ortho* carborane is yielded.[18] This reaction yields two equivalents of hydrogen for each equivalent of carborane formed, originating from the decaborane molecule.[36]

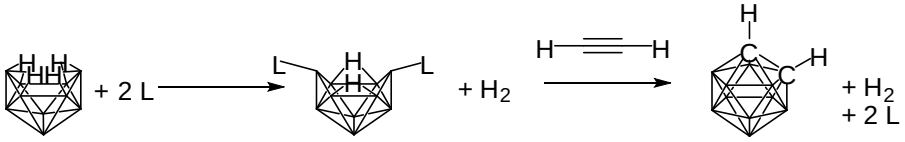

Figure 1–7: Formation of *ortho* carborane by reaction of decaborane with a Lewis base, L, followed by acetylene.

The primary way of making the *meta* isomer is by the thermal rearrangement of the *ortho* isomer, Figure 1–8, discussed below. Another method gives much lower yields and therefore is not ideal. It involves the reaction of B_2H_6

with 1,6-$C_2B_8H_{10}$.[37] It is also possible to synthesise this isomer by fusing two CB_5 units to give the C_2B_{10} skeleton, heating the units to 250 °C for several days.[38]

The synthesis of *para* carborane also makes use of thermal isomerisation, Figure 1–8. Just heating the carborane to very high temperatures leads to only a very low yield of the *para* isomer.[18] A much better synthesis, giving a 25 % yield of the desired isomer, requires passing the *ortho* isomer in a stream of nitrogen through a converter at 700 °C.[39,40]

1.5 Converting between carborane isomers

It is very useful to be able to convert between the isomers of the carboranes if a derivative of one isomer cannot be made by other methods. The two directions of conversions, shown in Figure 1–8, will be considered separately below.

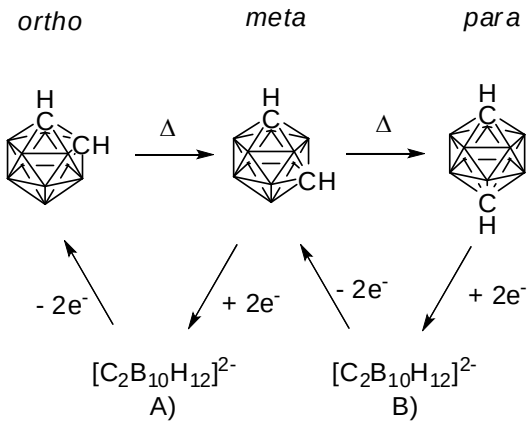

Figure 1–8: The conversion between isomers of $C_2B_{10}H_{12}$ by thermal and redox isomerisation.

1.5.1 *Ortho* to *meta* to *para* carborane (thermal isomerisation)

A method for the conversion of *ortho* carboranes to the *meta* and *para* isomers has been well established.[18] Heating the isomers to high temperatures produces an isomer where the carbon atoms are not adjacent to each other. This result is explained by the greater thermodynamic stability of the carborane when the more electronegative carbon atoms are further separated. Hoffmann and Lipscomb calculated, on the basis of MO theory, that the *meta* carborane isomer would be more stable than the *ortho* isomer.[41,42]

By heating the *ortho* compound, in an inert atmosphere, to high temperatures, conversion to the *meta* and *para* isomers respectively is achieved. To carry out the conversion to the *meta* isomer, reaction conditions which have proved successful include heating it to 460 °C for 24 hours, and a flow process in which it is heated to 600 °C for less than one minute.[39,43] The process of converting the *ortho* isomer to *meta* isomer is efficient as yields are nearly quantitative. The *para* isomer is formed by heating to 620-700 °C where an equilibrium exists between the *meta* and *para* isomers.[18] Also present in reaction mixtures will be bicarboranes and decomposed products.[18]

Grafstein and Dvorak carried out the complete isomerisation of 1,2-$C_2B_{10}H_{12}$ and 1-Me-1,2-$C_2B_{10}H_{11}$ to the respective 1,7 *meta* isomers.[43] Complete isomerisations have been shown for other carborane derivatives with thermally stable functional groups. When the derivatives have very bulky functional groups, this isomerisation is observed to occur at much lower temperatures. This may be explained by the favourable steric relief of the bulky groups when they move further apart.[44] For example, the conversion of the 1,2-$(MePh_2Si)_2$-1,2-$C_2B_{10}H_{10}$ to the *meta* isomer occurs at 260 °C.[18]

1.5.2 *Para* to *meta* to *ortho* carborane (redox isomerisation)

It was predicted by Hoffmann and Lipscomb that the reverse isomerisation, of the *para* to *meta* to *ortho* isomers, would not be possible with the neutral compounds.[41,42] Therefore in order to carry out this transformation it is necessary to introduce a negative charge into the carborane molecule, as anions based on the *ortho* structure are found to be more stable than those based on the *meta* or *para* structure.[41,42] As such, this reverse isomerisation process has three steps – reduction, isomerisation of the dianion followed by oxidation.

Primarily, the methodology used in the literature has used liquid ammonia as the solvent and sodium to reduce the carborane with potassium permanganate, $KMnO_4$, to oxidise the dianion.[45] This reaction is reported to convert the *para* isomer to the *meta*, and the *meta* to the *ortho*.[17,45,46] Zakharkin *et al* reported the

successful conversion of 1,7-$C_2B_{10}H_{12}$, 1-Me-1,7-$C_2B_{10}H_{11}$, 1,7-Me_2–1,7-$C_2B_{10}H_{10}$ and 1-Ph-1,7-$C_2B_{10}H_{11}$ to the *ortho* isomers.[17] Stanko *et al* demonstrated the conversion of *para*-carborane to *meta* carborane.[46] The solubility of the isomers in ammonia was found to be greatest for the *ortho* isomer, decreasing for the *meta* and *para* isomer.[46]

This isomerisation of carboranes has also been reported using THF as the solvent, instead of liquid ammonia.[17,47] The dianions formed are easily oxidised by molecular oxygen in an exothermic reaction.[17] This reaction was carried out on 1,7-Ph_2-1,7-$C_2B_{10}H_{10}$ and 1-Ph-1,7-$C_2B_{10}H_{11}$ by Zakharkin *et al*.[17,47] The reaction must be carried out in the presence of two equivalents of sodium, the electron source, in order to reduce the compound to the dianion. Naphthalene or biphenyl were also present, which were to act as electron carriers. Without the presence of an electron carrier the reaction was not found to work very effectively.[17] Alternatively, naphthlenesodium or biphenylsodium could be used. They also attempted the reaction using a liquid sodium/potassium alloy, instead of just sodium metal. Under these conditions the reaction proceeded easily, in the absence of electron carriers.[17]

1.6 Rearrangement mechanisms

A consensus on the mechanism of the rearrangement has not yet been reached. There has been considerable discussion of this in the literature, most of which is in reference to the thermal isomerisation from *ortho* to *meta* to *para*.[17,48,49]

1.6.1 *Ortho* to *meta* to *para* carborane (thermal isomerisation)

In an attempt to ascertain the mechanism of this transformation, carborane molecules were labelled with halogen substituents and the products formed from the thermal isomerisation reactions were compared with the expected products. None of the mechanisms that had been proposed at this stage gave satisfactory predictions that were in line with the real products for rearrangements.[50] It has also been found that under the conditions required for rearrangement, hydrogen

halogen exchange is possible, making this methodology for discovering the mechanism flawed.[51]

One mechanism put forward for thermal isomerisation is the diamond-square-diamond mechanism (DSD), Figure 1–9.[42,52] This mechanism however is unable to explain the formation of *para* carborane from either the *meta* or the *ortho* isomer, and also fails to account for experimentally found product distributions.[57]

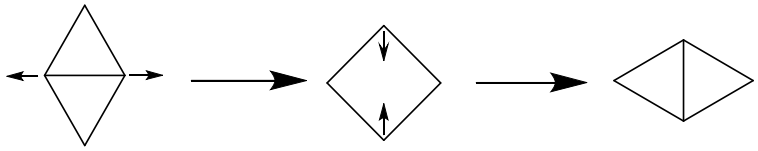

Figure 1–9: Schematic of the proposed DSD mechanism for thermal isomerisation.

Another mechanism put forward is the rotation of triangular faces (TFR), Figure 1–10.[53] In the transition state between isomers, this mechanism predicts 3 square faces.[54] This mechanism can be broken down into a series of DSD transitions.[54]

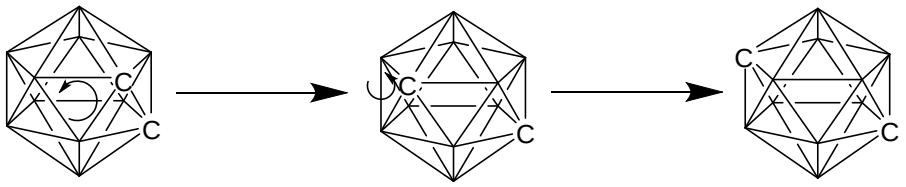

Figure 1–10: Schematic illustrating the proposed TFR mechanism for thermal isomerisation.

Proposed mechanisms that involved an intermediate of *nido* structure give the most accurate predictions. Calculations have pointed to a stepwise mechanism in preference to a concerted pathway.[55,56] The extended triangular rotation mechanism (ETR), a hybrid mechanism of the DSD and TFR, agrees with the experimental data well.[57] Labelling *ortho*-carborane molecules with a ^{10}B isotope and then heating the molecule to 350 °C led to the observation that the ^{10}B atom moved around in the molecule, forming isomers, faster than the carbon atoms moved from an *ortho* to *meta* conformation.[58] The ratio of the ^{10}B isomers with time was compared with proposed mechanisms. The mechanisms proposed which

involved the formation of a *nido* intermediate and had preferred B-B bond breaking are favoured.[58]

1.6.2 *Para* to *meta* to *ortho* carborane (redox isomerisation)

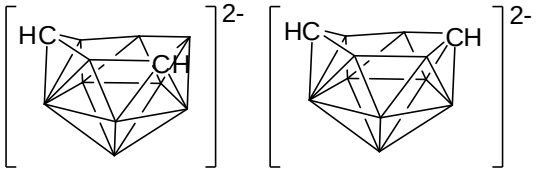

A) **B)**

Figure 1–11: Possible rearrangement intermediates in the redox isomerisation of carboranes from the *meta* to *ortho* isomer (A) [7,9-*nido*-$C_2B_{10}H_{12}]^{2-}$ and the *para* to *meta* isomer (B) [7,10-*nido*-$C_2B_{10}H_{12}]^{2-}$.

It is thought that the reduction of 1,2-$C_2B_{10}H_{12}$ and 1,7-$C_2B_{10}H_{12}$ lead to the formation of the same dianion, [7,9-*nido*-$C_2B_{10}H_{12}]^{2-}$, Figure 1–11(A).[59] Upon oxidation, this intermediate becomes the 1,2-$C_2B_{10}H_{12}$ isomer.[47] It has been suggested that the reduction of 1,12-$C_2B_{10}H_{12}$ gives rise to a different dianion, [7,10-*nido*-$C_2B_{10}H_{12}]^{2-}$, Figure 1–11(B).[60] It is thought that this intermediate is the reason why, on reduction then oxidation of *para* carborane species, the *meta* isomer is obtained instead of the *ortho*. According to Zlatogorsky *et al.* the reduced form of 1,12-Ph_2-1,12-$C_2B_{10}H_{12}$ is able to form the same [7,9-*nido*-$C_2B_{10}H_{12}]^{2-}$ species on reduction as the *ortho* and *meta* analogues.[61] They explain that the [7,10-Ph_2-*nido*-$C_2B_{10}H_{10}]^{2-}$ intermediate which is formed initially becomes [7,9-Ph_2-*nido*-$C_2B_{10}H_{10}]^{2-}$ on heating at reflux in THF.[61]

It has been calculated that oxidation of [7,9-*nido*-$C_2B_{10}H_{12}]^{2-}$ gives a basket-shaped intermediate, higher in energy than [7,9-*nido*-$C_2B_{10}H_{12}]^{2-}$.[62] This intermediate can then proceed via two different transition states; one leading to the *ortho* carborane cage, and the other to *meta* carborane.[62] It was found that the transition state leading to the *meta* carborane cage has a greater activation barrier than the transition state leading to *ortho* carborane.[62] As such, on reoxidation of [7,9-*nido*-$C_2B_{10}H_{12}]^{2-}$, *ortho* carborane is formed preferentially to *meta* carborane.[62]

1.7 Known synthetic routes to carboranes with aromatic substituents at the cage carbons

We are particularly interested in C-aryl carboranes, where an aryl group is directly bonded to the cage carbon, as such compounds are easily reduced and can form radical monoanions. There are several methods put forward in the literature as to how to make carboranes where one or both of the cage carbon atoms is directly bonded to another carbon atom of an aromatic ring. A common method involves using decaborane, *nido*-$B_{10}H_{14}$, and reacting it with Lewis bases, such as dialkylsulfides, acetonitrile or alkylamines. This leads to the formation of a compound with a general formula of $B_{10}H_{12}L_2$. On reacting this species with an alkyne with aromatic substituents, the corresponding aryl carborane is formed, shown in Figure 1–12.

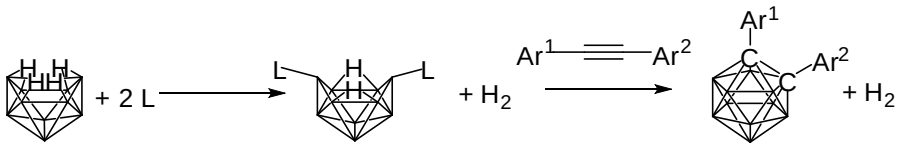

Figure 1–12: Reaction of decaborane with a Lewis base, L, to give the *arachno* $B_{10}H_{12}L_2$ which is reacted with an alkyne to give the carborane product, with liberation of hydrogen.

This reaction gives very low yields for some alkynes.[63] Lower yields are observed when making carboranes with two aromatic units. This reaction cannot be used when the aryl groups involved are acidic, reducible or susceptible to nucleophilic attack.[64] Groups that are nucleophilic may form stable complexes with the decaborane starting material which will additionally complicate the reaction.[63,64] If the *ortho* product is obtained it may be possible to convert it into the *meta* or *para* isomer by heating it to very high temperatures, as described above, but only if the groups Ar^1 and Ar^2 are thermally stable.

By using an Ullmann-type copper-coupling reaction it is possible to make mono and disubstituted carboranes for the *meta* and *para* isomers. Only mono-substituted carboranes have been reported for the *ortho* isomer, Figure 1-13. Similarly the use of the copper-coupling reaction has been reported using aromatic molecules with the easily displaced group -N_2BF_4 instead of iodide.[65]

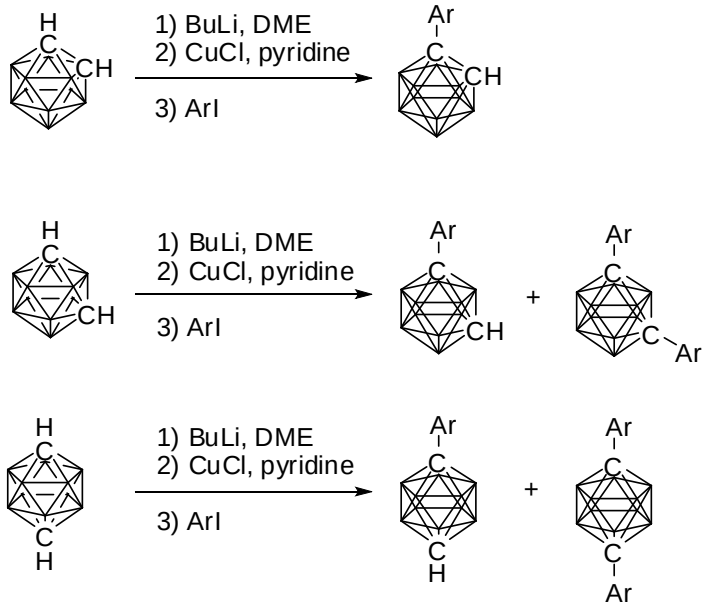

Figure 1–13: The formation of aryl substituted carboranes using a copper-coupling reaction.

The reaction of fluorinated aromatic groups with carborane cages has been shown to produce mono and di-aryl substituted carborane cages in good yields.[63,66,67,68,69,70,71] For example Figure 1–14 shows the synthesis of a di-aryl substituted *ortho* carborane.[67]

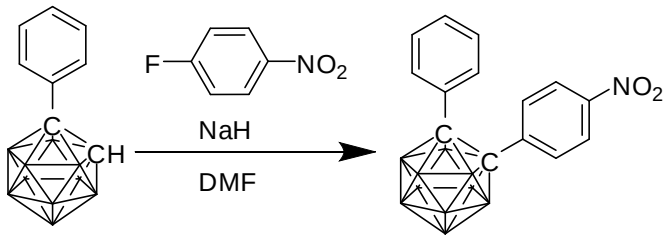

Figure 1–14: Synthesis of 1-Ph-2-(4'-NO_2-C_6H_4)-1,2-$C_2B_{10}H_{10}$ by reaction of 1-Ph-1,2-$C_2B_{10}H_{11}$ with 1-F-4-NO_2-C_6H_4.

Di-aryl substituted *ortho* carboranes have also been synthesised by the method in Figure 1–15.[72]

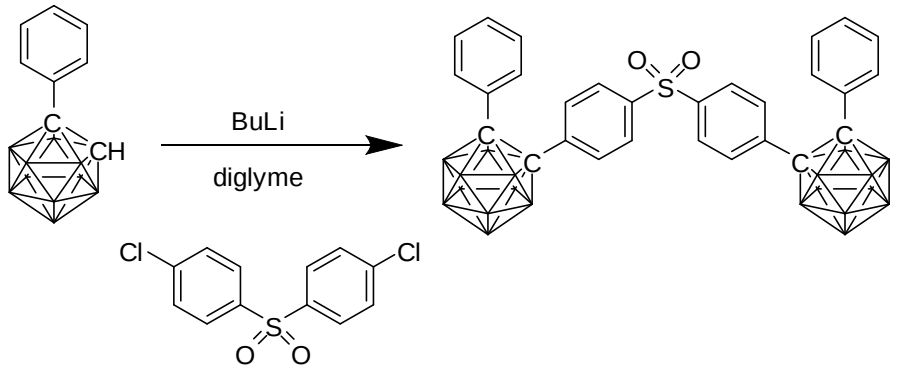

Figure 1–15: Synthesis of (1-Ph-1,2-$C_2B_{10}H_{10}$)$_2$-((C_6H_4)$_2SO_2$) by reaction of 1-Ph-1,2-$C_2B_{10}H_{11}$ with (4-Cl-C_6H_4)$_2SO_2$.

Using chromium tricarbonyl complexes of aryl halides, Henly *et al.* reported the formation of aryl substituted carboranes, but in very low yields, Figure 1–16.[73]

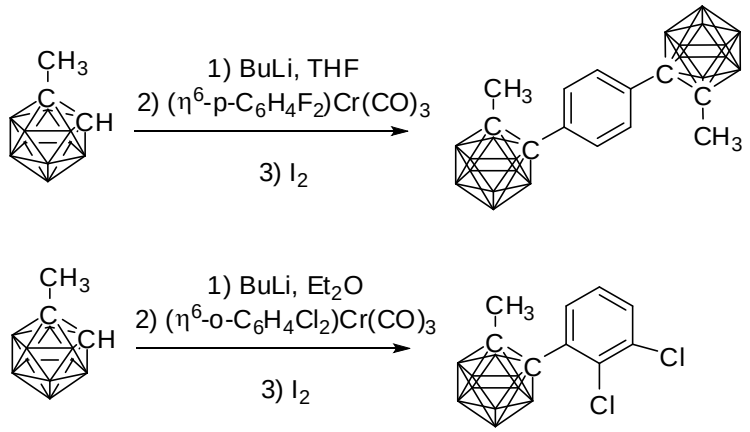

Figure 1–16: Synthesis of aryl substituted carboranes using chromium tricarbonyl complexes.

Heteroaryl carboranes have similarly been synthesised by the decaborane and copper-coupling methods.[74,75] Using the decaborane method, the reported yields are lower than those for the copper-coupling method.

Appendix 1 gives further examples and details, in a series of tables for each general method, of the reagents and yields obtained of carboranes with aromatic substituents.

1.8 Luminescence of Carboranes

Routes for the luminescence of molecules via fluorescence and phosphorescence are shown in Figure 1–17. After excitation of a molecule by a photon of light from the singlet ground state, S_0, to the first singlet excited state, S_1, the molecule will undergo vibrational relaxation to the lowest energy vibrational state in the S_1 state. From this state fluorescence emission can take place. Alternatively, intersystem crossing can take place to the first triplet excited state, T_1. Phosphorescence arises from relaxation from T_1 which is formally spin forbidden. This leads to a long lived emission lifetime. Phosphorescence is only observed in the absence of oxygen as its presence leads to non radiative relaxation.

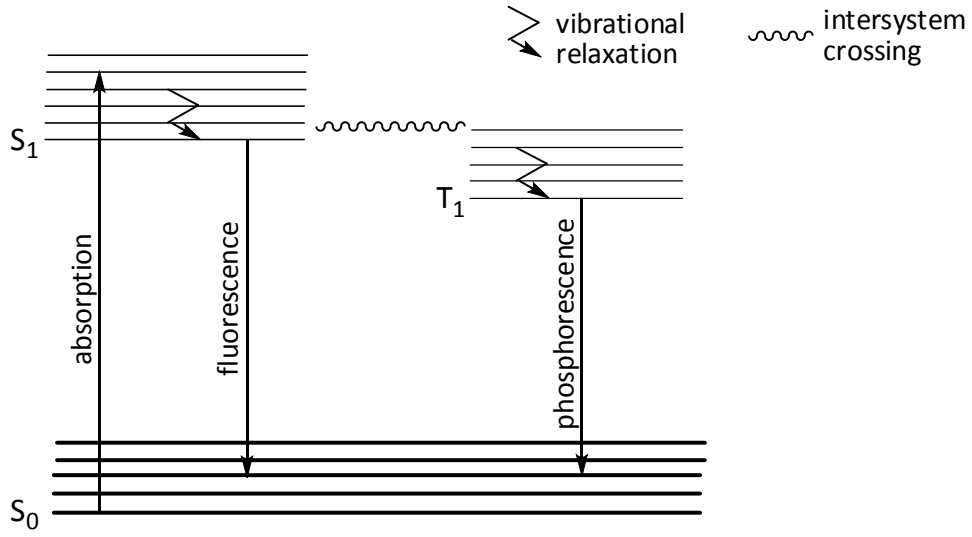

Figure 1–17: Jablonski diagram showing the pathways for fluorescent and phosphorescent emission.

The Stokes shift is the difference in the maxima of the absorption and emission bands. A small Stokes shift is typical of a rigid molecule which does not undergo a significant rearrangement on excitation. In contrast, a large Stokes shift can indicate a significant rearrangement to a lower energy state, hence increasing the difference in absorption and emission energies.

There is much work in the literature on the synthesis of compounds that give fluorescent or phosphorescent emission. The interest is due to the potential for such compounds to be used in OLEDs, organic light emitting diodes, which are of use in flat panel displays without the need for a backlight.

Carboranes are generally considered to have negligible luminescence properties. However, very recently carboranes with aromatic substituents have been reported to show luminescence properties.

The parent carboranes (*ortho*, *meta* and *para)* have been reported to be weakly luminescent in the solid state at room temperature (RT) and 77 K.[76,77,78] In solution they fail to show any emission. Kunkely and Crespo however disagree on the maximum wavelength of emission of *ortho* carborane, shown in Table 1–2.

Compound	λ_{em} / nm		
	RT	77 K	15 K
1,2-$C_2B_{10}H_{12}$	356[77] / 395[76]	354[77] / 441[76]	-
1,7-$C_2B_{10}H_{12}$	380[77]	390[77]	-
1,12-$C_2B_{10}H_{12}$	345[77]	320[77]	397[78]

Table 1–2: Reported fluorescence maxima wavelengths for the parent *ortho*, *meta* and *para* carboranes.

1.8.1 Luminescent *ortho* carborane containing compounds

At present the majority of carborane containing compounds reported to exhibit fluorescence use the *ortho* isomer. Many of these have a similar framework and are reported to exhibit aggregation induced emission in solutions of 1:99 THF:H_2O. Examples of compounds exhibiting such behaviour are shown in Figures 1-17 to 1-19.[79,80,81,82,83,84,85] The fluorescence quenching undergone in these compounds, in solvents that do not encourage aggregate formation, is attributed to the flexible cage C-C bond in *ortho* carborane.[82,83]

It has been shown that the emission wavelength can be tuned by using electron withdrawing and donating groups. Electron donating groups are expected to lengthen the cage C-C bond and with this lengthening a lower energy emission is observed.[84]

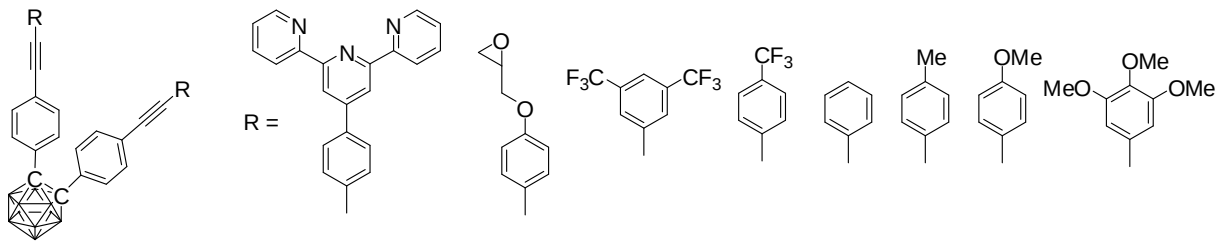

Figure 1–18: *Ortho* carborane monomers reported to exhibit AIE in 1:99 THF:H_2O solution.

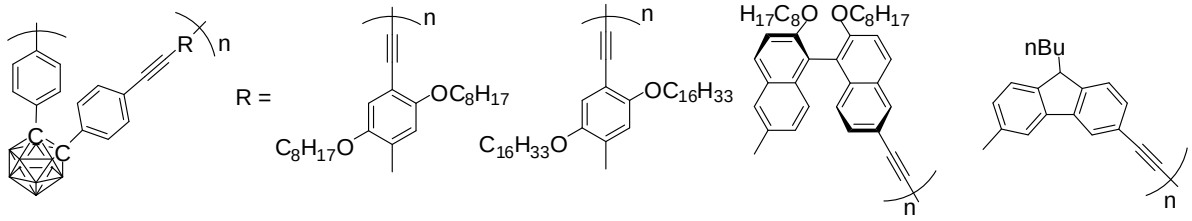

Figure 1–19: *Ortho* carborane polymers reported to exhibit AIE in 1:99 THF:H_2O solution.

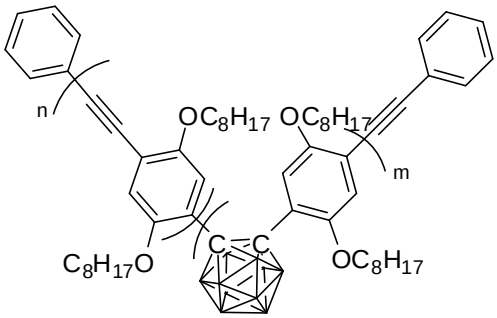

Figure 1–20: *Ortho* carborane polymer reported to exhibit AIE in 1:99 THF:H_2O solution.

Similarly, the compound in Figure 1–21 displays AIE with an emission of 517 nm and quantum yield of 24 %.[85]

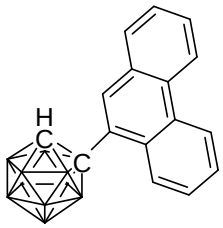

Figure 1–21: *Ortho* carborane phenanthrenyl monomer exhibiting AIE in 1:99 THF:H_2O solution.

The compound shown in Figure 1–22 clearly has many similarities to the compounds shown in Figure 1–18 and Figure 1–19. This compound however exhibits fluorescence in THF at 405 nm.[79] The quantum yield measured in THF is very low at <0.02 %. In a THF/H_2O solution the emission maximum is shifted to 485 nm and the fluorescence quantum yield is found to be 12 %.

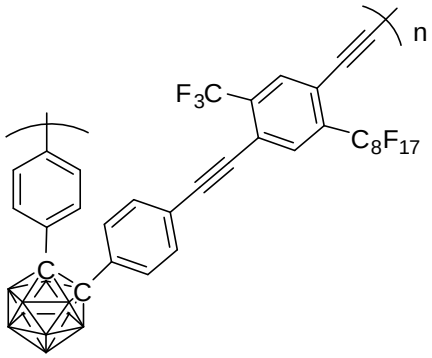

Figure 1–22: *Ortho* carborane polymer reported to exhibit emission in THF solution as well as AIE in 1:99 THF:H_2O solution.

The compound shown in Figure 1–23 however displays strong luminescence in a solution of THF with quantum yields varying from 51 to 40 %, depending on substituent R.[86] This is attributed to the benzocarborane structure, in which movement of the cage C-C bond length is restricted, which reduces the excited state quenching seen in solution for the similar compounds.[86] The HOMO in these cases is found to be on the p-phenylene-ethynylene and the LUMO is located on the butadiene unit of the benzocarborane.[86]

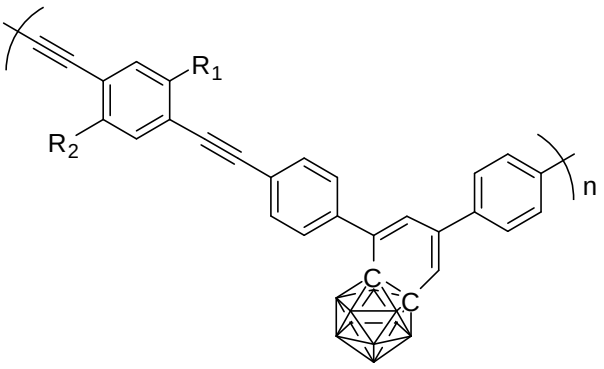

Figure 1–23: Benzocarborane polymer which displays strong luminescence in THF solution. R_1 and R_2= $OC_{12}H_{25}$ or $R_1 = C_8F_{17}$ and $R_2 = CF_3$.

The carboranyl-functionalised aryl ether derivatives, Figure 1–24, also emit in solutions of THF, and toluene, and so the *ortho* carborane cage C-C bond does not quench emission in this case.[87,88] The emission maximum in the compounds where R is methyl is found to vary between 333-370 nm, while those when R is phenyl have emissions between 369-381 nm.[87,88] The *nido* anionic derivatives of these compounds were also prepared and the emission properties compared to the *closo* versions.[87,88] Solvent effects were observed such that the *closo* versions of the molecules had the strongest emissions in non polar solvents, while the *nido* anionic molecules were strongest in polar solvents.[87,88]

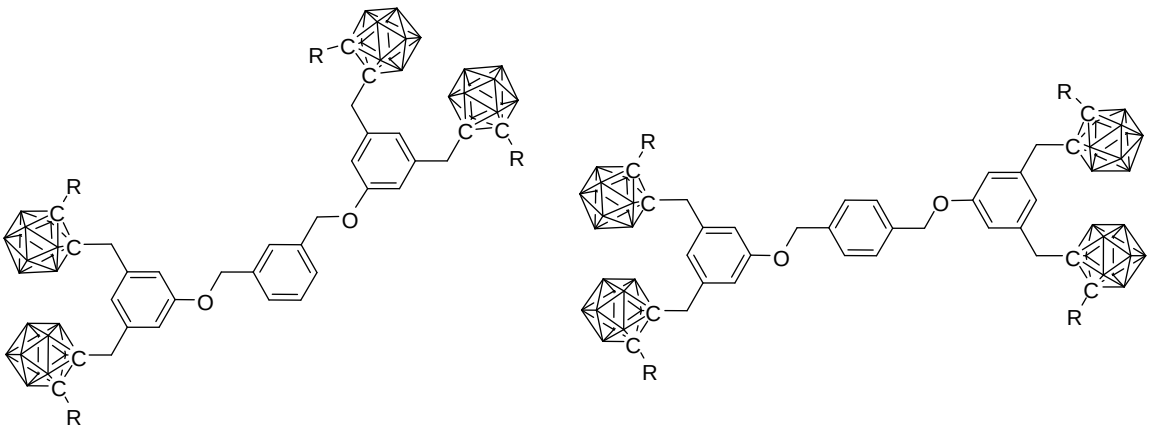

Figure 1–24: *Ortho* carborane containing aryl ether derivatives, where R is Ph or Me, reported to exhibit fluorescent emission in solution.

Polyfluorene-containing polymers, Figure 1–25, also emit in solution, but the emission is characteristic of annealed polyfluorenes.[89] The presence of the carboranes act only to raise the T_g of the polymer, hinder chain packing and increase the stability of the compounds.[89]

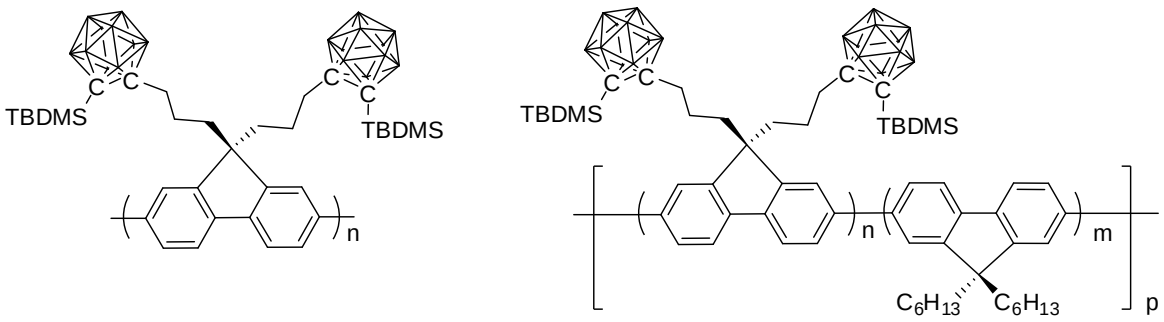

Figure 1–25: Polymers containing polyfluorene and *ortho* carborane units which emit in solution with a high T_g, due to the carborane group.

The carborane containing polymers, where the carborane cage is in the polymer backbone, in Figure 1–26 are the first to be integrated into polymer light emitting diodes (PLEDs).[90] The presence of the carborane cage disrupts the conjugation along the polymer and so there is a blue shift in absorption compared to the non carborane containing polymers.[90] The emission is red shifted by ~140 nm compared to the polymers without the carborane.[90] However, the PLEDs using polymers omitting the carborane cage require lower voltages to turn on than the carborane containing polymer devices.[90]

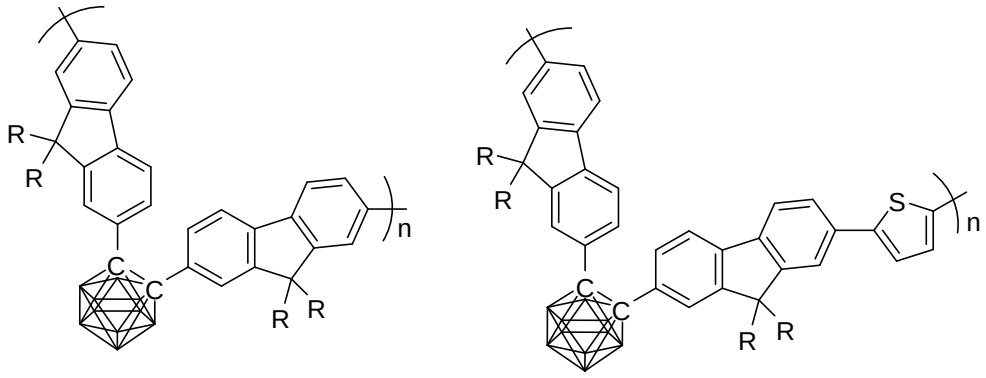

Figure 1–26: Polymers containing polyfluorene and *ortho* carborane units, which have been incorporated into a PLED. R = C_6H_{13}.

The polyfluorene containing *ortho* carborane in the main chain, Figure 1–27, exhibits emission maxima at 415 nm and 565 nm.[91] The higher energy blue emission, at 415 nm, is attributed to the fluorene units.[91] The presence of the carborane leads to a 30 nm bathochromic shift in the fluorescence emission, compared to the dihexyl fluorene dimer, which is attributed to the carborane cage

extending the conjugation length.[91] The lower energy emission, at 565 nm, is not seen without the incorporation of carborane cages.[91] This band is attributed partly to energy transfer from the fluorene groups to the electron withdrawing carborane cages, leading to emission at lower energy.[91] The other possibility raised is the aggregation of the molecule.[91]

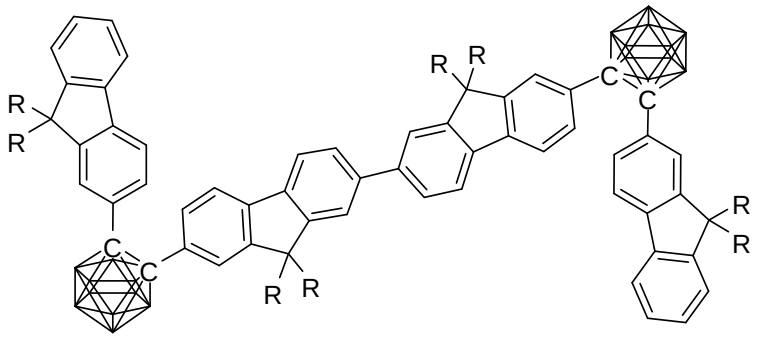

Figure 1–27: Polyfluorene containing *ortho* carborane in the main chain, exhibiting two emission bands. R = C_6H_{13}.

The carborane compounds in Figure 1–28 show a small red shift in the absorbance maximum and a large decrease in ε compared to the parent perylene compounds.[92] The emission of the carborane compounds are blue shifted and have higher emission intensity compared to the parent perylene compounds.[92] The parent perylenes therefore have larger Stokes shifts than the carborane compounds.[92]

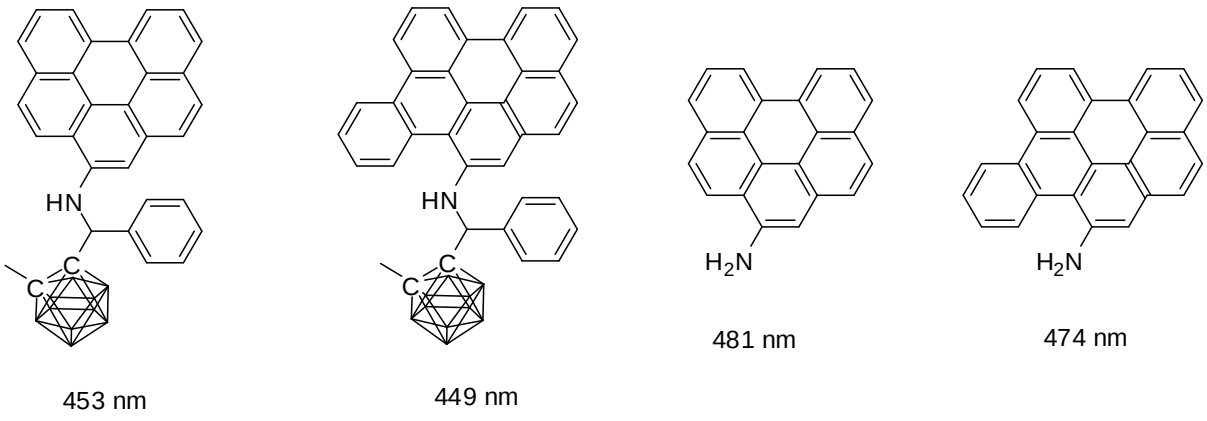

Figure 1–28: Emission maxima of perylene appended carboranes and their parent perylenes in THF solution.

A series of *ortho* carborane appended clusters have been synthesised, Figure 1–29.[93,94,95] These compounds are very thermally stable. This is attributed to the *ortho* carborane units. The photochemistry of compound H) is attributed solely to the hexaphenylbenzene core.[93] The report however does not give the precise emission and quantum yield data. Quantum yields are found to be higher for the carborane appended compounds C)-E) than the parent molecules A) and B).[94] The increase is attributed to the size and 3D structure of the *ortho* carborane units preventing π-π stacking interactions and hence minimising non radiative decay.[94] Compounds F) and G), however, have much reduced quantum yields compared to the core parent molecules.[95]

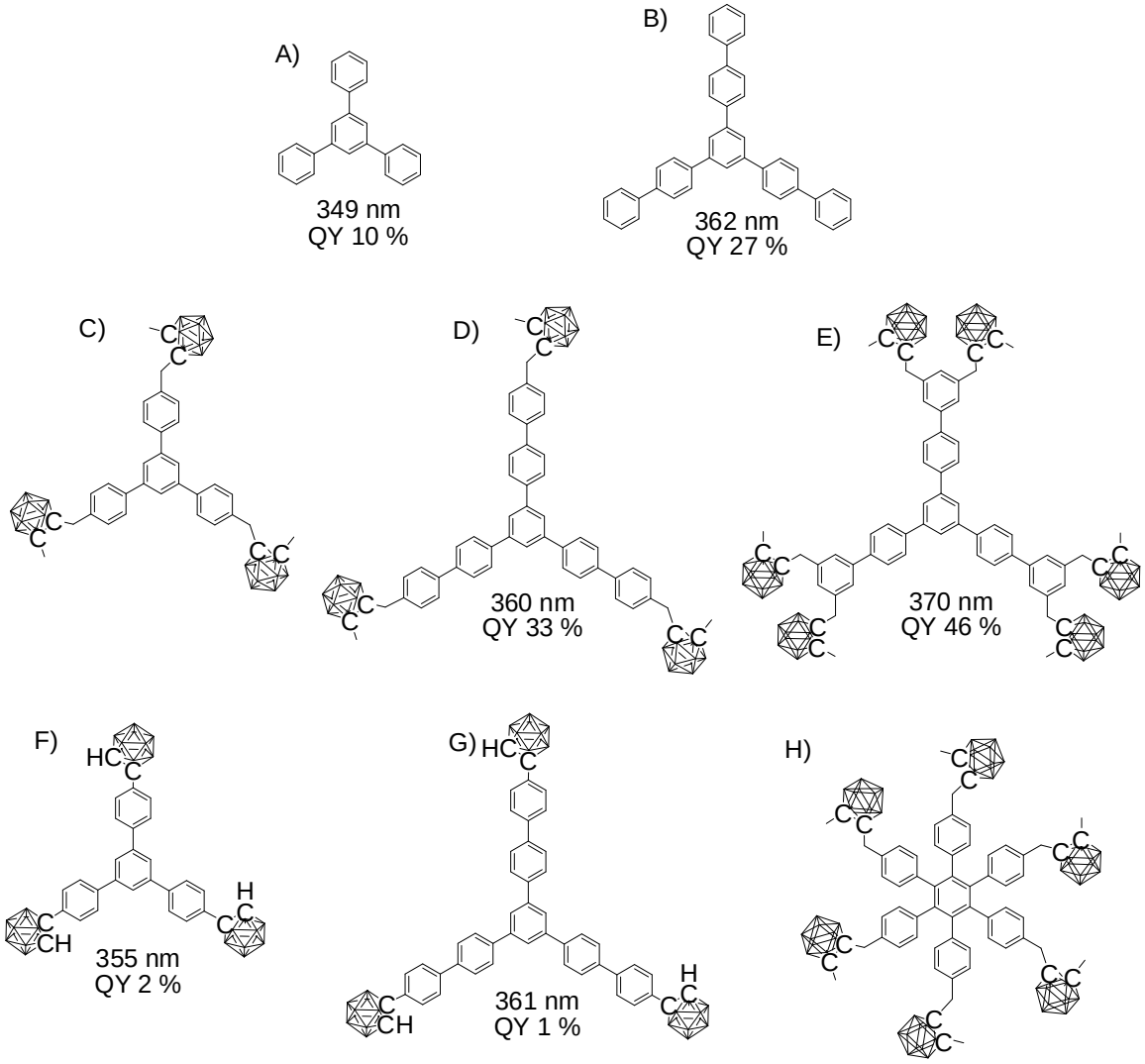

Figure 1–29: Fluoresent carborane appended trimers and parent unsubstituted molecules, with emission maxima and quantum yields in DCM solution, where reported.

The compounds shown in Figure 1–30 have absorptions assigned to the π-π* transition of the carbazole group.[102] The emission maximum is red shifted compared to the *meta* and *para* analogues.[102] The large solvatochromic shifts seen for these *ortho* carboranes are attributed to charge transfer.[102] It is also observed that there is extensive fluorescence quenching in the *ortho* isomers.[102]

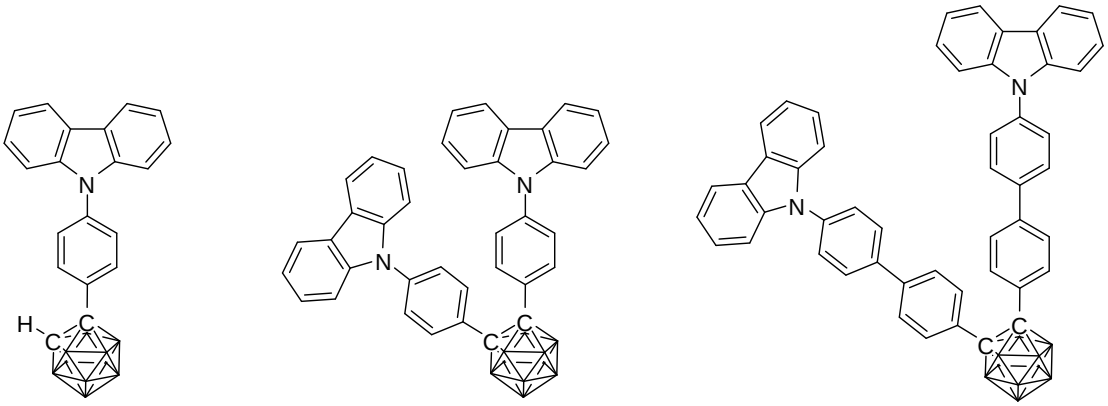

Figure 1–30: Carbazole *ortho* carboranes that emit in toluene solution.

Crespo *et al.* report the synthesis and luminescence spectra of gold disubstituted complexes of *ortho* carboranes with PPh_3 and PMe_3 substituents on the gold atoms, Figure 1–31.[77] The *meta* and *para* $AuPPh_3$ substituted isomers were also synthesised.[77] They give two weak emission bands in the solid state at 77 K and room temperature.[77] The λ_{em} bands are found to be between 367 - 403 nm and 506 – 555 nm.[77] The low energy band was assigned as MLCT.[77] As we saw in Table 1–2, they reported the parent carboranes to emit, in the same conditions, between 345 and 380 nm.[77] As such the higher energy band is assigned to intraligand transitions on the carborane cage.[77]

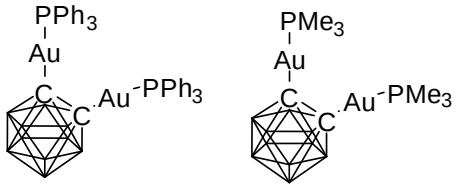

Figure 1–31: *Ortho* gold disubstituted carboranes which emit in the solid state.

The borolyl carboranes in Figure 1–32 have been shown to display interesting fluorescence properties.[96] Low energy emission bands, with high Stokes shifts, are attributed to a charge transfer transition between the carborane cage and the heterocyclic group which is dependent on the orientation of the diazaborolyl group with the cage C-C bond.[96] In the solid state quantum yields of up to 65 % are found.[96] In cyclohexane, two of these carboranes have been shown to display dual fluorescence.[96] In these cases there is a high energy emission due to a local transition on the borolyl substituent, and a low energy emission due to a charge transfer between the cage and the heterocycle.[96] Two distinct S_1 excited state conformations were found by TD-DFT for these two compounds, each attributed to the high or low energy emission band.[96]

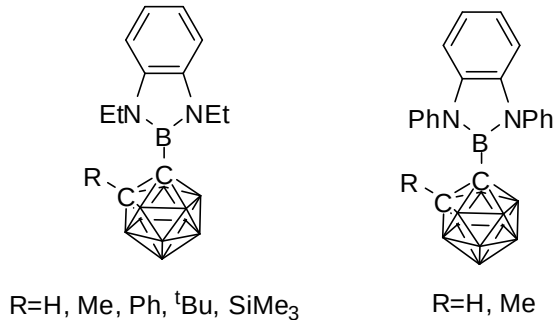

R=H, Me, Ph, ^{t}Bu, $SiMe_3$ R=H, Me

Figure 1–32: Borolyl carboranes reported to display fluorescence.

1.8.2 Luminescent *meta* and *para* carborane containing compounds

The *meta* carborane polymers, Figure 1–33, are shown to be fluorescent.[97] There is an intense blue emission in solution with a quantum yield of 11 to 25 % for the different Ar groups.[97] In this case the HOMO is located on the p-phenylene ethynylene group whilst in the LUMO there is a small contribution from *meta* carborane.[97]

The *ortho* carborane analogues displayed AIE and only emitted in a 1:99 THF:water solution. These *meta* carborane compounds however do not have the flexible cage C-C bond and as such do not show AIE but display fluorescence in chloroform solution.[97]

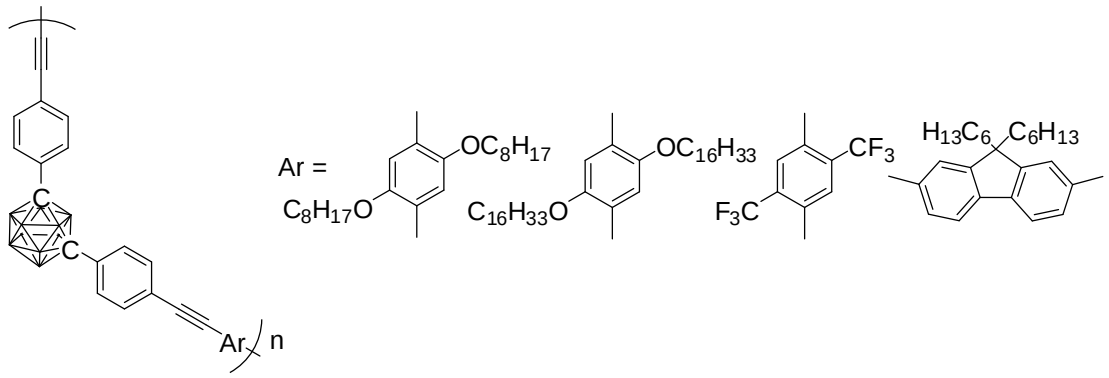

Figure 1–33: *Meta* carborane containing polymers reported to emit in chloroform solution.

Meta and *para* analogues of the compounds in Figure 1–29 are shown in Figure 1–34.[95] These compounds are not as thermally stable as the *ortho* analogues.[95] Similarly, the energy of the emission is much the same as that of the core parent molecules.[95] The quantum yields however are much enhanced compared to the *ortho* analogues, Figure 1–29 F) and G), and the core parent molecules, Figure 1–29 A) and B).[95]

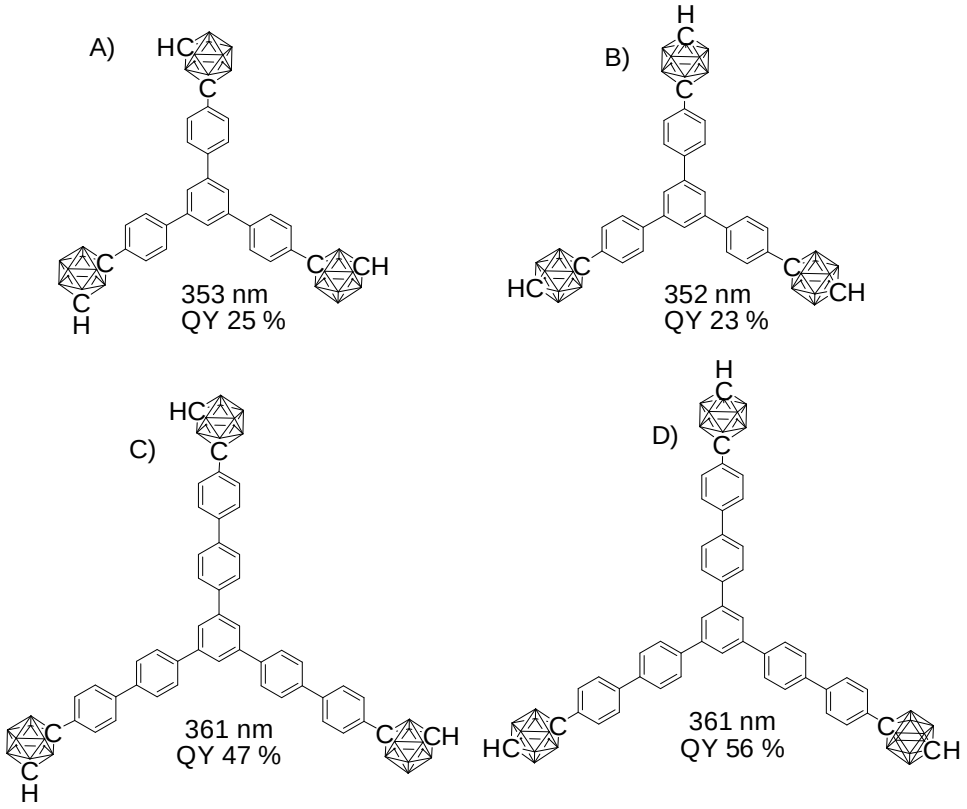

Figure 1–34: *Meta* and *para* carborane appended trimers exhibiting fluorescence, with emission maxima and quantum yields in DCM solution, where reported.

Meta carboranes substituted at 9-B with tolyl bipyridine, Figure 1–35, lead to a decrease in the quantum yields to 14 % and 21 % from 38 % for the parent molecule.[98] The emission is also red shifted for A) and B) compared to the parent molecule.[98] When coordinated to Zn(II) there is a small red shift in the emission wavelength and an increased quantum yield with the increased rigidity imparted to the bipyridyl group.[98]

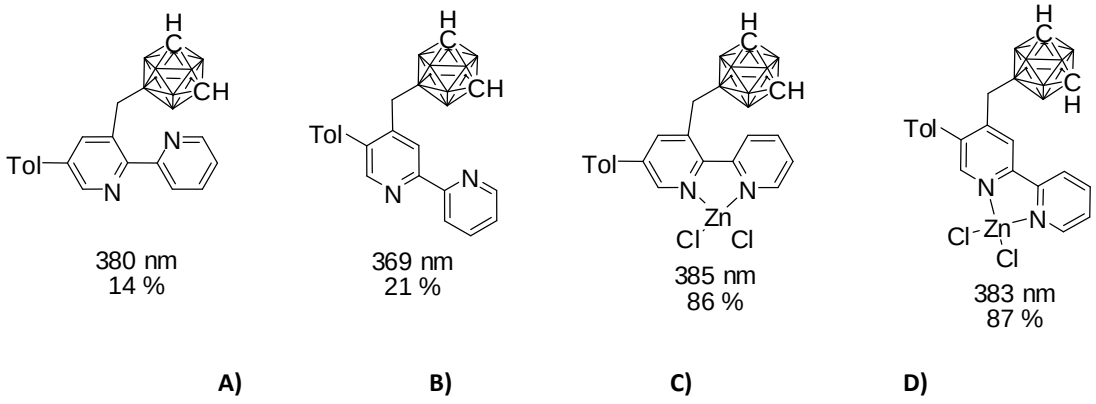

Figure 1–35: *Meta* tolyl bipyridyl carboranes which exhibit fluorescence emission in chloroform solution with emission maxima and quantum yields.

Compounds containing *para* carborane have also been shown to emit. Figure 1–36 shows an example of this.[99] These compounds all emit in DCM solutions. By varying the R group from H to $C_{12}H_{25}O$ or $Me(OCH_2CH_2)_3O$, the emission is seen to shift, such that A) emits at 496 nm, B) emits at 458 nm and C) emits at 438 nm.[99]

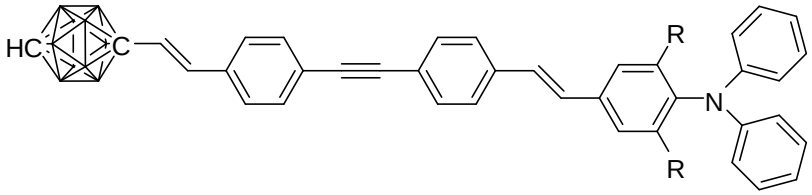

Figure 1–36: *Para* carborane containing compounds which exhibit fluorescence in DCM solution. A) R = H, B) R = $C_{12}H_{25}O$ and C) R = $Me(OCH_2CH_2)_3O$.

The compound in Figure 1–37 shows blue emission at 400 nm in chloroform.[100] As in the case of the *ortho* carboranes in Figure 1–25, the *para* carborane imparts stability to the polyfluorene structure and increases the T_g.[100]

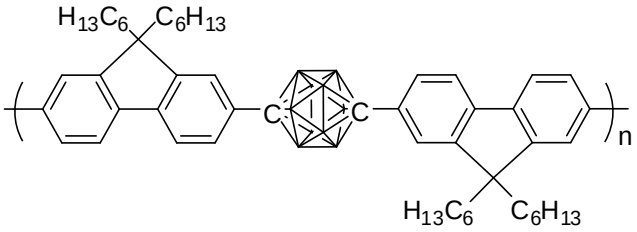

Figure 1–37: Polyfluorene containing polymer with *para* carborane in the backbone which exhibits emission in chloroform.

Para carborane has also been used as a backbone link between organic dyes, Figure 1–38.[101] The group labelled R emits at 538 nm and the group labelled G emits at 726 nm.[101] The compound GC, with *para* carborane bonded to the group labelled G, also emits at 726 nm.[101] Similarly, the compound RCG emits at 728 nm. The carborane is not found to have a significant electronic influence.[101]

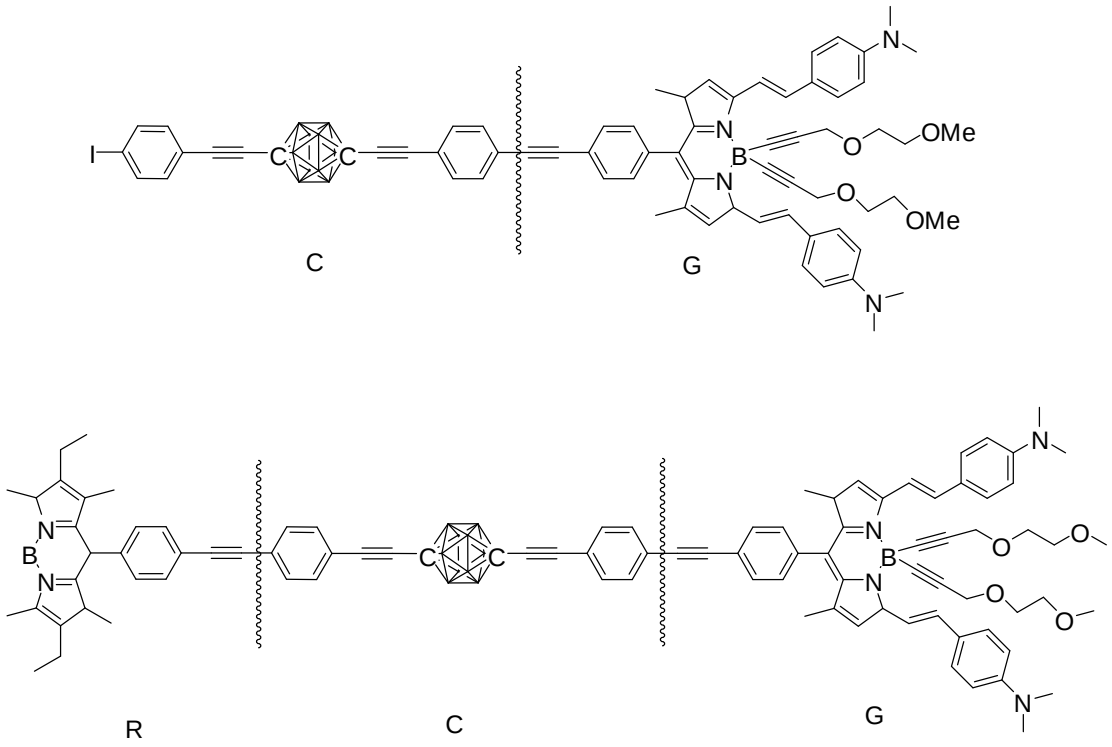

Figure 1–38: *Para* carborane as a backbone link between organic dyes.

The *meta* and *para* analogues of the compounds in Figure 1–30 are shown in Figure 1–39. As noted earlier, the photophysical properties are very different from those of the *ortho* isomers. The absorption, emission, lifetimes and quantum yields for these compounds are almost identical with those for the fluorescence of the carbazole chromophore.[102] The presence of the *meta* and *para* carborane cages in these cases, again, has only a very subtle effect.

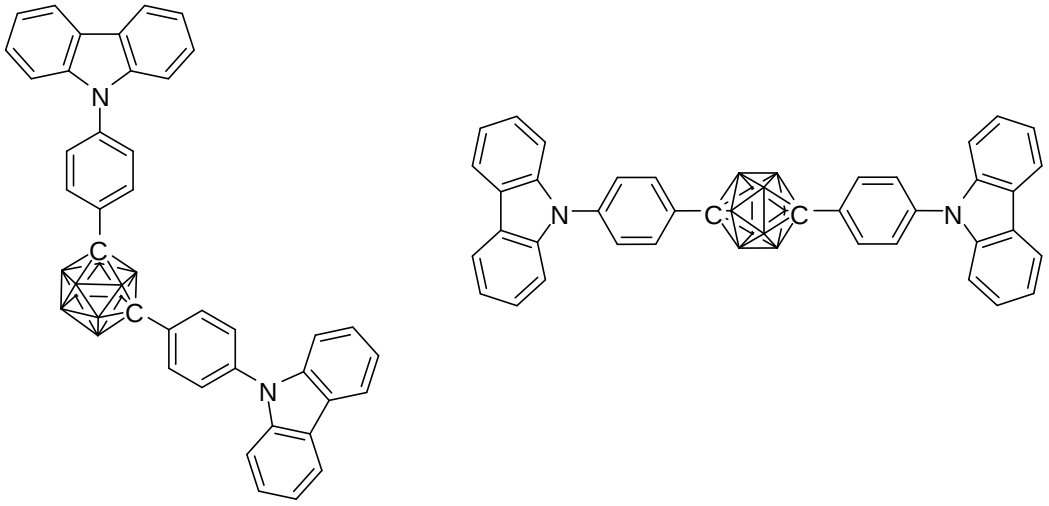

Figure 1–39: Fluorescent carbazole *meta* and *para* carboranes, reported to emit in toluene solution.

Bitner *et al* also found luminescence in carboranes compounds containing metals, Figure 1–40.[78] They conclude that the luminescence is based on $CpFe(CO)_2L$ instead of the carborane and is a ligand field (d-d) effect rather than charge transfer.[78]

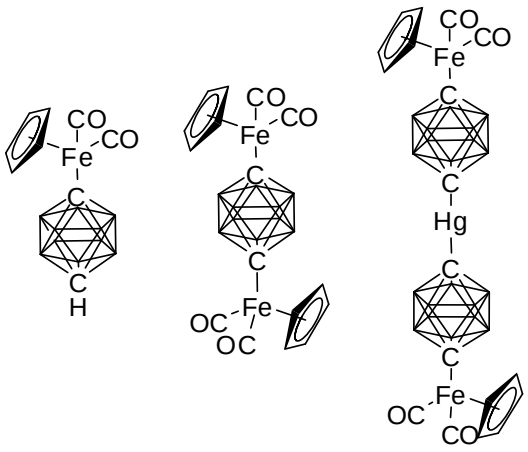

Figure 1–40: *Para* carborane compounds substituted with $CpFe(CO)_2$ groups, reported to emit in the solid state.

Absorption and emission data reported in the literature for carborane derivatives are summarised in tables in Appendix 2.

1.9 Electrochemistry and spectroelectrochemistry of carboranes

Electrochemistry can provide useful information about the redox activity of carborane compounds. Spectroelectrochemistry can provide further information with respect to the structures of the redox species.

The reduction potentials reported for some carboranes are shown below in Table 1–3. In the cases of 1,2-$C_2B_{10}H_{12}$, 1-Ph-1,2-$C_2B_{10}H_{11}$, 1-Me-1,2-$C_2B_{10}H_{11}$ and 1,2-Me_2-1,2-$C_2B_{10}H_{10}$ the reduction step is an irreversible two-electron reduction. Three oxidation peaks are seen for these molecules corresponding to the irreversible destruction of the dianions.[103] The first of these waves is assigned to the oxidation of the monoprotonated anion.[103] The first and second waves decrease in size with repeated sweeps, while the third increases in size.[103]

Compound	$-E_{1/2}$ V (reduction)
1,2-$C_2B_{10}H_{12}$	2.44[103], 2.51[109], 2.4[104], 2.42[105], 2.55[106]
1,2-$C_2B_{10}H_{12}$ with bipy	2.1[108]
1,1'-(1,2-$C_2B_{10}H_{12}$)$_2$	1.44[109]
1-Ph-1,2-$C_2B_{10}H_{11}$	1.78[103], 1.95[109], 1.82[107], 1.84[106]
1,2-Ph_2-1,2-$C_2B_{10}H_{10}$	1.14[109]
1-Me-1,2-$C_2B_{10}H_{11}$	2.30[103], 2.44[109], 2.35[104]
1,2-Me_2-1,2-$C_2B_{10}H_{10}$	2.26[103], 2.35[109]
1,7-$C_2B_{10}H_{12}$	>2.8[109,106]
1-1'-(1,7-$C_2B_{10}H_{12}$)$_2$	2.62[109]
1-Me-1,7-$C_2B_{10}H_{11}$	>2.8[109]
1-Ph-1,7-$C_2B_{10}H_{11}$	2.45[109]
1,7-Ph_2-1,7-$C_2B_{10}H_{10}$	2.35[109]

Table 1–3: Reported reduction and oxidation potentials for some simple carboranes.

The electro-reduction of 1,2-$C_2B_{10}H_{12}$ in the presence of 2,2'-bipyridyl (bipy) is easier than in the absence of bipy as reduction occurs at the potential of the first stage of bipy reduction.[108] As the bipy is reduced this electron is transferred to the *ortho* carborane, regenerating the bipy.[108] The *ortho* carborane radical anions formed then dispropotionate to form the dianion, shown below.[108]

$$bipy + e^- \rightarrow bipy^{-\cdot}$$

$$bipy^{-\cdot} + C_2B_{10}H_{12} \rightarrow bipy + C_2B_{10}H_{12}^{-\cdot}$$

$$2\ C_2B_{10}H_{12}^{-\cdot} \rightarrow C_2B_{10}H_{12}^{2-} + C_2B_{10}H_{12}$$

Such an effect is not seen for carboranes such as 1-Ph-1,2-$C_2B_{10}H_{11}$ which are reduced before the bipy reduction potential is reached.[108] It can be seen that *ortho* carborane is reduced more easily than the *meta* isomer. This is due to the greater electron affinity of *ortho* carborane. It is noted that introducing alkyl and aryl groups to the C atoms lowers the reduction potential showing an increase in electron affinity.[109]

The electrochemistry of halogen substituted carboranes has been investigated. There is a weakening of the electron acceptor properties from the *ortho* to *meta* to *para* isomers.[107] This corresponds to a larger reduction potential of the C-X bond for the *para* isomer, Table 1–4.[107] The difference in the reduction potentials between the Cl- and Br-substituted carboranes reduces from *para* to *meta* to *ortho*.[107]

Compound	$-E_{1/2}$ X=Cl	$-E_{1/2}$ X=Br	$\Delta E_{1/2}$
1-X-1,12-$C_2B_{10}H_{11}$	2.14	0.99	1.15
1-Me-7-X-1,7-$C_2B_{10}H_{11}$	1.67	0.66	1.00
1-X-1,2-$C_2B_{10}H_{11}$	1.12	0.50	0.62

Table 1–4: Reduction potentials for some halogenated carboranes.[107]

These halogen-substituted carborane reduction potentials correspond to a two-electron addition to the cages, forming dianions.[110] The basic *ortho* carborane molecule reduction observed is a two-electron process.[107] The introduction of a methyl group has only a small effect on the reduction potential.[107]

C-Phenyl carboranes are well known and many derivatives have been synthesised. The electrochemistry of these compounds has also been investigated.[111,112] Di-phenyl *ortho* carborane has been reported to form a stable radical anion with a 2n + 3 skeletal electron (SE) count where n is the number of vertices in the cluster.[111] The radical species is calculated to have an extended cage C-C length.[111] This is to be expected as the cage with a 2n + 3 SE count takes on a

structure that is an intermediate of the *closo* structure (with 2n + 2 SE) and the more open *nido* (with 2n + 4 SE), in which the cage C-C bond is broken.[111] Cyclic voltammetry shows two sequential chemically reversible and electrochemically quasi reversible one electron waves, separated by 170 mV.[111] This distance gives a measure of the stability of the radical anion with respect to disproportionation to the neutral and dianion species.[111] IR and UV-Vis spectroelectrochemistry confirm the high chemical stability of each redox process in the almost complete recovery of the starting spectrum after reduction.[111] DFT calculations carried out show an elongation in the cage C-C bond length on reduction to the radical anion, suggesting that the extra electron is located in the carborane cage rather than the phenyl groups.[111] ESR measurements confirm the paramagnetic nature of the anion and also suggest the extra electron is located in the cage.[111] Very similar CV results are observed for derivatives of di-phenyl *ortho* carborane, Figure 1–41.[112] Reduction potentials shift to more negative values as the substituent becomes more electron donating.[112] These observations confirm that electronic communication occurs between X and the carborane cage through the phenylene link.[112]

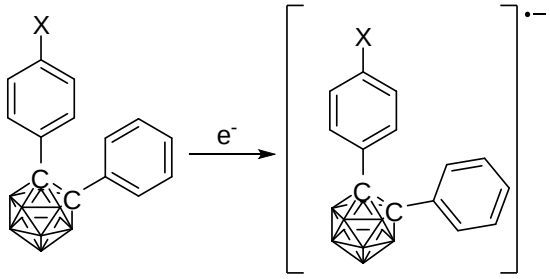

X= H / F / OMe / NMe_2 / NH_2

Figure 1–41: Carboranes, based on di-phenyl *ortho* carborane, reported to form radical anions.

A series of carboranes with fluorinated aryl groups have been reported, with CV data similar to diphenyl-*ortho*-carborane.[113] The *ortho* carborane compounds shown in Figure 1–42 display two sequential one electron reductions which are chemically reversible and electrochemically quasi reversible.[113] The separation in reduction potentials varies from 160 mV to 610 mV, with the greatest separation being for the most electron-withdrawing substituent, $C_6F_4CF_3$.[113] UV-vis and IR spectroelectrochemistry results are similar to those seen for the phenyl carboranes

without fluorination and confirm the stability of the redox products.[113] Again, EPR indicates that the extra electron in the radical anionic species is located in the carborane cage.[113] The analogous *meta* and *para* carborane species synthesised, shown in Figure 1–42, show very different cyclic voltammetry traces. They both display irreversible two-electron reductions.[113] These reductions lead to decomposition of the *meta* and *para* compounds.[113] In the case of the *ortho* isomers, the LUMO is found to be delocalised over the cage C-C and the aromatic rings.[113] In comparison, the LUMO of the *meta* and *para* isomers is localised on the aromatic rings.[113]

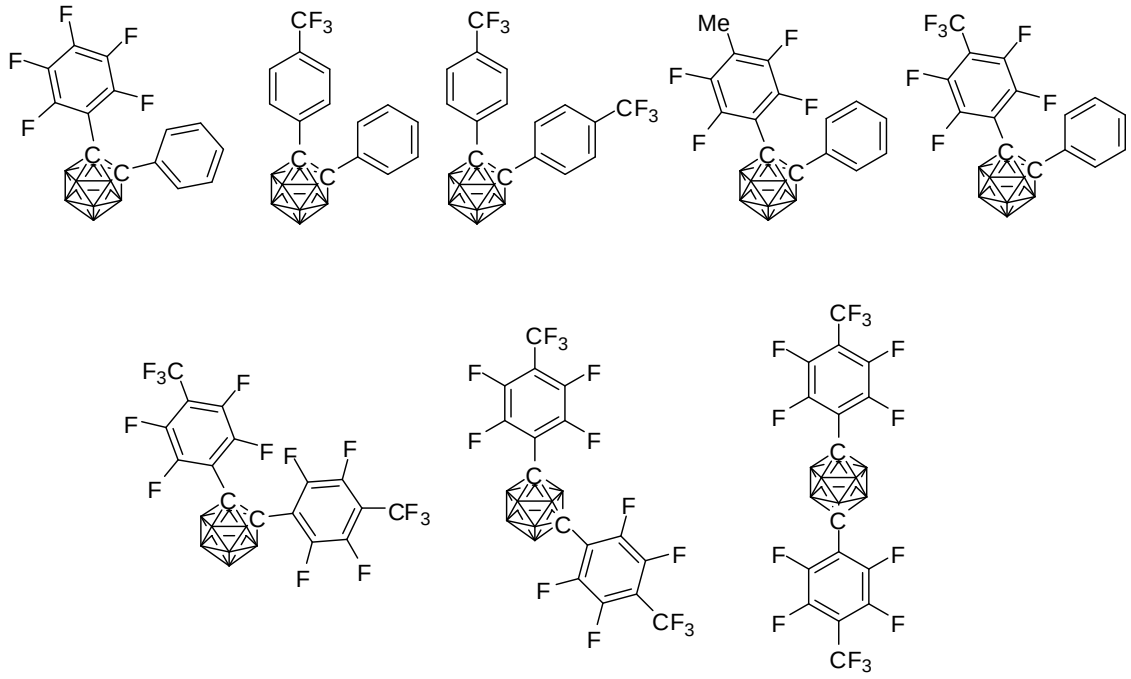

Figure 1–42: Carboranes with fluorinated aryl groups investigated by cyclic voltammetry, where the *ortho* carboranes are reported to form radical anions.

Diphenyl *ortho* carborane has been investigated as a mediator in electroorganic synthesis.[114] Carboranes have been investigated for this due to their high stability on reduction and the wide range of reduction potentials possible with different carborane derivatives. The electrocatalytic reduction of 1,2-dibromo-1,2-diphenylethane in the presence of 1 mol% of the carborane produced *trans* stilbene in a yield of 95 %.[114]

The compounds in Figure 1–43 both show a single irreversible oxidation peak, due to the oxidation of the pyrrole group, at 1.20 (A) and 1.06 V (B) (vs Ag/Ag^{+}).[115] The presence of an electron-withdrawing *ortho* carborane cage is shown to shift the oxidation potential of a pyrrole to a more positive potential compared with the unsubstituted pyrrole, which shows an oxidation peak at 1.04 V.[116] This shift in oxidation potential is due to the electron-withdrawing nature of the carborane cage.[115] The addition of another CH_2 in the spacer between the carborane cage and the pyrrole group in B) reduces the effect of the carborane cage substantially.[115]

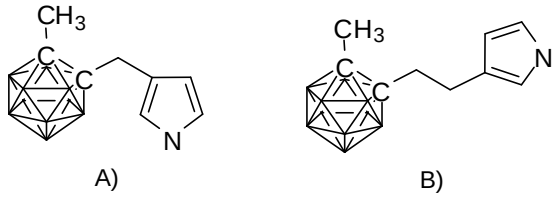

Figure 1–43: Pyrrole with electron withdrawing *ortho* carborane cage which increases the oxidation potential compared to pyrrole alone.

The disubstituted *ortho*, *meta* and *para* carboranes, Figure 1–44, show three irreversible oxidation peaks.[117] The oxidation potentials were found to increase from the *ortho* to the *meta* to the *para* isomer, at 0.9, 1.11 and 1.12 V respectively.[117,118] The oxidation peaks are assigned to the oxidation of the thienyl group to radical cation species.[117] The oxidation of the *ortho, meta* and *para* carboranes leads to the formation of conducting polymers on the surface of the electrode.[117,118] The species with two *ortho* carborane cages bridged by a phenylene group displays a single irreversible oxidation, and two quasi reversible reductions.[117]

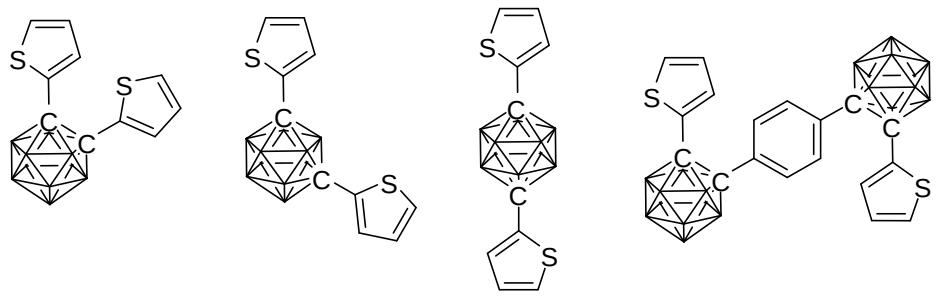

Figure 1–44: Thiophene substituted *ortho*, *meta* and *para* carboranes investigated by cyclic voltammetry.

Several bimetallic carborane compounds have been investigated using these techniques and found to display electronic communication between metal centres, through the carborane cage in some cases. In the Robin-Day classification system, Class I systems display very weak coupling leading to structural and spectroscopic properties of the two sites being retained. In Class II systems, the two sites are more strongly coupled but remain valence trapped with a double well potential ground state. New spectroscopic properties arise due to electron transfer between redox sites. Class III systems have so great a degree of mixing between redox states that the ground state potential has a single minimum and the system becomes completely delocalised, with the spectroscopic identity of the individual sites being lost.

The molecule, shown in Figure 1–45, displayed both oxidation and reduction processes.[119,120] A splitting of the redox waves showed electronic interaction within the molecule. If there was no electronic interaction between the metal centres it would be expected that both would oxidise at the same potential. It was concluded the *para* carborane cage is a conduit for electronic delocalisation.

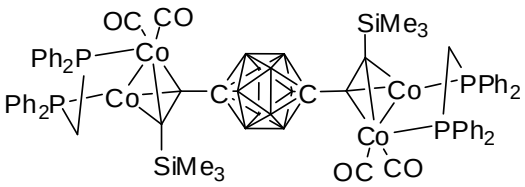

Figure 1–45: 1,12-($C_2SiMe_3Co_2(CO)_2(dppe)$)$_2$-1,12-$C_2B_{10}H_{10}$, an example of a bimetallic carborane compound displaying electronic communication between metal centres, through the carborane cage.

A variety of carborane compounds with a η^5-$CpFe(CO)_2$ substituent have been synthesised, Figure 1–46.[121] The simple monosubstituted *ortho*, *meta* and *para* carboranes showed one irreversible single electron oxidation wave, with a decrease in oxidation potentials from *ortho* to *meta* to *para*.[121] In the case of the *para* disubstituted compound, cyclic voltammetry showed two irreversible one electron oxidations which were within the same range.[121] This suggests that there is communication between the two iron centres through the carborane cage. The *para* carborane with two C≡CFe[$(CO)_2$Cp] groups, in contrast, only displays one oxidation potential.[121] This suggests that the alkynyl triple bond link stops electronic

communication, due to poor p orbital overlap between the ethynyl group and the p orbital of the carborane cage C atom.[121] When two monosubstituted *para* carborane cages were bridged by a mercury atom, only one oxidation potential was observed, indicating that there was no communication between the iron centres in this case.[121]

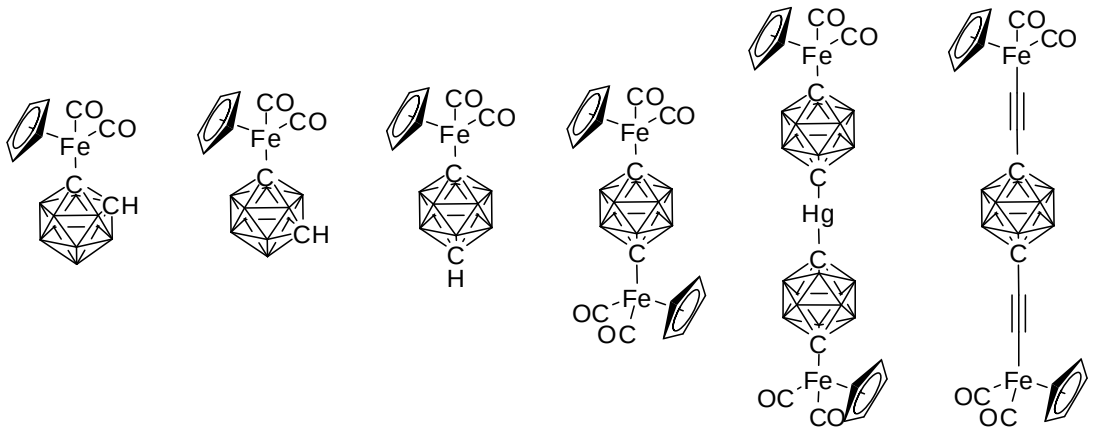

Figure 1–46: $CpFe(CO)_2$ substituted carboranes investigated by cyclic voltammetry, examining electronic communication through the carborane cage(s) between metal centres for bimetallic compounds.

The bimetallic compound shown in Figure 1–47 displays a separation of two 1- electron waves in the cyclic voltammogram showing that there was a stable intermediate in the redox products.[122] This molecule was also investigated using UV-Vis NIR and IR spectroelectrochemistry.[122] The electrochemical data reveal that the carborane orbitals do not mix significantly with the metal ethynyl-based orbitals and that communication is permitted between the two metal atoms.[122] Looking at the characteristic C≡C and BH bands in the IR spectra as the molecule is oxidised is revealing. There is a small shift in position of the BH band and the single C≡C band is replaced by two new bands when it is oxidised to the monocation.[122] When oxidised to the di-cation the BH band is further shifted to higher energy while the C≡C band is seen to be a single weak band.[122] This is consistent with the organometallic ethynyl moieties being distinct from the carborane unit.[122]

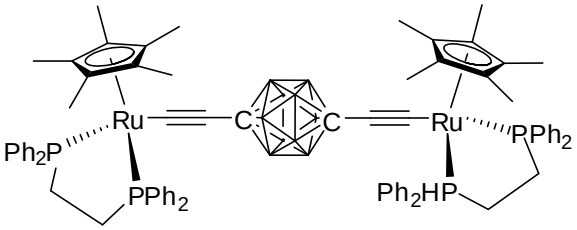

Figure 1–47: 1,12-(CC(Ru(dppe)(η-CpMe$_5$))$_2$-1,12-$C_2B_{10}H_{10}$, a bimetallic carborane compound exhibiting communication through the *para* carborane cage, between the metal centres.

The compound in Figure 1–48 also displays two electrochemically reversible, chemically reversible, 1-electron oxidation processes.[123] Using the Robin and Day mixed valence classification system, the compound is assigned to be a weakly coupled class II mixed valence system, such that electron transfer between the redox sites leads to new spectroscopic properties.[123,124]

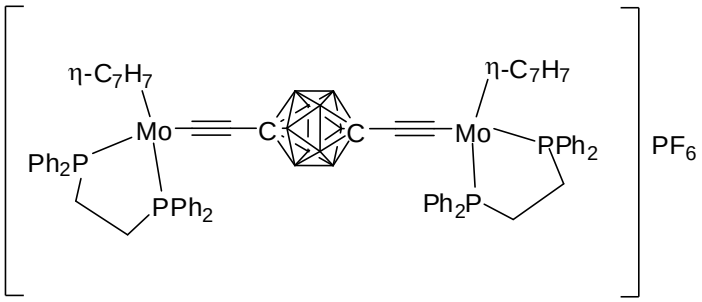

Figure 1–48: [1,12-(CC(Mo(dppe)(η-C_7H_7))$_2$-1,12-$C_2B_{10}H_{10}$]$^-$, a weakly coupled class II mixed valence system.

1.10 References

1. Grimes R. N., *J. Am. Chem. Soc.,* **1966**, 88, 1895-1899.
2. Onak T., Drake R. P. and Dunks G. B., *J. Am. Chem. Soc.*, **1965**, 87, 2505.
3. Hart H. and Lipscomb W. N., *Inorg. Chem.*, **1968**, 7, 1070-1075.
4. Koetzle T. F., Scarbrough F.E. and Lipscomb W. N., *Inorg. Chem.*, **1968**, 7, 1076-1084.
5. Garrett P. M., Smart J. C. and Hawthorne M. F., *J. Am. Chem. Soc.,* **1969**, 91, 4707-4710.
6. Tsai C. C. and Streib W. E., *J. Am. Chem. Soc.*, **1966**, 88, 4513-4514.
7. Grafstein D., Fein M. M, Vogel C., Paustian J. E., Smith H. F., Karlan S., Bobinski J. and Dvorak J., *Inorg. Chem.*, **1963**, 2, 1125-1128.
8. Dunks G. B. and Hawthorne M. F., *J. Am. Chem. Soc.*, **1968**, 90, 7355.
9. Onak T., Drake R. P. and Dunks G. B., *Inorg. Chem.*, **1964**, 3, 1686-1690.
10. Grimes R. N., Bramlett C. L. and Vance R. L., *Inorg. Chem.*, **1968**, 7, 1066-1070.
11. Franz D. A. and Grimes R. N., *J. Am. Chem. Soc.*, **1970**, 92, 1438.
12. Fox M. A., Greatrex R., Hofmann M., Schleyer P. V. R. and Williams R. E., *Angew. Chem. Int. Ed.*, **1997**, 36, 1498-1501.
13. Bausch J. W., Matoka D. J., Carroll P. J. and Sneddon L. G., *J. Am. Chem. Soc.*, **1996**, 118, 11423-11433.
14. Brellochs B., Backovsky J., Stibr B., Jelinek T., Holub J., Bakardjiev M., Hnyk D., Hofmann M., Cisarova I. and Wrackmeyer B., *Eur. J. Inorg. Chem.*, **2004**, 3605-3611.
15. Su K., Carroll P. J. and Sneddon L. G., *J. Am. Chem. Soc.*, **1993**, 115, 10004-10017.
16. Wade K., *Chem. Brit.*, **1975**, 11, 177-183.
17. Zakharkin L. I., Kalinin V. N. and Podvisotskaya L. S., *Bull. Acad. Sci. USSR Div. Chem. Sci.*, **1967**, 2212-2217.
18. Grimes R. N., *Carboranes*, Academic Press, **1970**.
19. Zhang J., Osgood A., Shirai Y., Morin J. F., Sasaki T., Tour J. M and Kelly K. F., 7th IEEE Conference on Nanotechnology, Hong Kong, **2007**.
20. Morin J. F., Shirai Y. and Tour J. M., *Organic Letters*, **2006**, 8, 1713-1716.
21. Sasaki T. and Tour J. M., *Organic Letters*, **2008**, 10, 897-900.
22. Morin J. F., Sasaki T., Shirai Y., Guerrero J. M. and Tour J. M., *J. Org. Chem.*, **2007**, 72, 9481-9490.
23. Valliant J. F., Guenther K. J., King A. S., Morel P., Schaffer P., Sogbein O. O. and Stephenson K. A., *Coord. Chem. Rev.*, **2002**, 232, 173-230.
24. Plesek J., *Chem. Rev.*, **1992**, 92, 269-278.
25. Armstrong A. F. and Valliant J. F., *Dalton Trans.*, **2007**, 4240-4251.
26. Endo Y., Iijima T., Yamakoshi Y., Yamaguchi M., Fukasawa H. and Shudo K, *J. Med. Chem.*, **1999**, 42, 1501-1504.
27. Endo Y., Iijima T., Yamakoshi Y., Kubo A. and Itai A., *Bioorg. Med. Chem. Lett.*, **1999**, 9, 3313-3318.
28. Endo Y., Yaguchi K., Kawachi E. and Kagechika H., *Bioorg. Med. Chem. Lett.*, **2000**, 10, 1733-1736.
29. Fujii S., Hashimoto Y., Suzuki T., Ohta S. and Endo Y., *Bioorg. Med. Chem. Lett.*, **2005**, 15, 227-230.
30. Papetti S., Schaeffer B. B, Gray A. P. and Heying T. L., *J. Polym. Sci. A Polym. Chem.*, **1966**, 4, 1623.

31. Mayes N., Green J. and Cohen M. S., *J. Polym. Sci. A Polym. Chem.*, **1967**, 5, 365.
32. Longuet-Higgins H. C. and Roberts M. D., *Proceedings of the Royal Society of London Series A-Mathematical and Physical Sciences*, **1955**, 230, 110-119.
33. Lipscomb W. N., *Science*, **1977**, 196, 1047-1055.
34. Wade K., *Adv. Inorg. Chem. Radiochem.*, **1976**, 18, 1-66.
35. Wade K., *J. Chem. Soc., Chem. Commun.*, **1971**, 792-793.
36. Hill W. E., Johnson F. A. and Novak R. W., *Inorg. Chem.*, **1975**, 14, 1244-1249.
37. Tebbe F. N., Garrett P. M. and Hawthorne M. F., *J. Am. Chem. Soc.*, **1968**, 90, 869-879.
38. Rietz R. and Hawthorne M. F., *Inorg. Chem.*, **1974**, 13, 755-756.
39. Papetti S., Obenland C. and Heying T. L., *Ind. Eng. Chem. Prod. Res. Dev.*, **1966**, 5, 334-337.
40. Sieckhaus J. F., Semenuk N. S., Knowles T. A. and Schroeder H., *Inorg. Chem.*, **1969**, 8, 2452-2457.
41. Hoffmann R. and Lipscomb W. N., *J. Chem. Phys.*, **1962**, 36, 3489-3493.
42. Hoffmann R. and Lipscomb W. N,, *Inorg. Chem.*, **1963**, 2, 231-232.
43. Grafstein D. and Dvorak J., *Inorg. Chem.*, **1963**, 2, 1128-1133.
44. Salinger R. M and Frye C. L., *Inorg. Chem.*, **1965**, 4, 1815-1816.
45. Zakharkin L. I. and Kalinin V. N., *Bull. Acad. Sci. USSR Div. Chem. Sci.*, **1969**, 192.
46. Stanko V. I., Brattsev V. A. and Goltyapin Y. V., *J. Gen. Chem. USSR*, **1969**, 39, 2623-2626.
47. Zakharkin L. I., Kalinin V. N, and Podvisotskaya L. S., *Bull. Acad. Sci. USSR Div. Chem. Sci.*, **1966**, 1444.
48. Zakharkin L. I. and Kalinin V. N., *Bull. Acad. Sci. USSR*, **1965**, 2173.
49. Hawthorne M. F., Young D. C., Garrett P. M., Owen D. A., Schwerin S. G., Tebbe F. N. and Wegner P. A., *J. Am. Chem. Soc.*, **1968**, 90, 862.
50. Wong H. S. and Lipscomb W. N., *Inorg. Chem.*, **1975**, 14, 1350-1357.
51. Zakharkin L. I. and Kalinin V. N., *Bull. Acad. Sci. USSR Div. Chem. Sci.*, **1969**, 3, 542-545.
52. Lipscomb W. N., *Science*, **1966**, 153, 373-378.
53. Gimarc B. M., Warren D. S., Ott J. J. and Brown C., *Inorg. Chem.*, **1991**, 30, 1598-1605.
54. Brown C. A. and McKee M. L., *J. Mol. Model.*, **2006**, 12, 653-664.
55. Wales D. J., Mingos D. M. P. and Lin Z. Y., *Inorg. Chem.*, **1989**, 28, 2754-2764.
56. Johnson B. F. G., *J. Chem. Soc., Chem. Commun.*, **1986**, 27-30.
57. Wu S. H. and Jones M., *J. Am. Chem. Soc.*, **1989**, 111, 5373-5384.
58. Edvenson G. M. and Gaines D. F., *Inorg. Chem.*, **1990**, 29, 1210-1216.
59. Dunks G. B., Wiersema R. J. and Hawthorne M. F., *J. Am. Chem. Soc.*, **1973**, 95, 3174-3179.
60. Ellis D., Lopez M. E., McIntosh R., Rosair G. M., Welch A. J. and Quenardelle R., *Chem. Commun.*, **2005**, 1348-1350.
61. Zlatogorsky S., Ellis D., Rosair G. M. and Welch A. J., *Chem. Commun,* **2007**, 2178-2180.
62. Hutton B. W., MacIntosh F., Ellis D., Herisse F., Macgregor S. A., McKay D., Petrie-Armstrong V., Rosair G. M., Perekalin D. S., Tricas H. and Welch A. J., *Chem. Commun.*, **2008**, 5345-5347.

63. Ohta K., Goto T. and Endo Y., *Inorg. Chem.*, **2005**, 44, 8569-8573.
64. Coult R., Fox M. A., Gill W. R., Herbertson P. L., MacBride J. A. H. and Wade K., *J. Organomet. Chem.*, **1993**, 462, 19-29.
65. Kovradov A. I., Shaujumbekova Z. S., Kazantsev V. A. and Zakharkin L. I., *J. Gen. Chem. USSR*, **1986**, 56, 2045.
66. Thomas R. L. and Welch A. J., *Polyhedron*, **1999**, 18, 1961-1968.
67. Ohta K., Goto T. and Endo Y., *Tetrahedron Lett.*, **2005**, 46, 483-485.
68. Zakharkin L. I. and Lebedev V. N., *Bull. Acad. Sci. USSR Div. Chem. Sci.*, **1970**, 914.
69. Zakharkin L. I. and Lebedev V. N., *Bull. Acad. Sci. USSR Div. Chem. Sci.*, **1972**, 2273-2275.
70. Thomas R. L. and Welch A. J., *Acta Crystallogr. C*, **1996**, 52, 1689-1691.
71. Batsanov A. S., Fox M. A., Howard J. A. K. and Wade K., *J. Organomet. Chem.*, **2000**, 597, 157-163.
72. Vyakaranam K., Rana G., Ratanasuwan A., Hosmane S. N., Maguire J. A. and Hosmane N. S., *Organometallics*, **2002**, 21, 3905-3912.
73. Henly T. J., Knobler C. B. and Hawthorne M. F., *Organometallics*, **1992**, 11, 2313-2316.
74. Alekseyeva E. A., Batsanov A. S., Boyd L. A., Fox M. A., Hibbert T. G., Howard J. A. K., MacBride J. A. H., Mackinnon A. and Wade K., *Dalton Trans*., **2003**, 475-482.
75. Ohta K., Goto T., Fijii S., Suzuki T., Ohta S. and Endo Y., *Bioorg. Med. Chem.*, **2008**, 16, 8022-8028.
76. Kunkely H. and Vogler A., *Inorg. Chim. Acta.*, **2004**, 357, 4607-4609.
77. Crespo O., Gimeno M. C., Laguna A., Ospino I., Aullon G. and Oliva J. M., *Dalton Trans.*, **2009**, 3807-3813.
78. Bitner T. W., Wedge T. J., Hawthorne M. F. and Zink J. I., *Inorg. Chem.*, **2001**, 40, 5428-5433.
79. Kokado K. and Chujo Y., *Macromolecules,* **2009**, 42, 1418-1420.
80. Kokado K., Tokoro Y. and Chujo Y., *Macromolecules*, **2009**, 42, 9238-9242.
81. Kokado K. and Chujo Y., *Polymer Journal*, **2010**, 42, 363-367.
82. Kokado K. and Chujo Y., *Dalton Trans.,* **2011**, 40, 1919-1923
83. Kokado K., Nagai A. and Chujo Y., *Macromolecules*, **2010**, 43, 6463-6468.
84. Kokado K. and Chujo Y., *J. Org. Chem.*, **2011**, 76, 316-319.
85. Kokado K., Nagai A. and Chujo Y., *Tetrahedron Lett.*, **2011**, 52, 293-296.
86. Kokado K., Tominaga M. and Chujo Y., *Macromol. Rapid Commun.*, **2010**, 31, 1389-1394.
87. Lerouge F., Vinas C., Teixidor F., Nunez R., Abreu A., Xochitiotzi E., Santillan R. and Farfan N., *Dalton Trans.*, **2007**, 1898-1903.
88. Lerouge F., Ferrer-Ugalde A., Vinas C., Teixidor F., Sillanpaa R., Abreu A., Xochitiotzi E., Farfan N., Santillan R. and Nunez R., *Dalton Trans.*, **2011**, 41, 7541-7550.
89. Simon Y. C., Peterson J. J., Mangold C., Carter K. R. and Coughlin E. B., *Macromolecules*, **2009**, 42, 512-516.
90. Davis A. R., Peterson J. J. and Carter K. R., *ACS Macro. Lett.*, **2012**, 1, 469-472.
91. Peterson J. J., Werre M., Simon Y. C., Coughlin E. B. and Carter K. R., *Macromolecules*, **2009**, 42, 8594-8598.

92. Pieters G., Gaucher A., Prim D., Besson T., Giner T., Planas J. G., Teixidor F., Vinas C., Light M. E. and Hursthouse M. B., *Chem. Commum.*, **2011**, 47, 7725-7727.
93. Dash B. P., Satapathy R., Maguire J. A. and Hosmane N. S., *Chem. Commun.*, **2009**, 3267-3269.
94. Dash B. P., Satapathy R., Gailliard E. R., Maguire J. A. and Hosmane N. S., *J. Am. Chem. Soc.*, **2010**, 132, 6578-6587.
95. Dash B. P., Satapathy R., Gaillard E. R., Norten K. M, Maguire J. A., Chug N. and Hosmane N. S., *Inorg. Chem.*, **2011**, 50, 5485-5493.
96. Weber L., Kahlert J., Brockhinke R., Bohling L., Brockhinke A., Stammler H-G., Neumann B., Harder R. A. and Fox M. A., *Chem. Eur. J.*, **2012**, 18, 8347-8357.
97. Kokado K., Tokoro Y. and Chujo Y., *Macromolecules*, **2009**, 42, 2925-2930.
98. Prokhorov A. M., Slepukhin P. A., Rusinov V. L., Kalinin V. N. and Kozhevnikov D. N., *Tetrahedron Lett.*, **2008**, 49, 3785-3789.
99. Nicoud J. F., Bolze F., Sun X. H., Hayek A. and Baldeck P., *Inorg. Chem.*, **2011**, 50, 4272-4278.
100. Peterson J. J., Simon Y. C., Coughlin B. E. and Carter K. R., *Chem. Commun.*, **2009**, 4950-4952.
101. Ziessel R., Ulrich D., Oliver J. H., Bura T and Sutter A., *Chem. Commun.*, **2010**, 46, 7978-7980.
102. Wee K-R., Han W-S., Cho D. W., Kwon S., Pac C. and Kang S. O., *Angew. Chem. Int. Ed.*, **2012**, 51, 2677-2680.
103. Yarosh M. V., Baranova T. V., Shirokii V. L., Erdman A. A. and Maier N. A., *Russian Journal of Electrochemistry*, **1994**, 30, 366-368.
104. Teixidor F., Pedrajas J. and Vinas C., *Inorg. Chem.*, **1995**, 34, 1726-1729.
105. Butin K. P., Rakhimov R. D., Kampel V. C., Petriashvili M. V., Bregadze V. I. and Godovikov N. N., *Organomet. Chem. USSR*, **1988**, 493-496.
106. Kampel V. C., Butin K. P., Bregadze M. V. and Godovikov V. I., *Institute Heteroorg. Compounds*, **1978**, 1318-1321.
107. Stanko V. I., Anorova G. A., Klimova T. V., Titova N. S., Butin K. P. and Beletskaya I. P., *J. Gen. Chem. USSR*, **1972**, 1320-1326.
108. Yarosh M. V., Shirokii V. L., Ryabtsev A. N., Baranova T. V. and Maier N. A., *Russian Journal of Electrochemistry*, **1995**, 31, 590-591.
109. Zakharkin L. I., Kalinin V. N. and Snyakin A. P., *Institute Heteroorg. Compounds*, **1968**, 194-196.
110. Stanko V. I., Butin K. P., Belokoneva N. A. and Beletskaya I. P., *J. Gen. Chem. USSR*, **1970**, 2214-2216.
111. Fox M. A., Nervi C., Crivello A. and Low P. J., *Chem. Commun.*, **2007**, 2372-2374.
112. Fox M. A., Nervi C., Crivello A., Batsanov A. S., Howard J. A. K., Wade K. and Low P. J, *J. Solid State Electrochem.*, **2009**, 13, 1483-1495.
113. Tricas H., Colon M., Ellis D., Macgregor S. A., McKay D., Rosair G. M., Welch A. J., Glukhov I. V., Rossi F., Laschi F. and Zanello P., *Dalton Trans.*, **2011**, 40, 4200-4211.
114. Hosoi K., Inagi S., Kubo T. and Fuchigami T., *Chem. Commun.*, **2011**, 47, 8632-8634.
115. Fabre B., Clark J. C. and Vicente M. G. H., *Macromolecules*, **2006**, 39, 112-119

116. Fabre B., Chayer S. and Vicente M. G. H., *Electrochemistry Communications*, **2003**, 5, 431-434.
117. Barrière F., Fabre B., Hao E., LeJeune Z. M., Hwang E., Garno J. C., Nesterov E. E. and Vicente M. G. H., *Macromolecules*, **2009**, 42, 2981-2987.
118. Hao E., Fabre B., Fronczek F. R. and Vicente M. G. H., *Chem. Commun.*, **2007**,4387-4389.
119. Fox M. A., Paterson M. A. J., Nervi C., Galeotti F., Puschmann H., Howard J. A. K. and Low P. J., *Chem. Commun.*, **2001**, 1610-1611.
120. Le Guennic B., Costuas K., Halet J-F., Nervi C., Peterson M. A. J., Fox M. A., Roberts R. L., Albesa-Jove D., Puschmann H., Howard J. A. K. and Low P. J., *C. R. Chimie.*, **2005**, 1833-1896
121. Wedge T. J., Herzog A., Huertas R., Lee M. W., Knobler C. B. and Hawthorne M. F., *Organometallics*, **2004**, 23, 482-489.
122. Fox M. A., Roberts R. L., Baines T. E., Le Guennic B., Halet J. F., Hartl F., Yufit D. S., Albesa-Jove D., Howard J. A. K. and Low P. J., *J. Am. Chem. Soc.*, **2008**, 130, 3566-3578.
123. Brown N. J., Lancashire H. N., Fox M. A., Collison D., Edge R., Yufit D. S., Howard J. A. K., Whiteley M. W. and Low P. J., *Organometallics*, **2011**, 30, 884-894.
124. Robin M. B. and Day P., *Adv. Inorg. Chem. Radiochem.*, **1967**, 10, 247.

2 : Synthesis and Fluorescence of C-Naphthyl and C-Anthracyl Carboranes

2.1 Introduction

This chapter describes the synthesis of a series of carboranes with naphthyl groups substituted at the cage carbon atoms. These naphthyl carboranes were found to exhibit fluorescence. These emission properties are compared with those of the well-known C-phenyl carboranes. In order to continue along the phenyl, naphthyl trend, we attempted to synthesise the anthracyl carboranes and carried out DFT calculations in an attempt to find a stable anthracyl carborane which is predicted to have interesting photophysical properties.

The 1-(1'-$C_{10}H_7$)-1,2-$C_2B_{10}H_{11}$ molecule investigated here has previously been synthesised by Ohta et al.[1] The molecule was made using both the decaborane route and a copper-coupling method, Figure 2–1, in yields of 52 and 84 %.[1] They also synthesised 1-(2'-$C_{10}H_7$)-1,2-$C_2B_{10}H_{11}$, Figure 2–2.[1] When reacting decaborane with 1 and 2-(phenylethynyl)naphthalene, forming 1-(1'-$C_{10}H_7$)-2-(C_6H_5)-1,2-$C_2B_{10}H_{10}$ and 1-(2'-$C_{10}H_7$)-2-(C_6H_5)-1,2-$C_2B_{10}H_{10}$, yields are significantly decreased to 10 % and 42% respectively compared to the equivalent compounds without the phenyl group substituted at the other cage carbon.[1] These *ortho* carboranes with both phenyl and naphthalene groups can only be synthesised by the decaborane methodology as the copper-coupling reaction will only give the mono substituted product.

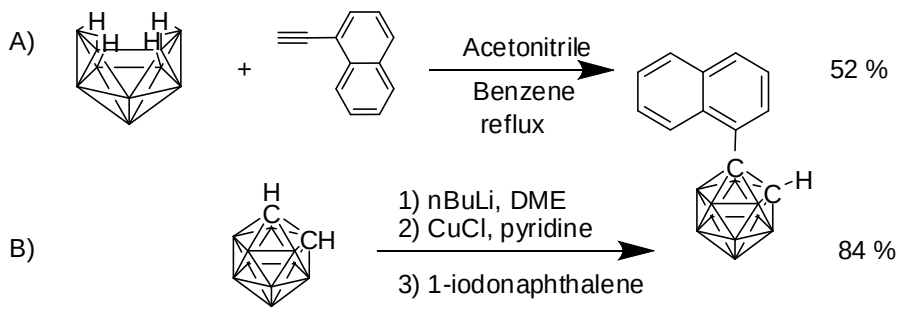

Figure 2–1:Synthesis of 1-(1'-$C_{10}H_7$)-1,2-$C_2B_{10}H_{11}$ A) by the decaborane method B) by the copper-coupling reaction.

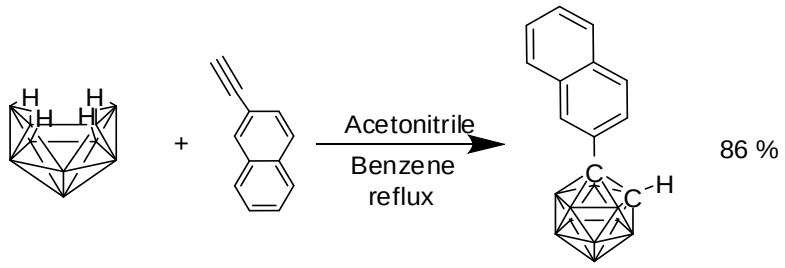

Figure 2–2: Synthesis of 1-(2'-$C_{10}H_7$)-1,2-$C_2B_{10}H_{11}$ by the decaborane method.

Eriksson et al. synthesised 2-(1'-$C_{10}H_7$)-1,12-$C_2B_{10}H_{11}$, with the naphthyl group on the boron atom, in a 93 % yield, Figure 2–3.[2] They used the Suzuki-Miyaura methodology. Fluoride ions from CsF act as an activating nucleophile and weak base, $Pd_2(dba)_3$ is a catalyst precursor and dppb is the bidentate ligand.[2]

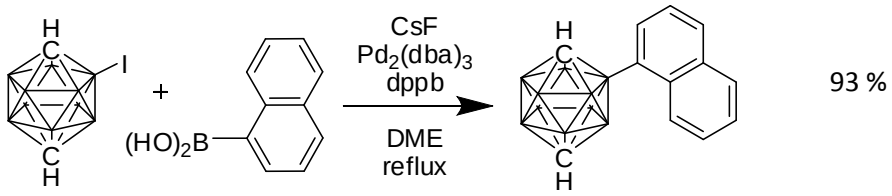

Figure 2–3: Synthesis of 2-(1'-$C_{10}H_7$)-1,12-$C_2B_{10}H_{11}$ by Suzuki-Miyaura methodology.

Kokado et al. have synthesised a similar molecule with a phenanthracenyl group, Figure 2–4, and noted its fluorescent emission at 517 nm.[3] In THF, emission was not observed but in a THF:H_2O 1:99 solution emission is seen. It is explained as being due to aggregation induced emission.

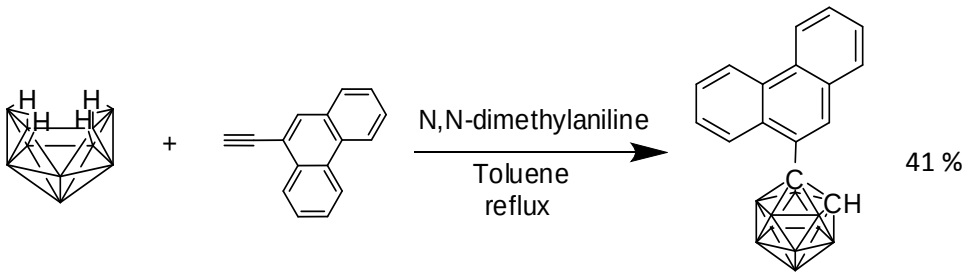

Figure 2–4: Synthesis of 1-(9'-$C_{14}H_9$)-1,2-$C_2B_{10}H_{11}$ by the decaborane method.

2.2 C-Naphthyl Carboranes

2.2.1 Syntheses

The *meta* and *para* mono and di-naphthyl carboranes were synthesised by a copper-coupling reaction, Figure 2–5 and Figure 2–6, as put forward by Fox et al.[4] By reacting the parent carborane in a 1:2 ratio with BuLi and CuCl followed by 1-iodonaphthalene both the mono and di-naphthyl carboranes were synthesised which were then separated and purified by column chromatography with hexane.

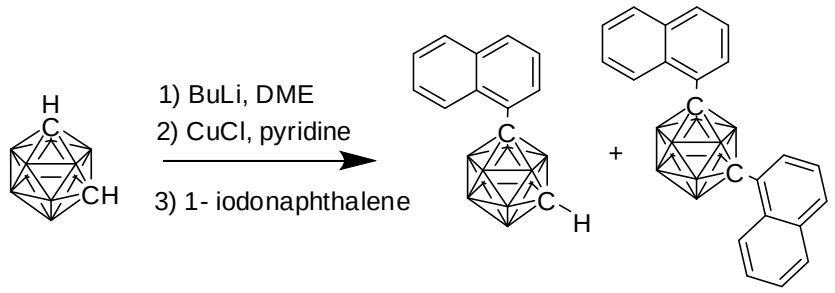

Figure 2–5: Synthesis of 1-(1'-$C_{10}H_7$)-1,7-$C_2B_{10}H_{11}$ and 1,7-(1'-$C_{10}H_7$)$_2$-1,7-$C_2B_{10}H_{10}$.

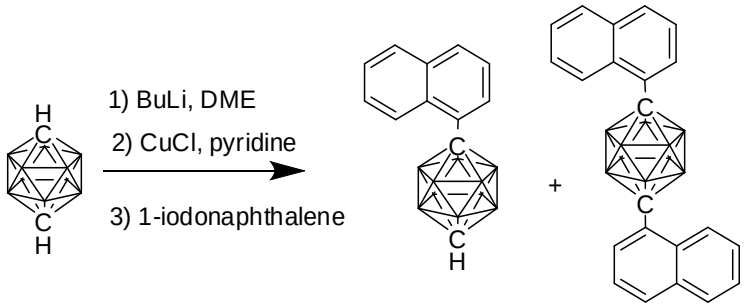

Figure 2–6: Synthesis of 1-(1'-$C_{10}H_7$)-1,12-$C_2B_{10}H_{11}$ and 1,12-(1'-$C_{10}H_7$)$_2$-1,12-$C_2B_{10}H_{10}$.

The copper-coupling reaction only gives the mono *ortho* carborane in appreciable yield, Figure 2–7. The mono *ortho* carborane can also be synthesised by reaction of decaborane with 1-ethynyl naphthalene, Figure 2–8, as reported by Ohta et al.[1]

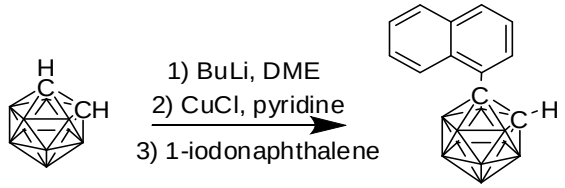

Figure 2–7: Synthesis of 1-(1'-$C_{10}H_7$)-1,2-$C_2B_{10}H_{11}$ by the copper-coupling method.

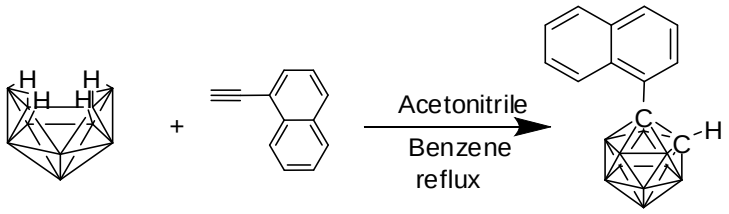

Figure 2–8: Synthesis of of 1-(1'-$C_{10}H_7$)-1,2-$C_2B_{10}H_{11}$ by the decaborane method.

In order to make the di-naphthyl *ortho* carborane we must employ an isomerisation reaction. By reducing either the *meta* or *para* di-naphthyl carboranes with sodium in THF and then reoxidising in air, the *ortho* isomer is formed.

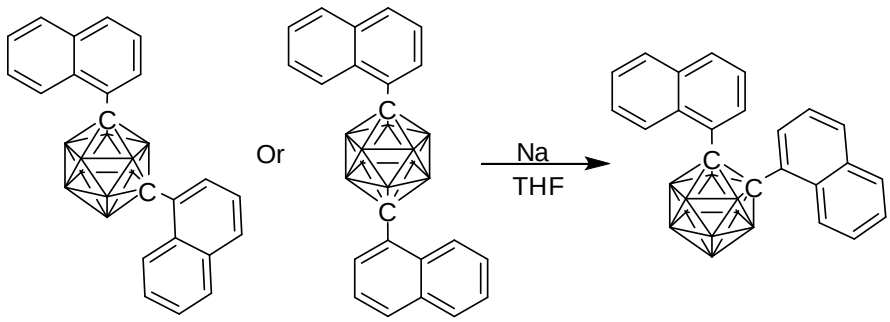

Figure 2–9: Synthesis of 1,2-(1'-$C_{10}H_7$)$_2$-1,2-$C_2B_{10}H_{10}$ by isomerisation from *meta* or *para* isomers.

2.2.2 X-ray crystallography

X-ray crystal structures have been obtained for five of the synthesised naphthyl carboranes, 1-(1'-$C_{10}H_7$)-1,2-$C_2B_{10}H_{11}$, 1,2-(1'-$C_{10}H_7$)$_2$-1,2-$C_2B_{10}H_{10}$, 1-(1'-$C_{10}H_7$)-1,7-$C_2B_{10}H_{11}$, 1-(1'-$C_{10}H_7$)-1,12-$C_2B_{10}H_{11}$ and 1,12-(1'-$C_{10}H_7$)$_2$-1,12-$C_2B_{10}H_{10}$. Molecular structures for these molecules are shown in Figures 2-10 to 2-12B. The crystal structure obtained of 1,12-(1'-$C_{10}H_7$)$_2$-1,12-$C_2B_{10}H_{10}$ however is of very poor quality and only the gross geometry is shown as a figure here. The cage C-C bond in 1,2-(1'-$C_{10}H_7$)$_2$-1,2-$C_2B_{10}H_{10}$ is longer than the cage C-C length in 1,2-Ph_2-1,2-$C_2B_{10}H_{10}$. This longer bond length can be explained by greater steric hindrances in this molecule between the two naphthyl groups. The corresponding monosubstituted 1-(1'-$C_{10}H_7$)-1,2-$C_2B_{10}H_{11}$ molecule, with a cage C1-C2 distance of 1.677 Å, has a smaller steric hindrance between the hydrogen atoms on C10 of the naphthalene and the B3 and B4 of the cage, and also on the other side of the molecule. The similar 1-Ph-1,2-$C_2B_{10}H_{11}$ has a smaller C-C bond length of 1.649 Å as there is less steric hindrance.[6] 1-(9'-$C_{14}H_9$)-1,2-$C_2B_{10}H_{11}$, Figure 2–4, has been found

to have a cage C-C bond length of the same order as that of 1-(1'-$C_{10}H_7$)-1,2-$C_2B_{10}H_{11}$.[3] This is to be expected as the steric hindrance in both of these cases is similar.

	Bond length (Å)		
	C(1) - C(2)	C(1) - C(1')	C(2) - C(1')
1,2-$C_2B_{10}H_{12}$ [5]	1.620(3)	-	-
1-Ph-1,2-$C_2B_{10}H_{11}$ [6]	1.649(2)	1.511(2)	-
1-(1'-$C_{10}H_7$)-1,2-$C_2B_{10}H_{11}$	1.677 (4)	1.516 (4)	-
1-(9'-$C_{14}H_9$)-1,2-$C_2B_{10}H_{11}$ [3]	1.6749(14)	1.5277(14)	-
1,2-Ph_2-1,2-$C_2B_{10}H_{10}$ [7]	1.726(2)	1.507(2)	1.505(2)
1,2-(1'-$C_{10}H_7$)$_2$-1,2-$C_2B_{10}H_{10}$	1.791(2)	1.517(2)	1.516(2)
1-(1'-$C_{10}H_7$)-1,7-$C_2B_{10}H_{11}$	-	1.5245 (19)	-
1-(1'-$C_{10}H_7$)-1,12-$C_2B_{10}H_{11}$	-	1.5330 (15) / 1.5280 (15)	-

Table 2–1: Selected bond lengths in naphthyl, phenyl and parent carboranes.

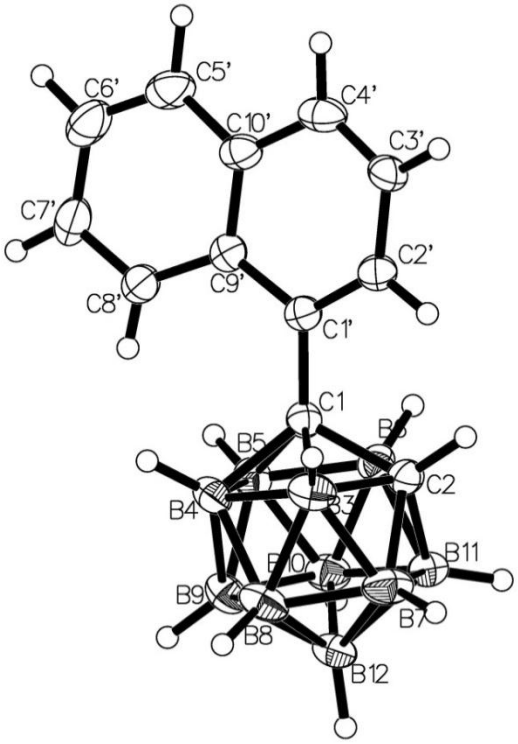

Figure 2–10: Molecular structure of 1-(1'-$C_{10}H_7$)-1,2-$C_2B_{10}H_{11}$.

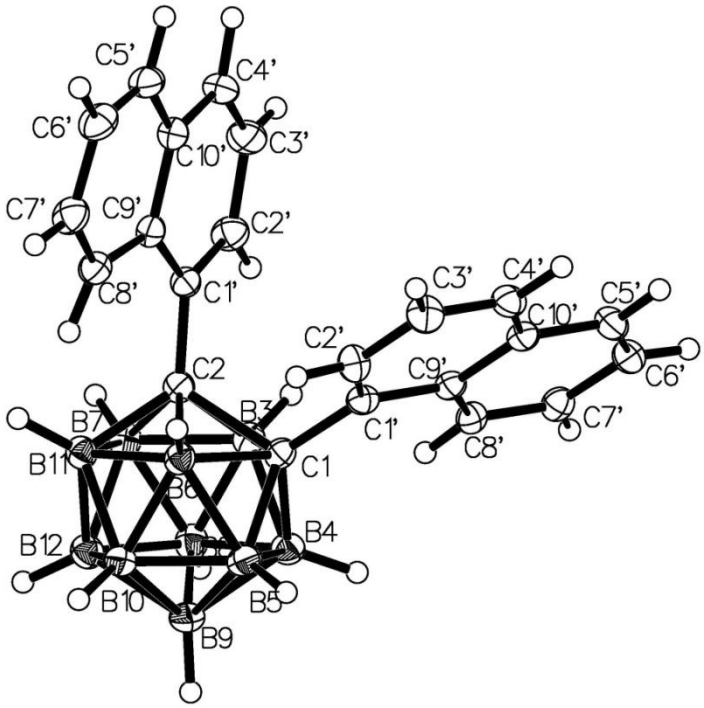

Figure 2–11: Molecular structure of 1,2-(1'-$C_{10}H_7$)$_2$-1,2-$C_2B_{10}H_{10}$.

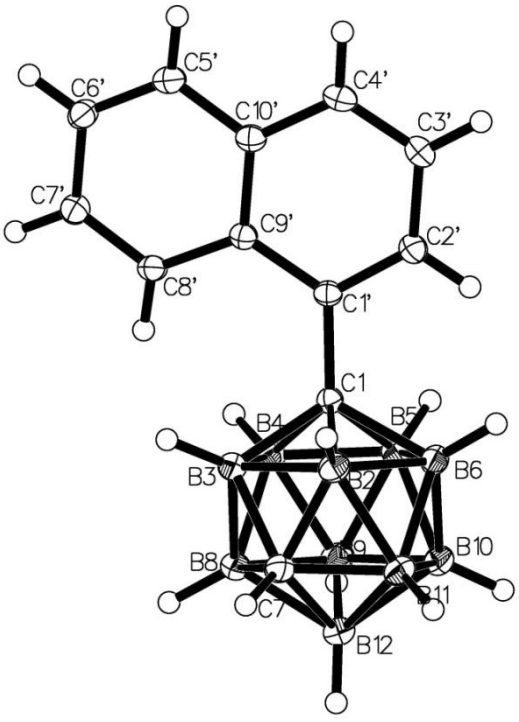

Figure 2–12A: Molecular structure of 1-(1'-$C_{10}H_7$)-1,7-$C_2B_{10}H_{11}$.

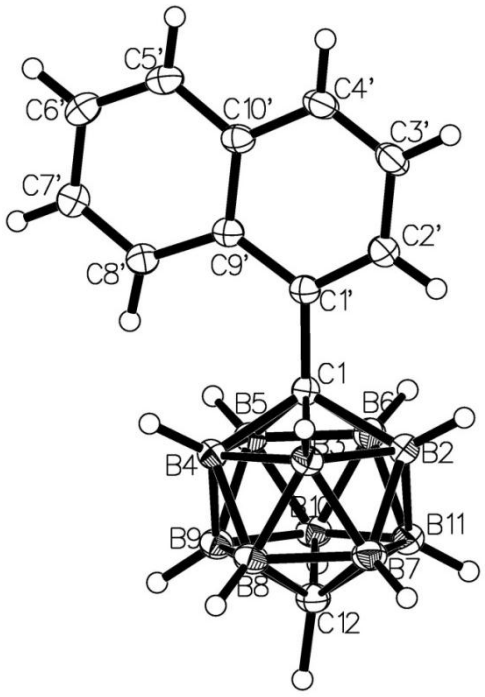

Figure 2–13A: Molecular structure of 1-(1'-$C_{10}H_7$)-1,12-$C_2B_{10}H_{11}$.

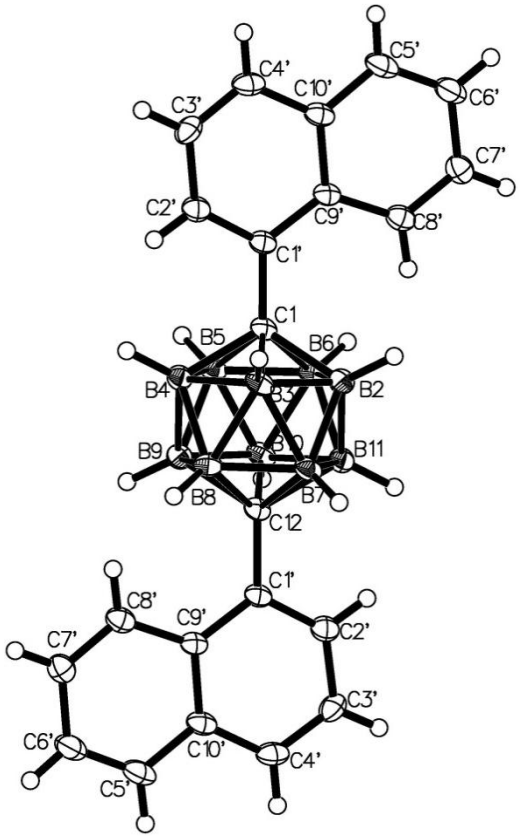

Figure 2–12B: Molecular structure of 1,12-(1'-$C_{10}H_7$)$_2$-1,12-$C_2B_{10}H_{10}$.

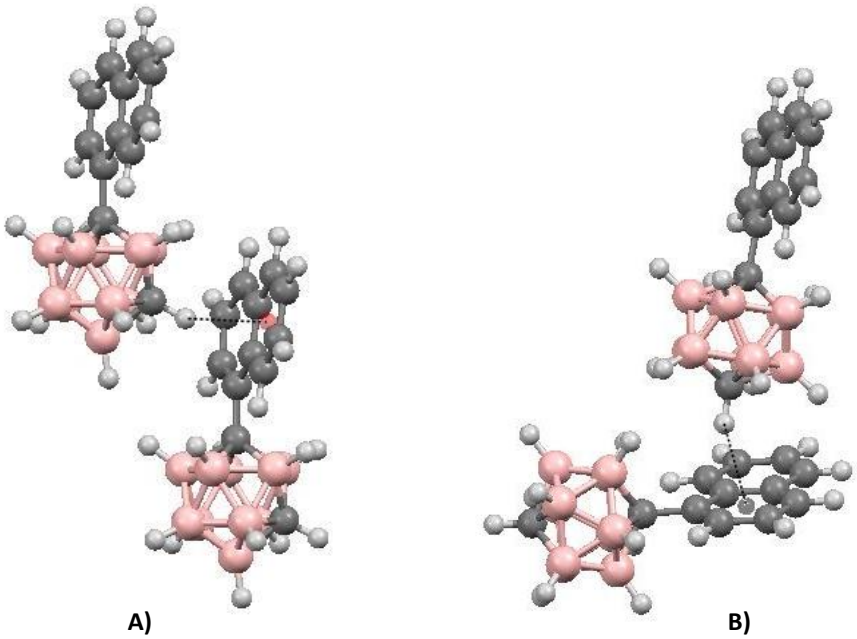

A) **B)**

Figure 2–13B: CH…X interactions between molecules in the crystalline state of A) 1-(1'-$C_{10}H_7$)-1,7-$C_2B_{10}H_{11}$ and B) 1-(1'-$C_{10}H_7$)-1,12-$C_2B_{10}H_{11}$.

The slightly acidic cage C-H hydrogen in the monosubstituted carboranes leads to weak interactions, where the distance between two atoms is less than the

sum of the van der Waals radii. These interactions between molecules in the crystalline state impart order on the structure.[8] *Ortho* mono naphthyl carborane is not seen to form cage CH…X interactions. BH…C (aromatic) and BH…B interactions are however observable, which may contribute to the ordering of this crystal structure. The *meta* and *para* naphthyl carboranes display cage CH…C (aromatic) distances of 2.687 and 2.620 Å respectively. BH…C (aromatic) interactions are also seen in each case.

2.2.2.1 Calculations

The calculated cage C-C bond lengths for *ortho* dinaphthyl and diphenyl carboranes are in line with the trends seen in the bond lengths observed, in that the cage C-C bond length is greater in the case of the *ortho* dinaphthyl than the *ortho* diphenyl carborane. *Ortho* dinaphthyl carborane has a calculated cage C-C bond length of 1.928 Å comparing to the observed C-C bond length of 1.791(2). The calculated *ortho* diphenyl carborane cage C- cage C bond length is in better agreement, at 1.749 Å, with the observed value of 1.726(2) Å.

Three optimised geometries were found for the ground state of o*rtho* mono naphthyl carborane, Figure 2–14. Figure 2–14 A) corresponds well to the observed geometry found by X-ray crystallography with a calculated cage C-C length of 1.673 Å and the naphthyl group running almost parallel to the cage C-C bond, with a dihedral C1-C2-C3-C4 angle of 0 °. Figure 2–14 B) shows an alternative geometry found for the molecule, also an energy minimum. In this case the cage C-C bond length is calculated to be greater at 1.692 Å and the naphthyl group is at an angle of 74 ° to the cage C-C bond. Conformation C), with a corresponding dihedral angle of 150 °, has a cage C- cage C bond length of 1.647 Å.

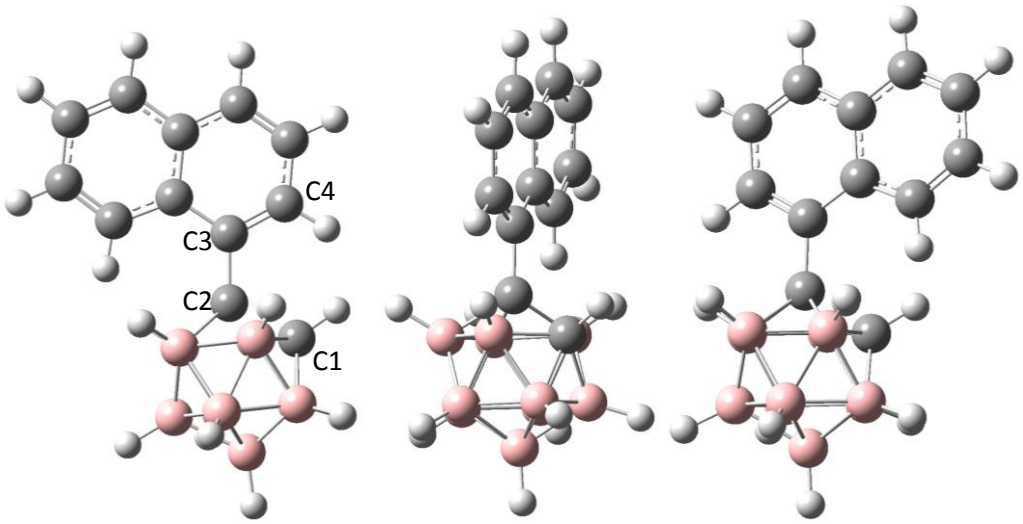

Figure 2–14: DFT calculated (B3LYP/6-31G*) optimised geometries found for 1-(1'-$C_{10}H_7$)-1,2-$C_2B_{10}H_{11}$.

In the ground state of the *ortho* naphthyl carborane there is free rotation around the C-C bond between the naphthyl group and the carborane cage. As can be seen in Figure 2–15, there is a small barrier to rotation between the minima geometries of 3 kcal/mol. In comparison, the similar *ortho* phenyl carborane has a barrier to rotation of less than 1 kcal/mol.

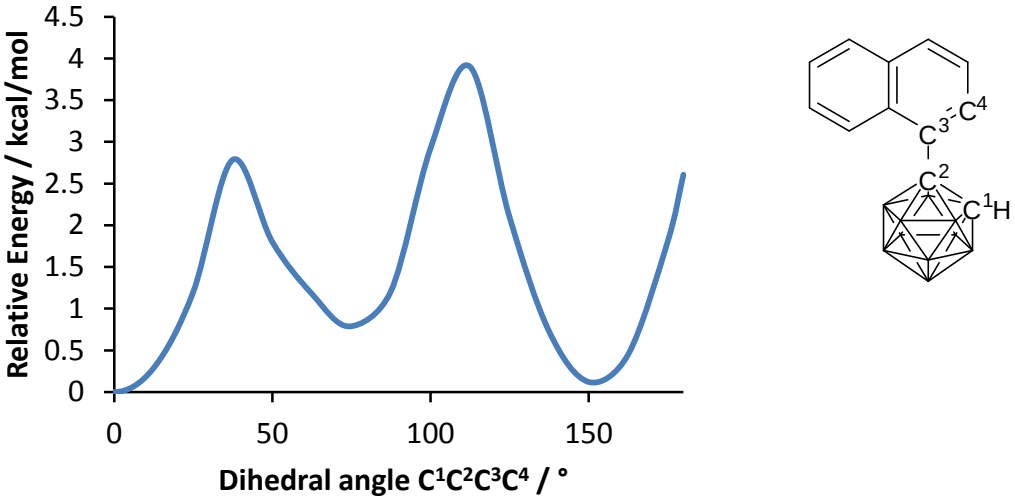

Figure 2–15: DFT calculated (B3LYP/6-31G*) barrier to rotation between naphthyl group and carborane cage.

The barrier to rotation in the *ortho* dinaphthyl carborane is much greater at 9.6 kcal/mol preventing rotation of the naphthyl groups at room temperature. The similar *ortho* diphenyl carborane, as expected, is found to display a smaller barrier to rotation of 4 kcal/mol.

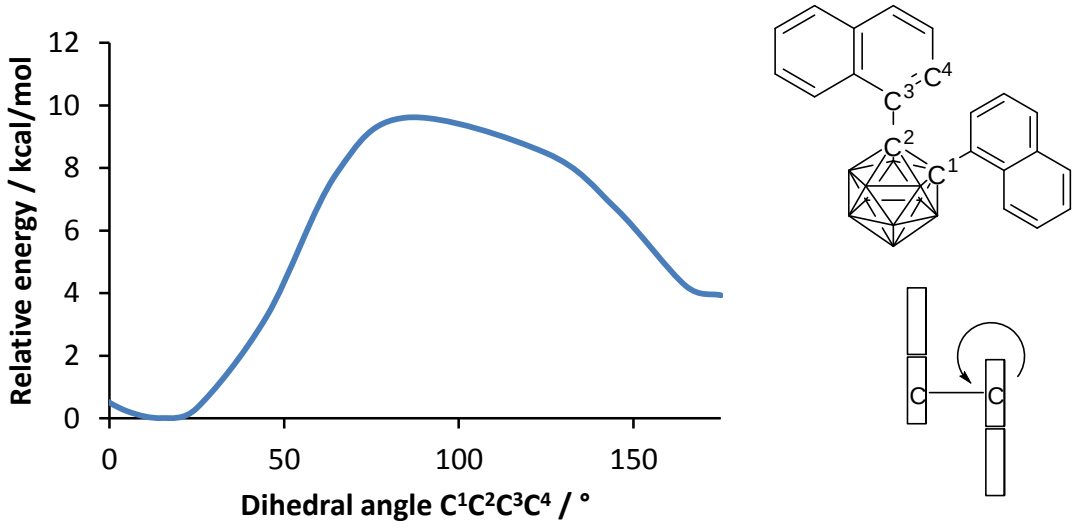

Figure 2–16: DFT calculated (B3LYP/6-31G*) barrier to rotation between a naphthyl group and carborane cage.

2.2.3 Fluorescence of the C-Naphthyl and C-Phenyl Carboranes

The naphthyl carboranes were found to exhibit fluorescence. Here we compare the naphthyl carboranes with the equivalent phenyl carboranes.

While the parent carboranes are not fluorescent in solution, naphthalene exhibits fluorescent emission at 322 nm, Figure 2–17. Benzene displays a weaker fluorescence emission, Figure 2–18, at 285 nm. Naphthyl groups are often chosen for use in molecules designed to be OLEDs in preference to phenyl groups as these molecules often have better photophysical properties.

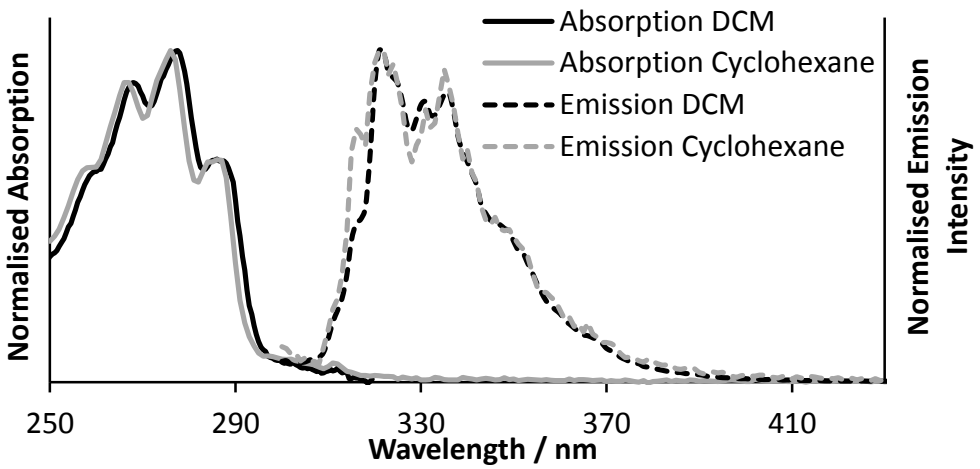

Figure 2–17: Absorption and Emission spectra of naphthalene in DCM and cyclohexane.

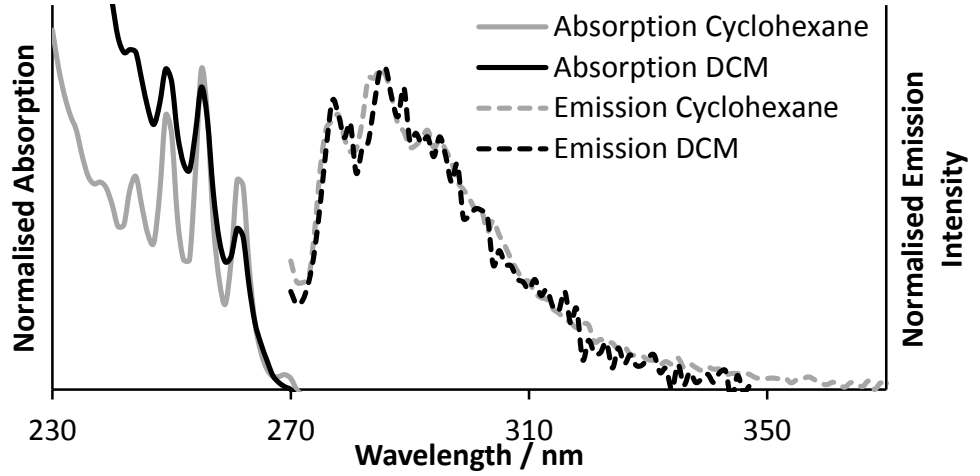

Figure 2–18: Absorption and Emission spectra of benzene in DCM and cyclohexane.

In Table 2–2 to Table 2–5 the absorption, emission and excitation data, collected in DCM and cyclohexane for the naphthyl and phenyl carboranes are summarised. Figure 2-21 to Figure 2–24 illustrate the absorption and emission spectra of the naphthyl carboranes.

Compound, in DCM	Absorption maximum			Emission wavelength	Excitation maximum		Excitation wavelength	High energy emission maximum		Low energy emission maximum		Stokes shift (cm^{-1})
	ε /$mol^{-1}dm^3cm^{-1}$	nm	cm^{-1}	nm	nm	cm^{-1}	nm	nm	cm^{-1}	nm	cm^{-1}	
1-(1'-$C_{10}H_7$)-1,2-$C_2B_{10}H_{11}$	8300	292	33200	545	322	31100	300	340	29400	548	18200	3800, 15000
1,2-(1'-$C_{10}H_7$)$_2$-1,2-$C_2B_{10}H_{10}$	10900	301	33200	580	309	32400	300	-	-	575	17400	15800
1-(1'-$C_{10}H_7$)-1,7-$C_2B_{10}H_{11}$	7000	290	34500	340	316	31700	292	331	30200	-	-	4300
1,7-(1'-$C_{10}H_7$)$_2$-1,7-$C_2B_{10}H_{10}$	14900	292	34200	345	291	34400	290	344	29100	-	-	5100
1 -(1'-$C_{10}H_7$)-1,12-$C_2B_{10}H_{11}$	2800	290	34500	340	320	31300	292	342	29200	-	-	5300
1,12-(1'-$C_{10}H_7$)$_2$-1,12-$C_2B_{10}H_{10}$	10400	293	34200	345	291	34400	290	344	29100	-	-	5100

Table 2–2: Absorption, emission and excitation data for the naphthyl carboranes in DCM.

Compound, in cyclohexane	Absorption maximum			Emission wavelength	Excitation maximum		Excitation wavelength	High energy emission maximum		Low energy emission maximum		Stokes shift (cm^{-1})
	ε /$mol^{-1}dm^3cm^{-1}$	nm	cm^{-1}	nm	nm	cm^{-1}	nm	nm	cm^{-1}	nm	cm^{-1}	
1-(1'-$C_{10}H_7$)-1,2-$C_2B_{10}H_{11}$	15100	299	33400	340	309	32400	292	330	30300	-	-	3100
1,2-(1'-$C_{10}H_7$)$_2$-1,2-$C_2B_{10}H_{10}$	11800	299	33500	350	299	33400	292	-	-	528	18900	14600
1-(1'-$C_{10}H_7$)-1,7-$C_2B_{10}H_{11}$	7200	289	34600	340	300	33300	300	332	30100	-	-	4500
1,7-(1'-$C_{10}H_7$)$_2$-1,7-$C_2B_{10}H_{10}$	19500	290	34500	340	295	33900	300	332	30100	-	-	4400
1 -(1'-$C_{10}H_7$)-1,12-$C_2B_{10}H_{11}$	5800	290	34500	340	300	33300	300	331	30200	-	-	4300
1,12-(1'-$C_{10}H_7$)$_2$-1,12-$C_2B_{10}H_{10}$	34200	291	34400	330	302	33100	300	331	30200	-	-	4200

Table 2–3: Absorption, emission and excitation data for the naphthyl carboranes in cyclohexane.

Compound, in DCM	Absorption maximum			Emission wavelength	Excitation maximum		Excitation wavelength	High energy emission maximum		Low energy emission maximum		Stokes shift (cm^{-1})
	ε /$mol^{-1}dm^3cm^{-1}$	nm	cm^{-1}	nm	nm	cm^{-1}	nm	nm	cm^{-1}	nm	cm^{-1}	
1-(C_6H_5)-1,2-$C_2B_{10}H_{11}$	200	265	37700	-	-	-	-	-	-	-	-	-
1,2-(C_6H_5)$_2$-1,2-$C_2B_{10}H_{10}$	500	267	37500	-	-	-	-	-	-	-	-	-
1-(C_6H_5) -1,7-$C_2B_{10}H_{11}$	300	266	37600	229	259	38600	262	285	35100	-	-	2500
1,7-(C_6H_5)$_2$-1,7-$C_2B_{10}H_{10}$	600	260	38500	292	260	38500	260	286	35000	-	-	3500
1 -(C_6H_5)-1,12-$C_2B_{10}H_{11}$	200	266	37600	292	259	38600	260	294	34000	-	-	3600
1,12-(C_6H_5)$_2$-1,12-$C_2B_{10}H_{10}$	800	266	37600	292	260	38500	260	285	35100	-	-	2500

Table 2–4:Absorption, emission and excitation data for the phenyl carboranes in DCM.

Compound, in cyclohexane	Absorption maximum			Emission wavelength	Excitation maximum		Excitation wavelength	High energy emission maximum		Low energy emission maximum		Stokes shift (cm^{-1})
	ε /$mol^{-1}dm^3cm^{-1}$	nm	cm^{-1}	nm	nm	cm^{-1}	nm	nm	cm^{-1}	nm	cm^{-1}	
1-(C_6H_5)-1,2-$C_2B_{10}H_{11}$	1300	265	37700	-	-	-	-	-	-	-	-	-
1,2-(C_6H_5)$_2$-1,2-$C_2B_{10}H_{10}$	1100	267	37500	-	-	-	-	-	-	-	-	-
1-(C_6H_5) -1,7-$C_2B_{10}H_{11}$	200	260	38500	290	259	38600	260	285	35100	-	-	3400
1,7-(C_6H_5)$_2$-1,7-$C_2B_{10}H_{10}$	300	260	38500	292	259	38600	260	287	34800	-	-	3700
1 -(C_6H_5)-1,12-$C_2B_{10}H_{11}$	200	260	38500	292	254	39400	260	286	35000	-	-	3500
1,12-(C_6H_5)$_2$-1,12-$C_2B_{10}H_{10}$	400	260	38500	292	259	38600	260	286	35000	-	-	3500

Table 2–5: Absorption, emission and excitation data for the phenyl carboranes in cyclohexane.

The fluorescence emission of the *meta* and *para* naphthyl isomers are very similar with maxima between 331 and 344 nm. In cyclohexane there are small solvatochromic shifts, of 6 – 13 nm, to lower wavelengths and higher energies. This effect is larger in the dinaphthyl *meta* and *para* isomers than in the mono. The small Stokes shift is only ~300 cm^{-1} greater than for the parent naphthalene. The small bathochromic shift can be attributed to the electron withdrawing nature of the carborane cage.

The spectra obtained for the *meta* and *para* phenyl carboranes, as with the related naphthyl carboranes, are very similar with maxima ranging from 285 - 294 nm. These maxima are slightly higher in energy than for their naphthyl counterparts which exhibit maxima ranging from 331 - 342 nm.

Ortho phenyl carboranes were not seen to exhibit fluorescence. The Stokes shifts observed for *ortho* dinaphthyl carborane in DCM and cyclohexane are much greater than that of the *meta* and *para* isomers.

Ortho mono naphthyl carborane is unusual as it exhibits two fluorescence bands, Figure 2–24. In DCM the emission maximum is a low energy band with a large Stokes shift. Also observed, however, is a high energy band, with a small Stokes shift, of the same order as for the *meta* and *para* isomers. In cyclohexane, only the higher energy band is observed. This is a striking contrast to the dinaphthyl *ortho* carborane, which maintains the emission with the high Stokes shift in cyclohexane. On varying the solvent polarity the low energy band is seen to undergo a solvatochromic effect, Figure 2–26. When in the most polar solvent, MeCN, the emission is at lower energy than in the least polar solvent, Table 2–6. The relative intensities of the high and low energy emission bands also change with varying solvent polarity, Figure 2–25. In cyclohexane only the high energy band is seen and in acetonitrile only the low energy band is seen. In a 50:50 DCM:cyclohexane solution the two emission bands are at approximately the same intensity.

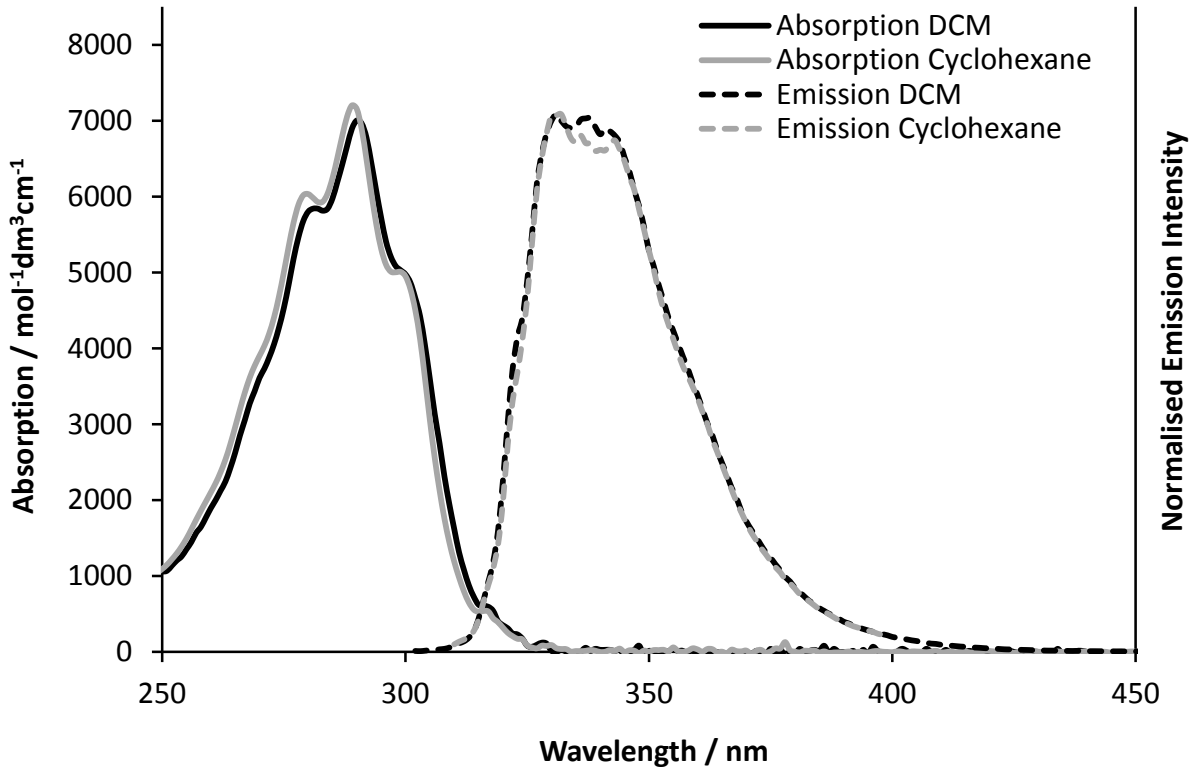

Figure 2–19: Absorption and emission spectra of 1-(1'-$C_{10}H_7$)-1,7-$C_2B_{10}H_{11}$ in DCM and cyclohexane.

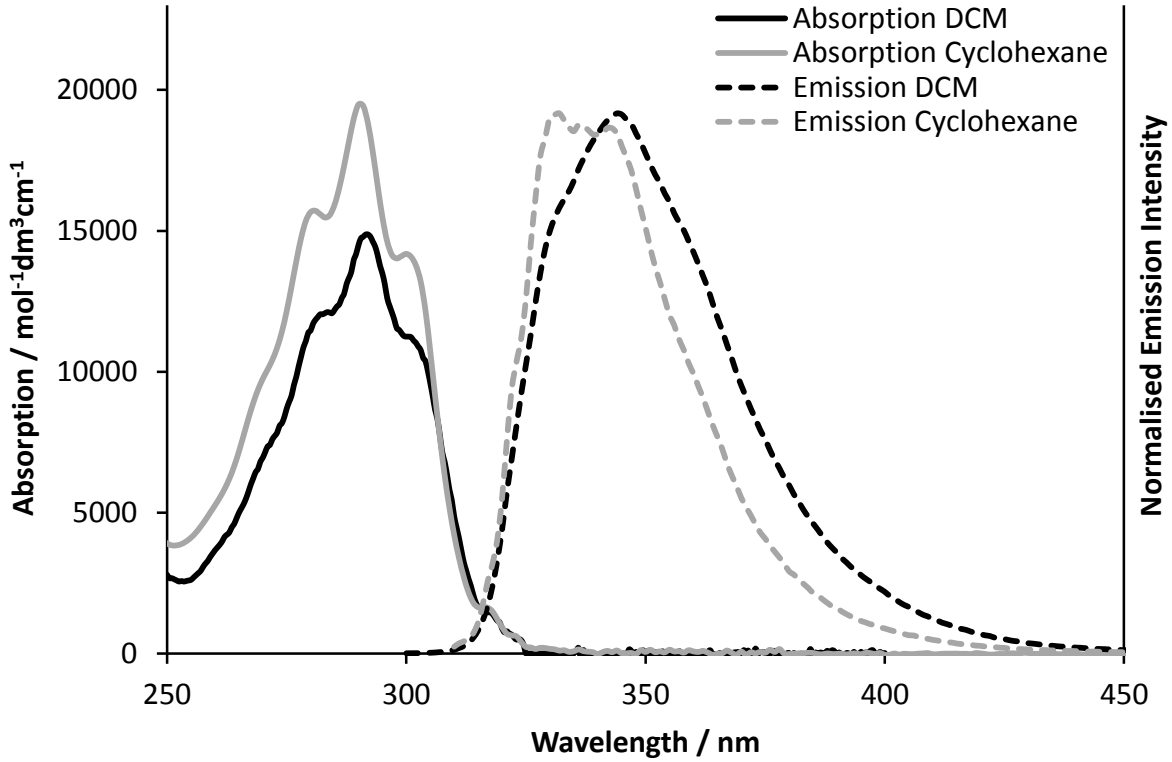

Figure 2–20: Absorption and emission spectra of 1,7-(1'-$C_{10}H_7$)$_2$-1,7-$C_2B_{10}H_{10}$ in DCM and cyclohexane.

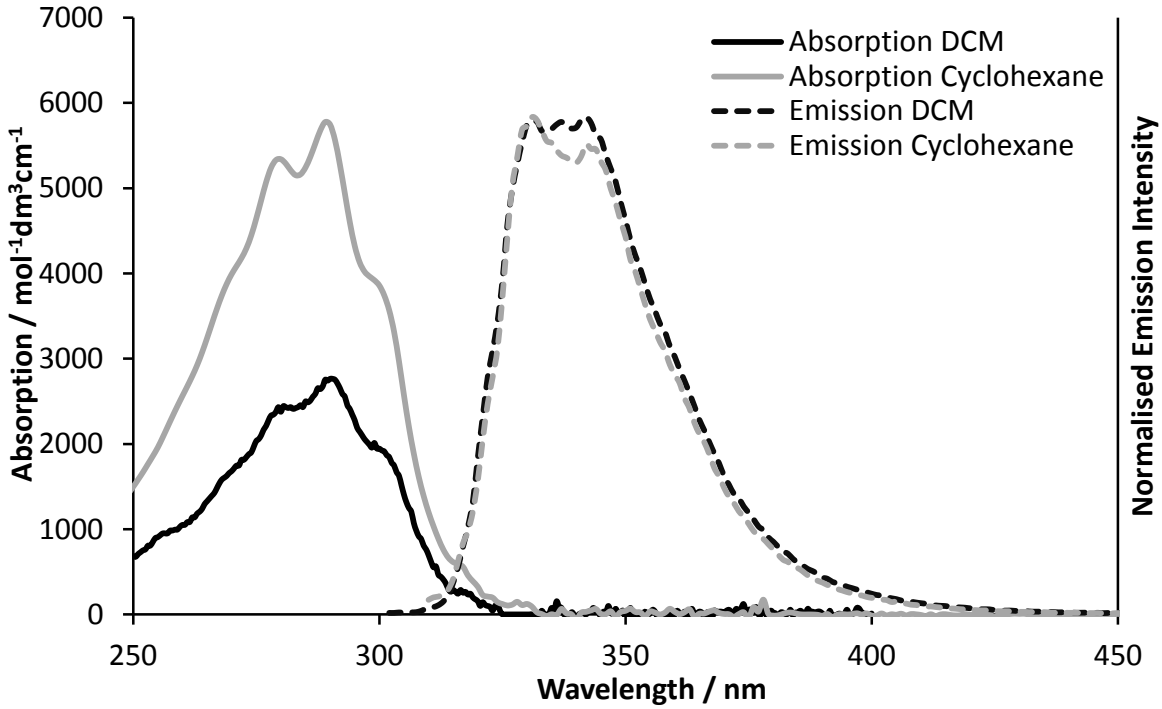

Figure 2–21: Absorption and emission spectra of 1-(1'-$C_{10}H_7$)-1,12-$C_2B_{10}H_{11}$ in DCM and cyclohexane.

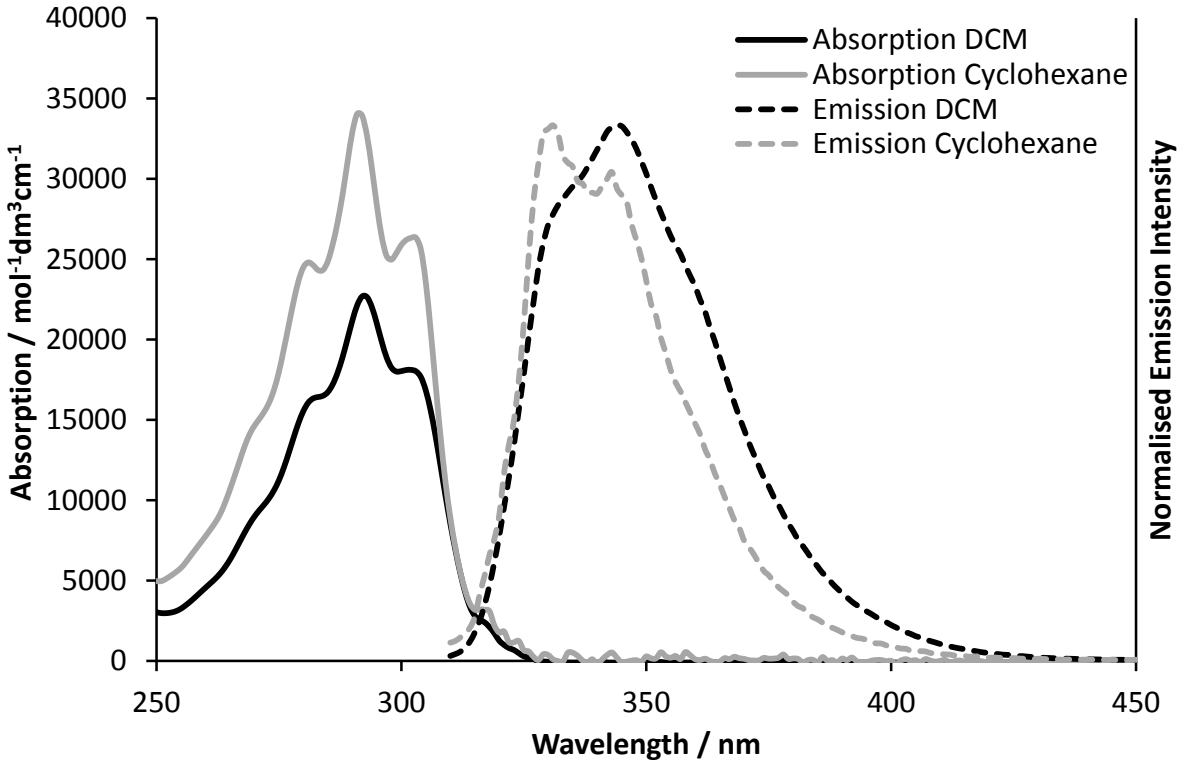

Figure 2–22: Absorption and emission spectra of 1,12-(1'-$C_{10}H_7$)$_2$-1,12-$C_2B_{10}H_{10}$ in DCM and cyclohexane.

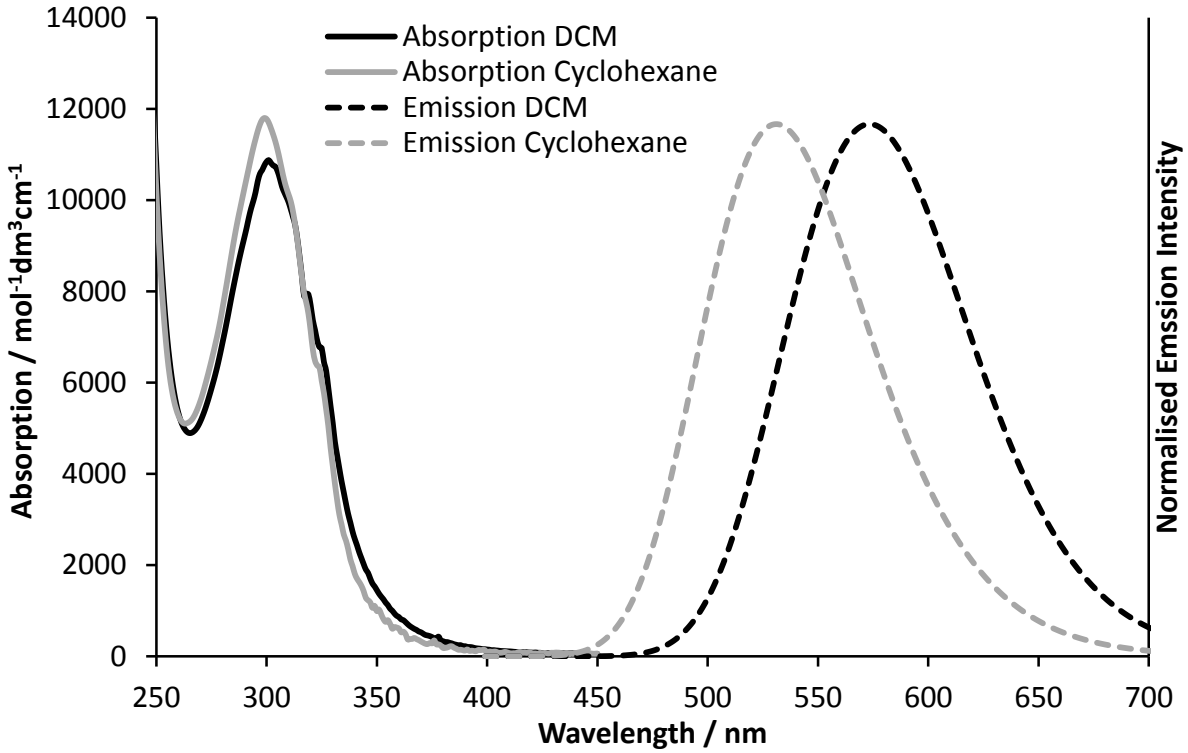

Figure 2–23: Absorption and emission spectra of 1,2-(1'-$C_{10}H_7$)$_2$-1,2-$C_2B_{10}H_{10}$ in DCM and cyclohexane.

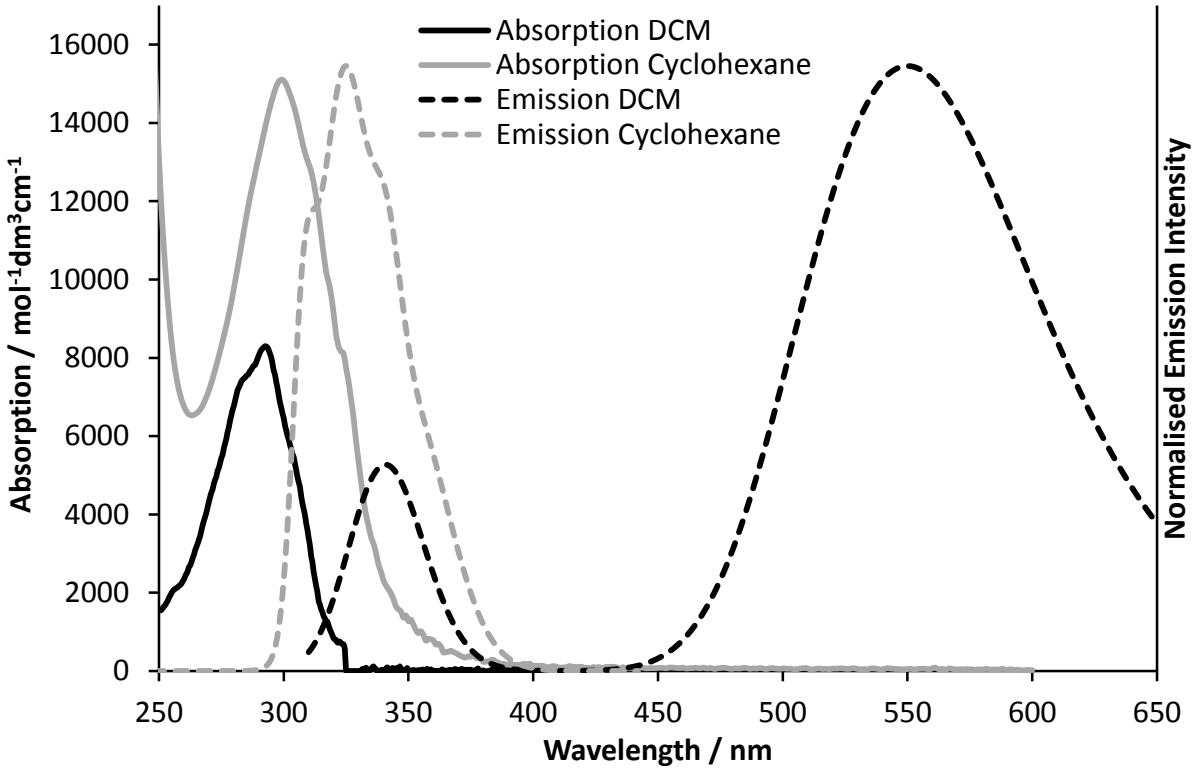

Figure 2–24: Absorption and emission spectra of 1-(1'-$C_{10}H_7$)-1,2-$C_2B_{10}H_{11}$ in DCM and cyclohexane.

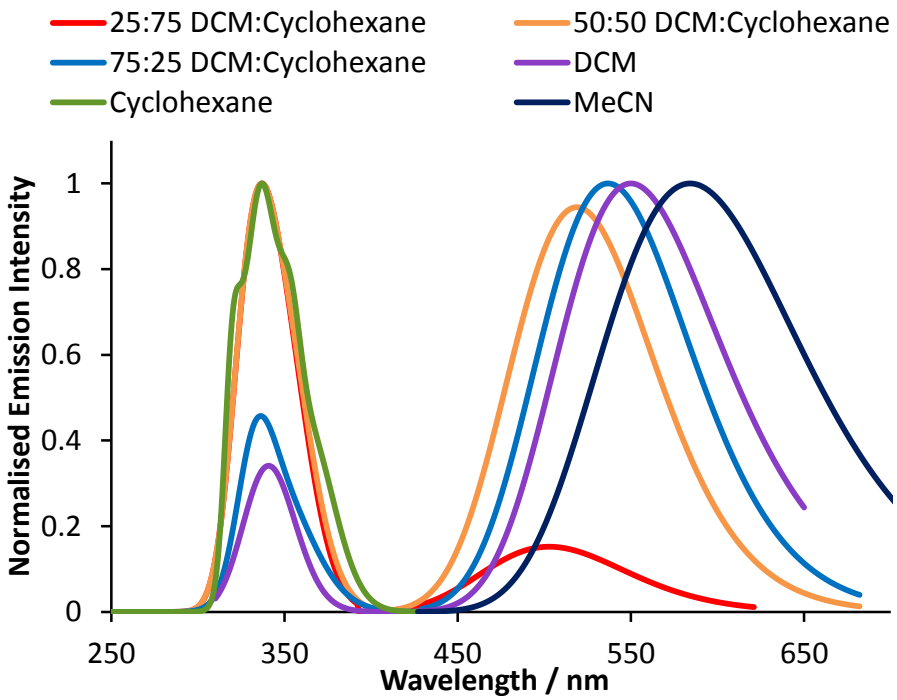

Figure 2–25: Relative emission intensities of 1-(1'-$C_{10}H_7$)-1,2-$C_2B_{10}H_{11}$ in different solvent polarities.

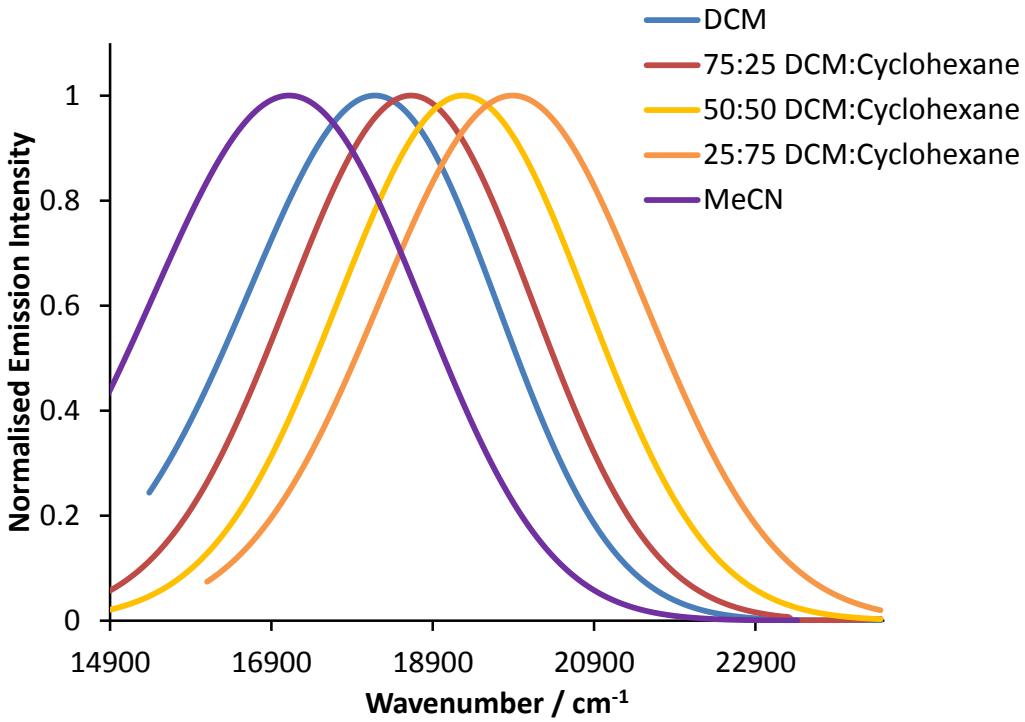

Figure 2–26: Solvatochromic shift of the low energy emission band of 1-(1'-$C_{10}H_7$)-1,2-$C_2B_{10}H_{11}$ in different solvents.

Solvent	Emission Maximum	
	nm	cm^{-1}
MeCN	584	17123
DCM	550	18181
75:25 DCM:Cyclohexane	537	18621
50:50 DCM:Cyclohexane	519	19267
25:75 DCM:Cyclohexane	503	19880

Table 2–6: The change in the low energy emission maximum of 1-(1'-$C_{10}H_7$)-1,2-$C_2B_{10}H_{11}$ on varying solvent polarity.

2.2.3.1 Calculations

Ultraviolet-visible (UV-Vis) spectroscopy looks at the ground state-excited state transition, whilst fluorescence looks at the excited state to ground state transition. Figure 2–27 shows the calculated HOMO LUMO energy gaps of the parent molecules benzene, naphthalene, anthracene and *ortho*, *meta* and *para* carboranes. The trends illustrated in this set of molecules help us to predict relative HOMO LUMO gaps of phenyl, naphthyl and anthracyl carboranes. Benzene is found to have a larger HOMO LUMO gap than naphthalene. As such phenyl carboranes will have larger HOMO LUMO energy gaps than naphthyl carboranes. This explains why phenyl carboranes have higher energy absorption maxima than the naphthyl carboranes. Likewise, as naphthalene has a greater HOMO LUMO gap than anthracene, we would expect naphthyl carboranes to have a larger HOMO LUMO gap than that of anthracyl carboranes. *Ortho* carboranes have lower energy absorptions than *meta* and *para* carboranes due to the smaller HOMO LUMO energy gap of the *ortho* carborane cage. We would expect smaller variations between the HOMO LUMO energy gaps on going from the *ortho* to *meta* and *para* naphthyl carboranes than in varying the group from phenyl to naphthyl and anthracyl.

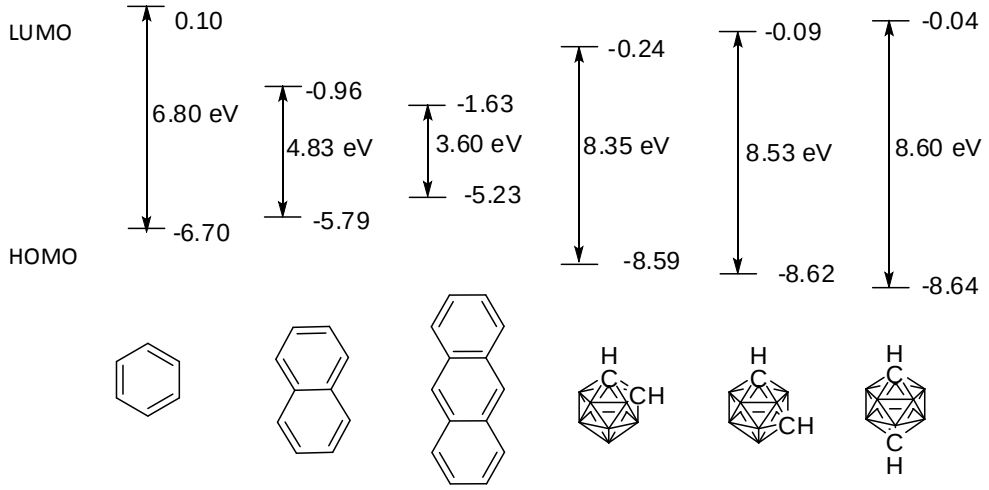

Figure 2–27: DFT calculated (B3LYP/6-31G*) HOMO LUMO energy gaps for parent molecules, benzene, naphthalene, anthracene and *ortho, meta* and *para* carboranes.

The calculated HOMO LUMO energy gaps of the naphthyl carboranes are in line with the observed UV-Vis maxima, Figure 2–28. 1,2-(1'-$C_{10}H_7$)$_2$-1,2-$C_2B_{10}H_{10}$ has the lowest HOMO LUMO energy gap and accordingly has the lowest energy UV-Vis absorption maximum observed.

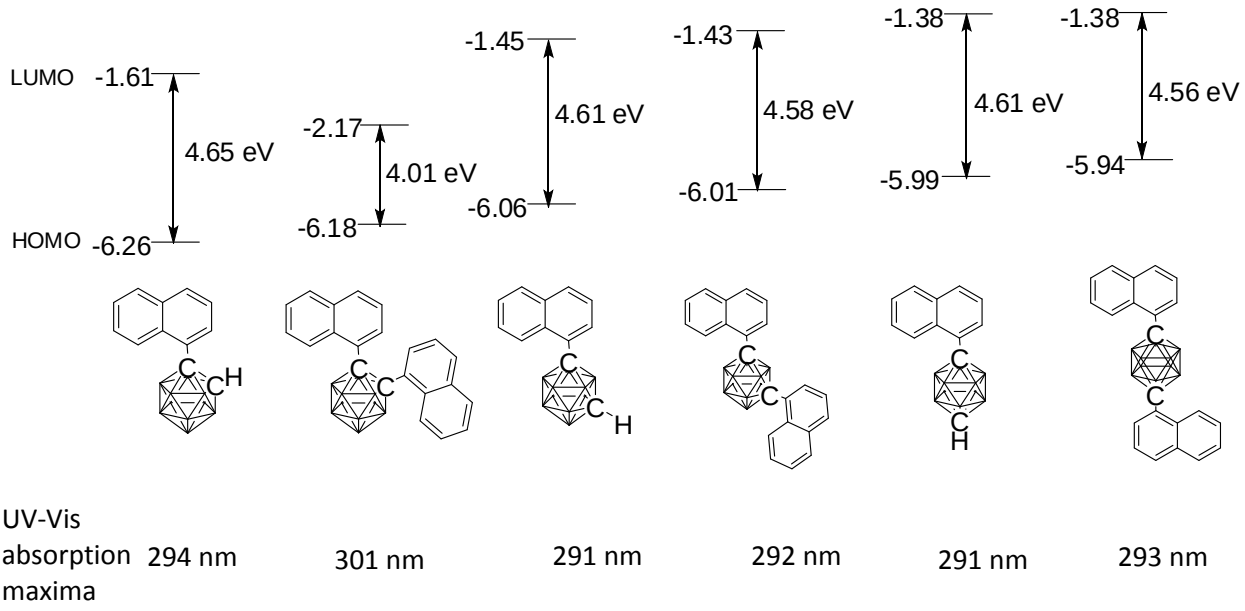

Figure 2–28: DFT calculated (B3LYP/6-31G*) HOMO LUMO energy gaps for the naphthyl carboranes and the corresponding observed maxima in the UV-Vis spectra in DCM.

As can be seen in Figure 2–29, on moving from the HOMO to the LUMO there is an increase in electron density on the carborane cage. It is clear therefore that the carborane cage is involved in the HOMO to LUMO transitions. This increase is particularly striking in the *ortho* di-naphthyl carborane which has a corresponding elongated cage C-C bond in the excited LUMO state. The molecular orbital contributions for all other naphthyl carboranes are largely the same.

O*rtho* di-naphthyl carborane only exhibits one emission band and accordingly one excited state geometry was located, Figure 2–30B), with the naphthyl groups running parallel. The predicted emission maximum of 499 nm is in good agreement with that observed, with a large Stokes shift. This geometry has a much smaller calculated energy gap on relaxation compared to the *meta* and *para* carboranes, accounting for the difference in Stokes shift in the isomers. We can see that this optimised geometry has an elongated carborane cage C-C bond length. With this elongation, we see the carborane cage opening up and correspondingly we see more electron density on the carborane cage in the excited state than for the more closed *meta* and *para* carboranes. The molecular orbitals as pictured for the *para* di-naphthyl carborane in Figure 2–30A) are typical for the *meta* and *para* naphthyl carboranes.

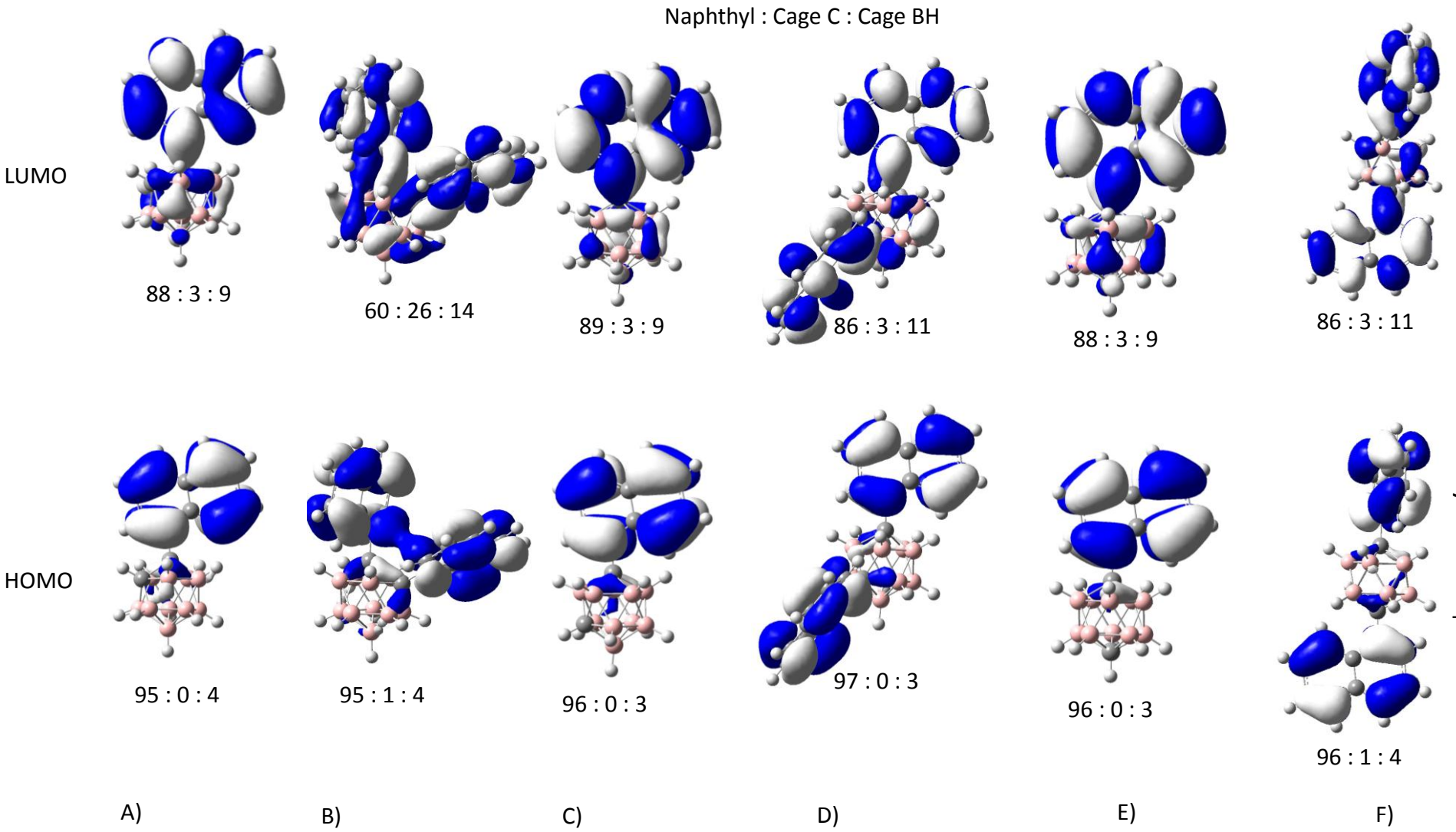

Figure 2–29: DFT calculated (B3LYP/6-31G*) molecular orbital contributions to the HOMO and LUMO of:

A) 1-(1'-$C_{10}H_7$) -1,2-$C_2B_{10}H_{11}$, B) 1,2-(1'-$C_{10}H_7$)$_2$-1,2-$C_2B_{10}H_{10}$, C) 1-(1'-$C_{10}H_7$) -1,7-$C_2B_{10}H_{11}$, D) 1,7-(1'-$C_{10}H_7$)$_2$-1,7-$C_2B_{10}H_{10}$, E) 1-(1'-$C_{10}H_7$) -1,12-$C_2B_{10}H_{11}$, F) 1,2-(1'-$C_{10}H_7$)$_2$-1,12-$C_2B_{10}H_{10}$

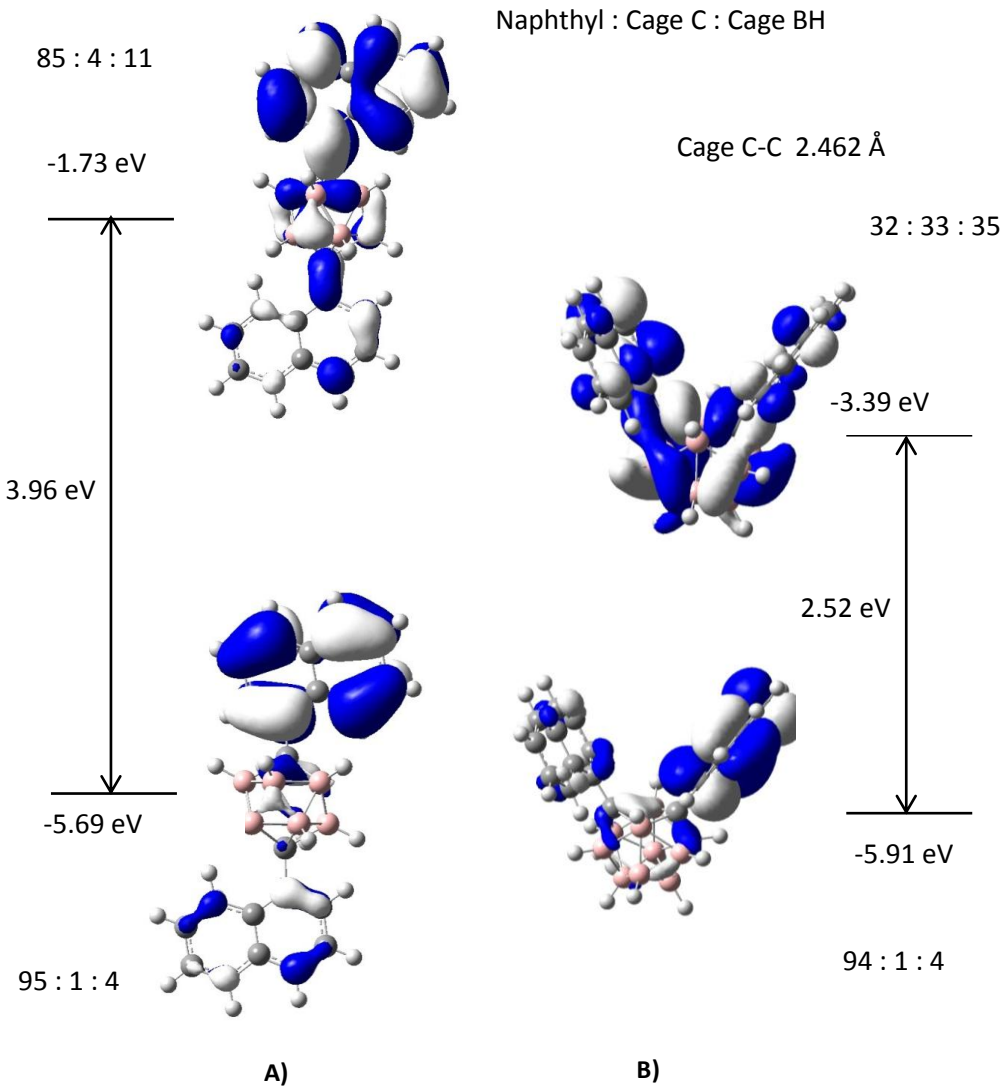

Figure 2–30: DFT calculated (B3LYP/6-31G*) HOMO and LUMO for the S_1 excited state of A) *para* di-naphthyl carborane, B) *ortho* di-naphthyl carborane.

Ortho mono naphthyl carborane displays two emission bands. Calculations suggest that the two different emission energies observed are due to two different excited state geometries, Figure 2–31. Free rotation in the ground state of the naphthyl group relative to the cage allows for the molecule to reach these conformations in the excited state, Figure 2–15. Conformation 1 is calculated to emit at 540 nm, while conformation 2 has a calculated emission of 356 nm. The higher energy band observed corresponds to the naphthyl group being parallel to the cage C-C bond, Figure 2–31 B). The lower energy band is due to the conformation when the naphthyl group is at right angles to the cage C-C bond,

Figure 2–31 A). In this case the cage C-C bond distance is elongated with the cage opening up. The excited state of conformation 1 has greater electron density on the carborane cage than in the closed cage of conformation 2. As seen in Figure 2–32, conformation 1, with the more open conformation shows a smaller energy gap on relaxation than conformation 2. This accounts for the difference in the Stokes shifts seen for the two emission bands.

As seen in Figure 2–24, these two excited state geometries are affected greatly by the solvent polarity. Calculations of the dipole moment in these two excited state geometries are in line with this observation. In the case of conformation 1 the calculated dipole is 13.9 Debye. For conformation 2 the calculated dipole is less, as expected, at 7.2 Debye. The more polar conformation 1 is indeed dominant in the more polar DCM. In cyclohexane, with a low polarity, the less polar conformation 2 is observable.

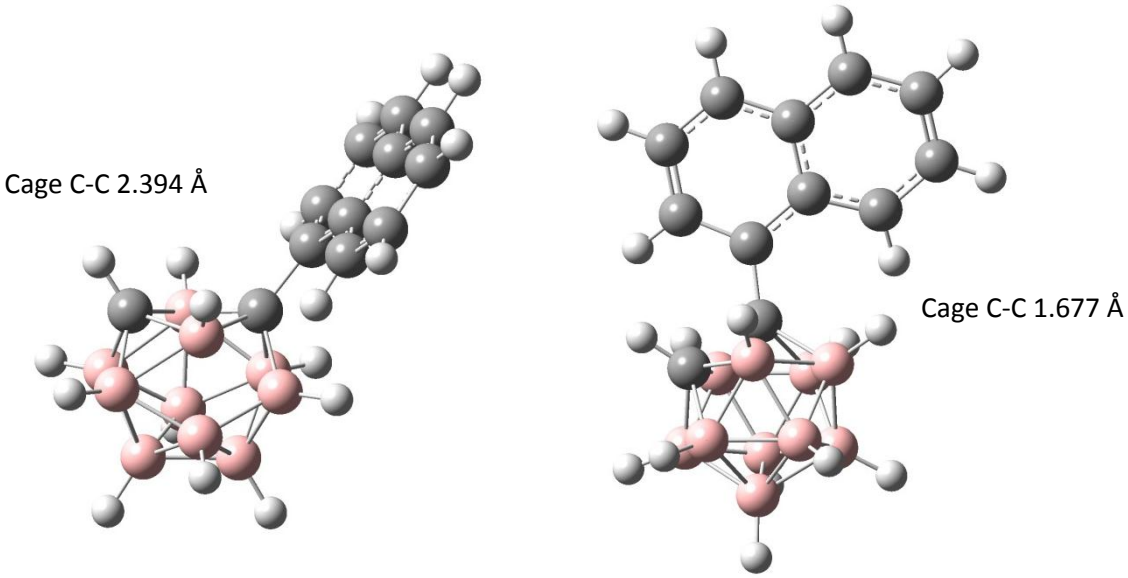

Figure 2–31: S_1 excited state optimised geometries obtained from DFT calculations (B3LYP/6-31G*)

A) Conformation 1 **B) Conformation 2**

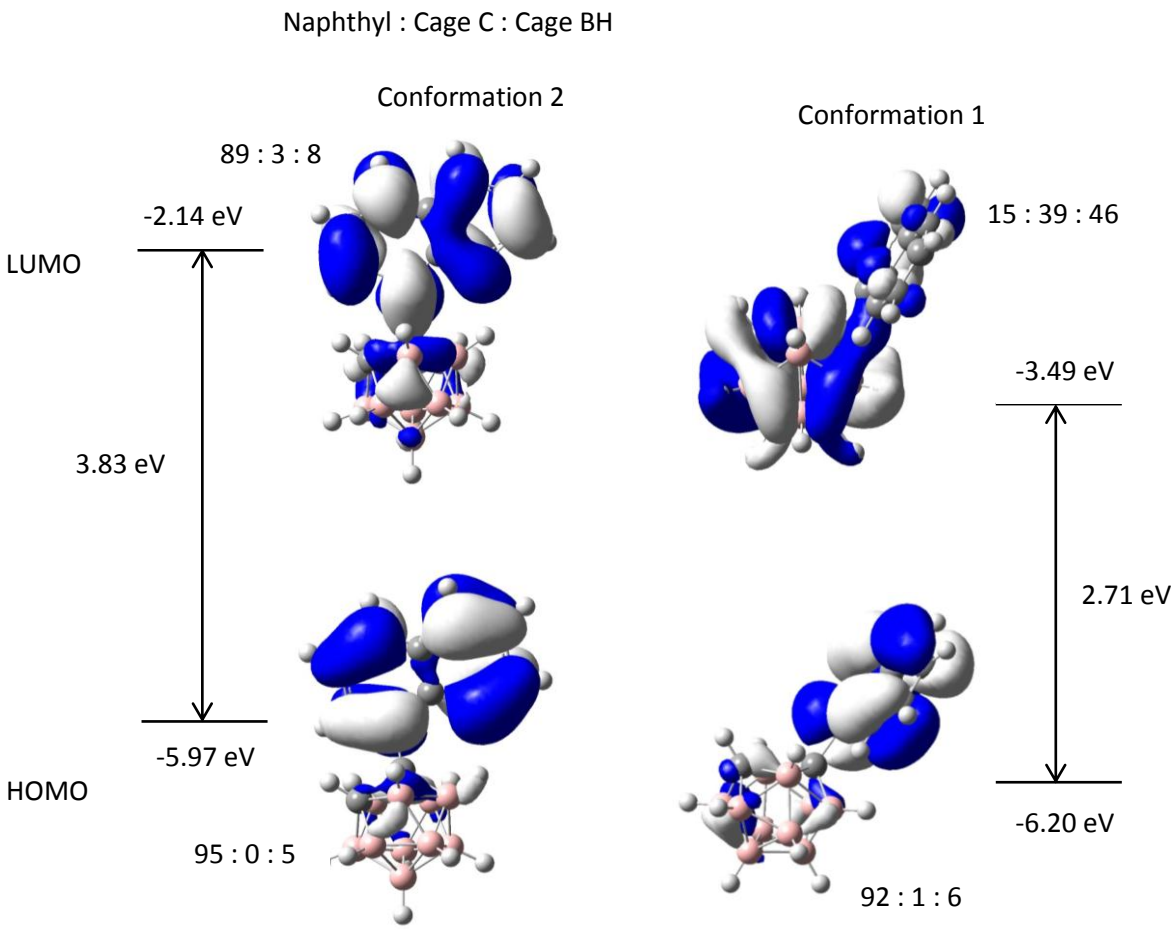

Figure 2–32: DFT calculated (B3LYP/6-31G*) HOMO and LUMO for the S_1 excited states, conformation 1 and conformation 2, of *ortho* naphthyl carborane.

2.3 C-Anthracyl Carboranes

Having seen that the naphthyl carboranes exhibited fluorescence the analogous anthracyl carboranes were investigated. Such species are expected to display fluorescence emission at lower energies.

2.3.1 Syntheses

There was a great deal of difficulty in attempting to synthesise 9-iodoanthracene in good yield. Several methods were attempted. One method attempted was the lithiation of anthracene with BuLi followed by addition of iodine. This was not successful. Lithiation of bromoanthracene followed by addition of iodine led to iodoanthracene in low yields.[9] As bromoanthracene is an expensive starting material compared to anthracene, a reaction that used anthracene as the starting material is to be desired. The reaction of anthracene with iodine in the presence of alumina supported copper (II) sulfate, again, gave small yields of iodoanthracene.[10] Anthracene was also reacted with iodine in the presence of copper(II) fluoride. This reaction yielded a large amount of unreacted anthracene with low yields of iodoanthracene and anthraquinone.

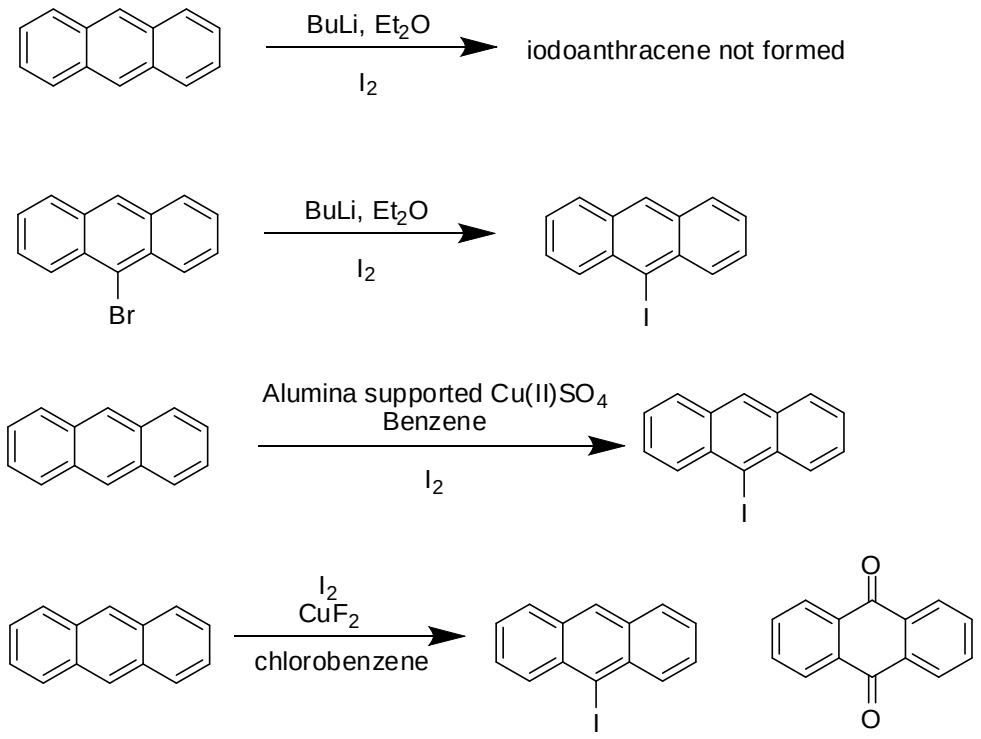

Figure 2–33: Methods by which the synthesis of 9-iodoanthracene was attempted.

A reaction mixture of anthracene, iodoanthracene and anthraquinone was used to carry out a small scale copper-coupling reaction with *meta* carborane. This trial confirmed that it was possible to synthesise *meta* anthracyl carborane. In the resulting reaction mixture we found trace amounts of *meta* anthracyl carborane by mass spectroscopy, m/z 320 corresponding to $C_{16}B_{10}H_{20}$. The reaction of *para* carborane with anthraquinone was attempted, to test if this was the source of the product. This reaction however did not give the desired product.

Having found some difficulty with the synthesis of 9-iodoanthracene, the reaction with the much cheaper 9-bromoanthracene with carborane was attempted. Surprisingly this did work but the reaction was not clean and many side products were formed.

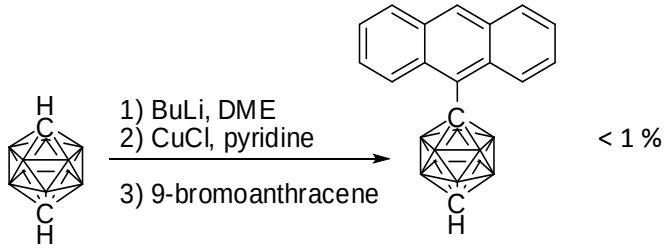

Figure 2–34: Synthesis of 1-(9'-$C_{14}H_9$)-1,12-$C_2B_{10}H_{11}$ by a copper-coupling reaction with bromoanthracene.

Purifying the anthracyl carborane was a difficult task. Purification by sublimation was attempted, but the compound degraded. The carborane could not be separated from the bromoanthracene by column chromatography. Purification could be carried out by column chromatography, eluting with hexane only, if none of the bromoanthracene starting material was present. As such a 10:1 excess of *para* carborane to bromoanthracene were reacted to ensure all the bromoanthracene was consumed. However, even in this case, not all of the bromoanthracene was consumed. This carborane is observed to emit blue light under a UV lamp. Calculations are in line with this observation, which predict that emission will occur at 497 nm.

Anthracyl carboranes which use a carbon-carbon triple bond as a spacer between the carborane cage and the anthracene group were synthesised. These have proved to be much more stable. They were synthesised by Sonogashira reactions, as shown in Figure 35 and 36. They were however also not obtained pure due to difficulty in separating the products from the anthracyl starting materials. Their presence was confirmed by mass spectrometry. For 1-Me-12-(C≡C-$C_{14}H_9$)-1,12-$C_2B_{10}H_{10}$, as shown in Figure 2–35, a m/z of 358 was found, corresponding to a molecular formula of $^{12}C_{19}{}^{1}H_{22}{}^{11}B_8{}^{10}B_2$ with typical carborane pattern from 351-361. For (1-Me-12-C≡C-1,12-$C_2B_{10}H_{10}$)$_2C_{14}H_8$, as shown in Figure 2–36, a m/z of 538 was found, corresponding to a molecular formula of $^{12}C_{24}{}^{1}H_{34}{}^{11}B_{16}{}^{10}B_4$ with typical carborane pattern at m/z 535-543.

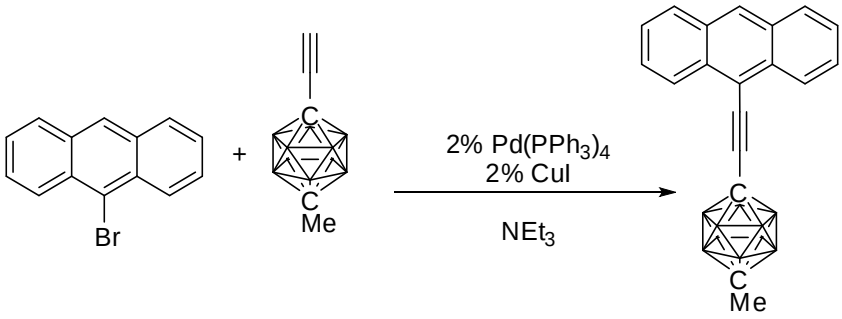

Figure 2–35: Synthesis of 1-(9'-C≡C-$C_{14}H_8$)-12-Me-1,12-$C_2B_{10}H_{10}$ by a Sonogashira cross coupling.

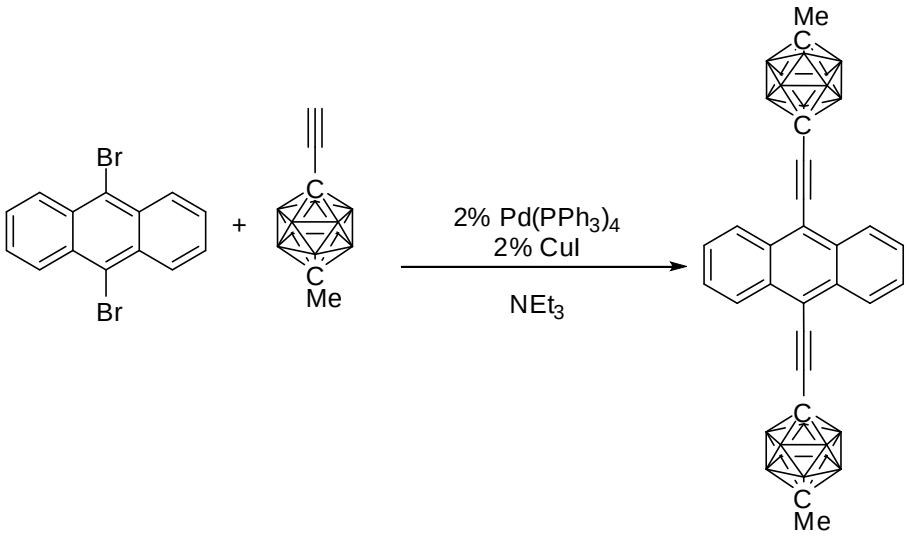

Figure 2–36: Synthesis of 9,10-(1-C≡C-12-Me-1,12-$C_2B_{10}H_{10}$)$_2$-$C_{14}H_8$ by a Sonogashira cross coupling.

2.3.1.1 Calculations

DFT calculations carried out on 1-(9'-$C_{14}H_9$)-1,12-$C_2B_{10}H_{11}$ show that the inherent instability in this molecule is due to the great strain the molecule is under, as can be seen in Figure 2–37.

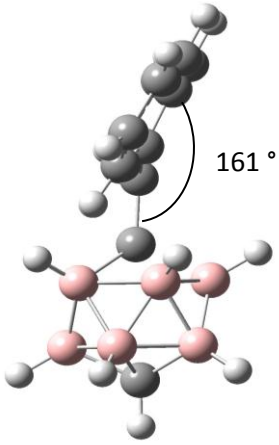

Figure 2–37: DFT calculated (B3LYP/6-31G*) optimised geometry of 1-(9'-$C_{14}H_9$)-1,12-$C_2B_{10}H_{11}$.

The *ortho* and *meta* isomers of this molecule are also shown to be unstable. Calculations suggest that the *ortho* isomer of this molecule, if isolated, would exhibit an extended cage C-C bond length of 2.345 Å in the excited state, compared to 1.727 Å in the ground state. Emission is predicted to be at 570 nm.

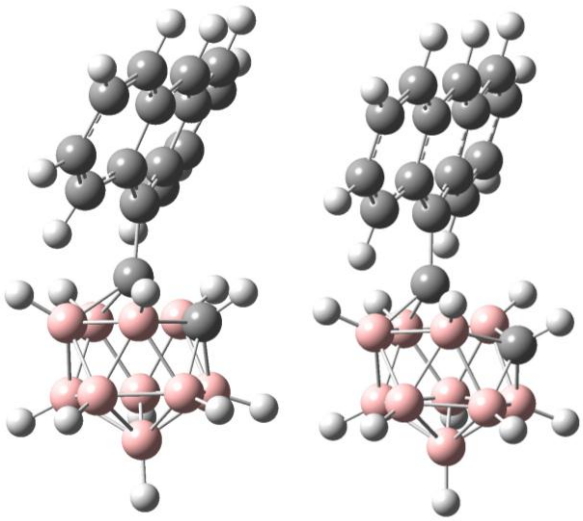

A) B)

Figure 2–38: DFT calculated (B3LYP/6-31G*) optimised geometry of 1-(9′-$C_{14}H_9$)-1,2-$C_2B_{10}H_{11}$ in A) the ground state B) the S_1 excited state.

The molecular orbitals of mono 9-anthracyl carboranes are shown in Figure 2–39 alongside those for the corresponding naphthyl carboranes. The HOMOs of both the naphthyl and anthracyl carboranes are predominantly on the aromatic rings. The LUMOs for the anthracyl carboranes have smaller contributions on the cage C and cage BH than in the case of the naphthyl carboranes. It can also be seen that the HOMO LUMO energy gap is smaller for the anthracyl carboranes than for the naphthyl carboranes.

Two S_1 excited state conformations are found for the *ortho* anthracyl carborane, as in the case of *ortho* naphthyl carborane. As before, one conformation has the anthracyl group adjacent to the cage C-C, while the other has the anthracyl group perpendicular to the cage C-C. In the case of the anthracyl group running perpendicular, the cage C-C bond length is increased to 2.345 Å, from 1.667 Å when the anthracyl group is parallel.

For the case when the anthracyl group is perpendicular, electron density for *ortho* anthracyl carborane shifts from predominantly the anthracyl group to the carborane cage on relaxation, Figure 2–40. The corresponding LUMO HOMO energy gap of the *ortho* anthracyl carborane, on relaxation from the S_1 to the

ground state, is 2.44 eV. This gap is smaller than that of the corresponding naphthyl carborane conformation, at 2.71 eV, Figure 2–32. This would correspond to a lower energy emission for the anthracyl carboranes than the naphthyl carboranes.

In the case of the anthracyl group parallel to the cage C-C, the electron density remains predominantly on the carborane cage, as in the case of the equivalent naphthyl carborane conformation. The energy gap of 2.77 eV is again smaller than that of the equivalent naphthyl carborane conformation, at 3.83 eV, Figure 2–32. This, again, indicates a lower energy emission than in the case of the naphthyl carborane.

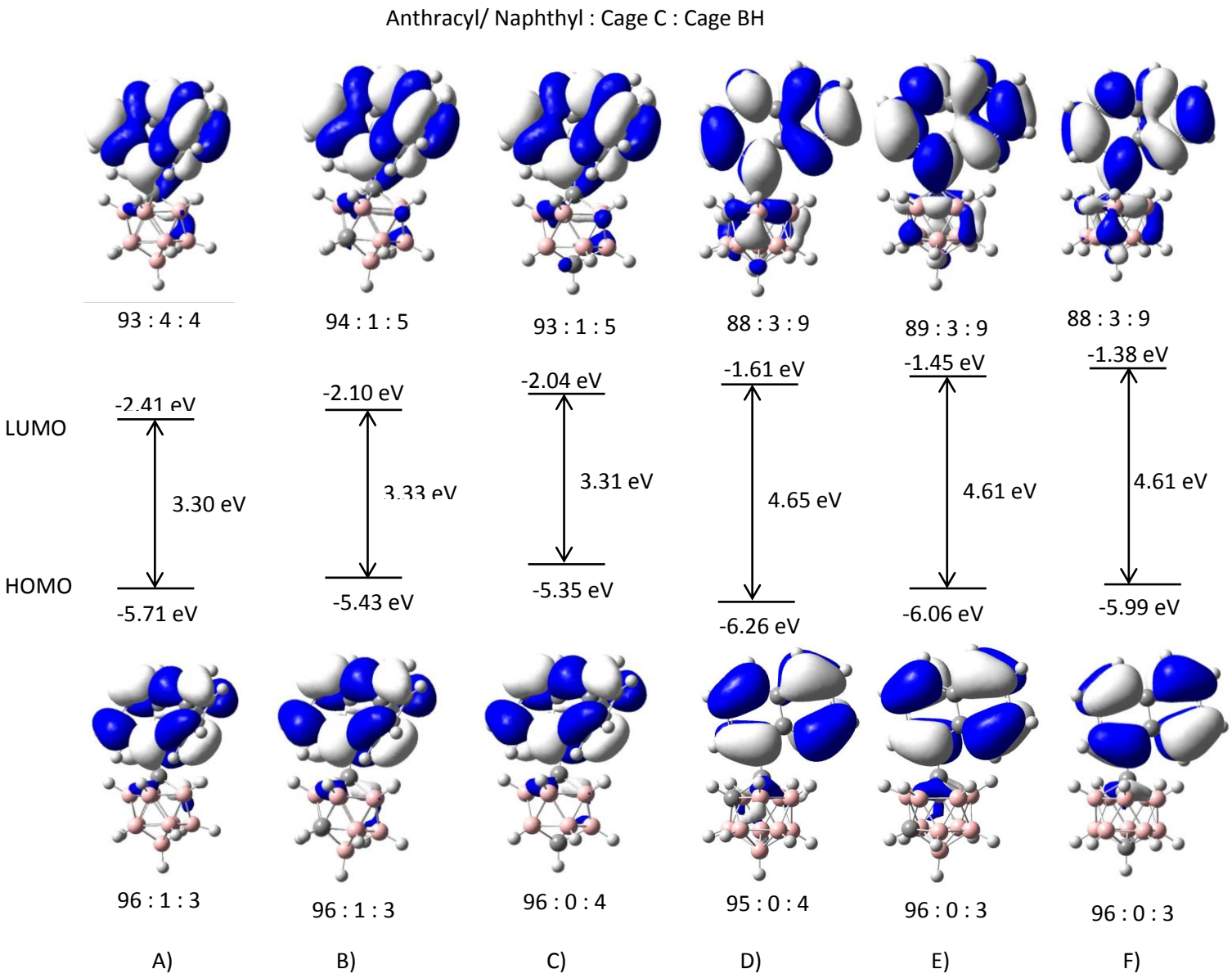

Figure 2–39: DFT calculated (B3LYP/6-31G*) HOMO and LUMO molecular orbital contributions and energy gaps for A) 1-(1'-$C_{14}H_9$)-1,2-$C_2B_{10}H_{11}$ B) 1-(1'-$C_{14}H_9$)-1,7-$C_2B_{10}H_{11}$ C) 1-(1'-$C_{14}H_9$)-1,12-$C_2B_{10}H_{11}$D) 1-(1'-$C_{10}H_7$)-1,2-$C_2B_{10}H_{11}$ E) 1-(1'-$C_{10}H_7$)-1,7-$C_2B_{10}H_{11}$ F) 1-(1'-$C_{10}H_7$)-1,12-$C_2B_{10}H_{11}$.

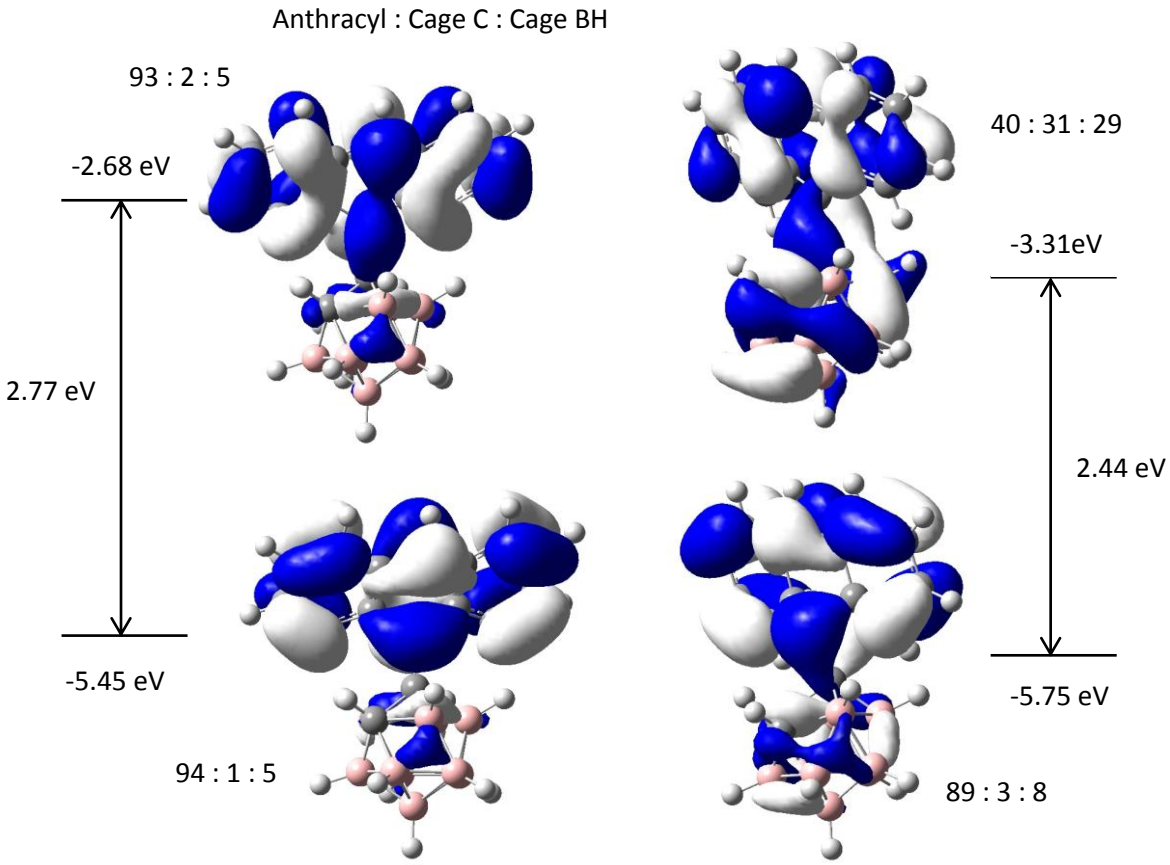

Figure 2–40: DFT calculated (B3LYP/6-31G*) HOMO and LUMO molecular orbital contributions and energy gaps for the two S_1 excited states found for *ortho* anthracyl carborane.

A series of calculations were carried out to find an anthracene containing molecule that would be more stable. The *ortho* isomer, with its flexible C-C bond, has potential to be the most interesting, so the calculations carried out concentrated on this.

Calculations suggest that the 1-(1′-$C_{14}H_9$)-1,2-$C_2B_{10}H_{11}$ molecule would be more stable. This is understandable as this molecule has a more striking similarity to the 9-naphthyl carboranes. In this case the extra aromatic ring is much further from the carborane cage and as such steric interactions are reduced.

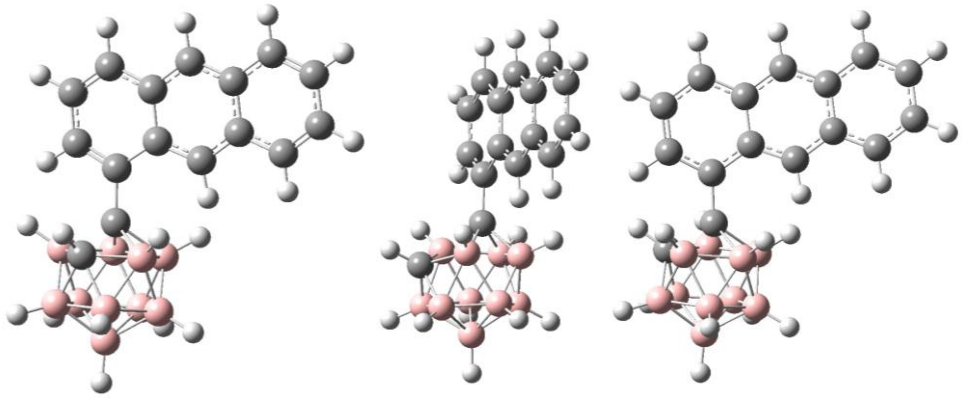

A) **B)** **C)**

Figure 2–41: DFT calculated (B3LYP/6-31G*) optimised geometry of 1-(1′-$C_{14}H_9$)-1,2-$C_2B_{10}H_{11}$ A) in the ground state B) and C) two S_1 excited state geometries found.

In Figure 2–41B), the first S_1 excited state geometry, the cage C-C bond length is extended from 1.691 Å in the ground state, to 2.371 Å. The predicted emission in this case is 682 nm. The second S_1 excited state geometry found, Figure 2–41C), does not have an extended cage C-C bond and has a predicted emission of 461 nm. These calculations suggest that if synthesised these molecules would show similar emission patterns to the *ortho* naphthyl carboranes. 1-Iodoanthracene is however not commercially available so synthesis would be difficult.

In order to find a more stable 9-anthracyl carborane derivative we investigated the effect of ethynyl and ethane spacer groups between the carborane and anthracyl.

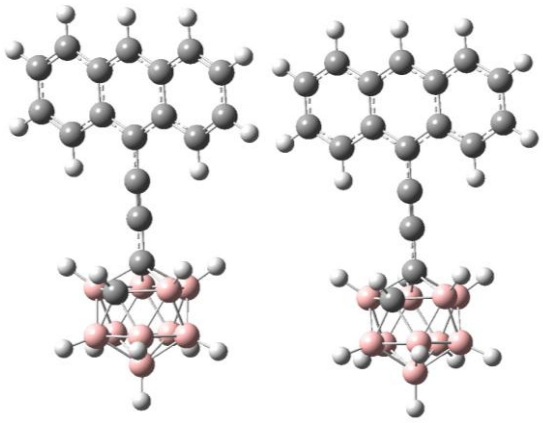

A) **B)**

Figure 2–42: DFT calculated (B3LYP/6-31G*) optimised geometry of 1-(CC-9-$C_{14}H_9$)-1,2-$C_2B_{10}H_{11}$ a) in the ground state b) S_1 excited state geometry.

In the case of the *ortho* mono ethynyl anthracyl carborane, the cage C-C bond length undergoes only a small increase on excitation from Figure 2–42A) to Figure 2–42B), from 1.667 Å to 1.699 Å. The predicted emission is 477 nm. In this case it is clear that the carborane cage is not involved in the fluorescence properties.

In the case of a ethane tether the *ortho* mono isomer does not exhibit an extended cage C-C bond length on excitation and the predicted emission wavelength is 447 nm. In the case of a CH_2 tether, again the *ortho* mono molecule does not show an extended cage C-C bond length and the predicted emission is at 447 nm.

In these cases it is clear that the carborane cage is not involved and the fluorescence emission is due to the anthracene molecule. This is confirmed by the molecular orbital contributions being found only on the anthracyl groups. In all cases, on excitation from the HOMO to LUMO and in the S_1 excited state, there is no change in the molecular orbital contributions.

2.4 Conclusion

A series of naphthyl carboranes have been synthesised which are found to be fluorescent. For the *meta* and *para* naphthyl carboranes small Stokes shifts are observed along with a small solvatochromic shift between DCM and cyclohexane. The *ortho* naphthyl carboranes have much larger Stokes shifts. The mono naphthyl *ortho* carborane displays two emission bands, each being assigned to a different excited state geometry. The position of the lower energy band varies with the solvent polarity, as do the relative intensities of the two bands. Although we have shown here that naphthyl carboranes are fluorescent, they are not considered to be useful for OLEDs as the emission is too high in energy.

We attempted to synthesise the anthracyl carboranes which proved to be unstable. Calculations suggest that, if synthesised, the mono anthracyl *ortho* carborane would display similar fluorescent properties to the naphthyl analogue, with two S_1 excited states and involvement from the carborane cage. Such

carboranes are calculated to have smaller HOMO LUMO energy gaps than the naphthyl carboranes and as such may be suitable for OLEDs. Introducing a spacer group between the anthracyl group and the carborane cage would impart more stability to the molecule, however calculations suggest that the tether would prevent carborane cage involvement and emission would be due to the anthracyl group.

2.5 Experimental

Pyridine and aniline were dried by stirring with KOH for 24 hours and then distilling under reduced pressure. Dry DME was obtained by stirring over sodium before distilling under reduced pressure. Dry CuCl was prepared by dissolving the powder in concentrated HCl, precipitating out the solid by addition of water, which was then filtered off and washed with ethanol and ether. The light grey solid is then heated under vacuum and stored under nitrogen.

Solution state NMR spectra were recorded on a Bruker Avance-400 spectrometer using $CDCl_3$ as the deuterated solvent. External references for the chemical shifts were $SiMe_4$ = 0.00 ppm for ^{1}H and ^{13}C, $BF_3.Et_2O$ = 0.0 ppm for ^{11}B. $CHCl_3$ was used as a reference for ^{1}H at 7.26 ppm and ^{13}C NMR at 77.0 ppm. Solid state IR spectra were recorded on a Perkin Elmer 1600 series FTIR spectrometer using a golden gate accessory. Elemental analysis was carried out on an Exeter Analytical E-440 Elemental Analyser. Mass spectra were carried out on a Thermoquest Trace spectrometer (EI) or LCT Premier XE mass spectrometer (ASAP). Melting points were measured by DSC using a TA DSC Q1000.

UV-vis measurements were taken using an ATI Unicam UV2-100 spectrometer. Fluorescence emission measurements were carried out using a Jobin-Yvon Horiba Fluorolog 3-22 Tau-3 spectrofluorimeter.

Computational studies

The input files and output files were created and analysed using GaussView 4.1.2.[11] Optimisations were carried out using starting geometries without symmetry constraints. Frequency calculations show these geometries to be true minima with no imaginary frequencies. The excited state geometries were optimised using TD-DFT and the Gaussian 09 package.[12] All other calculations were carried out using the Gaussian 03 package.[13] The predicted UV-vis and emission data were carried out on S_0 ground state and S_1 ground state geometries respectively with TD-DFT. The rotation energies were estimated by fixing the selected torsion angles and allowing the rest of the geometry to optimise. The MO orbital contributions were generated with the aid of the GaussSum package.[14] The level of theory used in all cases was B3LYP/6-31G*.[15,16]

2.5.1 Preparation of 1,7-(1'-$C_{10}H_7$)$_2$-1,7-$C_2B_{10}H_{10}$ and 1-(1'-$C_{10}H_7$)-1,7-$C_2B_{10}H_{11}$

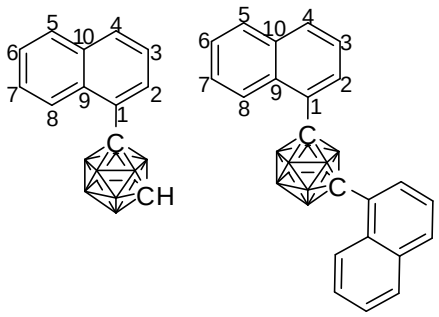

1,7-$C_2B_{10}H_{12}$ (1.17 g, 8.1 mmol) was dissolved in dry DME (20 ml) with stirring under nitrogen. The solution was cooled in an ice bath and *n*-BuLi (11 ml, 1.51 M in hexanes, 16 mmol) was added dropwise. The ice bath was removed and the solution was heated to 40 °C for 1 h. The solution was cooled in an ice bath and pyridine (5 ml) and CuCl (1.6 g, 16 mmol) were added. The ice bath was removed and the solution was heated to 40 °C for 1 h. 1-Iodonaphthalene (4.0 g, 16 mmol) was added. The solution was heated to reflux for 12 h. The solution mixture was allowed to cool and then poured over Et_2O (200 mL) with stirring. The solution was filtered and then washed with HCl (2 M) and dried over $MgSO_4$. The solvent was removed under reduced pressure. The resulting brown solid was sublimed to separate the unreacted 1,7-$C_2B_{10}H_{12}$ from the 1,7-(1'-$C_{10}H_7$)$_2$-1,7-$C_2B_{10}H_{10}$ and 1-(1'-$C_{10}H_7$)-1,7-$C_2B_{10}H_{11}$. The mono and disubstituted products were purified by silica gel chromatography with hexane to give 1,7-(1'-$C_{10}H_7$)$_2$-1,7-$C_2B_{10}H_{10}$ melting point 171 °C (520 mg, 1.3 mmol, 16%) and 1-(1'-$C_{10}H_7$)-1,7-$C_2B_{10}H_{11}$ melting point 139 °C (930 mg, 3.4 mmol, 43%) as white solids. Crystals of 1-(1'-$C_{10}H_7$)-1,7-$C_2B_{10}H_{11}$ suitable for X-ray crystallography were obtained from hexane.

1,7-(1'-$C_{10}H_7$)$_2$-1,7-$C_2B_{10}H_{10}$: **^{11}B** (128 MHz, $CDCl_3$): δ -10.4 (8B, d, J 138), -3.3 (2B,d, J 135).

^{1}H {^{11}B} (400 MHz, $CDCl_3$): δ 2.49 (2H, s, BH), 3.13 (6H, s, BH), 3.87 (2H, s, BH), 7.38 (2H, t, J=15.6 Hz, $C_3\underline{H}$), 7.48 (2H, t, J= 15.2 Hz, $C_6\underline{H}$), 7.55 (2H, t, J=15.6 Hz, $C_7\underline{H}$), 7.84 (4H, dd, J=13.2 Hz, $C_{4+5}\underline{H}$), 8.10 (2H, d, J=8.0 Hz, $C_2\underline{H}$), 8.95 (2H, d, J=8.8 Hz, $C_8\underline{H}$).

^{13}C (176 MHz, $CDCl_3$): δ 78.3 (cage C), 124.9 ($\underline{C}_3H$), 125.8 ($\underline{C}_{6/8}H$), 125.9 ($\underline{C}_{6/8}H$), 126.5 ($\underline{C}_7H$), 127.7 (C), 129.7 ($\underline{C}_{4/5}H$) , 130.3 ($\underline{C}_2H$), 130.5 (C), 131.2 ($\underline{C}_{4/5}H$), 135.1 (C).

MS (low res. EI) $^{12}C_{22}{}^{1}H_{24}{}^{11}B_8{}^{2}B_2$ FW = 396 g/mol. M^+ = m/z 396 (with typical carborane pattern from 389-399) .

IR: (ν_{max}/cm^{-1}): 3052w (aromatic CH stretch), 2644s (BH stretch), 2610s (BH stretch), 2564w, 1600w, 1512w, 1462w, 1398w, 1356w, 1282w, 1268w, 1242w, 1214w, 1174w, 1124w, 1040w, 1024w, 972w, 916w, 874w, 816s, 766s, 742s, 694w, 656w, 610w, 534w, 474w, 414w.

% CHN Anal. Calcd for $C_{22}B_{10}H_{24}$ C, 66.50; H, 6.05. Found C, 66.43; H, 6.38.

1-(1'-$C_{10}H_7$)-1,7-$C_2B_{10}H_{11}$: **^{11}B** (128 MHz, $CDCl_3$): δ -14.6 (2B, d), -13.2 (2B, d), -10.5 (3B, d, J 143), -9.0 (1B, d), -7.1 (1B, d, J 162), -2.9 (1B, d, J 161).

^{1}H {^{11}B} (400 MHz, $CDCl_3$): δ 2.34 (6 H, m, BH), 2.94 (2 H, s, BH), 3.07 (1H, s, cage C-H), 3.25 (2H, s, BH), 7.34 (1H, t, J 7.9, $C_3\underline{H}$), 7.49 (1H, t, J 14.7, $C_6\underline{H}$), 7.52 (1H, t, J 21.6, $C_7\underline{H}$), 7.83 (2H, dd, J 13.2, $C_5\underline{H}$+$C_4\underline{H}$), 8.01 (1H, d, J 7.6, $C_2\underline{H}$), 8.89 (1H, d, J 9.2, $C_8\underline{H}$).

^{13}C (176 MHz, $CDCl_3$): δ 54.6 (cage CH), 124.9 ($\underline{C}_3H$), 125.8 ($\underline{C}_6H$ or $\underline{C}_8H$), 125.9 ($\underline{C}_6H$ or $\underline{C}_8H$), 126.5 ($\underline{C}_7H$), 129.7 ($\underline{C}_5H$ or $\underline{C}_4H$), 130.3 ($\underline{C}_2H$), 130.5 (C), 131.2 ($\underline{C}_5H$ or $\underline{C}_4H$), 135.0 (C), 137.8 (C).

MS (low res. EI) $^{12}C_{12}{}^{1}H_{18}{}^{11}B_8{}^{10}B_2$ FW = 270 g/mol. M^+ = m/z 271 (with typical carborane pattern from 264-274).

IR: (ν_{max}/cm^{-1}): 3044w (CH), 2920w, 2852w, 2596s (BH stretch), 2574s (BH stretch), 1596w, 1508w, 1452w, 1392w, 1326w, 1262w, 1194w, 1114w, 1012w, 914w, 882w, 840w, 766s, 728s, 648w, 606w, 518w, 474w, 418w.

% CHN Anal. Calcd for $C_{12}B_{10}H_{18}$ C, 53.14; H, 6.64. Found C, 53.12; H, 6.29.

2.5.2 Preparation of 1,12-(1'-$C_{10}H_7$)$_2$-1,12-$C_2B_{10}H_{10}$

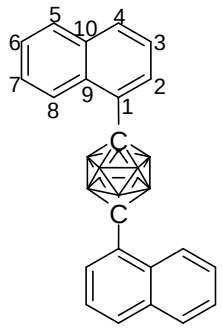

1,12-$C_2B_{10}H_{12}$ (1.44 g, 10 mmol) was dissolved in dry DME (40 ml) with stirring under nitrogen. The solution was cooled in an ice bath and *n*-BuLi (8.8 ml, 2.38 M in hexanes, 20 mmol) was added dropwise. The ice bath was removed and the solution was heated to 40 °C for 30 mins. Pyridine (2 ml) and CuCl (2.4 g, 25 mmol) were added. The solution was heated to reflux for 10 mins. 1-Iodonaphthalene (5.22 g, 20 mmol) was added. The solution was heated to reflux for 69 hours. The reaction mixture was allowed to cool and then poured over Et_2O (200 mL) with stirring. The green precipitate which formed was filtered off and washed with HCl (2 M). The precipitate was boiled in toluene and filtered whilst hot. This step was repeated. The toluene was removed and the resulting pink/brown solid was recrystallsed from xylene to give the product 1,12-(1'-$C_{10}H_7$)$_2$ -1,12-$C_2B_{10}H_{10}$ (2.10 g, 5.2 mmol, 53 %), melting point 305 °C.

^{11}B (128 MHz, $CDCl_3$): δ -11.6 (10B, d, J 150).

^{1}H {^{11}B}(699 MHz, $CDCl_3$): δ 3.03 (10H, d, J 29.8), 7.32 (2H, t, $C_3\underline{H}$, J 15.4, 7.7), 7.45 (2H, t, $C_{6/7}\underline{H}$, J 16.1, 8.4), 7.53 (2H, t, $C_{5/7}\underline{H}$, J 16.8, 8.4), 7.77 (2H, d, $C_4\underline{H}$, J 7.7), 7.81 (2H, d, $C_5\underline{H}$, J 9.1), 7.86 (2H, d, $C_2\underline{H}$, J 7.2), 8.87 (2H, d, $C_8\underline{H}$, J 8.3).

^{13}C (100 MHz, $CDCl_3$): δ 85.2 (cage C), 124.8 ($\underline{C}_3$H), 125.7 ($\underline{C}_{6/7}$H), 125.9 ($\underline{C}_8$H), 126.2 ($\underline{C}_{6/7}$H), 129.4 ($\underline{C}_2$H), 129.6 ($\underline{C}_5$H), 130.2 (C), 130.9 ($\underline{C}_4$H), 131.3 (C), 134.9 (C).

MS (low res. ASAP) $^{12}C_{22}{}^{1}H_{24}{}^{11}B_8{}^{2}B_2$ FW = 396 g/mol. M^+ = m/z 397 (with typical carborane pattern from 393-400).

IR: (ν_{max}/cm^{-1}): 3044w (aromatic CH stretch), 2610s (BH stretch), 2600s (BH stretch), 1598w, 1512w, 1398w, 1356w, 1330w, 1266w, 1240w, 1212w, 1172w, 1122w, 1040w, 1020w, 962w, 906w, 860w, 806w, 770s, 728s, 638w, 612w, 530w, 418w.

% CHN Anal. Calcd for $C_{22}B_{10}H_{24}$ C, 66.50; H, 6.05. Found C, 66.47; H, 6.07.

2.5.3 Preparation of 1-(1'-$C_{10}H_7$)-1,12-$C_2B_{10}H_{11}$

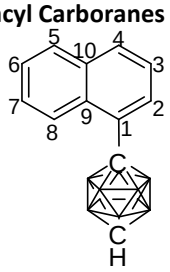

1,12-$C_2B_{10}H_{12}$ (0.72 g, 5 mmol) was dissolved in dry DME (15 ml) with stirring under nitrogen. The solution was cooled in an ice bath and *n*-BuLi (3.3 ml, 1.51 M in hexanes, 5 mmol) was added dropwise. The ice bath was removed and the solution was heated to 40 °C for 1 h. Pyridine (2 ml) and CuCl (0.5 g, 5 mmol) were added. The solution was heated to 40 °C for 1 h. 1-Iodonaphthalene (1.25 g, 5 mmol) was added. The solution was heated to reflux for 19 h. The reaction mixture was allowed to cool and then poured over Et_2O (200 mL) with stirring. The solution was filtered, washed with HCl, then dried over $MgSO_4$. The solvent was removed under reduced pressure. The resulting white solid was fractionally sublimed to separate the unreacted 1,12-$C_2B_{10}H_{12}$ and 1-(1'-$C_{10}H_7$)-1,12-$C_2B_{10}H_{11}$ (0.8 g, 3 mmol, 59 %). Crystals of 1-(1'-$C_{10}H_7$)-1,12-$C_2B_{10}H_{11}$ suitable for crystallography were obtained from hexane.

^{11}B (128 MHz, $CDCl_3$): δ -15.1 (5B, d, J 172), -11.3 (5B, d, J 158).

^{1}H {^{11}B}(699 MHz, $CDCl_3$): δ 2.43 (5H, s, BH), 2.88 (5H, s, BH), 2.96 (1H, s, cage CH), 7.29 (1H, t, $C_3\underline{H}$, J 15.4, 7.7), 7.43 (1H, t, $C_{6/7}\underline{H}$, J 15.4, 6.3), 7.50 (1H, t, $C_{6/7}\underline{H}$, J 17.5, 8.4), 7.74 (1H, d, $C_4\underline{H}$, J 8.4), 7.79 (2H, d, $C_{5+2}\underline{H}$, J 7.7), 8.83 (1H, d, $C_8\underline{H}$, J 9.0).

^{13}C (100 MHz, $CDCl_3$): δ 62.7 (cage CH), 87.7 (cage C), 124.4 ($\underline{C}_3$H), 125.3 ($\underline{C}_{6/7}$H), 125.6 ($\underline{C}_{6/7}$H), 129.1 ($\underline{C}_{2/5}$H), 129.3 ($\underline{C}_{2/5}$H), 129.8 (C), 130.5 ($\underline{C}_4$H), 131.5 (C), 134.6 (C).

MS (low res. EI) $^{12}C_{12}{}^{1}H_{18}{}^{11}B_8{}^{10}B_2$ FW = 270 g/mol. M^+ = m/z 270 (with typical carborane pattern from 263-273).

IR: (ν_{max}/cm^{-1}): 3052w (CH stretch), 2604s (BH stretch), 2360w, 1600w, 1512w, 1398w, 1356w, 1328w, 1260w, 1142w, 1120w, 1082w, 1062w, 1010w, 896w, 862w, 824s, 794s, 768s, 746s, 728s, 698w, 662w, 614w, 532w, 416w.

% CHN Anal. Calcd for $C_{12}B_{10}H_{18}$ C, 53.14; H, 6.64. Found C, 53.17; H, 6.67.

2.5.4 Preparation of 1,2-(1'-$C_{10}H_7$)$_2$-1,2-$C_2B_{10}H_{10}$

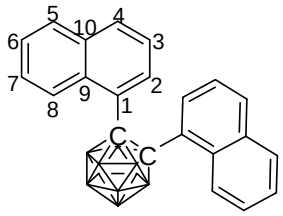

Isomerisation from *para*-dinaphthyl carborane: 1,12-(1'-$C_{10}H_7$)$_2$–1,12-$C_2B_{10}H_{10}$ (513 mg, 1.29 mol) was dissolved in dry THF (20 mL) with stirring under nitrogen. Sodium metal flakes (100 mg) were added and the mixture was left to stir under nitrogen at room temperature for 12 h. The reaction mixture changed from clear and colourless to dark purple. The THF was removed under reduced pressure using a rotary evaporator. The purple solid (1.304 g) was dissolved in DCM (20 mL) and washed with water (3 x 20 mL). The DCM solution was dried over $MgSO_4$ and then DCM was removed under reduced pressure to give a yellow solid 1,2-(1'-$C_{10}H_7$)$_2$ - 1,2-$C_2B_{10}H_{10}$ (398 mg, 1.00 mol, 77%). The solid was recrystallised from DCM:Hexane, melting point 271 °C.

Isomerisation from *meta*-dinaphthyl carborane: The method above was followed using 1,7-(1'-$C_{10}H_7$)$_2$–1,7-$C_2B_{10}H_{10}$ (50 mg) as the starting material. The yellow solid product was 1,2-(1'-$C_{10}H_7$)$_2$–1,2-$C_2B_{10}H_{10}$ (34 mg, 68%).

Crystals suitable for X-ray diffraction were grown from slow evaporation of a DCM solution of the carborane.

^{11}B (128 MHz, $CDCl_3$): δ -9.2 (8B, d, J 135), -1.2 (2B, d, J 141).

^{1}H {^{11}B}(400 MHz, $CDCl_3$): δ 2.74 (4H, s, BH), 2.92 (4H, s, BH), 4.16 (2H, s, BH), 6.95 (2H, t, J 7.9, C_3H), 7.44 (2H, t, J 7.4, C_6H), 7.60 (4H, dt, C_4H, C_7H), 7.61 (2H, d, J 8.1, C_5H), 7.78 (2H, d, J 7.7, C_2H), 9.02 (2H, d, J 9.0, C_8H).

^{13}C (100 MHz, $CDCl_3$): δ 93.2 (cage C), 124.1 (C_3H), 125.1 (C_8H), 125.8 (C), 125.9 (C_6H), 127.2 ($C_{4/7}$H), 129.7 (C_5H), 132.1 (C), 132.8 ($C_{4/7}$H), 133.7 (C_2H), 134.7 (C).

Mass (low res. EI) $^{12}C_{22}{}^{1}H_{24}{}^{11}B_8{}^{2}B_2$ FW = 396 g/mol. M^+ = m/z 396 (100 %) (with typical carborane pattern from 388-399).

IR: (ν_{max}/cm^{-1}): 3054w (aromatic CH stretch), 2688m, 2674m, 2612s (BH stretch), 2578s (BH stretch), 1597m, 1512s, 1395m, 1357w, 1331m, 1239w, 1124w, 891w, 880w, 860w, 815m, 806m, 767s, 602w, 517w, 417w.

% CHN Anal. Calcd for $C_{22}B_{10}H_{24}$ C, 66.50; H, 6.05. Found C, 65.66; H, 6.05.

2.5.5 Preparation of 1-ethynyl naphthalene.[1,17,18]

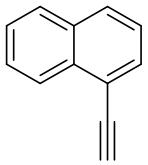

1-bromonaphthalene (3.8 g, 18 mmol), TMSA (10 g, 100 mmol), CuI (0.14 g, 7.36 mmol) and $Pd(PPh_3)_4$ (0.24g, 7.36 mmol) were added to degassed triethylamine (80 mL) and heated to reflux for 70 h. The reaction mixture was allowed to cool then filtered. The solvent was removed from the filtrate and the solid residue was dissolved in DCM, washed with 5 % HCl (100 mL) and water (3 x 100 mL). The solution was dried over $MgSO_4$ and then the solvent was removed in vacuo. The solid was then dissolved in wet methanol and K_2CO_3 was added. The reaction mixture was stirred at 20 °C under N_2 for 24 hours. It was then poured into water and the product was extracted with AcOEt. The organic phase was washed with saturated NaCl solution and then dried over $MgSO_4$. The solvent was removed and the product, 1-ethynyl naphthalene, was dried under vacuum.

^{1}H (400 MHz, $CDCl_3$): δ 3.38 (1H, s), 7.30 (1H, t, J 7.7), 7.41 (1H, t, J 7.5), 7.48 (1H, t, J 7.6), 7.65 (1H, d, J 7.0), 7.72 (2H, d, J 8.3), 8.30 (1H, d, J 8.3).

2.5.6 Preparation of 1-(1'-$C_{10}H_7$)-1,2-$C_2B_{10}H_{11}$.[1]

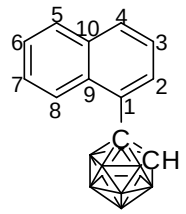

Isomerisation: The isomerisation method used in the synthesis of 1,2-(1'-$C_{10}H_7$)$_2$-1,2-$C_2B_{10}H_{10}$ was followed using 1-(1'-$C_{10}H_7$)-1,7-$C_2B_{10}H_{11}$ (400 mg) as the starting material. Separation was carried out by sublimation and white crystals of 1-(1'-$C_{10}H_7$)–1,2-$C_2B_{10}H_{11}$ (80 mg, 20%) were obtained from hexane.

Copper-coupling: 1,2-$C_2B_{10}H_{12}$ (0.72 g, 5 mmol) was dissolved in dry DME (20 ml) with stirring under nitrogen. The solution was cooled in an ice bath and *n*-BuLi (3.3 ml, 1.51 M in hexanes, 5 mmol) was added dropwise. The ice bath was removed and the solution was heated to 40 °C for 1 h. Pyridine (2 ml) and CuCl (0.5 g, 5 mmol) were added. The solution was heated to 40 °C for 1 h. 1-Iodonaphthalene (1.25 g, 5 mmol) was added. The solution was heated to reflux for 19 h. The reaction mixture was allowed to cool and was then poured over Et_2O (200 mL) with stirring. The green precipitate which formed was filtered off and filtrate was washed with HCl (2 M), then dried over $MgSO_4$. The solvent was removed and the resulting brown sticky solid was dissolved in dry Et_2O (10 mL) with stirring under nitrogen. The mixture of products was separated by sublimation to give 1-(1'-$C_{10}H_7$)–1,2-$C_2B_{10}H_{11}$ (310 mg, 23 %). 1-(1'-$C_{10}H_7$)–1,2-$C_2B_{10}H_{11}$ was recrystallised from hexane.

From decaborane: Decaborane (3.7 g, 30 mmol) was dissolved in benzene (40 mL) and cooled in an ice bath. A solution of 1-ethynyl naphthalene (4 g, 26 mmol) in MeCN (10 mL) was added. The ice bath was removed and the reaction mixture was slowly heated to reflux for 48 h. The solvent was removed and the remaining solid

was dissolved in the minimum amount of DCM and passed through a slilica plug eluting with hexane to give 1-(1'-$C_{10}H_7$)–1,2-$C_2B_{10}H_{11}$ (1.4 g, 5.2 mmol, 20 %).

Crystals suitable for X-ray diffraction were grown from slow evaporation of a hexane solution of the carborane.

^{11}B (128 MHz, $CDCl_3$): δ -13.2 (2B, d, J 170), -10.0 (4B, d, J 154), -8.8 (4B, d), -2.7 (2B, d, J 140).

^{1}H {^{11}B}(400 MHz, $CDCl_3$): δ 2.33 (2H, s, BH), 2.42 (2H, s, BH), 2.48 (1H, s, BH), 2.55 (1H, s, BH), 2.76 (2H, s, BH), 2.96 (2H, s, BH), 4.63 (1H, s, cage CH), 7.39 (1 H, $C_3\underline{H}$, t, *J* 7.9), 7.51 (1H, t, $C_6\underline{H}$, J 7.4), 7.58 (1H, $C_7\underline{H}$, t, J 5.0), 7.77 (1H, $C_4\underline{H}$, d, J 7.7), 7.88 (2H, $C_{2+5}\underline{H}$, d, J 8.2), 8.69 (1H, $C_8\underline{H}$, d, J 8.9).

^{13}C (100 MHz, $CDCl_3$): δ 61.3 (cage CH), 124.6 ($\underline{C}_8H$), 124.7 ($\underline{C}_3H$), 126.3 ($\underline{C}_6H$), 127.4 ($\underline{C}_7H$), 128.4 ($\underline{C}_4H$), 128.9 (C), 130.0 ($\underline{C}_{2/5}H$), 130.1 (C), 131.9 ($\underline{C}_{2/5}H$), 135.0 (C).

MS (low res. EI) $^{12}C_{12}{}^{1}H_{18}{}^{11}B_8{}^{10}B_2$ FW = 270 g/mol. M^+ = m/z 272 (with typical carborane pattern from 265-275).

IR: (ν_{max}/cm^{-1}) 3074w (aromatic CH stretch), 2958m, 2920m, 2850m, 2596m (BH stretch), 1598w, 1508w, 1458w, 1398w, 1354w, 1330w, 1258s, 1216w, 1068s, 1014s, 876w, 860w, 800s, 790s, 730m, 688w, 610w, 600w, 524w, 490w, 466w, 418w.

2.6 References

1. Ohta K., Goto T. and Endo Y., *Inorg. Chem*., **2005**, 44, 8569-8573.
2. Eriksson L., Beletskaya I. P., Bregadze V. I., Sivaev I. B. and Sjöberg S., *J. Organomet. Chem.,* **2002**, 267-272.
3. Kokado K., Nagai A. and Chujo Y., *Tetrahedron Lett.*, **2011**, 52, 293-296.
4. Fox M. A., MacBride J. A. H., Peace R. J. and Wade K., *J. Chem. Soc. Dalton Trans.*, **1998**, 3, 401-411.
5. Turner A. R., Robertson H. E., Borisenko K. B., Rankin D. W. H. and Fox M. A., *Dalton Trans.*, **2005**, 1310-1318.
6. Alekseyeva E. S., Fox M. A., Howard J. A. K., MacBride J. A. H. and Wade K., *Appl. Organomet. Chem.*, **2003**, 17, 499-508.
7. Fox M. A., Nervi C., Crivello A., Batsanov A. S., Howard J. A. K., Wade K. and Low P. J., *J. Solid State Electrochem.*, **2009**, 13, 1483-1495.
8. Fox M. A. and Hughes A. K., *Coord. Chem. Rev.*, **2004**, 248, 457-476.
9. Shao M., Dongare P., Dawe L. N., Thompson D. W., Zhao Y., *Org. Lett.*, **2010**, 12, 3050-3053.
10. Kodomari M., Amanokura N., Takeuchi K., Yoshitomi S., *Bull. Chem. Soc. Japan*, **1992**, 65, 306-308.
11. Dennington II R., Keith T., Millam J., GaussView, Version 4.1.2, Semichem., Inc., Shawnee Mission, KS, 2007.
12. Gaussian 09, Revision A.02, Frisch, M. J.; Trucks, G. W.; Schlegel, H. B.; Scuseria, G. E.; Robb, M. A.; Cheeseman, J. R.; Scalmani, G.; Barone, V.; Mennucci, B.; Petersson, G. A.; Nakatsuji, H.; Caricato, M.; Li, X.; Hratchian, H. P.; Izmaylov, A. F.; Bloino, J.; Zheng, G.; Sonnenberg, J. L.; Hada, M.; Ehara, M.; Toyota, K.; Fukuda, R.; Hasegawa, J.; Ishida, M.; Nakajima, T.; Honda, Y.; Kitao, O.; Nakai, H.; Vreven, T.; Montgomery, Jr., J. A.; Peralta, J. E.; Ogliaro, F.; Bearpark, M.; Heyd, J. J.; Brothers, E.; Kudin, K. N.; Staroverov, V. N.; Kobayashi, R.; Normand, J.; Raghavachari, K.; Rendell, A.; Burant, J. C.; Iyengar, S. S.; Tomasi, J.; Cossi, M.; Rega, N.; Millam, J. M.; Klene, M.; Knox, J. E.; Cross, J. B.; Bakken, V.; Adamo, C.; Jaramillo, J.; Gomperts, R.; Stratmann, R. E.; Yazyev, O.; Austin, A. J.; Cammi, R.; Pomelli, C.; Ochterski, J. W.; Martin, R. L.; Morokuma, K.; Zakrzewski, V. G.; Voth, G. A.; Salvador, P.; Dannenberg, J. J.; Dapprich, S.; Daniels, A. D.; Farkas, Ö.; Foresman, J. B.; Ortiz, J. V.; Cioslowski, J.; Fox, D. J. Gaussian, Inc., Wallingford CT, 2009.
13. Gaussian 03, Frisch, M. J.; Trucks, G. W.; Schlegel, H. B.; Scuseria, G. E.; Robb, M. A.; Cheeseman, J. R.; Montgomery, Jr., J. A.; Vreven, T.; Kudin, K. N.; Burant, J. C.; Millam, J. M.; Iyengar, S. S.; Tomasi, J.; Barone, V.; Mennucci, B.; Cossi, M.; Scalmani, G.; Rega, N.; Petersson, G. A.; Nakatsuji, H.; Hada, M.; Ehara, M.; Toyota, K.; Fukuda, R.; Hasegawa, J.; Ishida, M.; Nakajima, T.; Honda, Y.; Kitao, O.; Nakai, H.; Klene, M.; Li, X.; Knox, J. E.; Hratchian, H. P.; Cross, J. B.; Bakken, V.; Adamo, C.; Jaramillo, J.; Gomperts, R.; Stratmann, R. E.; Yazyev, O.; Austin, A. J.; Cammi, R.; Pomelli, C.; Ochterski, J. W.; Ayala, P. Y.; Morokuma, K.; Voth, G. A.; Salvador, P.; Dannenberg, J. J.; Zakrzewski, V. G.; Dapprich, S.; Daniels, A. D.; Strain, M. C.; Farkas, O.; Malick, D. K.; Rabuck, A. D.; Raghavachari, K.; Foresman, J. B.; Ortiz, J. V.; Cui, Q.; Baboul, A. G.; Clifford, S.; Cioslowski, J.; Stefanov, B. B.; Liu, G.; Liashenko, A.; Piskorz, P.; Komaromi, I.; Martin, R. L.; Fox, D. J.; Keith, T.; Al-Laham, M. A.; Peng,

C. Y.; Nanayakkara, A.; Challacombe, M.; Gill, P. M. W.; Johnson, B.; Chen, W.; Wong, M. W.; Gonzalez, C.; and Pople, J. A.; Gaussian, Inc., Wallingford CT, 2004.
14. O'Boyle N. M., Tenderholt A. L. and Langner K. M., *J. Comp. Chem.*, **2008**, 29, 839-845.
15. a) Becke A. D., *J. Chem. Phys.*, **1993**, 98, 5648–5652; b) Lee C., Yang W., Parr R. G., *Phys. Rev. B*, **1988**, 37, 785 –789.
16. a) Petersson G. A., Al-Laham M. A., *J. Chem. Phys.*, **1991**, 94, 6081–6090; b) Petersson G. A., Bennett A., Tensfeldt T. G., Al-Laham M. A., Shirley W. A., Mantzaris J., *J. Chem. Phys.*, **1988**, 89, 2193–2218.
17. Koumbis, A. E., Kyzas, C. M., Savva, A. and Varvoglis, A., *Molecules*, **2005**, 10, 1340-1350.
18. Neenan, T. X. and Whitesides, G. M., *J. Org Chem*., **1988**, 53, 2489-2496.

3 : Synthesis and Fluorescence of Carboranyl Triarylamines

3.1 Introduction

Triarylamines, such as those in Figure 3–1, are commonly used as hole transport materials in multi-layer organic light emitting diodes (OLEDs).[1] The triarylamine unit can be easily oxidised at the nitrogen centre.[2] Another important property of triarylamines is their ability to transport positive charge.[2] An unsubstituted triphenylamine undergoes dimerization after oxidation to an unstable monocation radical.[2] The dimer formed is more easily oxidised than the monomer.[2] A high glass transition temperature (T_g) and an amorphous character is required in a hole transport material in OLEDs.[3] They play important roles in improving device efficiencies and increasing the lifetimes of the devices.[3] The amorphous nature of triarylamine molecules has been found to increase when bulky substituents are attached.[2] In this chapter we describe the synthesis of carboranes substituted with triarylamine groups. The incorporation of highly thermally stable carboranes is expected to increase the thermal stability of the triarylamines.

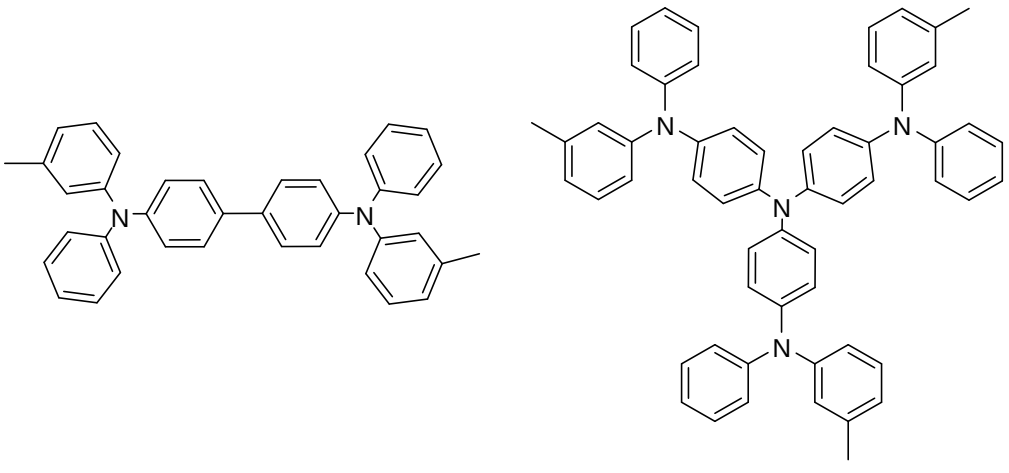

A) B)

Figure 3–1: Triarylamines used as hole transport materials in OLEDs, A) TPD (N,N'-Diphenyl-N,N'-bis(m-tolyl)-1,1'-biphenyl-4,4'-diamine) and B) MTDATA (m-methyl-tris(diphenylamine)triphenylamine).[1]

3.2 Syntheses

To synthesise the carboranyl triarylamines via a copper coupling reaction, an iodo triarylamine is required. 4-$IC_6H_4NTol_2$ was synthesised by the reaction scheme in Figure 3–2. An Ullmann reaction was used to synthesise the $C_6H_5NTol_2$ precursor, before a simple iodination with N-iodosuccinimide.

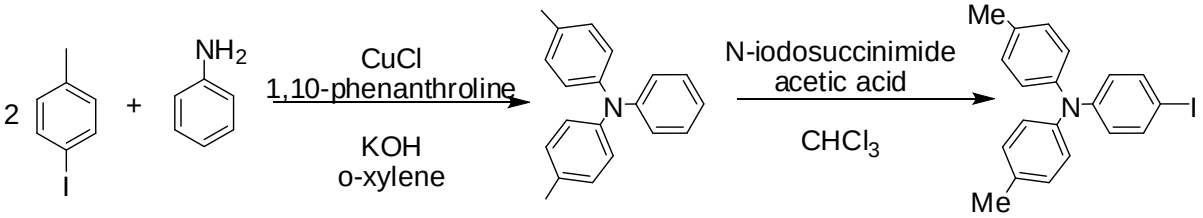

Figure 3–2: Synthesis of 4-$IC_6H_4NTol_2$.

The *meta* and *para* mono and di substituted products, **1**-**4**, were synthesised by a copper coupling method, Figure 3–3 and Figure 3–4. The slightly acidic carborane cage C-H bond is lithiated by two equivalents of BuLi, followed by substitution with copper(I). The iodo-triarylamine is then added to the cage C atom with the formation of CuI and the desired carborane. Low yields of the products are due to difficulty in separation of the mono and disubstituted products from the triarylamine starting material.

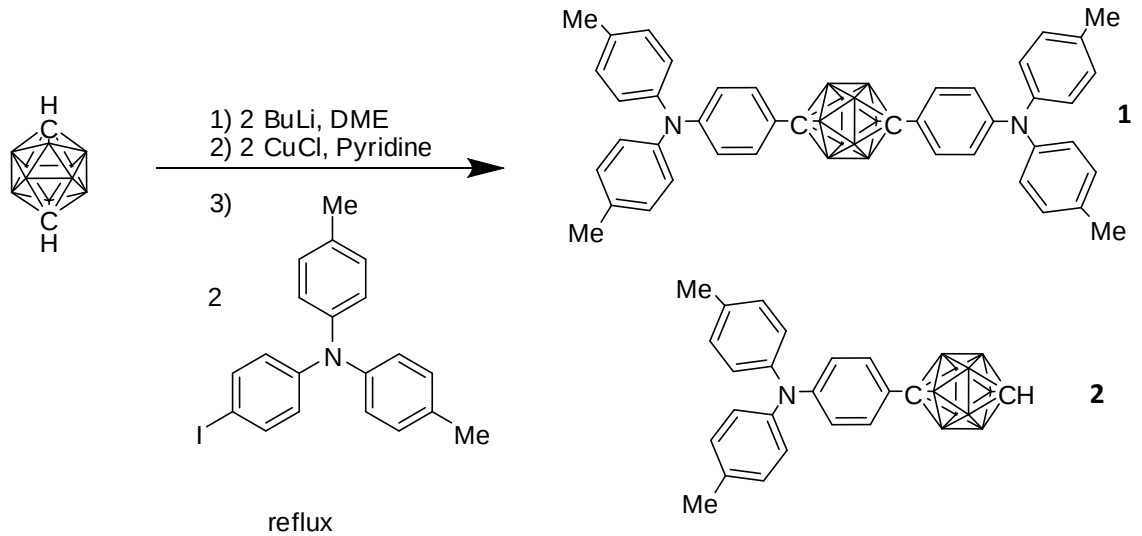

Figure 3–3: Synthesis of 1,12-$(C_6H_4NTol_2)_2$-1,12-$C_2B_{10}H_{10}$, 1, and 1-$(C_6H_4NTol_2)$-1,12-$C_2B_{10}H_{10}$, 2.

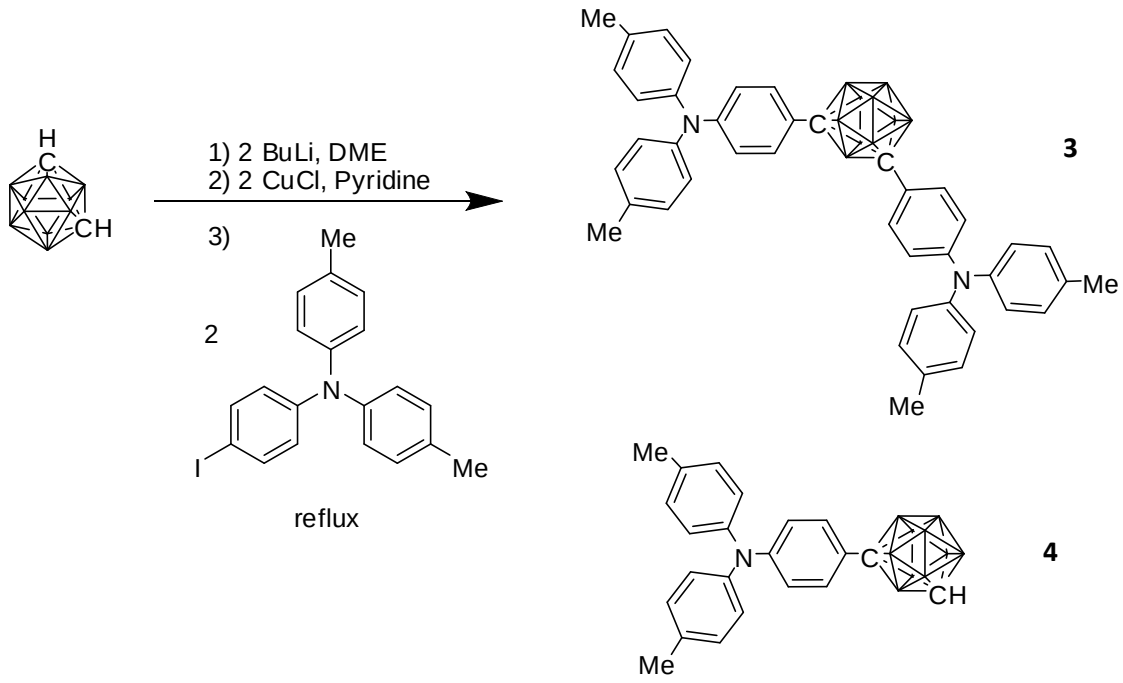

Figure 3–4: Synthesis of 1,7-($C_6H_4NTol_2$)$_2$-1,7-$C_2B_{10}H_{10}$, 3, and 1-($C_6H_4NTol_2$)-1,7-$C_2B_{10}H_{10}$, 4.

The *ortho* mono triarylamine carborane was also synthesised by a copper coupling method, Figure 3–5. In this case the carborane cage C atom is lithiated with one equivalent of butyllithium, followed by the addition of CuCl. The triarylamine group is then added, replacing the Cu on the cage carbon, with the formation of copper iodide and the carboranyl triarylamine **5**.

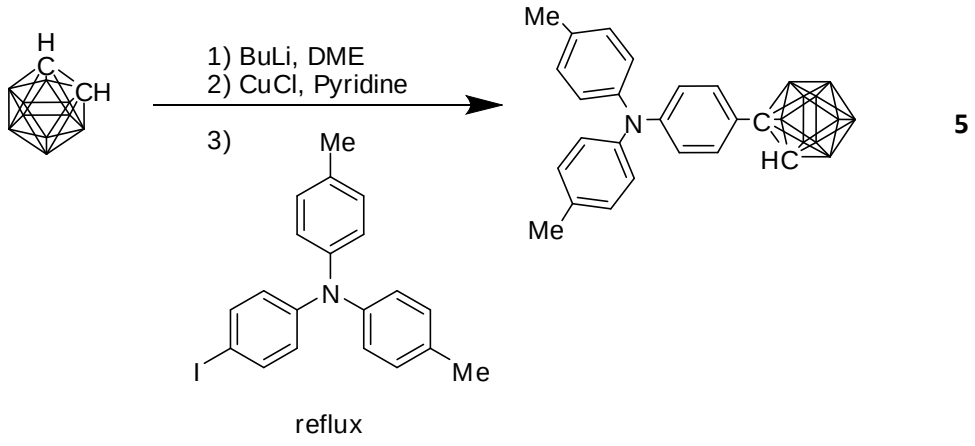

Figure 3–5: Synthesis of 1-($C_6H_4NTol_2$)-1,2-$C_2B_{10}H_{10}$, 5.

3.3 X-ray crystallography

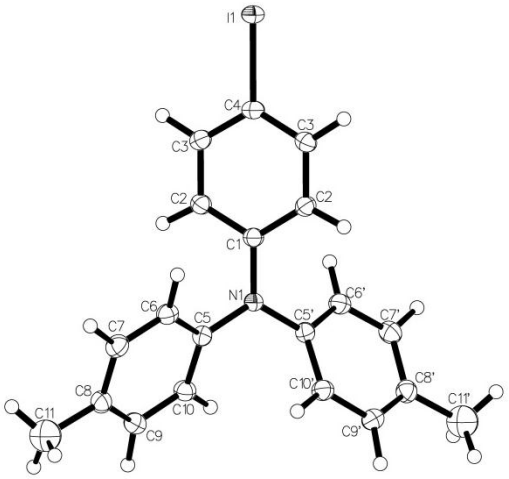

Figure 3–6: Molecular structure of 4-$IC_6H_4NTol_2$.

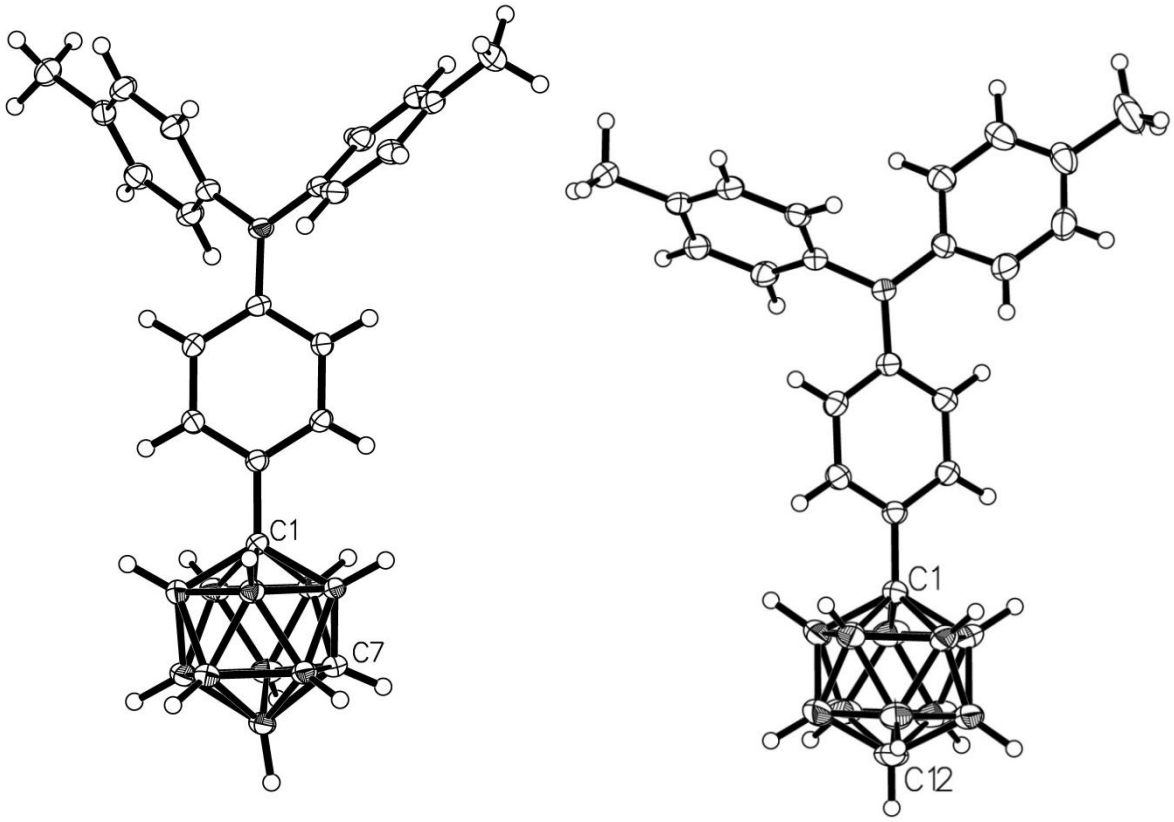

Figure 3–7: Molecular structure of 1-($C_6H_4NTol_2$)-1,7-$C_2B_{10}H_{11}$, 4.

Figure 3–8: Molecular structure of 1-($C_6H_4NTol_2$)-1,12-$C_2B_{10}H_{11}$, 2.

Compound	N1-C1 / Å	N1-C5 / Å	N1-C5' / Å	C5-N1-C5' / °
***p* mono 2**	1.4124(18) /1.4128(17)	1.4214(18) /1.4344(18)	1.4240(18) /1.4194(18)	118.90(11) /119.70(11)
***m* mono 4**	1.4101(17)	1.4245(18)	1.4304(17)	117.87(11)
4-$IC_6H_4NTol_2$	1.411(5)	1.424(3)	1.424(3)	120.8(4)

Table 3–1:Selected bond lengths and angles of compounds 2,4 and $IC_6H_4NTol_2$.

Molecular structures of monosubstituted *meta* and *para* carboranyl triarylamines are shown in Figure 3–7 and Figure 3–8 respectively. Selected bond lengths and angles of these compounds are compared with those of the iodotriarylamine starting material in Table 3-1. Very little change is found in the geometric parameters of the triarylamine moiety on replacing the iodine atom with a carboranyl group.

The weakly acidic nature of the cage C-H in monosubstituted carboranes leads to the possibility of hydrogen bonding between molecules. Such intermolecular interactions impart order in the crystals of such molecules, which would otherwise be subject to a high degree of rotational disorder.[4] Such interactions are particularly useful in identifying the position of the cage C atom in the *meta* isomers. Figure 3–9 shows the observed interactions between molecules in the crystalline state of A) the *meta* monosubstituted and B) the *para* monosubstituted carboranyl triarylamines. Observed cage C-H…C (aromatic) distances are in line with those reported in the literature, at 2.460 and 2.937 Å for the *meta* and *para* isomers respectively.[4] Cage B…HC aromatic interactions are also believed to contribute to the crystal ordering.

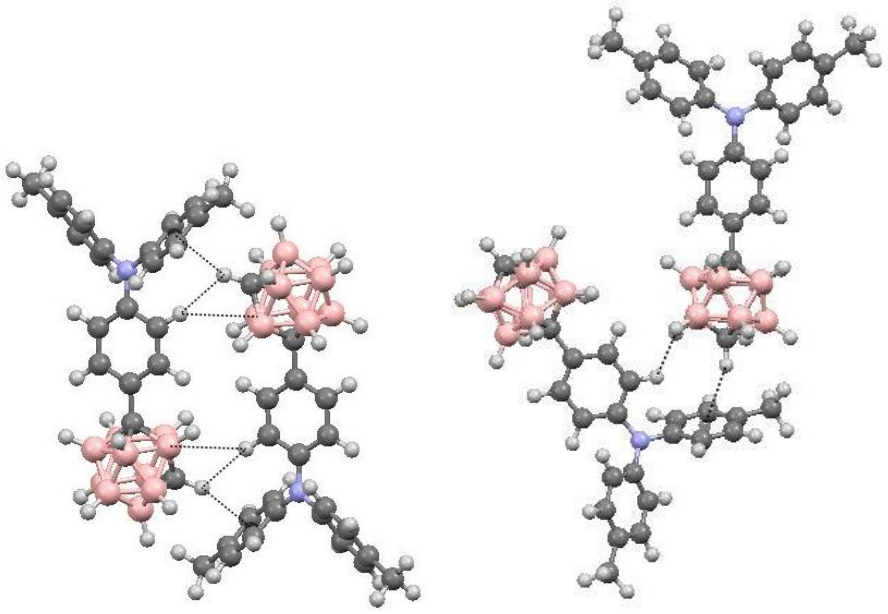

Figure 3–9: CH…X interactions between molecules in the crystalline state of A) 1-($C_6H_4NTol_2$)-1,7-$C_2B_{10}H_{11}$ and B) 1-($C_6H_4NTol_2$)-1,12-$C_2B_{10}H_{11}$.

Crystal suitable for X-ray crystallography could not be obtained for the disubstituted carboranes. It could be that the amorphous character of these compounds is a useful characteristic for OLEDs. Degradation of OLEDs and shortening the lifetime of OLED devices, can be attributed to crystallisation of organic layers in the device.[5]

3.3.1 Calculations

Optimised geometries of these carboranes were found by DFT (B3LYP/6-31G*). The calculated cage C-C bond length for the *ortho* disubstituted product is in good agreement with that observed. The calculated cage C-C bond length is smaller for the *ortho* monosubstituted carborane, due to a decreased steric interaction as compared to the disubstituted analogue. The parent 4-$IC_6H_4NTol_2$ could not be optimised at B3LYP/6-31G* with the software used for comparison with the other calculations. The similar $PhNTol_2$, however, can be. The C5-N1-C5' angle is calculated to be slightly greater for this parent $PhNTol_2$ with shorter N1-C1 and N1-C5 bond lengths as compared to the carboranyl triarylamines.

Compound	C-C / Å	N1-C1 / Å	N1-C5 / Å	N1-C5' / Å	C5-N1-C5' / °
***p* di 1**	-	1.412 1.413	1.425 1.425	1.425 1.425	119.1 119.0
***p* mono 2**	-	1.411	1.425	1.425	119.0
***m* di 3**	-	1.412 1.411	1.426 1.425	1.425 1.426	119.0 119.0
***m* mono 4**	-	1.411	1.425	1.426	118.8
***o* mono 5**	1.641	1.408	1.427	1.427	118.8
$PhNTol_2$	-	1.420	1.422	1.422	119.8

Table 3–2: DFT (B3LYP/6-31G*) calculated selected bond lengths of the carboranyl triarylamines.

3.4 Fluorescence

The absorption and emission properties of the carboranyl triarylamines were investigated and compared to parent triarylamines. The results of these studies are summarised in Table 3–3. Figure 3–10 illustrates the absorption and emission spectra of the carboranyl triarylamines.

The *meta* and *para* substituted carboranes show very similar absorptions and emissions in DCM solution. As in the case of the naphthyl carboranes, the carborane cages only have only a small effect on the emission when compared with parent triarylamines. The small bathochromic shift observed can be attributed to the slight electron withdrawing nature of the carborane cages.

The main effects of the carborane cage in the *meta* and *para* isomers are to increase the thermal stability and quantum yields of the products when compared to the triarylamine starting material. The *meta* and *para* carboranyl triarylamines have quantum yields between 11 and 16 %. The parent triarylamines we looked at have quantum yields of only 1 to 4 %. Quantum yields of the di substituted carboranes are found to be higher than those of the mono substituted products. The thermal stability of the carborane products is increased as shown by the high melting points of 134 to 289 °C, the highest being for the *para* disubstituted carborane. By comparison, 4-$IC_6H_4NTol_2$, is found to have a melting point of 90 °C.

In the case of the *ortho* mono substituted product, we see a dark red solid state emission under a UV lamp. However, when dissolved in DCM, no fluorescent emission is observable. This quenching may be due to the flexible cage C-C bond in

ortho carboranes leading to relaxation by a non radiative route. In a 1:99 THF:H_2O solution the fluorescent emission is observed. The use of THF:H_2O solution mimics the solid state so aggregation induced emission is seen. The Stokes shift observed is large and strikingly different from the small Stokes shifts seen in the *meta* and *para* isomers. It is also striking that only one emission band is observable, unlike the case of *ortho* mono naphthyl carborane. This may be due to the fact that emission for the *ortho* carboranyl triarylamine is only observable in a THF:H_2O solution and as such we are unable to probe the emission in a variety of solvent polarities, which led to the discovery of the two emission bands in the naphthyl analogue.

Emission of **5** is completely quenched in solution, as in the case of the *ortho* phenyl carborane, whilst the emission of *ortho* mono naphthyl carborane is observable in DCM and cyclohexane solution. This disparity may be due to a greater steric interaction present between the naphthyl group and carborane cage, than between the triarylamine group or phenyl group and the carborane cage. This smaller steric hindrance effect for **5** would allow for a greater degree of conformational freedom, allowing the flexible cage C-C bond length greater freedom to change length, leading to a greater degree of quenching for **5**.

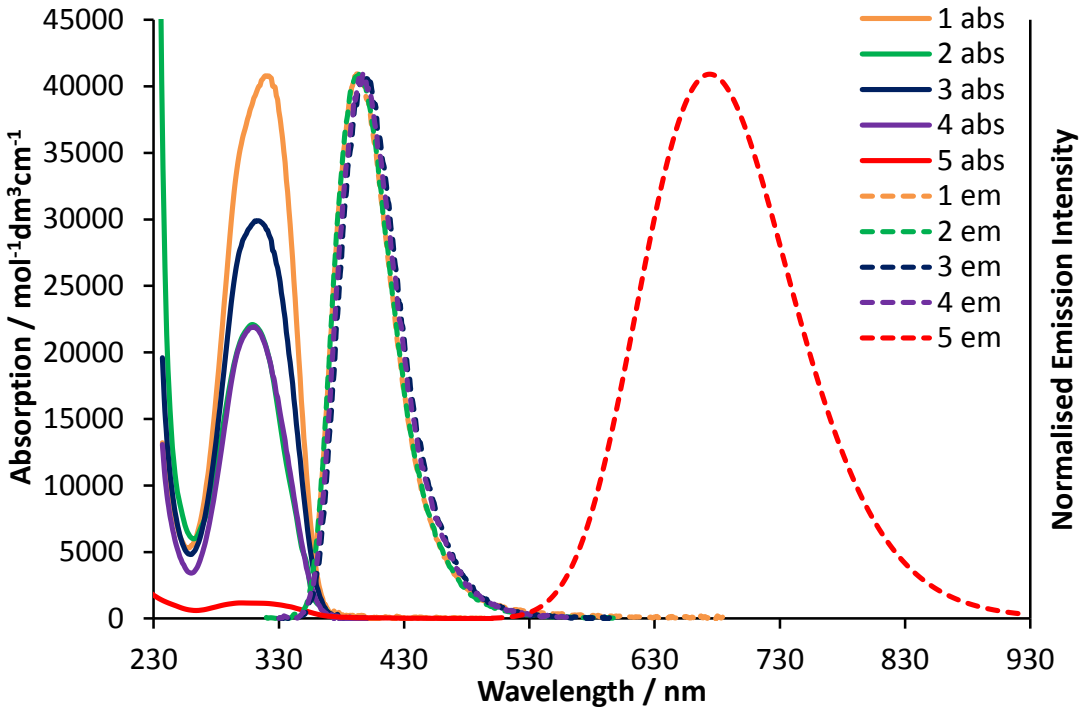

Figure 3–10: Absorption and emission spectra of 1 (*p* di), 2 (*p* mono), 3 (*m* di) and 4 (*m* mono) in DCM and 5 (*o* mono) in 1:99 THF:H_2O.

Compound	Absorption maximum			Excitation maximum		Excitation wavelength	Emission maximum		Stokes shift / cm^{-1}	QY / %
	ε / $mol^{-1}dm^3cm^{-1}$	nm	cm^{-1}	nm	cm^{-1}	nm	nm	cm^{-1}		
1	40800	320	31300	323	31000	350	392	25500	5800	15
2	22100	308	32500	304	32900	310	394	25400	7100	11
3	30000	313	32000	302	33100	320	398	25100	6900	16
4	21900	311	32200	302	33100	320	397	25200	7000	13
5	1200	300	33300	288	34700	370	690	14500	18800	1
$PhNTol_2$	17600	301	33200	298	33600	300	367	27200	6000	4
$NTol_3$	16000	300	33300	295	33900	300	373	26800	6500	2
$4\text{-}BrC_6H_4NTol_2$	25000	303	33000	295	33900	303	398	25100	7900	1
$4\text{-}IC_6H_4NTol_2$	23000	303	33000	297	33700	303	375	26700	6300	2

Table 3–3: Absorption and emission data in DCM for 1,2,3,4, $PhNTol_2$, $NTol_3$, $4\text{-}BrC_6H_4NTol_2$, $4\text{-}IC_6H_4NTol_2$ and in 1:99 THF:H_2O for 5.

3.4.1 Calculations

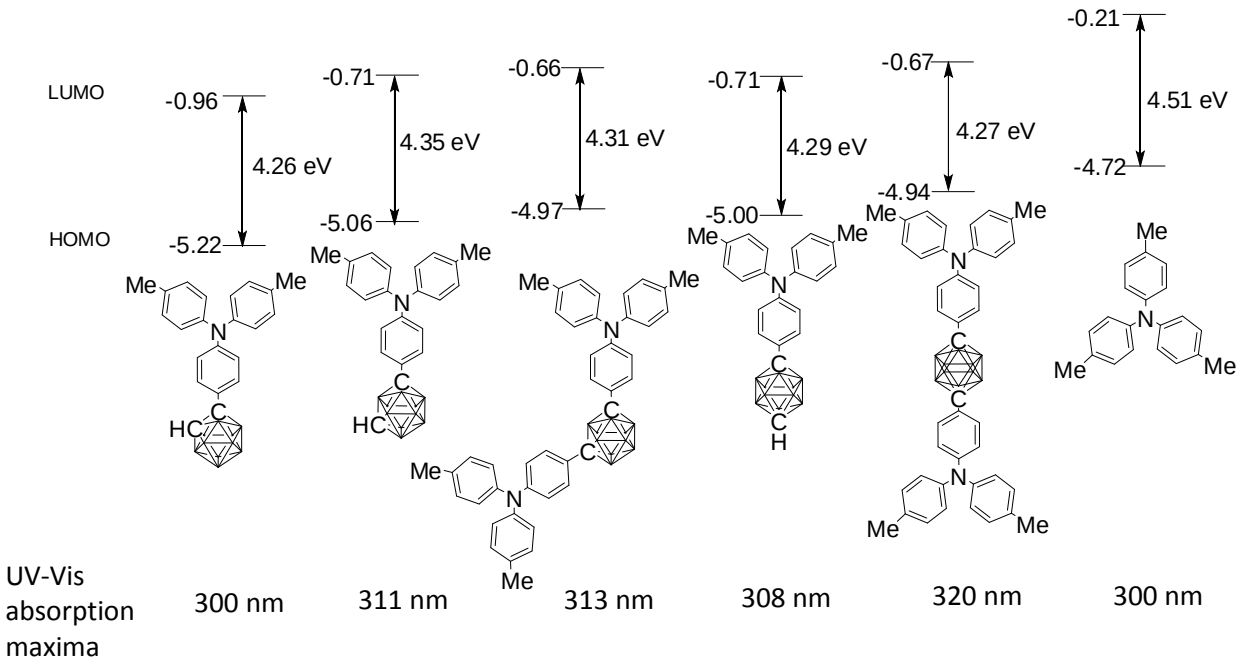

Figure 3–11: DFT (B3LYP/6-31G*) calculated HOMO LUMO energy gaps for carboranyl triarylamines and the corresponding observed maxima in the UV-Vis spectra.

The HOMO and LUMO energy levels of the carboranyl triarylamines are shown in Figure 3–11. The molecular orbital contributions of the frontier orbitals are shown in Figure 3–12. The absorption maximum for **1** is 20 nm higher than for tritolylamine. This lower energy absorption is in line with the smaller calculated HOMO LUMO energy gap for **1** compared to the tritolylamine parent molecule. Compounds **2**-**5** have calculated HOMO LUMO energy gaps of 4.26 – 4.35 eV (corresponding to wavelengths of 291-285 nm) and absorption maxima of 300-313 nm.

The HOMOs of compounds **1**-**5** are based on the triarylamine group whilst the LUMOs are also on the triarylamine but have a greater electron density on the carborane cage.

The *ortho* monosubstituted carboranyl triarylamine, **5**, has a calculated cage C-C bond length of 1.641 Å in the ground state. Unlike some *ortho* carboranes under a greater steric strain, such as *ortho* di naphthyl carborane (chapter 2), the *ortho* carborane cage remains closed, with similar bond lengths to the *meta* and

para isomers. As such, there are no great differences in the calculated HOMO and LUMO energy levels and molecular orbital contributions. If the disubstituted *ortho* analogue were synthesised it would be likely to be under a greater steric strain, leading to an elongated cage C-C bond.

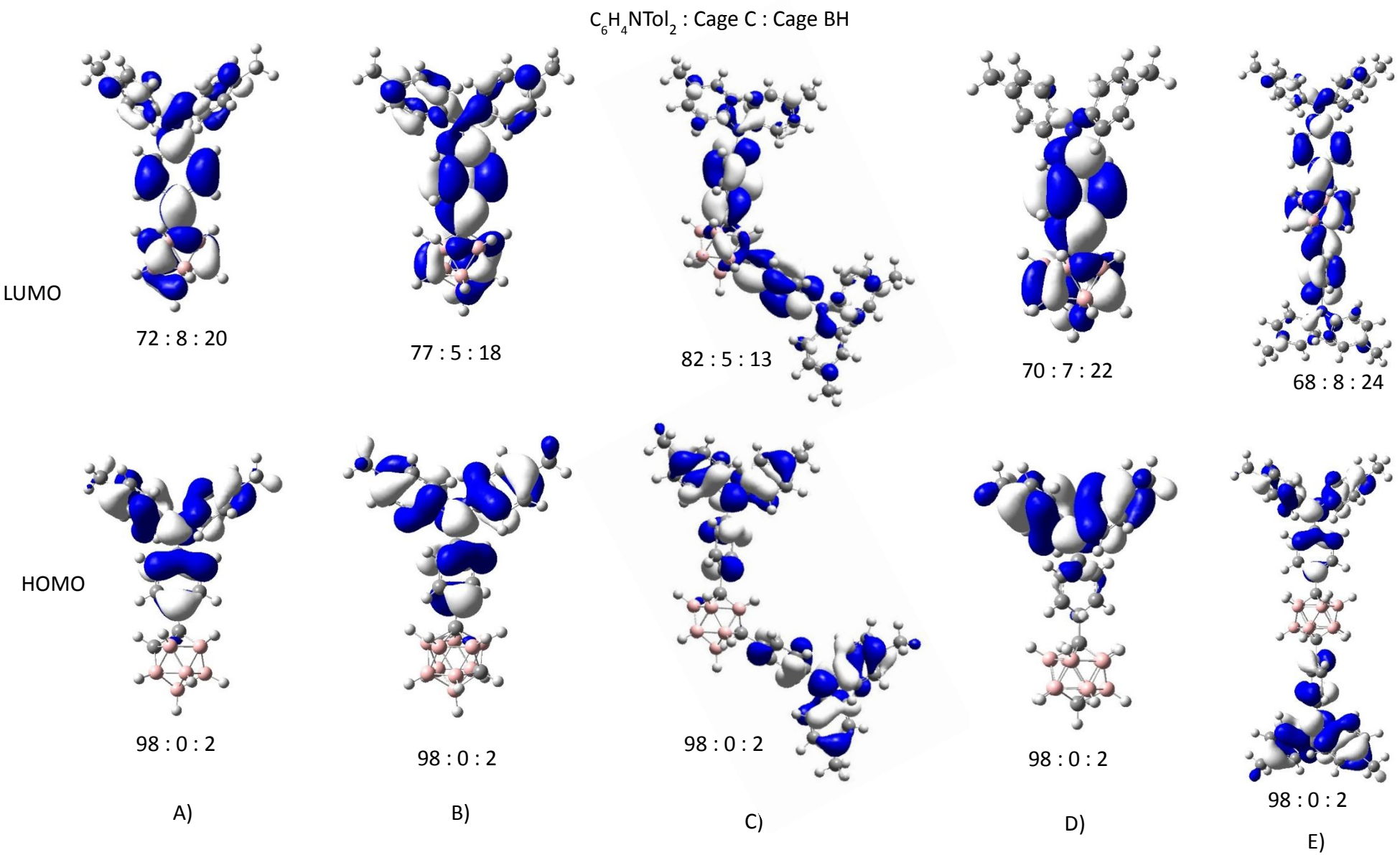

Figure 3–12: DFT (B3LYP/6-31G*) calculated molecular orbital contributions to the HOMO and LUMO of A) 5, *ortho* mono, B) 4, *meta* mono, C) 3, *meta* di, D) 2, *para* mono and E) 1, *para* di.

The barrier to rotation about the C-C bond between the carborane cage and the triarylamine group for **5**, is less than 1 kcal/mol, allowing for free rotation at room temperature. This is a similar barrier to that observed in the case of *ortho* phenyl carborane, which is to be expected due to the structural similarities. The barrier to rotation for *ortho* mono naphthyl carborane is greater, at 3 kcal/mol (chapter 2), whilst still allowing free rotation at room temperature. This is in agreement with the suggestion that there is a smaller degree of steric hindrance for **5**, which could allow a greater flexibility of the cage C-C bond than in the case of *ortho* mono naphthyl carborane, leading to a greater degree of fluorescence quenching in solution for **5**.

Using TD-DFT, S_1 excited state optimised geometries of the carboranyl triarylamines were found. The *ortho* mono substituted carborane has a cage C-C bond length of 2.443 Å. This means that the carborane cage has a more open geometry than in the case of the *meta* and *para* isomers where the carborane cage remains closed on excitation. Accordingly, in the excited state, the carborane cage has a greater predicted electron density for the *ortho* isomer than for the *meta* and para. The energy gap on emission for the *ortho* is also calculated to be much smaller than that which we find for the *meta* and *para* isomers, accounting for the difference in the Stokes shifts seen for the *ortho* and the *meta* and *para*, Figure 3–13. The calculated absorption and emission spectra are in good agreement with those observed. *Para* carboranyl triarylamine has a calculated absorption maximum at 329 nm and emission maximum at 375 nm. *Ortho* carboranyl triarylamine, in contrast, has a calculated absorption maximum at 330 nm and emission at 548 nm.

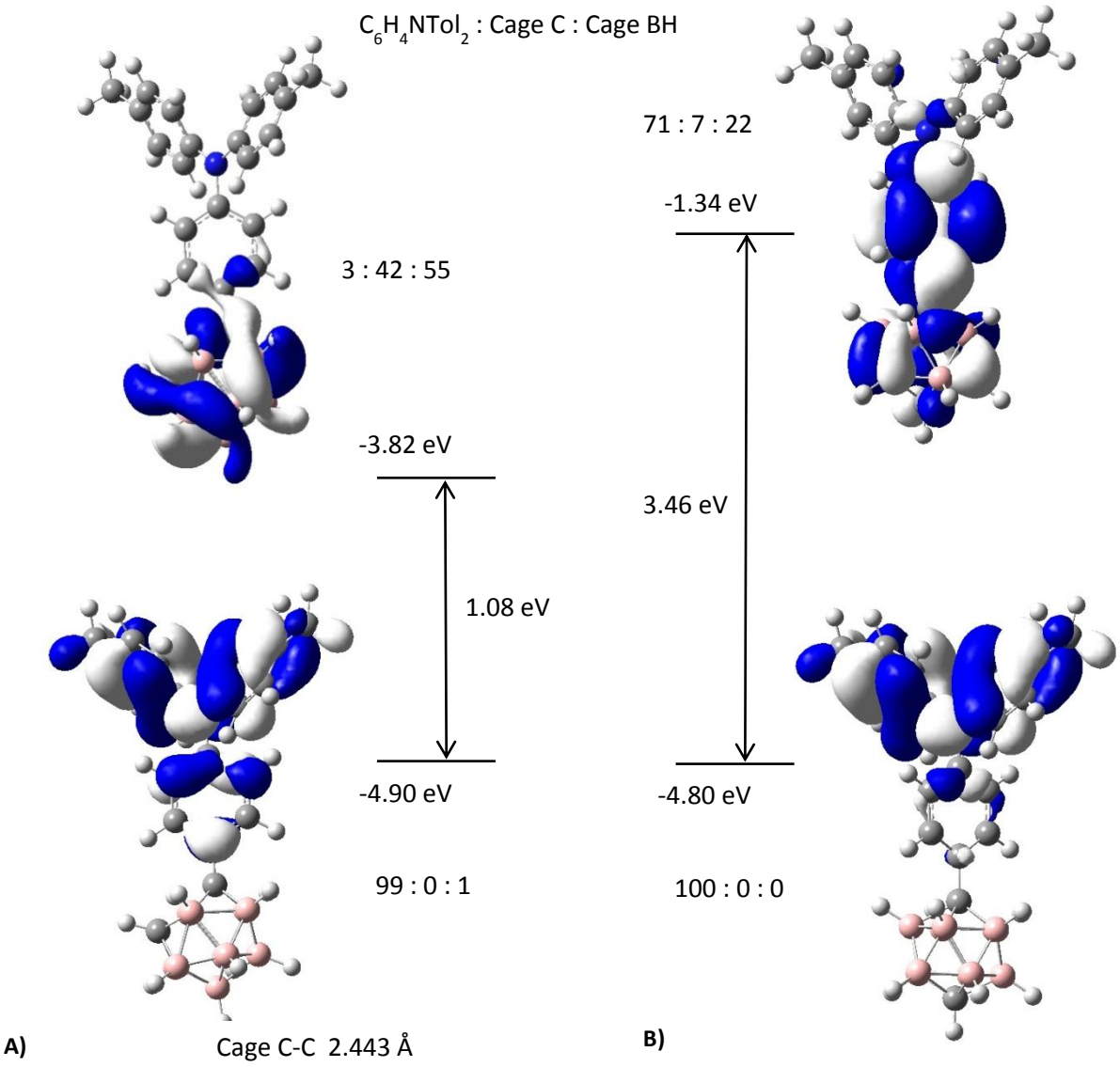

Figure 3–13: TD-DFT (B3LYP/6-31G*) calculated HOMO and LUMO of the S_1 excited states for A) *ortho* mono and B) *para* mono carboranyl triarylamines.

3.5 Conclusions

The electron withdrawing nature of the carborane cage is seen to give rise to a bathochromic shift in the absorption and emission properties of *meta* and *para* carboranyl triarylamines. The *meta* and *para* carborane cages are also found to increase the thermal stability and quantum yields of the parent triarylamines. The *ortho* carborane cage has a striking effect on the emission properties of the triarylamines due to the flexibility of the carborane cage C-C bond. In solution there is quenching of the emission, but when forming aggregates, there is fluorescent emission with a large Stokes shift (18800 cm^{-1}). TD-DFT calculations have confirmed that in the excited state the *ortho* carborane cage opens up, with a longer cage C-C bond, and so there is a greater electron density on the carborane cage, giving rise to a lower energy excited state than for the closed cage *meta* and *para* carboranes and hence a lower energy charge transfer transition to the ground state.

3.6 Experimental

Experimental conditions, reagent preparation, equipment and computational studies are the same as those detailed in section 2.5. Quantum yields were measured using an integrating sphere, as described in the literature.[6]

3.6.1 Preparation of $C_6H_4NTol_2$.[7]

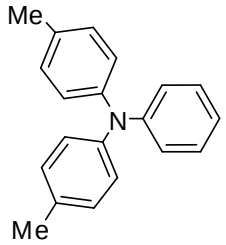

4-Iodotoluene (20 g, 92 mmol), aniline (4.2 ml, 46 mmol), 1,10-phenanthroline (0.4 g, 2.2 mmol), CuCl (0.32 g) and o-xylene (30 ml) were mixed in a round bottomed flask with an overhead stirrer and reflux condenser, under N_2. The mixture was stirred for 30 mins at 130 °C. Powdered KOH was added to the reaction mixture, which was then heated to reflux overnight. The solution was neutralised with 2 M acetic acid and filtered. The filtrate was poured into water and the aqueous layer was extracted with DCM. The organic layers were combined, washed with water (3 x 50 ml) and dried over $MgSO_4$. The solvent was removed under reduced pressure. The resulting solid was passed through a silica plug with hexane, giving an off white solid (2.46 g, 9 mmol, 20 %), melting point 90 °C

^{1}H (400 MHz, $CDCl_3$): δ 2.31 (3H, s), 6.77 (2H, d, J 9.2), 6.97 (4H, d, J 8.4), 7.07 (4H d, J 8.0), 7.45 (2H, d, J 8.8).

^{13}C (100 MHz, $CDCl_3$): δ 20.9 (CH), 121.8 (CH), 123.2 (CH), 124.8 (CH), 129.2 (CH), 130.1 (CH), 132.4 (C), 145.6 (C), 148.5 (C).

IR (υ_{max}/cm^{-1}) 2918w (aryl C-H stretch), 1482s (aryl C=C), 1269s (C-N).

% CHN Anal. Calcd for $C_{20}H_{19}N$ requires C, 87.87; H, 7.01; N, 5.12. Found C, 87.45; H, 7.10; N, 5.12.

3.6.2 Preparation of 4-$IC_6H_4NTol_2$.[8]

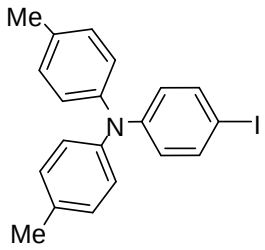

Di-p-tolylphenylamine (2.46 g, 9 mmol), NIS (2.48 g, 11 mmol) and acetic acid (20 ml) were stirred in chloroform (30 ml) in air with the exclusion of light at room temperature for 18 hours. The reaction mixture was then poured into water (10 ml) and washed with 10 % sodium thiosulfate solution. DCM was added and the organic phase was washed with water followed by drying over $MgSO_4$. The solvent was then removed and the solid was purified with a silica plug, eluting with hexane to give the product as a white solid (1.5 g, 4mmol, 40 %), melting point 90 °C.

^{1}H (400 MHz, $CDCl_3$) δ 2.31 (3H, s), 6.77 (2H, d, J 9.2), 6.97 (4H, d, J 8.4), 7.07 (4H d, J 8.0), 7.45 (2H, d, J 8.8).

^{13}C (100 MHz, $CDCl_3$): δ 19.8 (CH), 82.4 (C), 123.1 (CH), 123.8 (CH), 129.0 (CH), 132.1 (C), 136.8 (CH), 143.8 (C), 147.1 (C).

IR (υ_{max}/cm^{-1}) 2918w (aryl C-H stretch), 1482s (aryl C=C), 1269s (C-N).

% CHN Anal. Calcd for $C_{20}H_{18}NI$ C, 60.16; H, 4.54; N, 3.51. Found C, 60.57; H, 4.72; N, 3.47.

3.6.3 Preparation of 1,12-(4'-$C_6H_4NTol_2$)$_2$-1,12-$C_2B_{10}H_{10}$

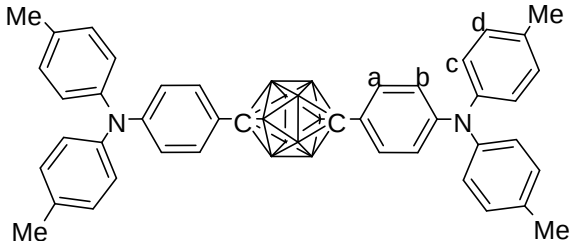

1,12-$C_2B_{10}H_{12}$ (0.63 g, 4.3 mmol) was dissolved in dry DME (15 ml) with stirring, under nitrogen. The solution was cooled in an ice bath and *n*-BuLi (8 ml, 1.51 M in hexanes, 10 mmol) was added dropwise. Cooling was removed and the solution was heated to 40 °C for 60 mins. Pyridine (3 ml) and CuCl (1 g, 10 mmol) were added. The reaction mixture was heated to 40 °C for 60 mins. 4-$IC_6H_4NTol_2$ (3.4 g, 8.6 mmol) was added. The solution was heated to reflux for 66 hours. The reaction mixture was allowed to cool and then poured over Et_2O (200 mL) with stirring. The green precipitate which formed was filtered off and the filtrate was washed with HCl (2 M) then dried over $MgSO_4$. The yellow solid was passed through a silica plug eluting with hexane, giving mainly mono substituted product, and then DCM, separating the disubstituted product. A substantial amount of the mono substituted product was obtained but could not be isolated. The disubstituted product was filtered, washing with hexane, and a white solid was filtered off, 1,12-(4'-C_6H_4N(4''-$CH_3C_6H_4$)$_2$)$_2$-1,12-$C_2B_{10}H_{10}$ (460 mg, 0.7 mmol, 16 %), melting point 289 °C.

^{11}B (128 MHz, $CDCl_3$): δ -12.4 (10B, d, J 161).

^{1}H{^{11}B} (700 MHz, $CDCl_3$): δ 2.29 (12H, s, CH_3), 2.57 (10H, s, cage BH), 6.73 (4H, d, $CH_{a/b}$, J 8.4), 6.94 (8H, d, $CH_{c/d}$, J 9.1), 6.98 (4H, d, $CH_{a/b}$, J 9.1), 7.04 (8H, d, $CH_{c/d}$, J 8.4).

^{13}C (100 MHz, $CDCl_3$): δ 21.2 (CH_3), 82.7 (cage C), 120.6 ($CH_{a/b}$), 125.6 ($CH_{c/d}$), 128.1 ($CH_{a/b}$), 129.1 (C), 130.4 ($CH_{c/d}$), 133.6 (C), 145.1 (C), 148.7 (C).

MS (low res. ASAP) $^{12}C_{42}{}^{1}H_{46}{}^{14}N_2{}^{11}B_8{}^{10}B_2$ FW = 686 g/mol. M^+ = m/z 687 (with typical carborane pattern at 680-690).

IR: (ν_{max}/cm^{-1}): 3020w (aromatic CH), 2604m (BH), 1604m, 1503s, 1321s, 1271s, 1198m, 1185m, 1081s, 1014m, 813s, 715m, 683w, 564m, 514s, 499m.

% CHN Anal. Calcd for $C_{42}B_{10}H_{46}N_2$ C, 73.42; H, 6.75; N, 4.08. Found C, 71.70; H, 6.68; N 3.94.

3.6.4 Preparation of 1-(4'-$C_6H_4NTol_2$)-1,12-$C_2B_{10}H_{11}$

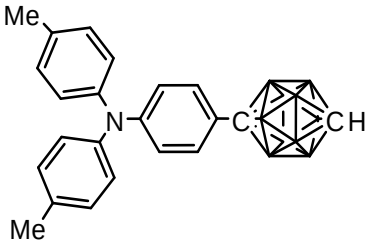

1,12-$C_2B_{10}H_{12}$ (0.18 g, 1.25 mmol) was dissolved in dry DME (5 ml) with stirring, under nitrogen. The solution was cooled in an ice bath and *n*-BuLi (1.6 ml, 1.6 M in hexanes, 2.5 mmol) was added dropwise. The cooling was removed and the solution was heated to 40 °C for 60 mins. Pyridine (0.8 ml) and CuCl (0.13 g, 1.25 mmol) were added. The reaction mixture was heated to 40 °C for 60 mins. 4-$IC_6H_4NTol_2$ (0.50 g, 1.25 mmol) was added. The solution was heated to reflux for 16 hours. The reaction mixture was allowed to cool and then poured over Et_2O (200 mL) with stirring. The green precipitate which formed was filtered off and the filtrate was washed with HCl (2 M) and then dried over $MgSO_4$. The product was then purified by column chromatography eluting with 1:1 DCM:hexane, giving 1-(4'-$C_6H_4NTol_2$)-1,12-$C_2B_{10}H_{11}$ (0.07 g, 0.17 mmol, 14 %).

^{11}B (128 MHz, $CDCl_3$): δ -15.0 (5B, d, J 165), -12.2 (5B, d, J 165).

^{1}H {^{11}B} (400 MHz, $CDCl_3$): δ 2.29 (5H, s, BH), 2.32 (6H, s), 2.54 (5H, s, BH), 2.75 (1H, s, cage CH), 6.76 (2H, d, J 12.0), 6.97 (6H, m), 7.07 (4H, d, J 8.0).

^{13}C (100 MHz, $CDCl_3$): δ 59.2 (cage CH), 86.9 (cage C), 120.3 (CH), 125.3 (CH), 127.7 (CH), 130.1 (CH), 133.3 (C), 144.8 (C), 148.4 (C).

MS (low res. ASAP) $^{12}C_{22}{}^{1}H_{29}{}^{14}N^{11}B_8{}^{10}B_2$ FW = 415 g/mol. M^+ = m/z 415 (with typical carborane pattern at 411-418).

IR: (ν_{max}/cm^{-1}):2920w (aryl CH stretch), 2602s (B-H), 1604m (aryl C=C), 1502s (aryl C=C), 1268s (C-N).

% CHN Anal. Calcd for $C_{22}B_{10}H_{29}N$ C,63.58; H,7.03; N,3.37. Found C,63.66 ; H, 7.24; N, 3.20.

3.6.5 Preparation of 1,7-(4'-$C_6H_4NTol_2)_2$-1,7-$C_2B_{10}H_{10}$

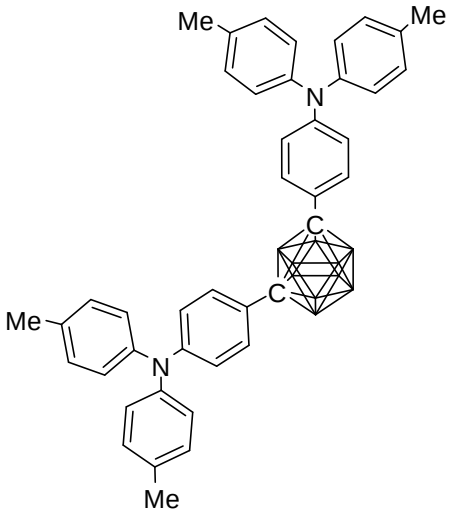

1,7-$C_2B_{10}H_{12}$ (0.18 g, 1.25 mmol) was dissolved in dry DME (5 mL) with stirring under nitrogen. The solution was cooled in an ice bath and *n*-BuLi (1.6 mL, 1.6 M in hexanes, 2.5 mmol) was added dropwise. The cooling was removed and the solution was heated to 40 °C and allowed to stir for 45 mins. The mixture was cooled in an ice bath followed by the addition of pyridine (0.8 mL) and CuCl (0.25 g, 2.5 mmol). The reaction mixture was then heated to 40 °C and stirred for 60 mins. The solution was cooled in an ice bath followed by the addition of $Tol_2NC_6H_4I$ (1 g, 2.5 mmol). The solution was heated to reflux for 16 hours. The reaction mixture was allowed to cool and then poured over Et_2O with stirring. The precipitate which formed was filtered and the filtrate was then added to water (10 mL) followed by dilute hydrochloric acid (2 mL), and the two phases were separated. The organic phase was then washed with water (3 x 10 mL) before the solvent and remaining pyridine were removed under reduced pressure, leaving a dark orange/brown oil which was then purified by column chromatography, eluting with 1:1 DCM : hexane. The resulting solid was then recrystallised from DCM/EtOH, yielding 1,7-(4'-$C_6H_4NTol_2)_2$-1,7-$C_2B_{10}H_{10}$ as a white solid (0.32 g, 0.48 mmol, 38%), melting point 194 °C.

^{11}B (128 MHz, $CDCl_3$):δ -10.6 (10 B, broad overlapped peaks).

^{1}H{^{11}B} (400 MHz, $CDCl_3$):δ 2.32 (6H, s), 2.49 (8H, s, BH), 3.16 (2H, s, BH), 6.82 (2H, d, J 8.0), 6.99 (4H, d, J 12.0), 7.08 (4H, d, J 8.0), 7.22 (2H, d, J 8.0).

^{13}C (100 MHz, $CDCl_3$):δ 21.0 (CH), 120.5 (CH), 125.3 (CH), 127.6 (C), 128.5 (CH), 130.2 (CH), 133.5 (C), 144.8 (C), 148.7 (C).

MS (low res. ASAP) $^{12}C_{42}{}^{1}H_{46}{}^{14}N_2{}^{11}B_8{}^{10}B_2$ FW = 686 g/mol. M^+ = m/z 686 (with typical carborane pattern at 680-690).

% CHN Anal. Calcd for $C_{42}B_{10}H_{46}N_2$ C, 73.4; H, 6.75; N, 4.08. Found: C, 69.28; H, 6.79; N, 3.77.

IR (υ_{max}/cm^{-1}): 2585m (B–H), 1603m (aryl C=C), 1502s (aryl C=C), 1271s (C-N).

3.6.6 Preparation of 1-(4'-$C_6H_4NTol_2$)-1,7-$C_2B_{10}H_{11}$

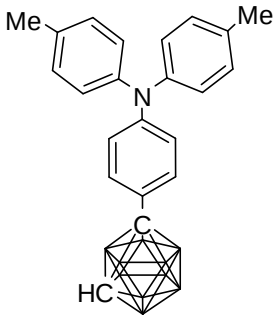

1,7-$C_2B_{10}H_{12}$ (0.83 g, 5.76 mmol) was dissolved in dry DME (15 mL) with stirring under nitrogen. The solution was cooled in an ice bath and *n*-BuLi (4 mL, 1.6 M in hexanes, 6.4 mmol) was added dropwise. The cooling was removed and the solution was heated to 40 °C and allowed to stir for 45 mins. The mixture was cooled in an ice bath followed by the addition of pyridine (3.5 mL) and CuCl (0.58 g, 5.9 mmol). The reaction mixture was heated to 40 °C for 60 mins. The mixture was cooled in an ice bath and 4-$IC_6H_4NTol_2$ (2.45 g, 6.1 mmol) was added. The solution was heated to reflux for 16 hours. The reaction mixture was allowed to cool and then poured over Et_2O (200 mL) with stirring. The green precipitate which formed was filtered off and the filtrate was washed with HCl (2 M) and then dried over $MgSO_4$. The solvent was removed under reduced pressure. The resulting oil was transferred to a round-bottomed flask, to which $Pd(PPh_3)_4$ (0.2 g, 0.2 mmol), CuI (0.04 g, 0.2 mmol) and triethylamine (150 mL, degassed using the freeze-pump-thaw method) were added under nitrogen. The mixture was stirred for 30 mins, after which TMSA (2.5 mL) was added and the reaction mixture was heated to reflux overnight. The mixture was cooled to room temperature and filtered, after which the solvent was removed under reduced pressure. The carborane and the silated amine were then separated by column chromatography eluting in hexanes followed by a slowly increasing ratio of DCM : hexane (up to 1:1) once the first product had been removed from the column, yielding yellow/white crystals of 1-(4'-$C_6H_4NTol_2$)-1,7-$C_2B_{10}H_{11}$ (0.63 g, 1.5 mmol, 26 %), melting point 135 °C.

^{11}B (128 MHz, $CDCl_3$): δ -15.1 (2B, d, J 204), -13.5 (3B, d, J 172), -10.5 (4B, d, J 148), -3.9 (1B, d, J 160).

^{1}H{^{11}B} (400MHz, $CDCl_3$): δ 2.19 (2H, s, BH), 2.26 (4H, s, BH), 2.32 (3H, s), 2.51 (2H, s,

BH), 2.66 (2H, s, BH), 2.95 (2H, s, BH), 3.03 (1H, s, cage CH), 6.81 (2H, d, J 8.0), 6.98 (4H, d, J 8.0), 7.08 (4H, d, J 12.0), 7.17 (2H, d, J 12.0).

^{13}C (100 MHz, $CDCl_3$): δ 21.0 (CH), 55.0 (C), 100.1 (C), 120.4 (CH), 125.4 (CH), 127.3 (C), 128.5 (CH), 130.2 (CH), 133.5 (C), 144.8 (C), 148.8 (C).

MS (low res. EI) $^{12}C_{22}{}^{1}H_{29}{}^{14}N^{11}B_8{}^{10}B_2$ FW = 415 g/mol. M^+ = m/z 415 (with typical carborane pattern at 410-419).

% CHN Anal. Calcd $C_{22}B_{10}H_{29}N$ C, 63.58; H,7.03; N,3.37. Found: C 63.21, H 7.09, N 3.14.

IR: (υ_{max}/cm^{-1}): 3050w (aryl C-H stretch), 2594b (B-H), 1601m (aryl C=C), 1503s (aryl C=C), 1269s (C-N).

3.6.7 Preparation of 1-(4'-$C_6H_4NTol_2$)-1,2-$C_2B_{10}H_{11}$

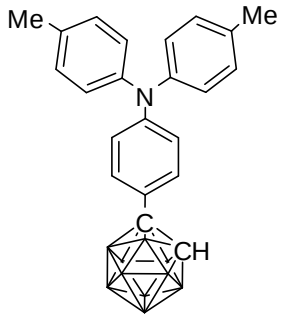

1,2-$C_2B_{10}H_{12}$ (0.83 g, 5.76 mmol) was dissolved in dry DME (15 ml) with stirring, under nitrogen. The solution was cooled in an ice bath and *n*-BuLi (4 ml, 1.6 M in hexanes, 6.4 mmol) was added dropwise. The cooling was removed and the solution was heated to 40 °C for 45 mins. Pyridine (3.5 ml) and CuCl (0.58 g, 5.9 mmol) were added. The reaction mixture was heated to 40 °C for 45 mins. 4-IC6H4NTol2 (2.45 g, 6.1 mmol) was added. The solution was heated to reflux for 16 hours. The reaction mixture was allowed to cool and then poured over Et_2O (200 mL) with stirring. The green precipitate which formed was filtered off and the filtrate was washed with HCl (2 M), and then dried over $MgSO_4$. Unreacted *ortho* carborane was removed by sublimation. The product 1-(4'-$C_6H_4NTol_2$)-1,2-$C_2B_{10}H_{11}$ was purified by column chromatography, eluting with hexane, as a white powder (0.52 g, 1.25 mmol, 22 %), melting point 187 °C.

^{11}B (128 MHz, $CDCl_3$): δ -12.7 (2B, d, J 150), -11.5 (2B, d, J 120), -10.6 (2B,d, J 180), -9.2 (2B, d, J 160), -4.9 (1B, d, J 120), -2.0 (1B, d, J 150).

^{1}H{^{11}B} (400MHz, $CDCl_3$): δ 2.25 (4H, s, BH), 2.33 (3H, s), 2.46 (4H, s, BH), 2.63 (2H, s, BH), 3.84 (1H, s, cage CH), 6.83 (2H, d, J 8.0), 6.99 (4H, d, J 8.0), 7.10 (4H, d, J 8.0), 7.24 (2H, d, J 8.0).

^{13}C (100 MHz, $CDCl_3$): δ 21.1 (CH), 61.3 (cage CH), 119.8 (CH), 124.6 (C), 125.8 (CH), 128.7 (CH), 130.4 (CH), 134.2 (C), 144.3 (C), 149.9 (C).

MS (low res. EI) $^{12}C_{22}{}^{1}H_{29}{}^{14}N{}^{11}B_8{}^{10}B_2$ FW = 415 g/mol. M^+ = m/z 415 (with a typical carborane pattern at 409-419).

% CHN Anal. Calcd $C_{22}B_{10}H_{29}N$ C, 63.58; H, 7.03; N, 3.37. Found C, 63.03; H, 7.04; N, 3.23.

IR (υ_{max}/cm^{-1}): 3046w (aryl C-H stretch), 2594b (B-H), 1600m (aryl C=C), 1503 (aryl C=C), 1270 (C-N).

3.7 References

1. Nuyken O., Jungermann S., Wiederhirn V., Bacher E. and Meerholz K., *Monatshefte für Chemie*, **2006**, 137, 811-824.
2. Thelakkat M., *Macromol. Mater. Eng.*, **2002**, 287, 442-461.
3. Chen J. P., Tanabe H., Li X-C., Thoms T., Okamura Y. and Ueno K., *Synthetic Metals*, **2003**, 132, 173-176.
4. Fox M. A. and Hughes A. K., *Coord. Chem. Rev.*, **2004**, 248, 457-476.
5. Aziz H., Popovic Z., Xie S., Hor A.-M., Hu N.-X., Tripp C. and Xu G., *Appl. Phys. Lett.*, **1998**, 72, 756-758.
6. Porrès L., Holland A., Pålsson L.-O., Monkman A. P., Kemp C. and Beeby A., *J. Fluoresc.*, **2006**, 16, 2, 267-272.
7. Marsden R. J. B., *J. Chem. Soc.*, **1937**, 627.
8. Plater J. M. and Jackson T., *Tetrahedron*, **2003**, 59, 4687–4692.

4 : Synthesis and Fluorescence of Bridged Carboranes

4.1 Introduction

Some of the carborane compounds which have been reported to display fluorescent emission contain two or more carborane cages, as discussed in chapter 1. Bridged carboranes, such as those in Figure 4–1, have been reported in the literature but their photophysical properties have not been reported.[1,2,5]

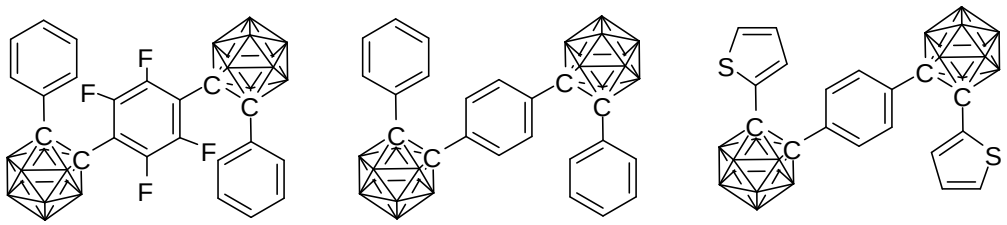

Figure 4–1: Known carboranes of the type (1-R-1,2-$C_2B_{10}H_{10}$)$_2$X, where R is Ph or C_4SH_2 and X is C_6F_4 or C_6H_4.

We set out to synthesise some bridged carboranes, Figure 4–2, with some different R and X groups. Their syntheses are discussed here. Many of these were found to exhibit fluorescence.

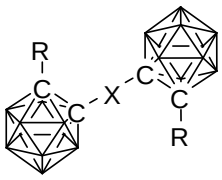

Figure 4–2: Template of carboranes synthesised here, of the type (1-R-1,2-$C_2B_{10}H_{10}$)$_2$X.

4.2 Syntheses

A Sonogashira cross coupling reaction between diiodobiphenyl and phenylacetylene gave 4,4'-bis(phenylethynyl)-1,1'-biphenyl.

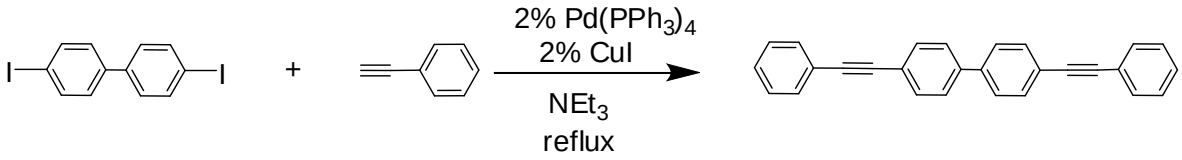

Figure 4–3: Synthesis of 4,4'-(CC-Ph)-1,1'-$(C_6H_4)_2$.

This was then reacted with a decaborane derivative to give 4,4'-bis(phenyl-*ortho*-carborane)-1,1'-biphenyl in a 16 % yield.

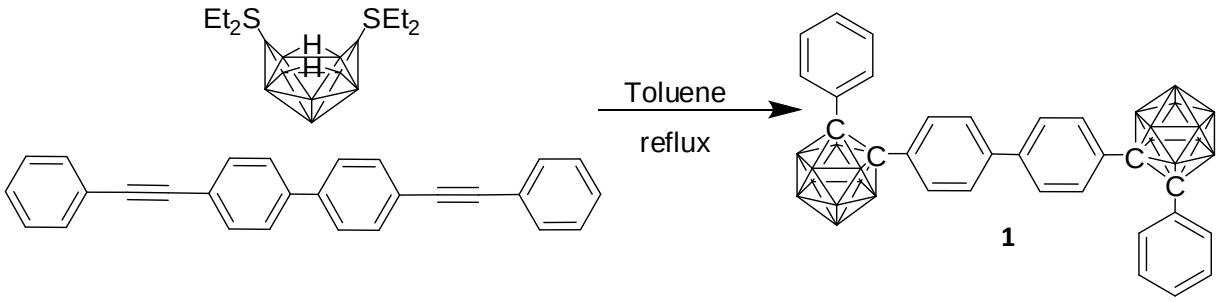

Figure 4–4: Synthesis of 4,4'-(1''-Ph-1'',2''-$C_2B_{10}H_{10})_2$-1,1'-$(C_6H_4)_2$.

Similarly, a Sonogashira reaction between dibromothiophene and phenylacetylene gave 2,5-bis(phenylethynyl)thiophene.

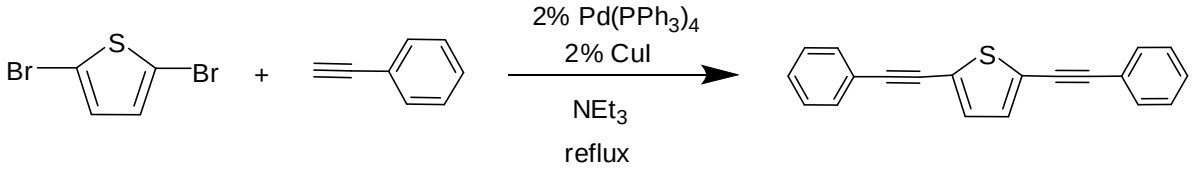

Figure 4–5: Synthesis of 2,5-$(CC\text{-}Ph)_2$-C_4SH_2.

This was then reacted with the decaborane derivative to give the product, 2,5-bis(1-phenyl-*ortho*-carboranyl)thiophene in a very low yield (6 %).

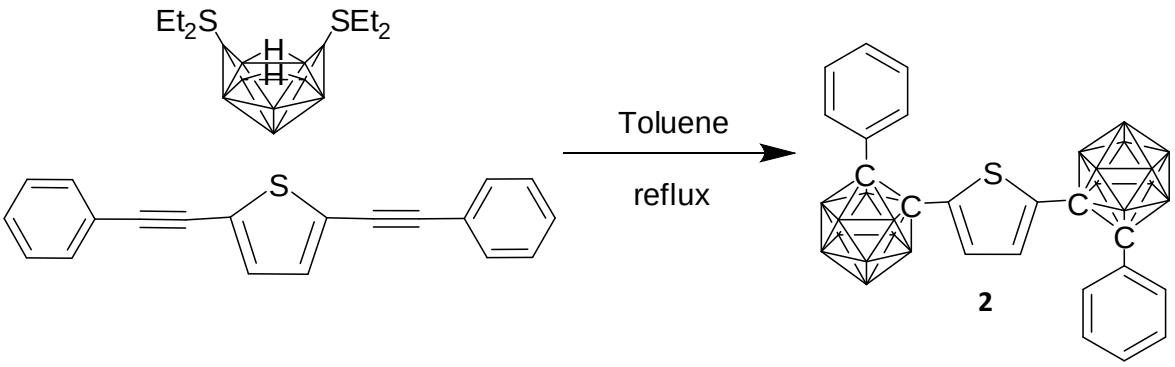

Figure 4–6: Synthesis of 2,5-(1'-Ph-1',2'-$C_2B_{10}H_{10}$)$_2$-C_4SH_2.

1,4-(1'-(4''-^{t}Bu-C_6H_4)-1',2'-$C_2B_{10}H_{10}$)$_2$-C_6H_4 was synthesised by reacting 1,4-bis(^{t}butyl-phenylethynyl)benzene with the decaborane derivative.

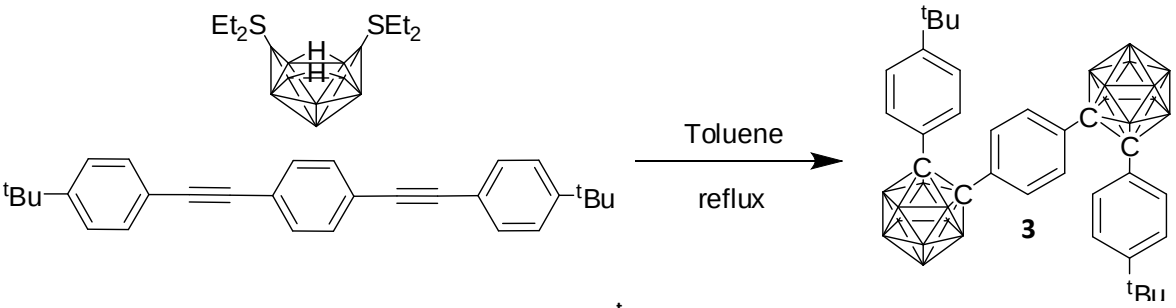

Figure 4–7: Synthesis of 1,4-(1'-(4''-^{t}Bu-C_6H_4)-1',2'-$C_2B_{10}H_{10}$)$_2$-C_6H_4.

To bridge two *ortho* carboranyl triarylamines with a phenylene group, the procedure in Figure 4–8 is followed to synthesise the required alkyne. An Ullmann reaction is used to synthesise 4-BrC_6H_4NTol_2, which is then reacted with TMSA in a Sonogashira reaction. The TMS group is then removed, followed by a Sonogashira reaction, coupling two HC≡C(C_6H_4)NTol_2 molecules to 1,4-diiodophenylene to give 1,4-(C≡C(C_6H_4)NTol_2)$_2$-C_6H_4.

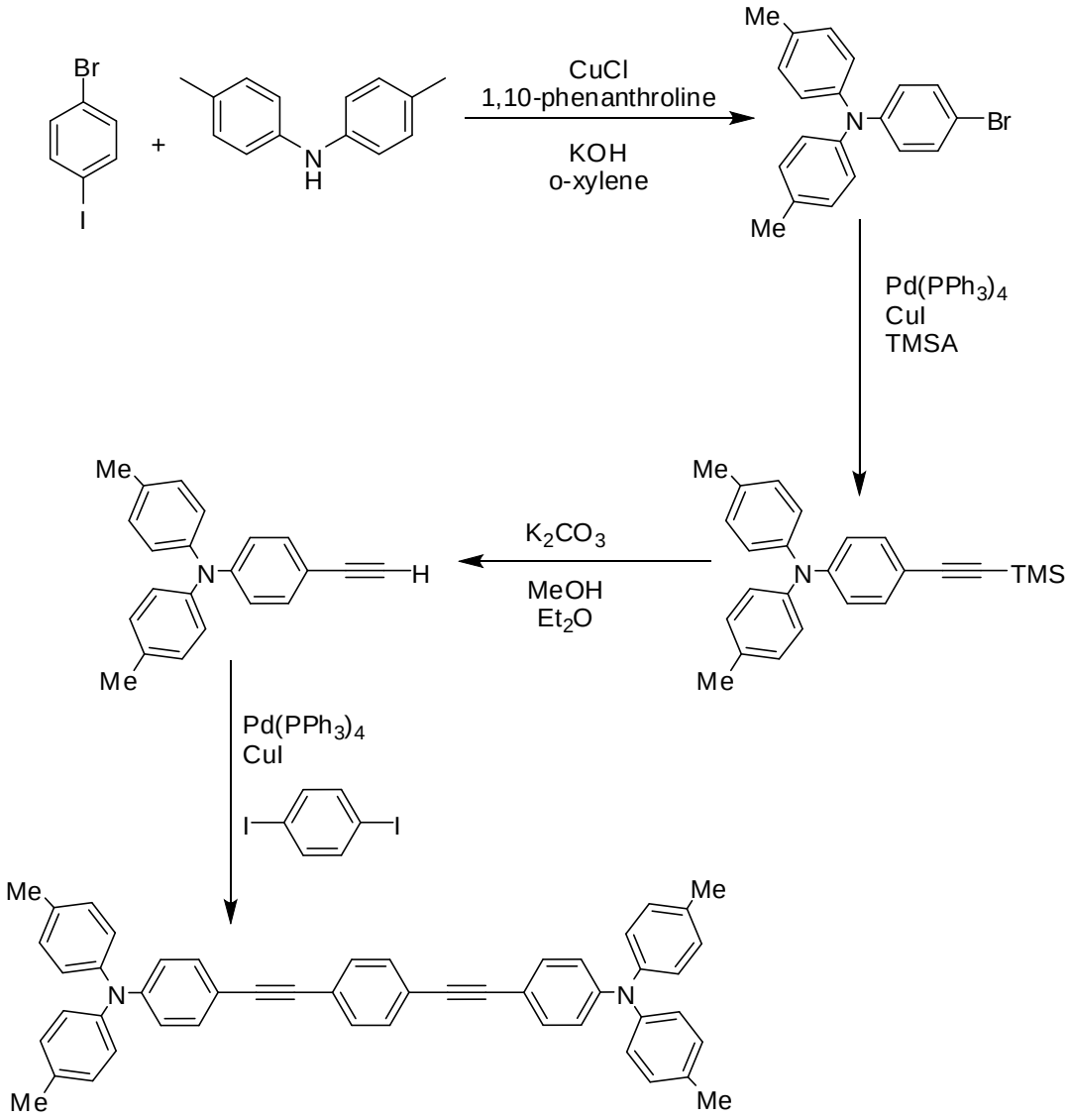

Figure 4–8: Synthetic route to 1,4-(C≡C(C_6H_4)NTol$_2$)$_2$-C_6H_4.

This alkyne is then reacted with the decaborane derivative to give 1,4-(1'-(4''-(NTol$_2$)C_6H_4)-1',2'-$C_2B_{10}H_{10}$)$_2$-C_6H_4 in a 15 % yield.

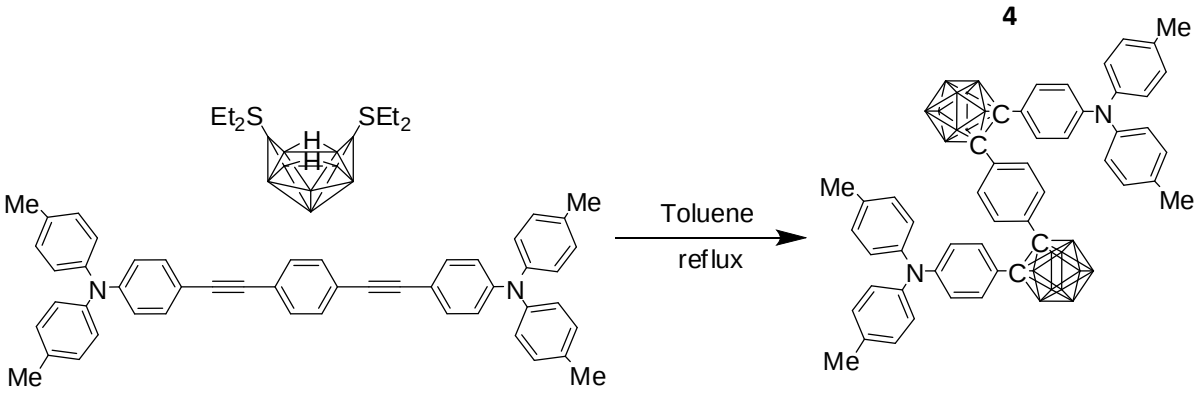

Figure 4–9: Synthesis of 1,4-(1'-$C_6H_4NTol_2$-1',2'-$C_2B_{10}H_{10}$)$_2$-C_6H_4.

The tetrafluorobenzene bridged triarylamine carborane can be synthesised more simply, as shown in Figure 4–10, in a yield of 38 %. Two equivalents of *ortho* mono carboranyl triarylamine, synthesised as described in chapter 3, were lithiated at the acidic cage CH, followed by the addition of one equivalent of hexafluorobenzene.

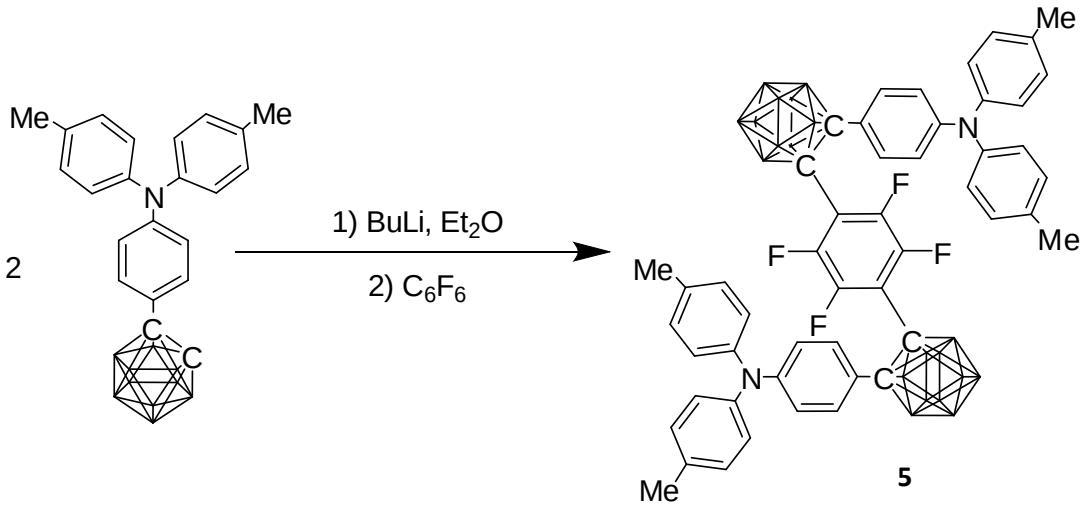

Figure 4–10: Synthesis of 1,4-(1'-$C_6H_4NTol_2$-1',2'-$C_2B_{10}H_{10}$)$_2$-C_6F_4.

A naphthyl substituted bridged carborane system was synthesised, analogous to the already reported compound 1,4-(C_6H_5-1,2-$C_2B_{10}H_{10}$)$_2$-C_6F_4.[2] 1,4-(1'-$C_{10}H_7$-1',2'-$C_2B_{10}H_{10}$)$_2$-C_6F_4 was synthesised from 1-(1'-$C_{10}H_7$)–1,2-$C_2B_{10}H_{11}$, as reported in chapter 2, by lithiating the unsubstituted carbon of the cage using

butyllithium, followed by the addition of hexafluorobenzene, to give the product in a 19 % yield.

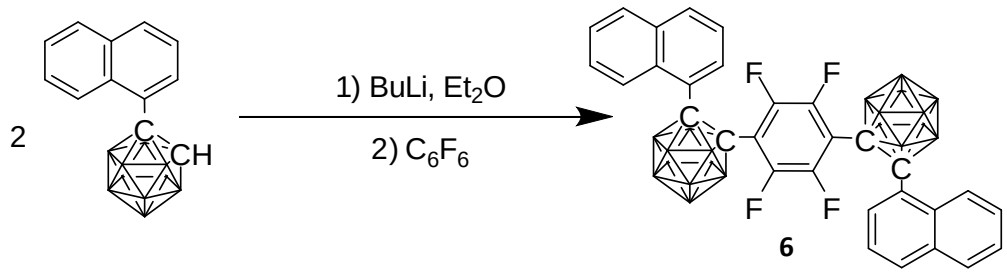

Figure 4–11: Synthesis of 1,4-(1'-$C_{10}H_7$-1',2'-$C_2B_{10}H_{10}$)$_2$-C_6F_4.

4.3 X-ray crystallography

Crystals suitable for X-ray diffraction were obtained for compounds **1**, **2**, **3**, **4** and **6**, with molecular structures shown in Figure 4-12 to 4-16. Figure 4–16 shows the molecular structures observed in the crystal of 1,4-(1'-$C_{10}H_7$-1',2'-$C_2B_{10}H_{10}$)$_2$-C_6F_4, where two conformations (i and ii) are observed. In all cases the cage C-C bond length is greater than that observed for the unsubstituted *ortho* carborane cage due to steric interactions between the groups substituted onto the cage C atoms. Compounds **2**, **3**, **4** and **6**(ii) have an inversion centre through the centre of their bridging groups, leading to identical cage C-C bond lengths for the two cages (A and B) in these compounds.

Compound		C(1)-C(2) Bond length (Å)	
		Cage A	Cage B
4,4'-(1''-Ph-1'',2''-$C_2B_{10}H_{10})_2$-1,1'-$(C_6H_4)_2$	**1**	1.786(2)	1.7280(19)
2,5-(1'-Ph-1',2'-$C_2B_{10}H_{10})_2$-C_4SH_2	**2**	1.7231(19)	1.7231(19)
1,4-(1'-(4''-^{t}Bu-C_6H_4)-1',2'-$C_2B_{10}H_{10})_2$-C_6H_4	**3**	1.729(4)	1.729(4)
1,4-(1'-(4''-(NTol$_2$)C_6H_4)-1',2'-$C_2B_{10}H_{10})_2$-C_6H_4	**4**	1.7119(19)	1.7119(19)
1,4-(1'-$C_{10}H_7$-1',2'-$C_2B_{10}H_{10})_2$-C_6F_4	**6**(i)	1.797(5)	1.795(5)
1,4-(1'-$C_{10}H_7$-1',2'-$C_2B_{10}H_{10})_2$-C_6F_4	**6**(ii)	1.782(6)	1.782(6)

Table 4–1:Cage carbon-carbon bond lengths for the bridged carboranes.

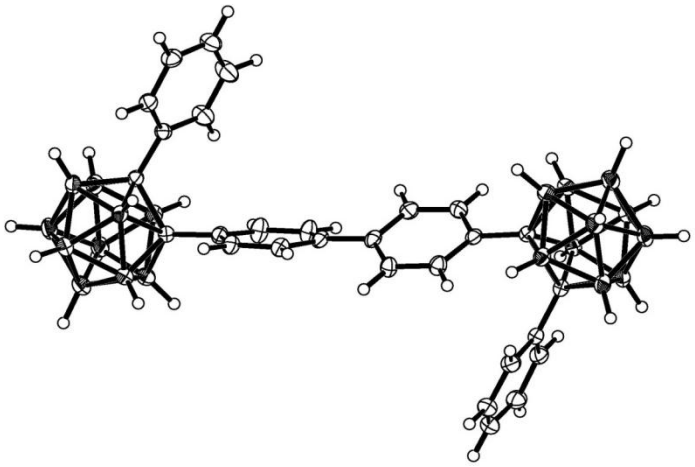

Figure 4–12: Molecular structure of 1, 4,4'-(1''-Ph-1'',2''-$C_2B_{10}H_{10})_2$-1,1'-$(C_6H_4)_2$.

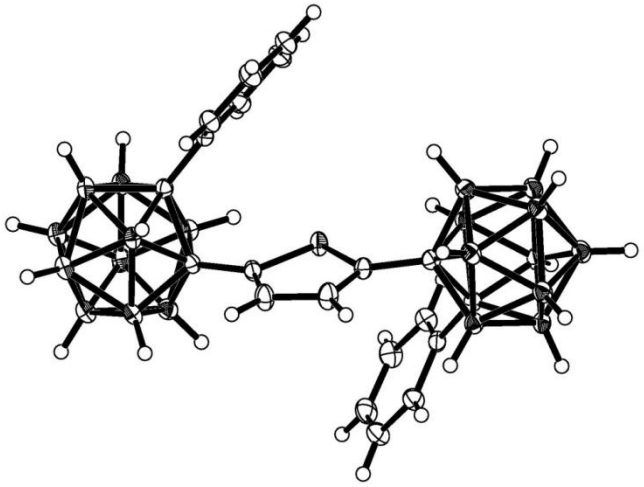

Figure 4–13: Molecular structure of 2, 2,5-(1'-Ph-1',2'-$C_2B_{10}H_{10}$)$_2$-C_4SH_2.

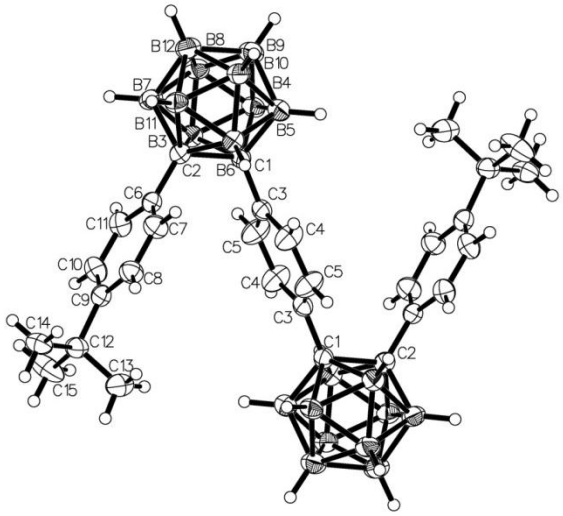

Figure 4–14: Molecular structure of 3, 1,4-(1'-(4''-^{t}Bu-C_6H_4)-1',2'-$C_2B_{10}H_{10}$)$_2$-C_6H_4.

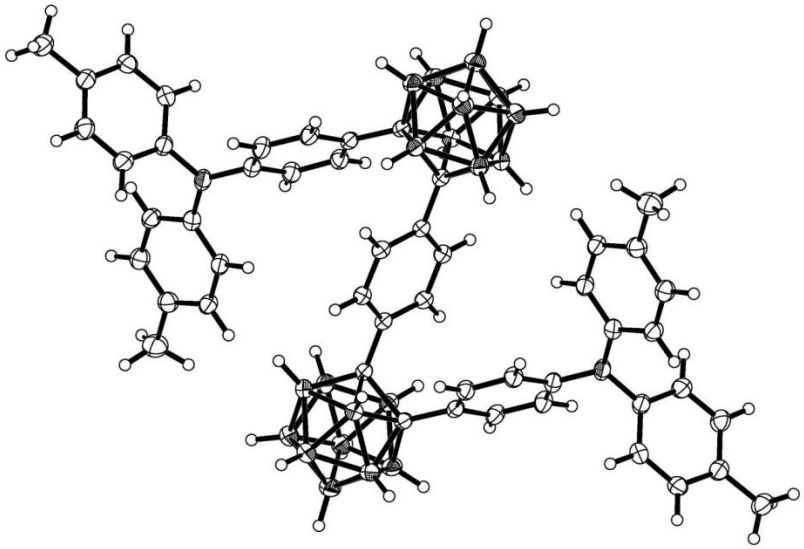

Figure 4–15: Molecular structure of 4, 1,4-(1'-($C_6H_4NTol_2$)-1',2'-$C_2B_{10}H_{10}$)$_2$-C_6H_4.

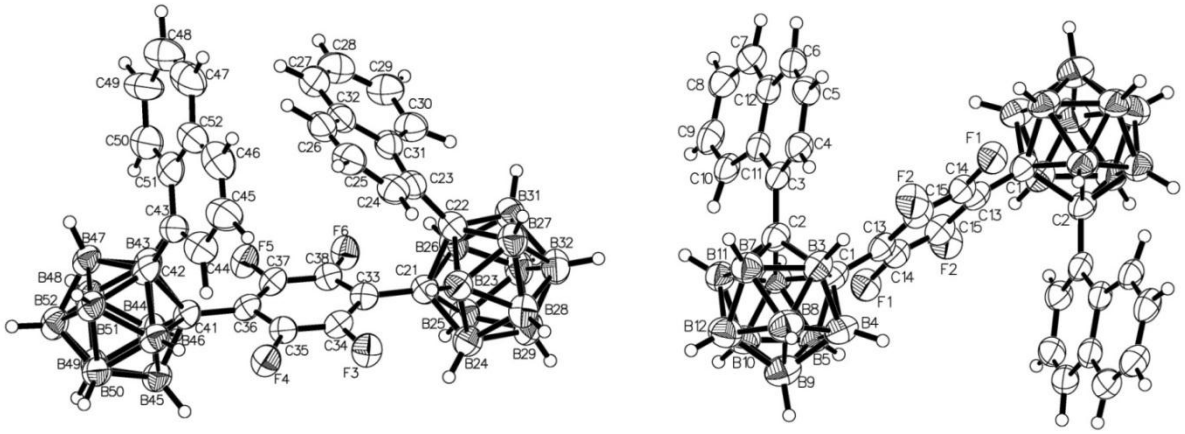

i) **ii)**

Figure 4–16: Molecular structure of 6, 1,4-(1'-$C_{10}H_7$-1',2'-$C_2B_{10}H_{10}$)$_2$-C_6F_4, in two conformations i) and ii).

4.3.1 Calculations

Optimised geometries of these carboranes found by DFT (B3LYP/6-31G*) are in line with those observed. The calculated cage C-C bond lengths for some bridged carboranes are shown in Table 4–2. In all of these compounds we see an extended cage C-C bond length compared to the parent *ortho* carborane molecule, in agreement with the observed bond lengths. Compounds **1** – **5** have conformations

such that the dihedral angles, C_3-C_1-C_1'-C_3' in Table 4–2, are close to 180 ° such that the R groups on the two carborane cages are as far away as possible, reducing steric interactions. The barrier to rotation for compounds **1** and **3** are calculated to be low, at 2.3 and 2.2 kcalmol^{-1} respectively, allowing free rotation at room temperature in solution. Compounds **2**, **4** and **5** have greater energy barriers to rotation, preventing the free rotation of the carborane cages with respect to each other. **2** has a barrier of 8.4 kcalmol^{-1}. In **4** and **5** it is not possible to decrease the dihedral angle (C_3-C_1-C_1'-C_3') beyond 50 ° as the triarylamine groups would intercept after this point.

Two conformations were observed for 1,4-(1'-$C_{10}H_7$-1,2-$C_2B_{10}H_{10}$)$_2$-C_6F_4, Figure 4–17. Both geometries were found to be energy minima. Calculations show that, as expected, ii) is the most thermodynamically stable by 1.0 kcalmol^{-1}, with the two naphthyl groups at maximum separation. The barrier to rotation between these two conformations is 3.5 kcalmol^{-1}, rotating around the C_2-C_4 bond.

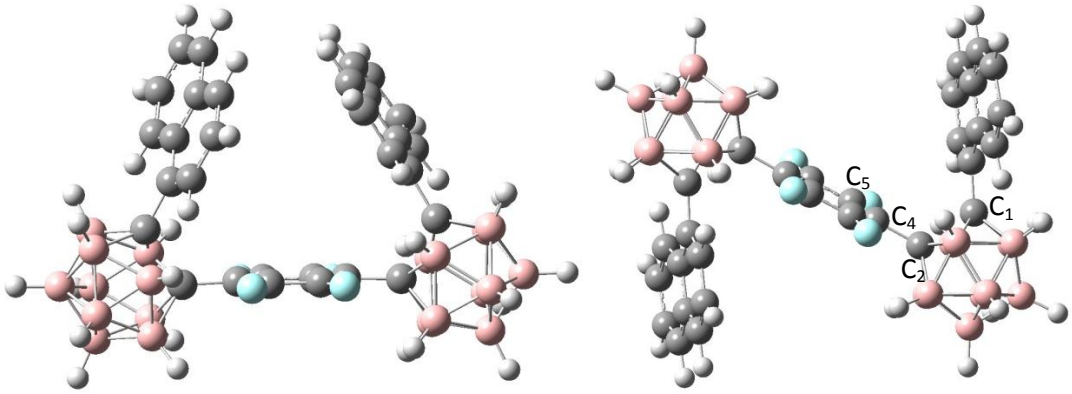

i) ii)

Figure 4–17: DFT calculated (B3LYP/6-31G*) conformations of 1,4-(1'-$C_{10}H_7$-1',2'-$C_2B_{10}H_{10}$)$_2$-C_6F_4

Compound		C(1)-C(2) Bond length (Å)		Dihedral angle C_3-C_1-C_1'-C_3' (°)
		Cage A	Cage B	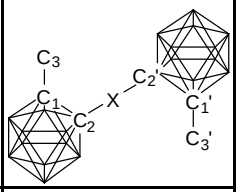
4,4'-(1'-Ph-1',2'-$C_2B_{10}H_{10})_2$-1,1'-$(C_6H_4)_2$	**1**	1.75665/ 1.7386(19)	1.75636/ 1.7280(19)	179
2,5-(1'-Ph-1',2'-$C_2B_{10}H_{10})_2$-C_4SH_2	**2**	1.76997	1.76997	176
1,4-(1-(4'-^{t}Bu-Ph)-1,2-$C_2B_{10}H_{10})_2$-C_6H_4	**3**	1.76228	1.76235	180
1,4-(1'-$(C_6H_4NTol_2)$-1',2'-$C_2B_{10}H_{10})_2$-C_6H_4	**4**	1.78281	1.78178	178
1,4-(1'-$(C_6H_4NTol_2)$-1',2'-$C_2B_{10}H_{10})_2$-C_6F_4	**5**	1.83344	1.83254	179
1,4-(1'-$C_{10}H_7$-1,2-$C_2B_{10}H_{10})_2$-C_6F_4	**6** i)	1.84357	1.88484	22
1,4-(1'-$C_{10}H_7$-1,2-$C_2B_{10}H_{10})_2$-C_6F_4	**6** ii)	1.84929	1.84476	178

Table 4–2: Selected bond lengths and angles of DFT calculated (B3LYP/6-31G*) optimised geometries of bridged carboranes.

4.4 Fluorescence

We found that some of these compounds exhibited fluorescence in the solid state when placed under a UV lamp. Because of this we decided to investigate the fluorescence of some bridged carborane compounds that have been previously synthesised, Figure 4–18: 7-10.[3,4,5,6]

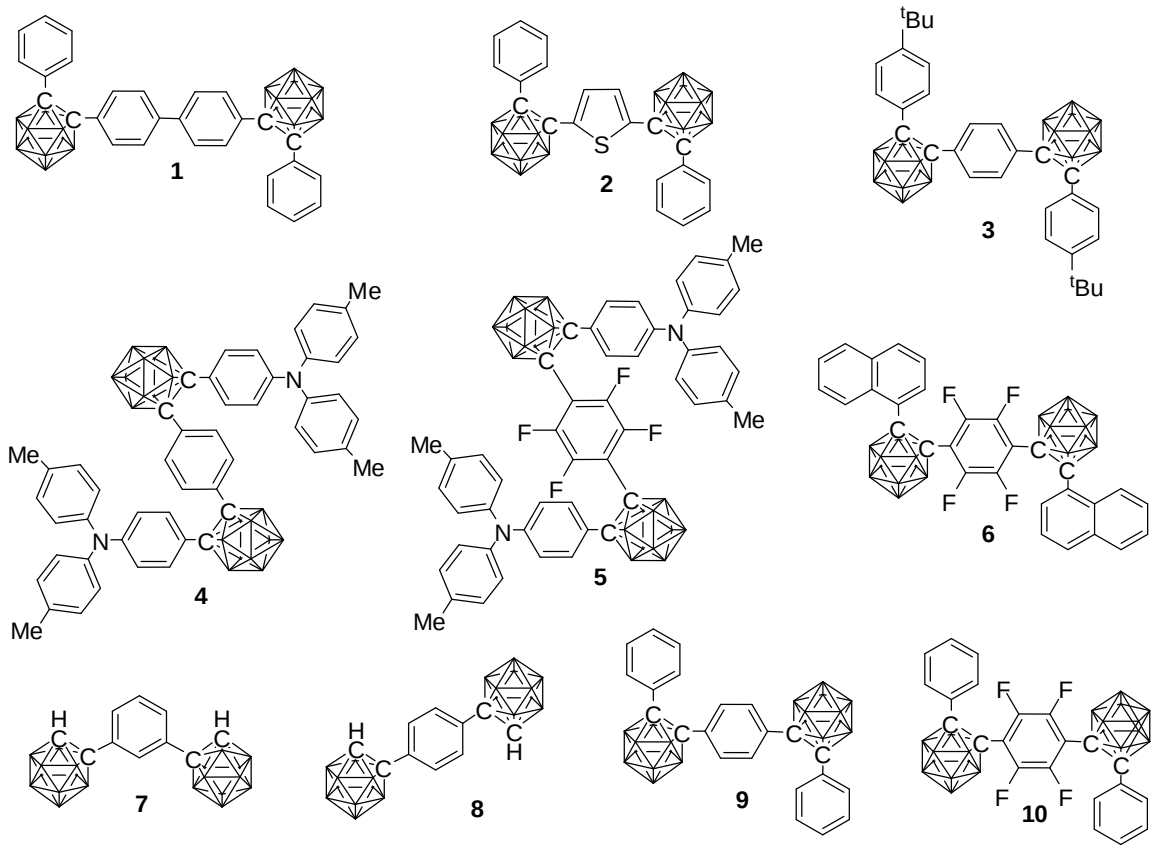

Figure 4–18 : Bridged carborane compounds investigated for fluorescence emission in DCM and 1:99 THF:H_2O solution.

The known bridged compounds we investigated did not exhibit fluorescence emission in solution. This is summarised in Table 4–3.

Compound		Solvent	
		DCM	THF : H_2O
4,4'-(1'-Ph-1',2'-$C_2B_{10}H_{10})_2$-1,1'-$(C_6H_4)_2$	**1**	✓	✓
2,5-(1'-Ph-1',2'-$C_2B_{10}H_{10})_2$-C_4SH_2	**2**	×	✓
1,4-(1'-(4'-^{t}Bu-Ph)-1',2'-$C_2B_{10}H_{10})_2$-C_6H_4	**3**	×	×
1,4-(1'-($C_6H_4NTol_2$)-1',2'-$C_2B_{10}H_{10})_2$-C_6H_4	**4**	×	✓
1,4-(1'-($C_6H_4NTol_2$)-1',2'-$C_2B_{10}H_{10})_2$-C_6F_4	**5**	✓	✓
1,4-(1'-$C_{10}H_7$-1',2'-$C_2B_{10}H_{10})_2$-C_6F_4	**6**	✓	✓
1,3-(1',2'-$C_2B_{10}H_{11})_2$-C_6H_4 [3]	**7**	×	×
1,4-(1',2'-$C_2B_{10}H_{11})_2$-C_6H_4 [4,3]	**8**	×	×
1,4-(1'-Ph-1',2'-$C_2B_{10}H_{10})_2$-C_6H_4 [5]	**9**	×	×
1,4-(1'-Ph-1',2'-$C_2B_{10}H_{10})_2$-C_6F_4 [6]	**10**	×	×

Table 4–3: Summary of the data collected while testing for fluorescence of bridged carboranes in different solvents. ✓ - fluorescence observed, × - fluorescence not observed.

In Table 4–4 the absorption and emission data for the compounds found to exhibit fluorescence are summarised. From highest to lowest energy, the compounds display absorption maxima in the order **2**>**1**>**6**>**5**>**4**. Emission is seen over a range of wavelengths, from 355 to 763 nm, Figure 4–19. From highest to lowest energy, the compounds display emission in the order **2**>**1**>**6**>**4**>**5**. It is to be expected that **4** and **5** display emission at lower energy than **6** as we showed in chapters 2 and 3 that *ortho* carboranyl triarylamine displayed emission at lower energy than the *ortho* naphthyl carborane. In chapter 2 we found that *ortho* mono and di phenyl carboranes did not display emission in solution. **1** and **3** contain this phenyl *ortho* carborane motif so we may expect similarities in properties. **3** was not emissive whereas **1** did display emission in solution.

Compound	Absorption maximum *			Excitation wavelength # (nm)	Emission maximum #		Stokes shift (cm^{-1})
	ε / mol^{-1} dm^3cm^{-1}	nm	cm^{-1}		nm	cm^{-1}	
4,4'-(1'-Ph-1',2'-$C_2B_{10}H_{10})_2$-1,1'-$(C_6H_4)_2$ **1**	147000	283	35300	310	491	20400	14900
1,4-(1'-(C_6H_5)-1',2'-$C_2B_{10}H_{10})_2$-C_4H_2S **2**	15200	269	37200	280	355	28200	9000
1,4-(1'-(4'-$NTol_2(C_6H_4)$)-1',2'-$C_2B_{10}H_{10})_2$-C_6H_4 **4**	31400	301, 348	33200, 28700	400	681	14700	14000
1,4-(1'-(4'-$NTol_2(C_6H_4)$)-1',2'-$C_2B_{10}H_{10})_2$-C_6F_4 **5**	51300	296, 327	33800, 30600	390	763	13100	17500
1,4-(1'-$C_{10}H_7$-1',2'-$C_2B_{10}H_{10})_2$-C_6F_4 **6**	22900	291	34300	250	590	16900	17400

Table 4–4: Absorption and fluorescence emission data for bridged compounds. * collected in THF. # collected in 1:99 THF:H_2O.

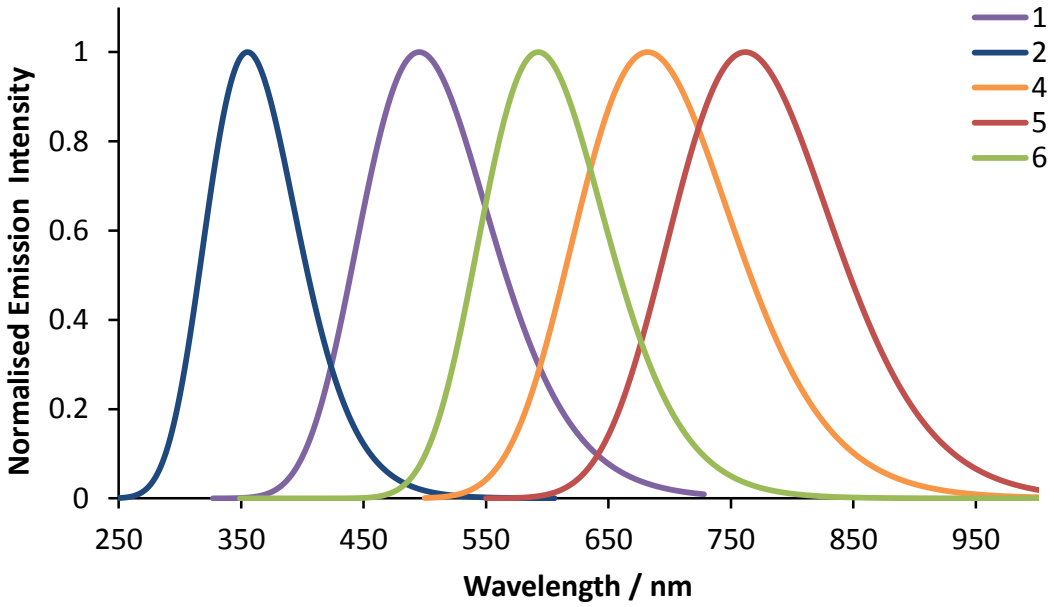

Figure 4–19: Normalised emission intensity for 1,2,4,5 and 6 in 1:99 THF:H_2O.

4.4.1 Calculations

Calculation of absorption and emission values can be carried out by two methods. Table 4–5 compares values taken from a calculation of the UV-vis spectrum and a wavelength derived from the HOMO LUMO gap, with the observed values. Both sets of absorption wavelength calculations correlate well with the observed trend. In the case of the predicted emission values, the frontier orbitals calculations give a trend in line with that observed. The UV-vis "emission" calculations are not in complete agreement with the trend observed.

Compound	Absorption / nm			Emission / nm		
	Observed	Frontier orbitals gap calculation	Calculated UV-vis maximum	Observed	Frontier orbitals gap calculation	Calculated UV-vis maximum
1	283	258	285	491	551	389
2	269	250	278	355	521	457
4	348	366	417	681	911	729
5	327	434	507	763	1051	779
6	291	334	387	590	561	677

Table 4–5: Observed and calculated absorption and emission values for bridged compounds 1,2,4,5 and 6.

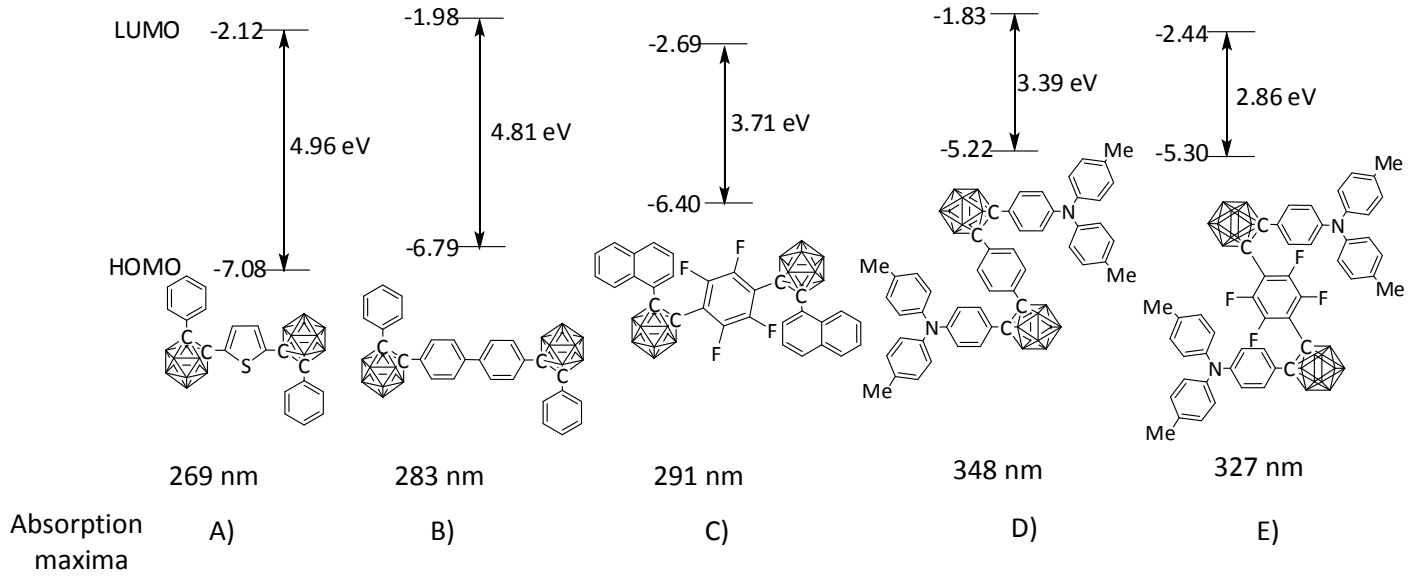

Figure 4–20: DFT calculated (B3LYP/6-31G*) HOMO and LUMO energy gaps for A) 1,4-(1'-(C_6H_5)-1',2'-$C_2B_{10}H_{10}$)$_2$-C_4H_2S, B) 4,4'-(1''-Ph-1'',2''-$C_2B_{10}H_{10}$)$_2$-1,1'-(C_6H_4)$_2$, C) 1,4-(1'-$C_{10}H_7$-1',2'-$C_2B_{10}H_{10}$)$_2$-C_6F_4, D) 1,4-(1'-($C_6H_4NTol_2$)-1',2'-$C_2B_{10}H_{10}$)$_2$-C_6H_4 and E) 1,4-(1'-($C_6H_4NTol_2$)-1',2'-$C_2B_{10}H_{10}$)$_2$-C_6F_4.

As can be seen in Figure 4–20, the calculated HOMO LUMO energy gaps are in order with the observed absorption. The largest HOMO LUMO gap corresponds to the highest energy absorption.

The HOMO and LUMO molecular orbitals, with the percentage contributions to the different groups, are shown in Figure 4–21. In the case of 1,4-(1-$C_{10}H_7$-1,2-$C_2B_{10}H_{10}$)-C_6F_4, the HOMO is based on the naphthyl R groups. On excitation to the LUMO there is a charge transfer such that the molecular orbitals are based on the carborane cage and the bridging X group. Similarly the carboranyl triarylamines bridged by C_6H_4 and C_6F_4 have a greater electron density on the carborane cages and bridging groups in the LUMO than in the triarylamine based HOMO. Conversely, the compounds with phenyl R groups have a HOMO based primarily on the bridging group, with a greater electron density on the carborane cage C atoms in the LUMO.

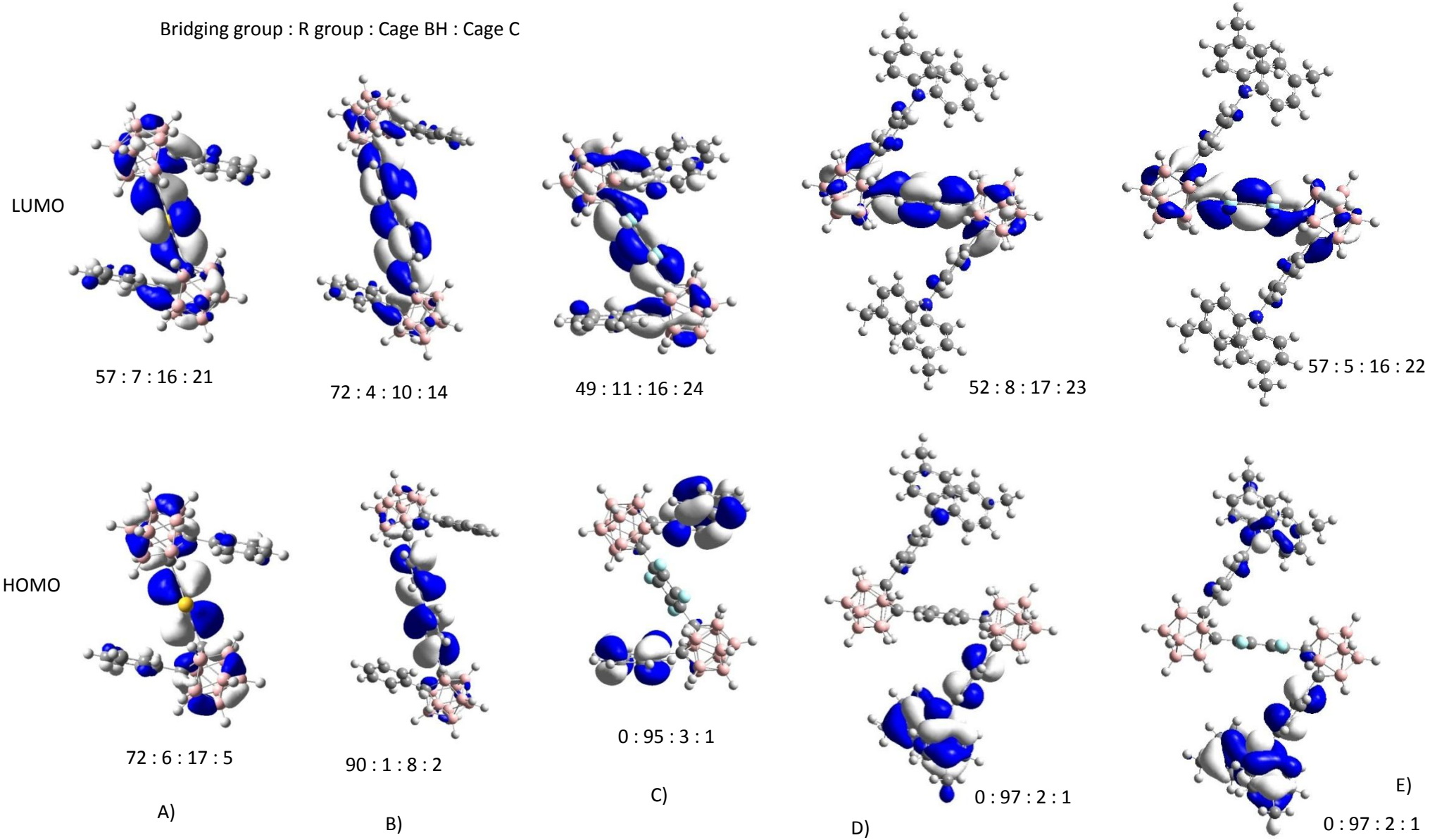

Figure 4–21: DFT calculated (B3LYP/6-31G*) HOMO and LUMO molecular orbitals for A) 1,4-(1'-(C_6H_5)-1',2'-$C_2B_{10}H_{10})_2$-C_4H_2S, B) 4,4'-(1''-Ph-1'',2''-$C_2B_{10}H_{10})_2$-1,1'-$(C_6H_4)_2$, C) 1,4-(1'-$C_{10}H_7$-1',2'-$C_2B_{10}H_{10})_2$-C_6F_4, D) 1,4-(1'-($C_6H_4NTol_2$)-1',2'-$C_2B_{10}H_{10})_2$-C_6H_4 and E) 1,4-(1'-($C_6H_4NTol_2$)-1',2'-$C_2B_{10}H_{10})_2$-C_6F_4.

The S_1 excited state geometry of 4,4'-(1''-Ph-1'',2''-$C_2B_{10}H_{10})_2$-1,1'-$(C_6H_4)_2$ is shown in Figure 4–22. On relaxation we expect a charge transfer transition from a carborane cage to the bridging biphenylene group. The cage calculated to have the greater electron density in the excited state also has an extended cage C-C bond length. The calculated energy gap of 2.25 eV is equivalent to 551 nm, which is in the same order as the observed emission at 491 nm.

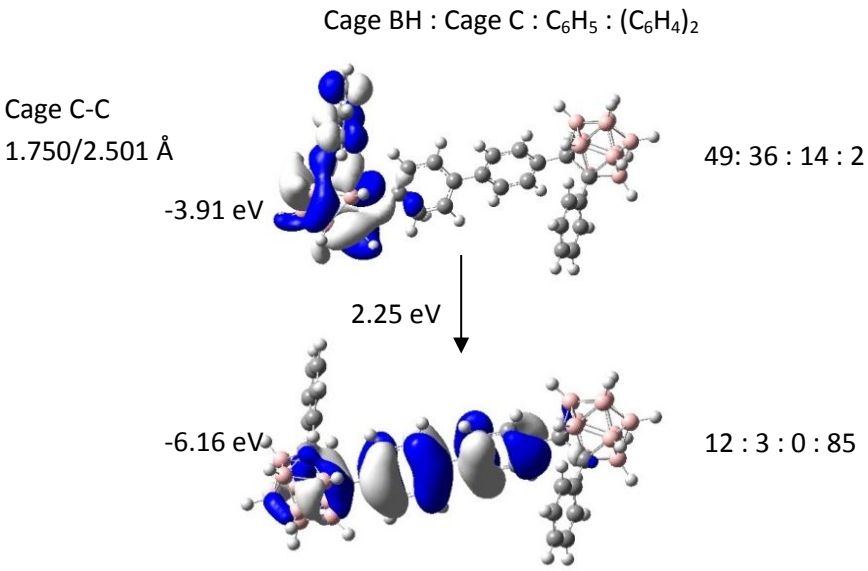

Figure 4–22: TD-DFT calculated (B3LYP/6-31G*) molecular orbital contributions to the S_1 excited state of 4,4'-(1''-Ph-1'',2''-$C_2B_{10}H_{10})_2$-1,1'-$(C_6H_4)_2$.

The S_1 excited state optimised geometry of 1,4-(1'-(C_6H_5)-1',2'-$C_2B_{10}H_{10})_2$-C_4H_2S is shown in Figure 4–23. Calculations predict that in the excited state the molecular orbitals are based primarily on the carborane cage and the bridging group, whilst after relaxation there is a shift in the position of the molecular orbitals to the phenyl group. The cage calculated to have the greater electron density displays an extended cage C-C bond length. The calculated energy gap for relaxation is 2.38 eV which corresponds to a wavelength of 521 nm.

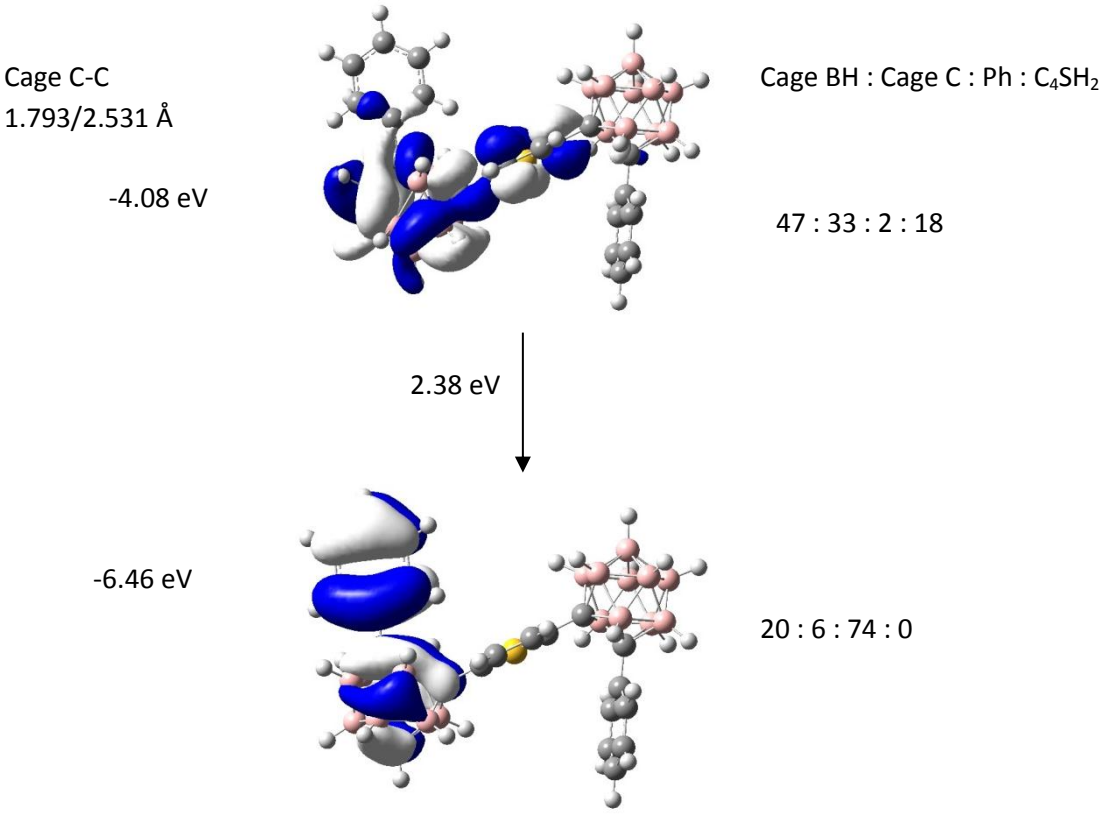

Figure 4–23: TD-DFT calculated (B3LYP/6-31G*) molecular orbital contributions to the S_1 excited state of 1,4-(1'-(C_6H_5)-1',2'-$C_2B_{10}H_{10}$)$_2$-C_4H_2S.

The S_1 excited state geometry of 1,4-(1'-($C_6H_4NTol_2$)-1',2'-$C_2B_{10}H_{10}$)$_2$-C_6H_4 is shown in Figure 4–24. In the excited state the molecular orbitals are primarily located on one of the carborane cages. On relaxation we expect the molecular orbitals to be based on one of the triarylamine groups. The carborane cage with the greater electron density in the excited state is found to have a longer carborane cage C-C bond length than the other. The predicted fluorescent emission of 1,4-(1'-($C_6H_4NTol_2$)-1',2'-$C_2B_{10}H_{10}$)$_2$-C_6H_4, 729 nm is in good agreement with the observed emission maximum wavelength of 681 nm.

The S_1 excited state geometry of the similar 1,4-(1'-($C_6H_4NTol_2$)-1',2'-$C_2B_{10}H_{10}$)$_2$-C_6F_4 is shown in Figure 4–25. The molecular orbital contributions, cage C-C bond lengths are very similar.

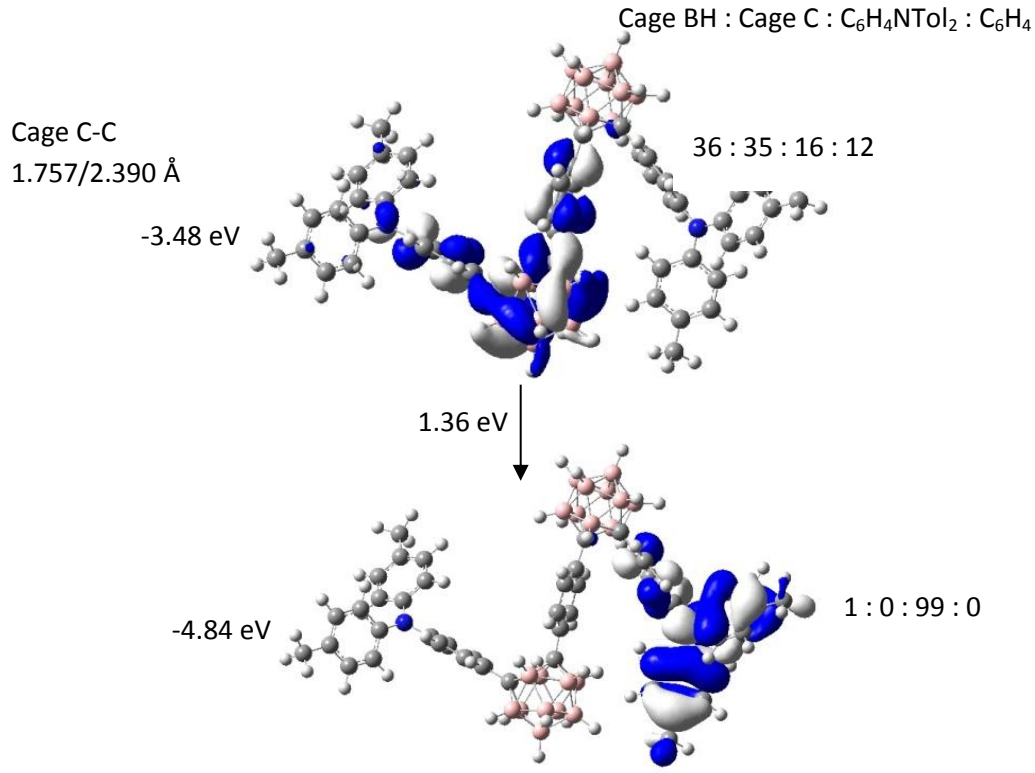

Figure 4–24: TD-DFT calculated (B3LYP/6-31G*) molecular orbital contributions to the S_1 excited state of 1,4-(1'-($C_6H_4NTol_2$)-1',2'-$C_2B_{10}H_{10}$)$_2$-C_6H_4.

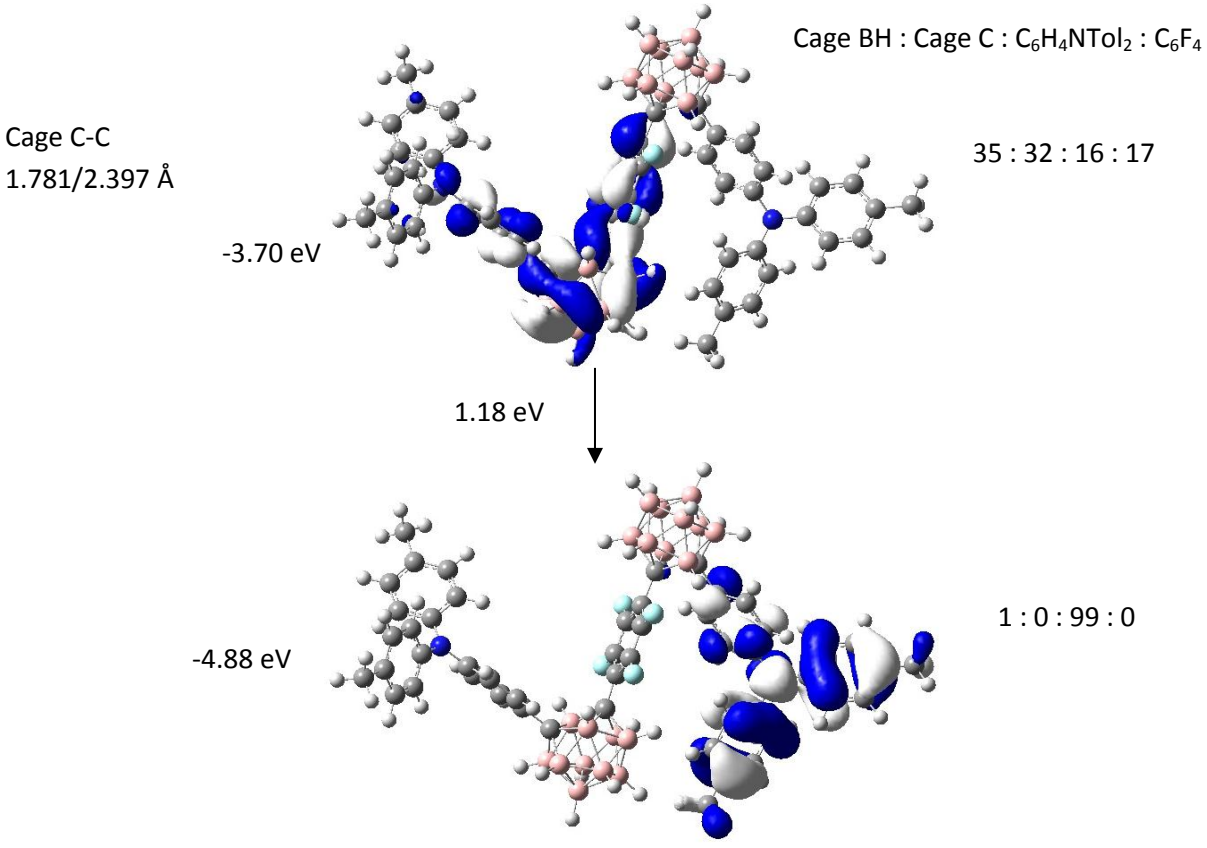

Figure 4–25: TD-DFT calculated (B3LYP/6-31G*) molecular orbital contributions to the S_1 excited state of 1,4-(1'-($C_6H_4NTol_2$)-1',2'-$C_2B_{10}H_{10}$)$_2$-C_6F_4.

The S_1 excited state geometry of 1,4-(1'-$C_{10}H_7$-1',2'-$C_2B_{10}H_{10}$)-C_6F_4 is shown in Figure 4-26. As before, calculations suggest that the emission is a charge transfer transition. In this case the excited state has molecular orbitals based on the carborane cage and bridging C_6F_4 group. In the relaxed state, molecular orbitals are based on the naphthyl R group. Both carborane cages are calculated to house the molecular orbitals in the excited state and as such both carborane cages are calculated to have extended cage C-C bond lengths.

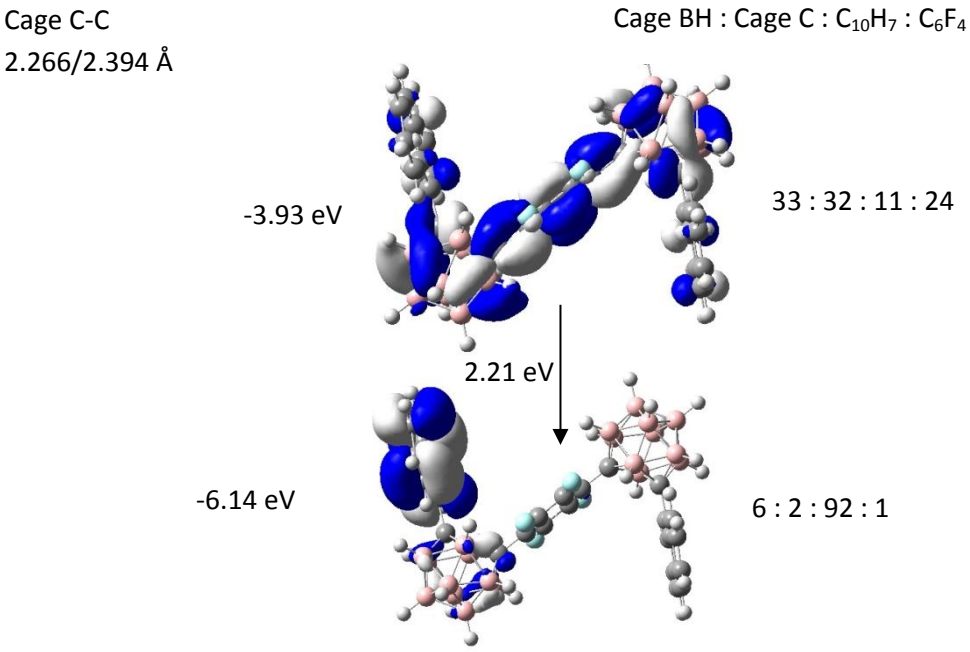

Figure 4–26: TD-DFT calculated (B3LYP/6-31G*) molecular orbital contributions to the S_1 excited state of 1,4-(1-$C_{10}H_7$-1,2-$C_2B_{10}H_{10}$)-C_6F_4.

For 1,4-(1'-$C_{10}H_7$-1',2'-$C_2B_{10}H_{10}$)-C_6F_4 two excited state optimised geometries are found which have different predicted emission wavelengths, Figure 4–27. The observed value of 590 nm is in between the two predicted values, Figure 4–28.

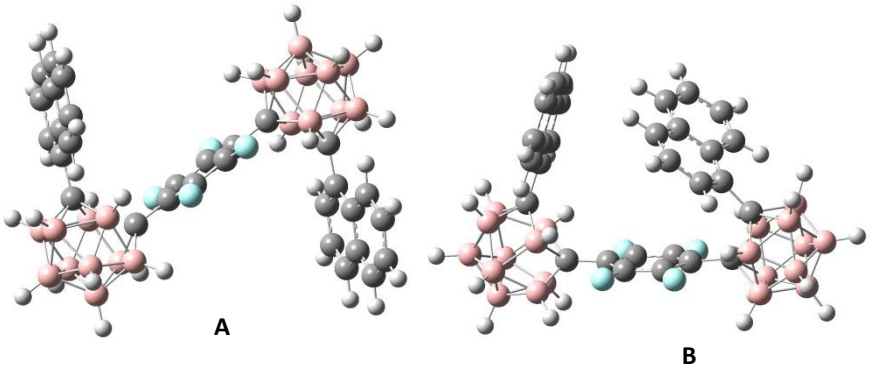

Figure 4–27: TD-DFT calculated (B3LYP/6-31G*) excited state optimised geometries of 1,4-(1-$C_{10}H_7$-1,2-$C_2B_{10}H_{10}$)-C_6F_4, A and B.

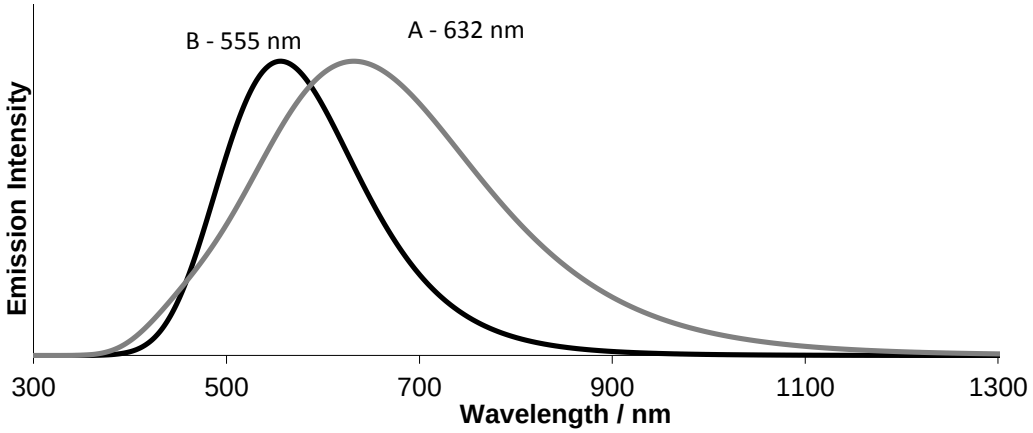

Figure 4–28: TD-DFT calculated (B3LYP/6-31G*) emission maxima for conformations A and B of 1,4-(1-$C_{10}H_7$-1,2-$C_2B_{10}H_{10}$)-C_6F_4.

4.5 Conclusions

A series of bridged carborane compounds of the type (1-R-1,2-$C_2B_{10}H_{10}$)$_2$-X have been synthesised and their photophysical properties have been investigated. Bridged carboranes, where R=Ph, X=(C_6H_4)$_2$/ R=Ph, X=C_4SH_2/ R=4'-$C_6H_4NTol_2$, X=C_6H_4/ R=4'-$C_6H_4NTol_2$, X=C_6F_4 or R=$C_{10}H_7$, X=C_6F_4, can be seen to undergo fluorescence emission. These compounds display emissions over a wide range of the visible spectrum, with maxima from 355 to 763 nm, varying as groups R and X are changed. DFT calculations suggest these molecules have extended carborane cage C-C bond lengths in the excited state, giving rise to charge transfer emissions.

4.6 Experimental

Experimental conditions, reagent preparation, equipment and computational studies are the same as those detailed in chapter 2.5.

4.6.1 Preparation of 4,4'-(C≡C-C_6H_5)$_2$-1,1'-(C_6H_4)$_2$.[7]

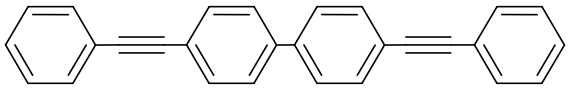

$Pd(PPh_3)_4$ (0.167 g, 0.24 mmol), copper iodide (0.098 g, 0.24 mmol), phenylacetylene (2.64 g, 26 mmol) and 4,4-diiodobiphenyl (5.00 g, 12 mmol) were added to degassed, dry triethylamine (20 ml). The reaction mixture was heated to reflux overnight. It was then allowed to cool to room temperature and was filtered. The grey solid was dissolved in DCM and washed with water, dried over $MgSO_4$ and then the solvent was removed under vacuum giving the product (3.52 g, 10 mmol, 83 %).

^{1}H (400 MHz, $CDCl_3$) δ 7.35 (m, 6H), 7.54 (m, 4H), 7.59 (s, 8H).

4.6.2 Preparation of 4,4'-(1''-C_6H_5-1'',2''-$C_2B_{10}H_{10}$)$_2$-1,1'-(C_6H_4)$_2$.

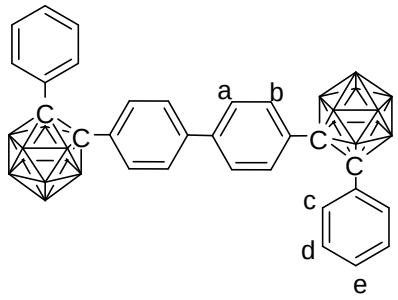

Bis(diethyl sulphide)decaborane (2.57 g, 13 mmol) and 4,4'-bis(phenylethynyl)-1,1'-biphenyl (1.78 g, 5 mmol) were dissolved in dry toluene (90 ml). The reaction mixture was slowly heated to reflux overnight. The solution was allowed to cool to room temperature and methanol (50 ml) was added. The solution was allowed to stir for 5 hours. The solvent was removed under vacuum and the residue underwent a soxhlet extraction with hexane. The solid remaining after the hexane was removed was dissolved in the minimum amount of DCM and methanol was added. This was passed through a silica plug giving the product (0.47 g, 0.8 mmol, 16 %). Crystals suitable for X-ray crystallography were formed from DCM : Hexane.

Proton assignments from calculations.

^{11}B (128 MHz, $CDCl_3$) δ -10.2 (d, 16B, J 137.6), -2.4 (d, 4B, J 137.2).

^{1}H{^{11}B} (400 MHz, $CDCl_3$) δ 2.40 (s, 4H, BH), 2.58 (s, 12H, BH), 3.29 (s, 4H, BH), 7.14 (t, 4H, J 7.9, H_a), 7.23 (m, 6H, H_{d+e}), 7.45 (d, 8H, J 7.7, H_{b+c}).

^{13}C (100 MHz, $CDCl_3$) δ 84.9 (cage C), 85.5 (cage C), 126.9 ($CH_{d/e}$), 128.6 (CH_a), 130.4 ($CH_{d/e}$), 130.7 (C), 130.8 ($CH_{b/c}$), 131.3 ($CH_{b/c}$), 141.0 (C).

MS (low res. ASAP) $^{12}C_{28}{}^{1}H_{38}{}^{11}B_{16}{}^{10}B_4$ FW = 590 g/mol. M^+ = m/z 591 (with typical carborane pattern from 584-594).

IR: (ν_{max}/cm^{-1}): 2636w (aromatic CH), 2564s (BH stretch), 1492m, 1446m, 1396m, 1192w, 1074s, 1004m, 886m, 868m, 828m, 754m, 726m, 688s, 580s, 510m, 482m

CHN Anal. Calcd for $C_{28}B_{20}H_{38}$ C, 56.92; H, 6.48. Found C, 56.97; H, 6.45.

4.6.3 Preparation of 2,5-(C≡C-C_6H_5)$_2$-C_4SH_2.[8]

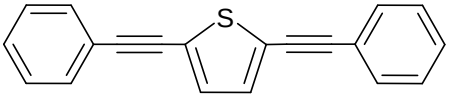

$Pd(PPh_3)_4$ (0.167 g, 0.25 mmol), copper iodide (0.098 g, 0.25 mmol), phenylacetylene (3 g, 29 mmol) and 2,5-dibromothiophene (3.15 g, 13 mmol) were added to degassed, dry triethylamine (100 ml). The reaction mixture was heated to reflux for 48 hours. It was then allowed to cool to room temperature and was filtered. The grey solid was dissolved in toluene and hexane was added. This solution was filtered and the solvent was removed under vacuum giving the product (3.64 g, 13 mmol).

^{1}H (400 MHz, $CDCl_3$) δ 7.14 (s, 2H), 7.34 (m, 6H), 7.51 (m, 4H).

4.6.4 Preparation of 2,5-(1'-C_6H_5-1',2'-$C_2B_{10}H_{10}$)$_2$-C_4SH_2.

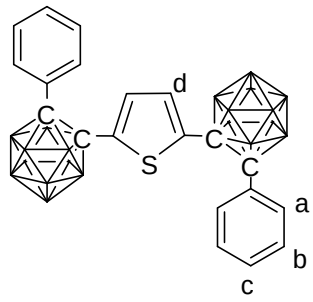

Bis(diethyl sulphide)decaborane (6.5 g, 31 mmol) and 2,5-Bis(phenylethynyl)-thiophene (3.63 g, 13 mmol) were dissolved in dry toluene (50 ml). The reaction mixture was slowly heated to reflux for 48 hours. The solution was allowed to cool to room temperature and methanol (50 ml) was added. The solution was allowed to stir for 5 hours. The solvent was removed under vacuum and the residue underwent a soxhlet extraction with hexane. The solid remaining in the thimble was passed through a silica column using 1:1 DCM:hexane giving the product (0.4 g, 0.8 mmol, 6%) which was recrystallised from DCM:hexane giving crystals suitable for X-ray crystallography.

^{11}B (128 MHz, $CDCl_3$): δ -10.3 (d, 16B, J 138), -2.4 (d, 4B, J 145).

^{1}H{^{11}B} (400 MHz, $CDCl_3$): δ 2.24 (s, 5H, BH), 2.34 (s, 2H, BH), 2.46 (s, 10H,BH), 2.93 (s, 8H,BH), 6.59 (s, 2H, H_d), 7.18 (t, 4H, J 7.9, H_b), 7.33 (t, 2H, J 7.4, H_c), 7.36 (4H, d, J 7.6, H_a).

^{13}C (100 MHz, $CDCl_3$): δ 78.6 (C), 85.8 (C), 128.6 (CH_b), 130.3 (C), 130.8 (CH_c), 131.1 (CH_{a+d}), 138.0 (C).

MS (low res. ASAP) $^{12}C_{20}{}^{1}H_{32}{}^{32}S{}^{11}B_{16}{}^{10}B_4$ FW = 520 g/mol. M^+ = m/z 520 (with typical carborane pattern from 514-524).

IR: (ν_{max}/cm^{-1}): 2604s (BH stretch), 2578s (BH stretch), 1492m, 1446m, 1064m, 1004m, 964w, 920m, 880m, 840m, 808m, 752s, 722s, 686s, 624m, 586s, 526w, 482s.

CHN Anal. Calcd for $C_{20}B_{20}H_{32}S$ C, 46.13; H, 6.19. Found C, 46.04; H, 6.16.

4.6.5 Preparation of 1,4-(1'-(4''-^{t}Bu-C_6H_4)-1',2'-$C_2B_{10}H_{10}$)$_2$-C_6H_4.

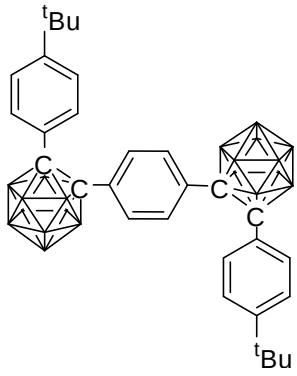

Bis(diethyl sulphide)decaborane (0.34 g, 0.87 mmol) and 1,4-(^{t}Bu-$C_6H_4CC)_2C_6H_4$ (0.47 g, 1.9 mmol) were dissolved in dry toluene (40 ml). The reaction mixture was slowly heated to reflux for 16 hours. The solution was allowed to cool to room temperature and methanol (40 ml) was added. The solution was allowed to stir for 5 hours. The solvent was removed under vacuum and the resulting solid was passed through a silica column using 1:1 DCM:hexane giving the product (0.25 g, 0.40 mmol, 46 %) which was recrystallised from hexane giving crystals suitable for X-ray crystallography.

^{11}B (128 MHz, $CDCl_3$): δ -10.3 (16B, s), -2.6 (4B, s).

^{1}H{^{11}B} (400 MHz, $CDCl_3$): δ 1.23 (18H, s), 2.29 (8H, s, BH), 2.49 (8H, s, BH), 3.03 (4H, s, BH), 7.07 (4H, s), 7.12 (4H, d, J 8.4), 7.19 (4H, d, J 8.4).

^{13}C (100 MHz, $CDCl_3$): δ 31.1 (CH), 34.8 (C), 83.1 (cage C), 85.3 (cage C), 125.4 (CH), 127.4 (C), 130.1 (CH), 130.4 (CH), 132.7 (C), 154.0 (C).

MS (low res. ASAP) $^{12}C_{30}{}^1H_{50}{}^{11}B_{16}{}^{10}B_4$ FW = 626 g/mol. M^+ = 627 m/z (with typical carborane pattern from 623-630).

IR: (ν_{max}/cm^{-1}): 2960s (CH), 2574s (BH), 1260s, 1078s, 1022s, 798s.

CHN Anal. Calcd for $C_{30}B_{20}H_{50}$ C, 57.11; H, 7.99. Found C, 47.81; H, 7.27.

4.6.6 Preparation of 4-$BrC_6H_4NTol_2$.[9]

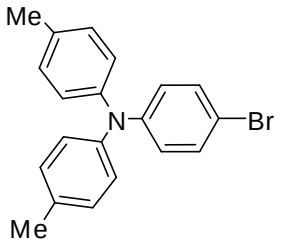

1-Bromo-4-Iodobenzene (21.5 g, 76 mmol), ditolylamine (9.6 g, 49 mmol), 1,10-phenanthroline (0.9 g, 5 mmol), CuCl (0.7 g, 7.1 mmol) and o-xylene (70 ml) were mixed in a round bottomed flask with an overhead stirrer and reflux condenser, under a nitrogen atmosphere. The mixture was stirred at reflux for 30 mins. Powdered KOH (45 g) was added to the reaction mixture, which was then refluxed overnight. The solution was neutralised with 2 M acetic acid and filtered. The filtrate was poured into water and the aqueous layer was extracted with DCM. The organic layers were combined, washed with water (3 x 50 ml) and dried over $MgSO_4$. The solvent was removed under reduced pressure. The resulting solid was passed through a silica plug with hexane giving a white solid (6.0 g, 17 mmol, 35 %).

^{1}H (400 MHz, $CDCl_3$) δ 2.31 (6H, s), 6.88 (2H, d), 6.97 (4H, d), 7.07 (4H, d), 7.27 (2H, d).

4.6.7 Preparation of TMSC≡C-$C_6H_4NTol_2$.[10]

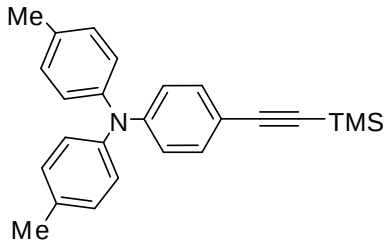

$Pd(PPh_3)_4$ (0.41 g, 0.35 mmol), copper iodide (0.07g, 0.35 mmol), TMSA (2.5 ml, 18 mmol) and $BrC_6H_4N(C_6H_4CH_3)_2$ (5.00 g, 14 mmol) were added to dry degassed triethylamine (30 ml). The reaction mixture was heated to reflux overnight. It was then allowed to cool to room temperature and was filtered. The solvent was removed from the filtrate and the resulting solid was dissolved in Et_2O and washed with water, dried over $MgSO_4$ and then the solvent was removed under vacuum. The solid was purified by column chromatography, eluting with hexane giving the product (3.5 g, 9.5 mmol, 67 %).

^{1}H (400 MHz, $CDCl_3$) δ 0.23 (9H, s), 2.32 (6H, s), 6.89 (2H, d), 6.98 (4H, d), 7.07 (4H, d), 7.27 (2H, d).

4.6.8 Preparation of $HC{\equiv}C\text{-}C_6H_4NTol_2$.[10]

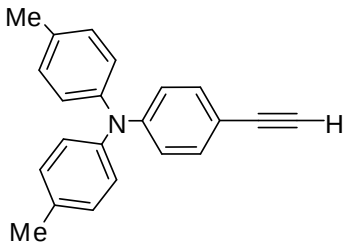

$TMSC{\equiv}C\text{-}C_6H_4N(C_6H_4CH_3)_2$ (3.5 g, 9.5 mmol) was dissolved in Et_2O (30 ml) and added to methanol (500 ml). Potassium carbonate (5 g, 36 mmol) was added and this suspension was stirred for 48 hours under N_2. This solution was added to water and the product was extracted with DCM. The organic layer was dried over $MgSO_4$ and the solvent was removed to give the product (1.75 g, 5.9 mmol, 62 %).

^1H (400 MHz, $CDCl_3$) δ 2.32 (6H, s), 3.00 (1H, s), 6.90 (2H, d), 6.99 (4H, d), 7.08 (4H, d), 7.28 (2H, d).

4.6.9 Preparation of 1,4-(C≡C-$C_6H_4NTol_2$)$_2$-C_6H_4.[10]

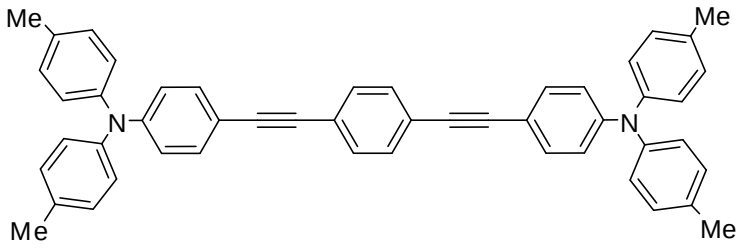

$Pd(PPh_3)_4$ (0.19 g, 0.17 mmol), copper iodide (0.03g, 0.17 mmol), 1,4-diiodobenzene (1.1 g, 3.2 mmol) and HC≡C-$C_6H_4N(C_6H_4CH_3)_2$ (1.75 g, 5.9 mmol) were added to degassed, dry triethylamine (30 ml). The reaction mixture was heated to reflux overnight. It was then allowed to cool to room temperature and was filtered. The solvent was removed from the filtrate and the orange solid was washed with cold hexane to give the product (1.7 g, 2.5 mmol, 86 %).

^{1}H (400 MHz, $CDCl_3$): δ 2.32 (12H, s), 6.94 (4H, d, J 4.4), 7.01 (8H, d, J 4.8), 7.09 (8H, d, J 4.8), 7.32 (4H, d, J 4.8), 7.44 (4H, s).

^{13}C (100 MHz, $CDCl_3$): δ 21.1 (CH), 88.5 (C), 91.9 (C), 115.0 (C), 121.2 (C), 123.3 (C), 125.5 (CH), 130.3 (CH), 131.5 (CH), 132.7 (CH), 133.6 (CH), 144.9 (C), 148.9 (C).

MS (low res. EI) $^{12}C_{50}{}^{1}H_{40}{}^{14}N_2$ FW = 668 g/mol. M^+ = m/z 668.

4.6.10 Preparation of 1,4-(1'-(4'-$C_6H_4NTol_2$)-1',2'-$C_2B_{10}H_{11}$)$_2$-C_6H_4.

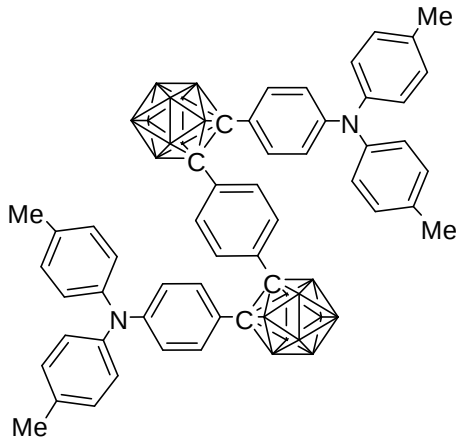

Diethyl sulphide (4.0 mL, 37 mmol) and decaborane (0.37 g, 3.0 mmol) were stirred together under nitrogen and refluxed for 16 hours. The solution was allowed to cool to room temperature, and then cooled in an ice bath. 1,4(C≡C-C_6H_4N(4'-$CH_3C_6H_4$)$_2$)$_2C_6H_4$ (0.67 g, 1 mmol) and dry toluene (15 mL) were added to the reaction mixture. The reaction mixture was slowly heated to reflux for 16 hours. The solution was allowed to cool to room temperature and methanol (50 ml) was added. The solution was allowed to stir for 5 hours. The solvent was removed under vacuum and the residue was purified using preparative thin layer chromatography (1:1 hexane:DCM) and then recrystallized from hot acetone (0.15 g, 0.02 mmol, 15 %).

^{11}B (128 MHz, $CDCl_3$): δ -10.7 (s, 16B), -2.9 (s, 4B).

^{1}H{^{11}B} (400 MHz, $CDCl_3$): δ 2.30 (12H, s), 2.46 (6H, s, BH), 2.53 (8H, s, BH), 3.03 (6H, s, BH), 6.54 (4H, d, J 9.2), 6.83 (8H, d, J 8.0), 7.01 (8H, d, J 9.2), 7.04 (4H, d, J 8.8), 7.19 (4H, s).

^{13}C (100 MHz, $CDCl_3$): δ 20.8 (CH), 83.4 (cage C), 86.3 (cage C), 119.2 (CH), 119.6 (C), 124.9 (CH), 125.3 (CH), 129.7 (CH), 131.0 (CH), 132.2 (C), 134.0 (C), 144.0 (C), 149.9 (C).

MS (low res. ASAP) $^{12}C_{50}{}^{1}H_{60}{}^{11}B_{16}{}^{10}B_{4}{}^{14}N_{2}$ FW = 904 g/mol. M^{+} = m/z 904 (with typical carborane pattern from 901-908).

IR (υ_{max}/cm^{-1}): 2922w (aryl C-H stretch), 2572b (B-H), 1598m (aryl C=C), 1505 (aryl C=C), 1272 (C-N).

CHN Anal. Calcd for $C_{50}B_{20}H_{60}N_{2}$ C, 66.04; H, 6.66; N, 3.08. Found C, 57.42; H, 6.95; N, 2.23.

4.6.11 Preparation of 1,4-(1'-(4'-$C_6H_4NTol_2$)-1',2'-$C_2B_{10}H_{11}$)$_2$-C_6F_4.

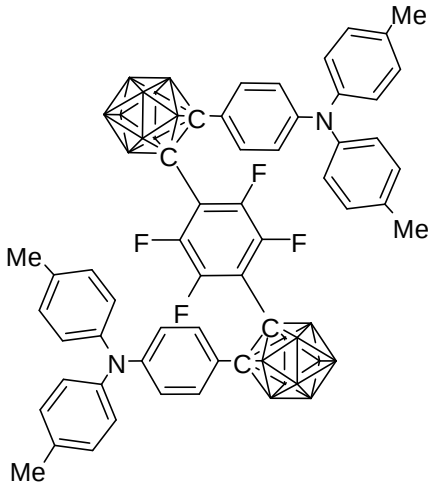

1-$C_6H_4N(C_6H_4CH_3)_2$-1,2-$C_2B_{10}H_{11}$ (0.28 g, 0.67 mmol) was dissolved in 20 mL dry Et_2O under nitrogen. The solution was cooled in an ice bath followed by the dropwise addition of *n*-BuLi (0.7 mL, 1.6 M in hexanes, 1 mmol). The reaction mixture was allowed to warm to room temperature and was stirred for 3 hours. The solution was cooled in an ice bath followed by the addition of hexafluorobenzene (0.1 g, 0.54 mmol). The reaction mixture was stirred at room temperature for 48 hours. The solution was diluted with DCM and washed with water (3 x 20 mL), followed by the removal of the organic solvents. The resulting solid was passed through a hexane silica plug, followed by recrystallization from DCM:hexane, giving the orange product (0.25 g, 0.26 mmol, 38%).

^{11}B (128 MHz, $CDCl_3$): δ -9.3 (16B, s), -4.3, (2B, s), 1.3 (2B, s).

^{1}H{^{11}B} (400 MHz, $CDCl_3$): δ 2.31 (12H, s), 2.44 (12H, s, BH), 2.72 (4H, s, BH), 3.34 (4H, s, BH), 6.65 (4H, d, J 8.8), 6.89 (8H, d, J 8.4), 7.07 (8H, d, J 8.0), 7.19 (4H, d, J 9.2).

^{19}F (658 MHz, $CDCl_3$): δ -130.0 (s, 4F).

^{13}C (100 MHz, $CDCl_3$): δ 21.0 (C), 74.7 (C), 89.0 (C), 118.9 (CH), 121.0 (C), 126.0 (CH), 130.4 (CH), 131.2 (CH), 134.6 (C), 143.8 (C), 150.7 (C).

MS (low res. ASAP) $^{12}C_{50}{}^{1}H_{56}{}^{19}F_{4}{}^{14}N_{2}{}^{11}B_{16}{}^{10}B_{4}$ FW = 976 g/mol. M^{+} = m/z 976 (with typical carborane pattern from 971-981).

IR: (ν_{max}/cm^{-1}): 2916w (aryl C-H), 2590s (B-H), 1596s (C=C), 1502s (C=C), 1320s (C-F), 1266s (C-N).

CHN Anal. Calcd for $C_{50}B_{20}H_{56}F_{4}N_{2}$ C, 61.45; H, 5.78; N, 2.87. Found C, 53.24; H, 5.92; N, 2.21.

4.6.12 Preparation of 1,4-(1'-$C_{10}H_7$-1',2'-$C_2B_{10}H_{10}$)$_2$-C_6F_4.

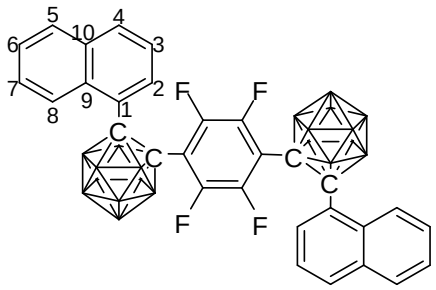

1-(1'-$C_{10}H_7$)-1,2-$C_2B_{10}H_{11}$ (0.5 g, 1.85 mmol) was dissolved in Et_2O (20 mL). The solution was cooled in an ice bath and n-BuLi (1.6 M in hexanes, 1.2 mL, 2 mmol) was added dropwise. The reaction mixture was stirred at 40 °C for 3 hours and then cooled in an ice bath again. Hexafluorobenzene (0.18 g, 1 mmol) was added and the reaction mixture was heated to reflux for 16 hours. The solution was allowed to cool to room temperature and was washed with water (3 x 20 mL) and then the organic phase was dried over $MgSO_4$. The solid was passed through a silica plug eluting with 1:1 DCM:hexane. Removing the solvent gave the product 1,4-(1-$C_{10}H_7$-1,2-$C_2B_{10}H_{10}$)-C_6F_4 as a yellow powder (0.25 g, 0.36 mmol, 19%). Crystals suitable for X-ray crystallography were grown from DCM:hexane.

^{11}B (128 MHz, $CDCl_3$): δ -8.8 (16B, s), -2.4 (2B, s), 0.4 (2B, s).

^{1}H {^{11}B}(400 MHz, $CDCl_3$): δ 7.00 (2H, t, J 7.9, $C_3\underline{H}$), 7.54 (2H, t, J 7.3, $C_6\underline{H}$), 7.60 (2H, t, J 7.9, $C_7\underline{H}$), 7.71 (2H, d, J 8.1, $C_4\underline{H}$), 7.83 (2H, d, J 7.8, $C_5\underline{H}$), 7.88 (2H, d, J 7.7, $C_2\underline{H}$), 8.86 (2H, d, J 9.0, $C_8\underline{H}$).

^{19}F (658 MHz, $CDCl_3$): δ -129.6 (s, 4F).

^{13}C (100 MHz, $CDCl_3$): δ 78.5 (C), 90.6 (C), 113.7 (C), 123.9 ($\underline{C}_3$H), 125.1 ($\underline{C}_8$H), 126.4 ($\underline{C}_6$H), 127.6 ($\underline{C}_7$H), 129.7 ($\underline{C}_5$H), 131.3 (C), 132.9 ($\underline{C}_2$H), 133.6 ($\underline{C}_4$H), 134.7 (C), 146.2 (C), 147.7 (C).

MS (low res. ASAP) $^{12}C_{30}{}^{1}H_{34}{}^{19}F_4\ {}^{11}B_{16}{}^{10}B_4$ FW = 686 g/mol. M^+ = m/z 687 (with typical carborane pattern from 682-692).

IR: (ν_{max}/cm^{-1}): 2914m (CH stretch), 2564s (BH stretch), 1510w, 1448s, 1396w, 1330w, 1308w, 1232w, 1160w, 1094w, 1038w, 988s, 858w, 852w, 796w, 764s, 718s, 610w, 564w, 518w, 426w, 430w.

CHN Anal. Calcd for $C_{30}B_{20}H_{38}F_4$ C,52.16; H, 5.54. Found C, 49.78; H, 5.70.

4.7 References

1. Barrière F., Fabre B., Hao E., LeJeune Z. M., Hwang E., Garno J. C., Nesterov E. E. and Vicente M. G. H., *Macromolecules*, **2009**, 42, 2981-2987.
2. Thomas R. LL. and Welch A. J., *Acta. Cryst.*, **1996**, C52, 1689-1691.
3. Songkram C., Ohta K., Yamaguchi K., Pichierri F. and Endo Y., *Inorg. Chem.*, **2010**, 49, 11174–11183.
4. Endo Y., Songkram C., Ohta K. and Yamaguchi K., *J. Organomet. Chem.*, **2005**, 11, 2750–2756.
5. Songkram C., Takaishi K., Yamaguchi K., Kagechika H. and Endo Y., *Tetrahedron Lett.*, **2001**, 42, 6365–6368.
6. Zakharkin L. I. and Lebedev V. N., *Russ. Chem. Bull.*, **1970**, 19, 4, 914.
7. Birckner, E., Grummt U.-W., Göller A. H., Pautzsch T., Egbe D. A. M., Al-Higari M. and Lkemm E., *J. Phys. Chem. A*, **2001**, 105(45), 10307-10315.
8. Siddle J. S., Ward R. M., Collings J. C., Rutter S. R., Porrès L., Applegarth L., Beeby A., Batsanov A. S., Thompson A. L., Howard J. A. K., Boucekkine A., Costuas K., Halet J.-F. and Marder T. B., *New J. Chem.*, **2007**, 31(6), 841-851.
9. Goodbrand H. B. and Hu N.-X., *J. Org. Chem.,* **1999**, 64, 670-674.
10. Plater J. M. and Jackson T., *Tetrahedron*, **2003**, 59, 4687–4692.

5 : Electrochemistry of Carboranes

5.1 Introduction

The redox properties of carboranes in the literature are discussed in chapter 1. Here we collect together the electrochemical data for some simple carboranes and the carboranes synthesised as part of this thesis. We found the clearest definition of redox waves using acetonitrile as the solvent and a glassy carbon working electrode.

5.2 Simple Carboranes

The parent *meta* and *para* carboranes are not reduced within the solvent window used in cyclic voltammetry. The parent *ortho* carborane undergoes an irreversible reduction at -3.09 V. Many of the substituted *ortho* carboranes undergo reduction more readily at -1 to -2 V.

Di phenyl *ortho* carborane and derivatives have been reported to display two sequential one electron, chemically reversible, electrochemically quasi reversible reduction waves. The first of these reduction waves is attributed to a stable radical anion with a 2n + 3 SE count, before the second reduction to the 2n + 4 SE dianion. The cyclic voltammetry of di phenyl *ortho* carborane and other simple carborane compounds are summarised in Table 5–1 with experimental details. The redox waves of these compounds are illustrated in Figure 5–1 to Figure 5-14, along with that of the internal reference (ferrocene or decamethylferrocene).

The di pyridyl substituted *ortho* carborane is seen to show the same splitting of the reoxidation peak as in the case of the di phenyl carborane, forming the same 2n + 3 SE radical anion. Likewise the pyridyl and phenyl substituted carborane has the same behaviour.

Mono phenyl and pyridyl *ortho* carboranes do not display the formation of a radical anion seen in their disubstituted counterparts. The other simple carboranes investigated here also do not display this behaviour.

R^1	R^2	$E(Red_1)$ cathodic V	$E(Red_1)$ anodic V	$E_{1/2}$ (Red_1) V	Red_1 p-p mV	$E(Red_2)$ cathodic V	$E(Red_2)$ anodic V	$E_{1/2}$ (Red_2) V	Red_2 p-p mV	$\Delta E_{1/2}$ $(Red_1$-$Red_2)$ mV	E(Ox) V	Fc p-p mV
H	**H**	-3.09	-	-	-	-	-	-	-	-	-	146
Ph	**Ph**	-1.79	-1.42	-1.61	370	-1.79	-1.66	-1.73	140	120	-	93
Ph	**H**	-2.48	-1.63	-2.06	850	-	-	-	-	-	-	85
Ph	**PPh_2**	-1.75	-1.33	-1.54	420	-	-	-	-	-	-	76
PPh_2	**PPh_2**	-1.98	-0.71	-1.35	1260	-1.98	-1.03	-1.5	950	150	-	88
PPh_2	**H**	-2.54	-0.38	-1.46	2160	-2.54	-1.28	-1.91	1260	450	-	78
Ph	**Me**	-2.24	-1.68	-1.96	560	-	-	-	-	-	-	112
Ph	**2-Py**	-1.91	-1.35	-1.63	550	-1.91	-1.58	-1.74	330	110	-	90
2-Py	**H**	-2.59	-1.51	-2.05	1080	-	-	-	-	-	-	115
2-Py	**2-Py**	-1.75	-1.33	-1.54	427	-1.75	-1.55	-1.65	200	110	-	76
$SiMe_3$	**H**	-3.01	-1.47	-2.24	1540	-	-	-	-	-	-	93
Me	**Me**	-3.00	-1.68	-2.34	1320	-	-	-	-	-	-	88
Me	**H**	-3.12	-1.48	-2.30	1640	-	-	-	-	-	-	127
SH	**SH**	-1.43#	-0.6#	-0.74#	1370#	-	-	-	-	-	-	70#
		-1.46*	0.21*	-0.62*	1670*	-	-	-	-	-	-	90*
SMe	**SMe**	-1.76	-1.36	-1.56	400	-	-	-	-	-	-	107

Table 5–1: Reduction and oxidation potentials of simple *ortho* carboranes, 1-R^1-2-R^2-1,2-$C_2B_{10}H_{10}$ in 0.1 M NBu_4PF_6 in MeCN, 100 mV/s, relative to an internal reference of ferrocene at 0.00 V, using a glassy carbon working electrode, unless otherwise stated. # Using a platinum working electrode. * Using decamethyl ferrocene as the internal reference.

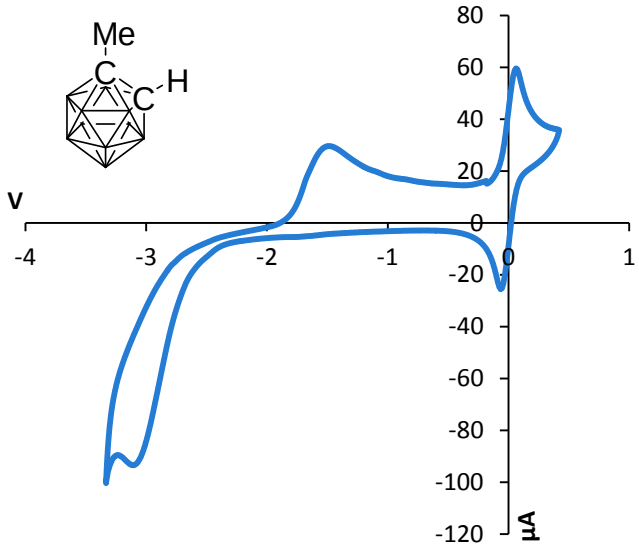

Figure 5–1: CV of 1-Me-1,2-$C_2B_{10}H_{11}$.[#]

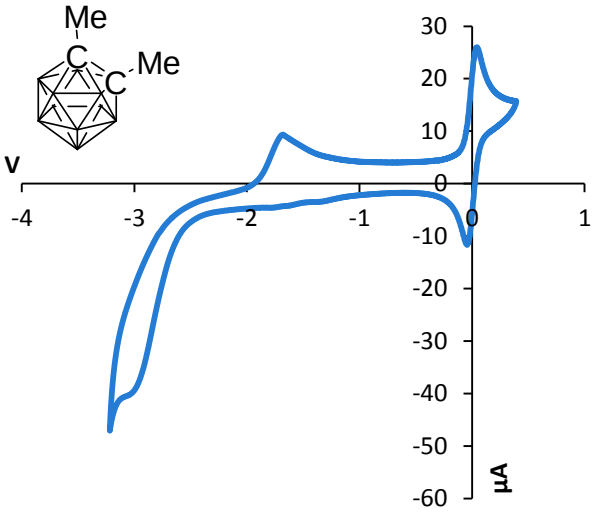

Figure 5–2: CV of 1,2-Me_2-1,2-$C_2B_{10}H_{10}$.[#]

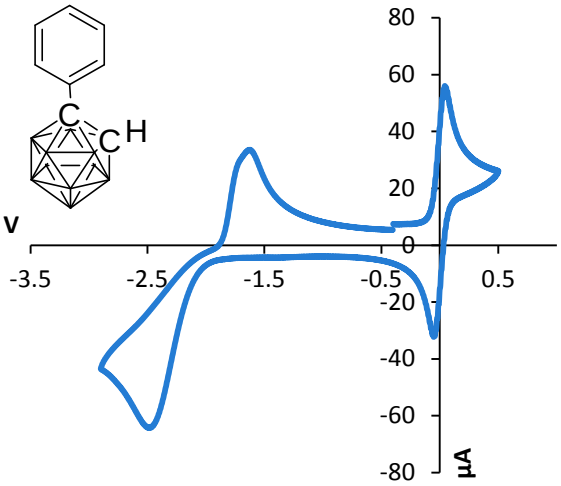

Figure 5–3: CV of 1-Ph-1,2-$C_2B_{10}H_{11}$.[#]

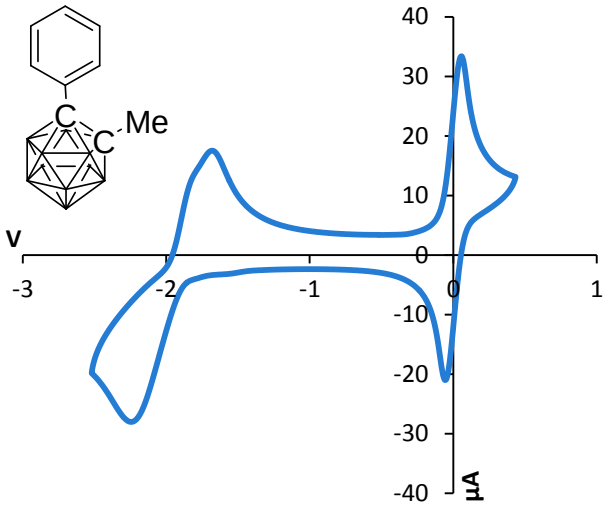

Figure 5–4: CV of 1-Me-2-Ph-1,2-$C_2B_{10}H_{10}$.[#]

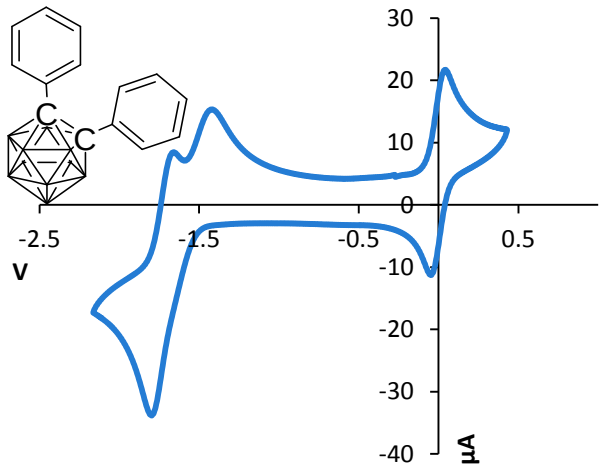

Figure 5–5: CV of 1,2-Ph_2-1,2-$C_2B_{10}H_{10}$.[#]

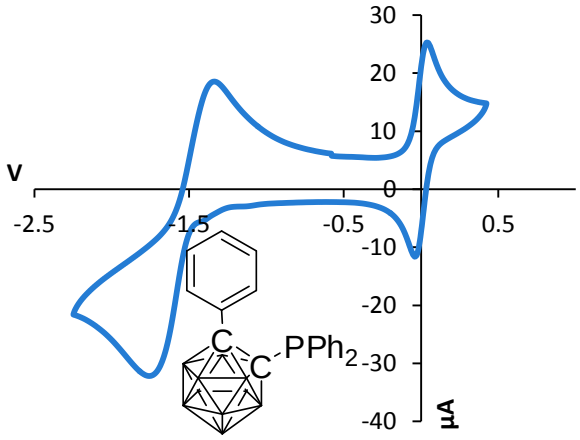

Figure 5–6: CV of 1-PPh_2-2-Ph-1,2-$C_2B_{10}H_{10}$.[#]

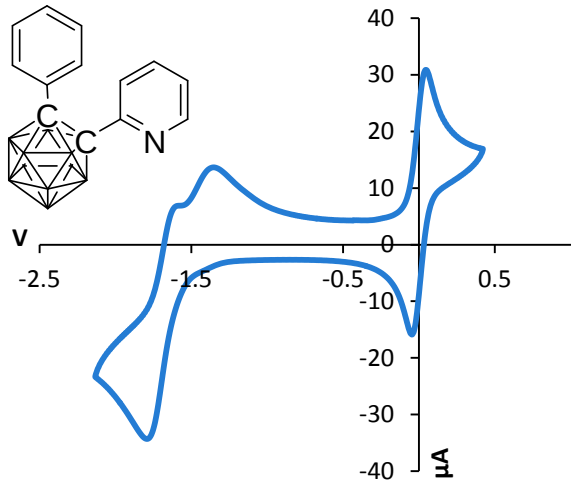

Figure 5–7: CV of 1-(2'-Py)-2-Ph-1,2-$C_2B_{10}H_{10}$.[#]

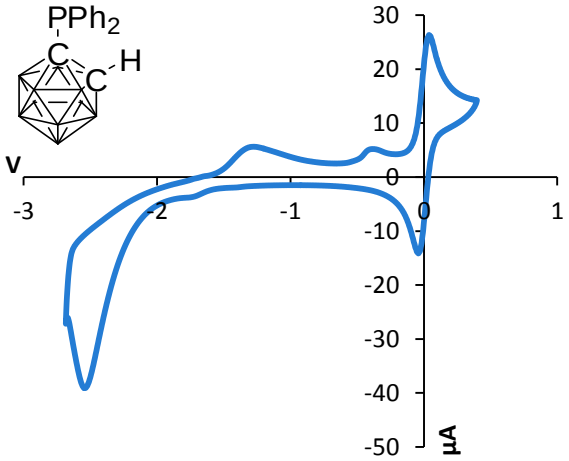

Figure 5–8: CV of 1-PPh_2-1,2-$C_2B_{10}H_{11}$.[#]

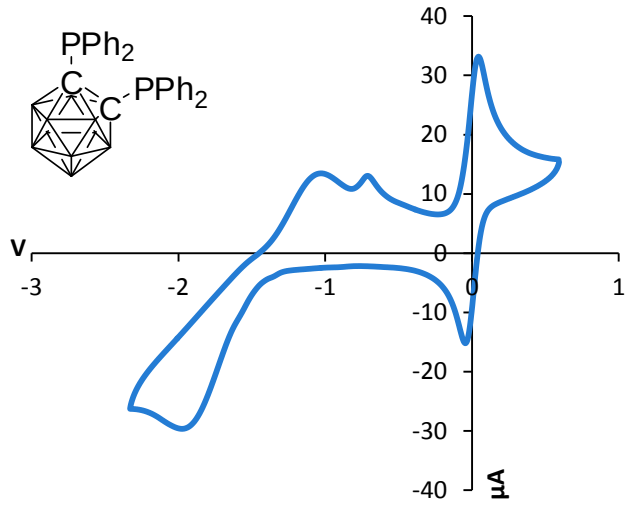

Figure 5–9: CV of 1,2-PPh_2-1,2-$C_2B_{10}H_{10}$.[#]

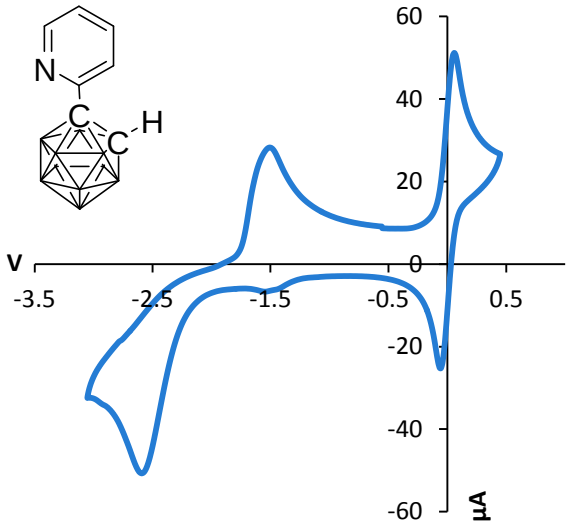

Figure 5–10: CV of 1-(2'-Py)-1,2-$C_2B_{10}H_{11}$.[#]

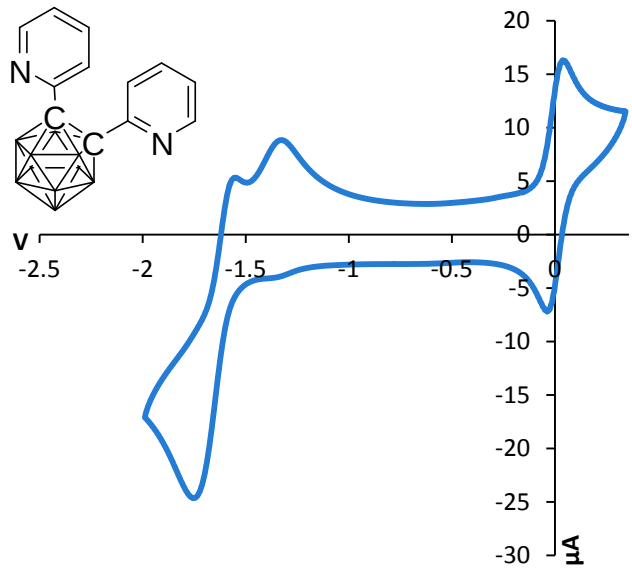

Figure 5–11: CV of 1,2-$(2'\text{-Py})_2$-1,2-$C_2B_{10}H_{10}$.[#]

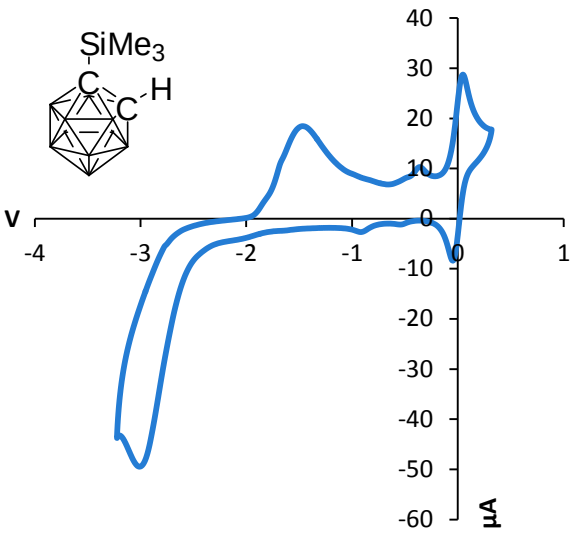

Figure 5–12: CV of 1-$SiMe_3$-1,2-$C_2B_{10}H_{11}$.[#]

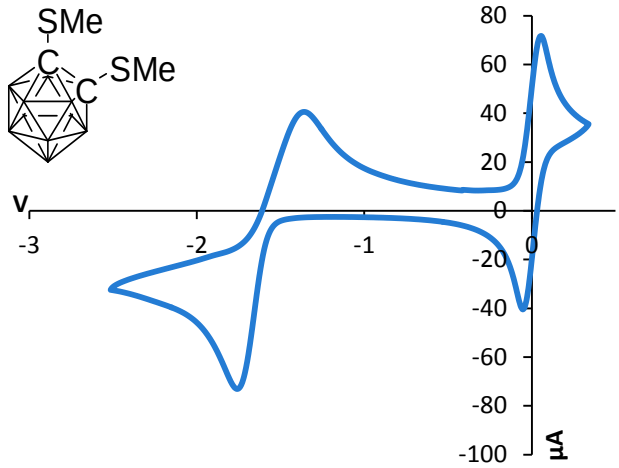

Figure 5–13: CV of 1,2-$(SMe)_2$-1,2-$C_2B_{10}H_{10}$.[#]

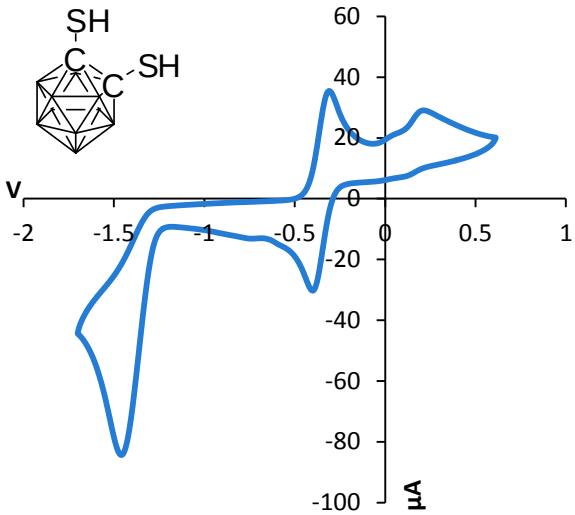

Figure 5–14: CV of 1,2-$(SH)_2$-1,2-$C_2B_{10}H_{10}$.[#]*

[#] 0.1 M NBu_4PF_6 in MeCN, 100 mV/s, with a glassy carbon working electrode, relative to an internal reference of ferrocene at 0.00 V unless otherwise stated.
*Decamethyl ferrocene as the internal reference and a platinum working electrode.

5.2.1 Calculations

The parent *ortho*, *meta* and *para* carboranes have calculated LUMO energies that are in line with the observation that the *ortho* carborane cage is more easily reduced than the *meta* and *para* isomers, Figure 5–15. The LUMO of *ortho* carborane is calculated to be much lower than for the *meta* and *para* cages and therefore it is easier to add electrons to the *ortho* carborane cage.

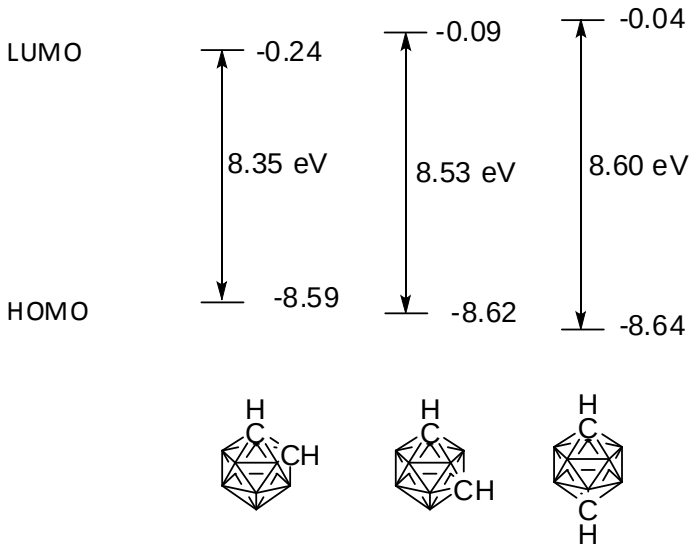

Figure 5–15: DFT calculated (B3LYP/6-31G*) HOMO and LUMO energies of *ortho*, *meta* and *para* carborane cages.

Calculation of the HOMO and LUMO energies of these simple carboranes are shown in Figure 5–16. The compound in Table 5–1 which is shown to reduce most easily is 1,2-$(SH)_2$-1,2-$C_2B_{10}H_{10}$. Calculations, however, predict that 1,2-Py_2-1,2-$C_2B_{10}H_{10}$ would be the easiest to reduce, with the lowest LUMO energy. The compound that is most difficult to reduce, from this series of compounds, is 1-Me-1,2-$C_2B_{10}H_{11}$. Calculations however would predict that 1-$SiMe_3$-1,2-$C_2B_{10}H_{11}$ would be most easily reduced. The calculated LUMO energy levels are not in good agreement with the observed pattern of reduction potentials and therefore are not suitable for predicting the reduction potentials of these *ortho* carboranes.

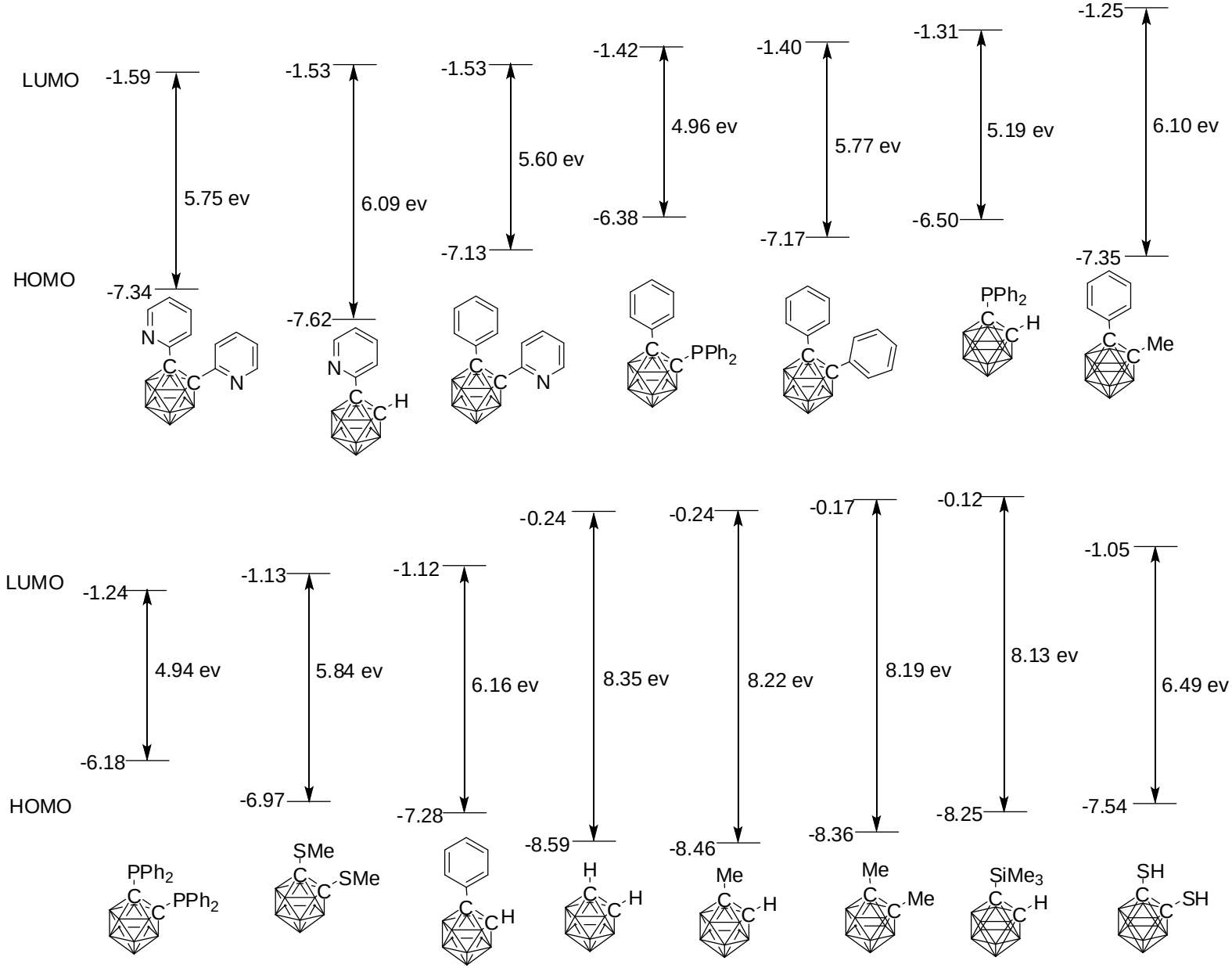

Figure 5–16: DFT calculated (B3LYP/6-31G*) HOMO and LUMO energies of simple *ortho* carboranes, 1-R^1-2-R^2-1,2-$C_2B_{10}H_{10}$.

Calculated cage C-C bond lengths in the neutral state vary from 1.626 to 1.868 Å, elongating with an increasing steric bulk between the R^1 and R^2 groups. Table 5–2 shows the E(red_1) cathodic values for these compounds, in order of reduction potential, alongside the calculated LUMO energy levels and cage C-C bond lengths. The cage C-C bond lengths in the neutral state can be seen to correlate better to the ease of reduction than the calculated LUMO energy levels.

The greater the cage C-C bond length in the ground state, the more open the geometry of the carborane cage, and therefore the closer the geometry is to a *nido* dianion geometry, with the additional electrons located on the carborane cage. This allows the reduction of a carborane with a longer cage C-C bond length to take place more readily.

R^1	R^2	Calculated C1-C2 / Å	Observed E(red_1) cathodic / V	Calculated LUMO energy / eV
Me	**H**	1.626	-3.12	-0.24
H	**H**	1.626	-3.09	-0.24
$SiMe_3$	**H**	1.655	-3.01	-0.12
Me	**Me**	1.663	-3.00	-0.17
Py	**H**	1.632	-2.59	-1.53
PPh_2	**H**	1.656	-2.54	-1.31
Ph	**H**	1.646	-2.48	-1.12
Ph	**Me**	1.720	-2.24	-1.25
PPh_2	**PPh_2**	1.791	-1.98	-1.24
Ph	**Py**	1.724	-1.91	-1.53
Ph	**Ph**	1.763	-1.79	-1.40
SMe	**SMe**	1.868	-1.76	-1.13
Ph	**PPh_2**	1.772	-1.75	-1.42
Py	**Py**	1.692	-1.75	-1.59
SH	**SH**	1.804	-1.46	-1.05

Table 5–2: E(red_1) cathodic for simple carboranes 1-R^1-2-R^2-1,2-$C_2B_{10}H_{10}$, taken from Table 5–1, compared to DFT(B3LYP/6-31G*) calculated cage C-C lengths and LUMO energy levels.

The calculated geometries of the mono and di-anions of these compounds are found to undergo an extension of the cage C-C bond length on reduction. Three different cage conformations, with varying cage C-C bond lengths, have been found to be possible for the dianions of simple *ortho* carborane cages. Representative examples of these geometries for 1-(2'-Py)-1,2-$C_2B_{10}H_{11}$ are shown in Figure 5–17. Conformation m2-A displays a closed cage geometry and is the highest energy conformation. The open cage, m2-B, with a near-planar open face, has a lower calculated energy than m2-A. Increasing the distance between the cage C atoms, further opening the cage conformation, leads to m2-C. In the case of unsubstituted *ortho* carborane and 1-(PPh_2)-1,2-$C_2B_{10}H_{11}$ the conformation with the lowest calculated energy is the open m2-B. In all other cases, m2-C is the lowest energy conformation.

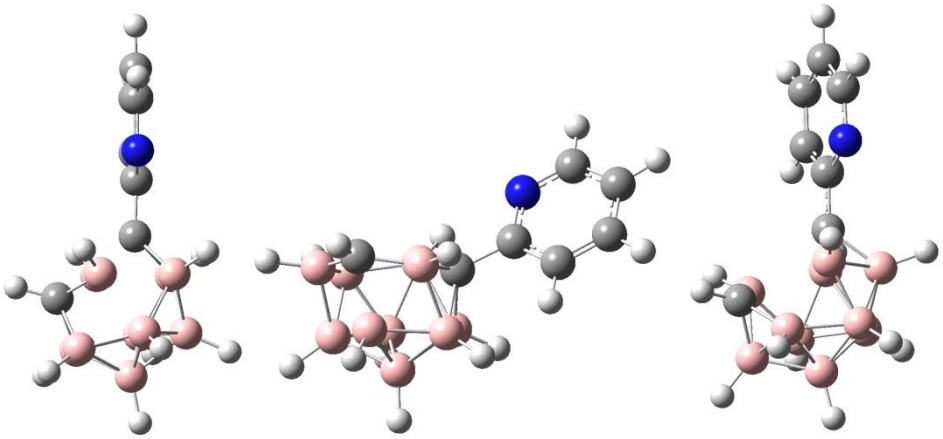

m2-A **m2-B** **m2-C**

Figure 5–17: DFT calculated (B3LYP/6-31G*) optimised geometries for the dianion of 1-(2'-Py)-1,2-$C_2B_{10}H_{11}$, m2-A, m2-B, m2-C.

R^1	R^2	m2-A		m2-B		m2-C	
		Calculated C1-C2 / Å	Relative Calculated Energy / kcal/mol	Calculated C1-C2 / Å	Relative Calculated Energy / kcal/mol	Calculated C1-C2 / Å	Relative Calculated Energy / kcal/mol
Me	H	2.554	+9	2.776	+2	2.963	0
H	H	2.550	+9	2.740	0	2.961	+2
$SiMe_3$	H	2.562	+36	2.768	+6	2.948	0
Me	Me	2.589	+2	2.796	+2	2.957	0
Py	H	2.524	+4	2.775	+11	2.891	0
PPh_2	H	2.697	0	2.770	+11	2.948	+2
Ph	H	2.532	+5	2.774	+8	2.915	0
Ph	Me	2.551	+6	2.794	+6	2.924	0
PPh_2	PPh_2	2.597	+10	2.787	+5	2.984	0
Ph	Py	2.514	+5	2.799	+13	2.901	0
Ph	Ph	2.523	+5	2.803	+10	2.913	0
SMe	SMe	2.544	+10	2.756	+3	2.932	0
Ph	PPh_2	2.565	+6	2.801	+8	2.952	0
Py	Py	2.504	+4	2.803	+15	2.887	0
SH	SH	2.530	+4	2.737	+1	2.964	0

Table 5–3: DFT calculated (B3LYP/6-31G*) cage C-C distances and energies of conformations m2-A, B and C of the simple carboranes 1-R^1-2-R^2-1,2-$C_2B_{10}H_{10}$.

5.3 Naphthyl Carboranes

The di-naphthyl *ortho* carborane molecule bears an obvious resemblance to the di-phenyl *ortho* carborane. As such we expect this molecule to also form a radical anion with the novel 2n + 3 SE count. Therefore we will compare the properties of the two molecules. We can also compare these results with those for the *ortho* mono naphthyl carborane and the *ortho* mono phenyl carborane.

The results for the *ortho* naphthyl carboranes are summarised in Table 5–4, whilst the cyclic voltammogram traces for the di and mono substituted naphthyl carboranes are shown in Figure 5–18 and # Figure 5–19 respectively.

R^1	R^2	E (Red_1) cathodic V	E (Red_1) anodic V	$E_{1/2}$ (Red_1) V	Red_1 p-p mV	E(Red_2) cathodic V	E (Red_2) anodic V	$E_{1/2}$ (Red_2) V	Red_2 p-p mV	$\Delta E_{1/2}$ (Red1-Red2) mV	Fc p-p mV
Nap	**H**	-1.79	-1.55	-1.67	240	-	-	-	-	-	107
Nap	**Nap**	-1.23	-1.14	-1.19	90	-1.55	-1.36	-1.46	190	270	83
Ph	**H**	-2.48	-1.63	-2.06	850	-	-	-	-	-	85
Ph	**Ph**	-1.79	-1.42	-1.61	370	-1.79	-1.66	-1.73	140	120	93

Table 5–4: Reduction and oxidation potentials of the *ortho* naphthyl carboranes, 1-R^1-2-R^2-1,2-$C_2B_{10}H_{10}$, in 0.1 M NBu_4PF_6 in MeCN, 100 mV/s, relative to an internal reference of ferrocene at 0.00 V, using a glassy carbon working electrode.

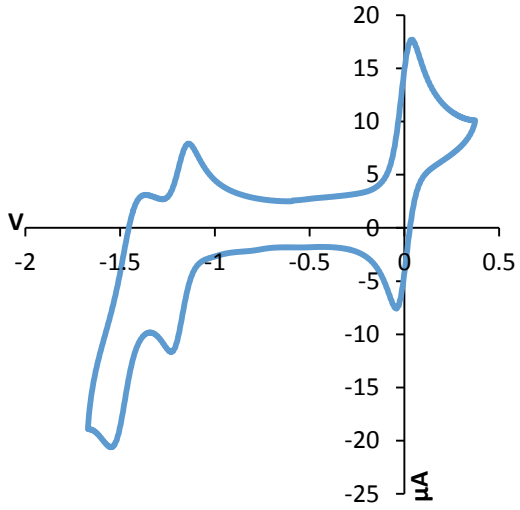

Figure 5–18: CV of 1,2-(1'-$C_{10}H_7$)$_2$-1,2-$C_2B_{10}H_{10}$.[#]

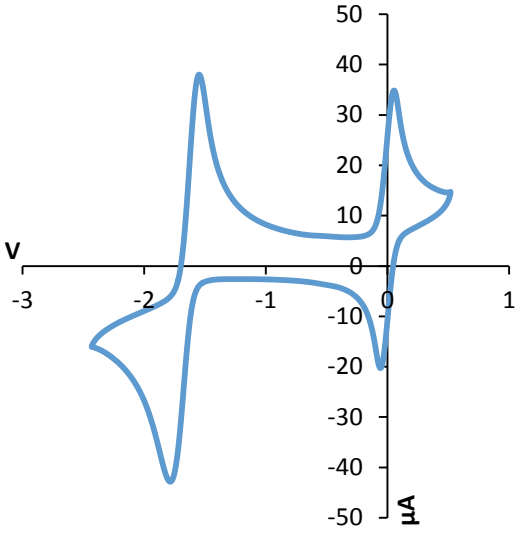

Figure 5–19: CV of 1-(1'-$C_{10}H_7$)-1,2-$C_2B_{10}H_{11}$.[#]

[#] In 0.1 M NBu_4PF_6 in MeCN, 100 mV/s, relative to an internal reference of ferrocene at 0.00 V, using a glassy carbon working electrode.

Di-naphthyl *ortho* carborane displays two sequential, electrochemically quasi reversible, chemically reversible reduction waves. In the case of di-naphthyl *ortho* carborane, we see a greater separation of the two reduction waves than for the di-phenyl analogue, at 270 mV compared to 120 mV. Reduction is more facile than for the diphenyl analogue. Mono naphthyl *ortho* carborane shows one electrochemically reversible, chemically reversible, reduction wave. Mono phenyl *ortho* carborane, Figure 5–3, by contrast displays an electrochemically quasi-reversible and chemically reversible reduction wave at 390 mV higher potential.

Both the di-naphthyl and di-phenyl *ortho* carboranes have been characterised by X-ray diffraction studies. As shown in Table 5–5, a striking difference in the structures is the cage C-C bond distance, which is longer for the di-naphthyl. This long bond length is probably due to greater steric hindrance in this molecule, between the hydrogen atoms on C10 of the naphthyl and the B3 and B4 of the cage, and also on the other side of the molecule (C20, B6, B7). We know that, on adding an electron forming the radical species the C-C bond will get longer as the carborane takes on a more open geometry. As such we expect di-naphthyl *ortho* carborane to form the radical species more readily and for the radical to be more stable than in the case of di-phenyl species. The mono substituted naphthyl *ortho* carborane also has a slightly longer cage C-C bond length than the mono phenyl analogue. This may contribute to the more facile reduction for the naphthyl carborane.

Compound	Cage C-C bond length / Å
1,2-$(C_6H_5)_2$-1,2-$C_2B_{10}H_{10}$ [1]	1.726(2)
1-(C_6H_5)-1,2-$C_2B_{10}H_{11}$ [2]	1.649(2)
1,2-(1'-$C_{10}H_7)_2$-1,2-$C_2B_{10}H_{10}$	1.791(2)
1-(1'-$C_{10}H_7$)-1,2-$C_2B_{10}H_{11}$	1.677 (4)

Table 5–5: Cage C-C bond lengths found by X-ray crystallography for naphthyl and phenyl *ortho* carboranes.

5.3.1 Calculations

The LUMO for the di-naphthyl *ortho* carborane is lower than for di-phenyl *ortho* carborane, Figure 5–20, as discussed in chapter 2. This is in line with the observation that *ortho* di-naphthyl carborane is easier to reduce than *ortho* di-phenyl carborane. The same is true of the mono substituted equivalents. The lower energy LUMO of the mono naphthyl carborane makes it easier to reduce than the mono phenyl carborane.

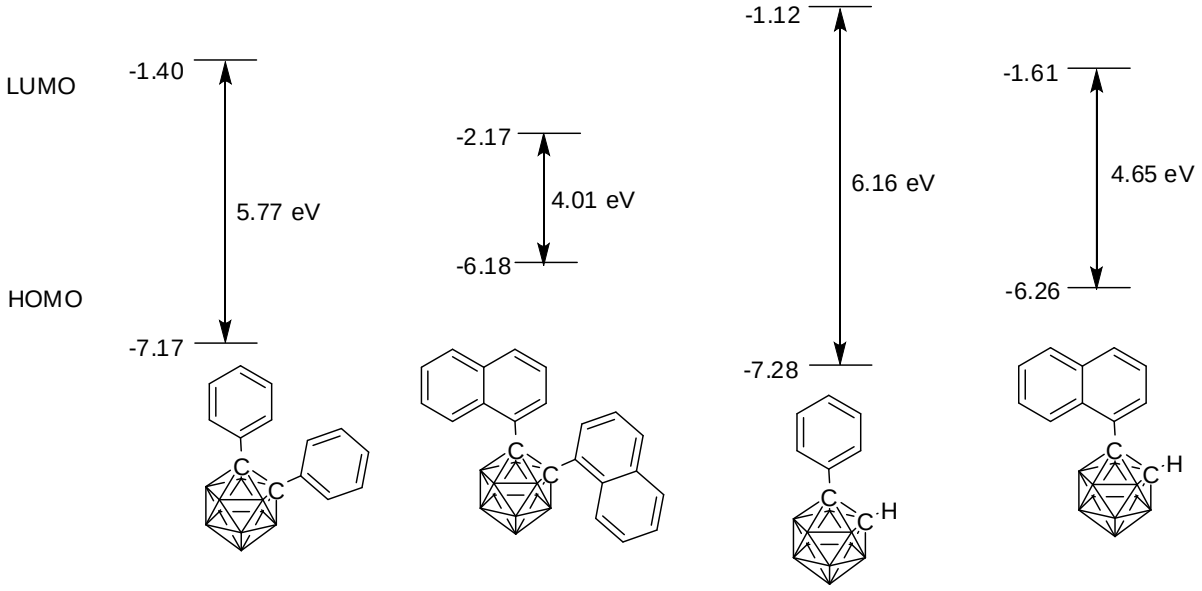

Figure 5–20: DFT calculated (B3LYP/6-31G*) HOMO LUMO energy gaps of *ortho* di-naphthyl, di-phenyl, mono naphthyl and mono phenyl carboranes.

5.3.2 Spectroelectrochemistry

5.3.2.1 Ortho di-naphthyl carborane

Spectroelectrochemistry and calculations can give us clues as to the location of the electrons added on reduction. In IR spectroelectrochemistry of the carboranes we can see the change in energy of the cage B-H band on reduction.

The IR spectroelectrochemistry results for the di-naphthyl and di-phenyl compounds are similar. The boron-hydrogen stretching frequencies are shifted to lower energies as the compound is reduced, Figure 5–21. The peak for the neutral di-naphthyl carborane species is shifted by 30 cm^{-1} to give the radical anion. The *ortho* di-phenyl carborane displays a greater shift in B-H stretching frequency, of 80

cm^{-1}.[3] For the di-phenyl analogue the B-H stretches are shifted by a further 100 cm^{-1} on going through the second reduction wave.[3] This is again slightly more than for the case of the di-naphthyl carborane where the shift is a further 90 cm^{-1}. On reoxidation, the original neutral band is recovered in both cases.

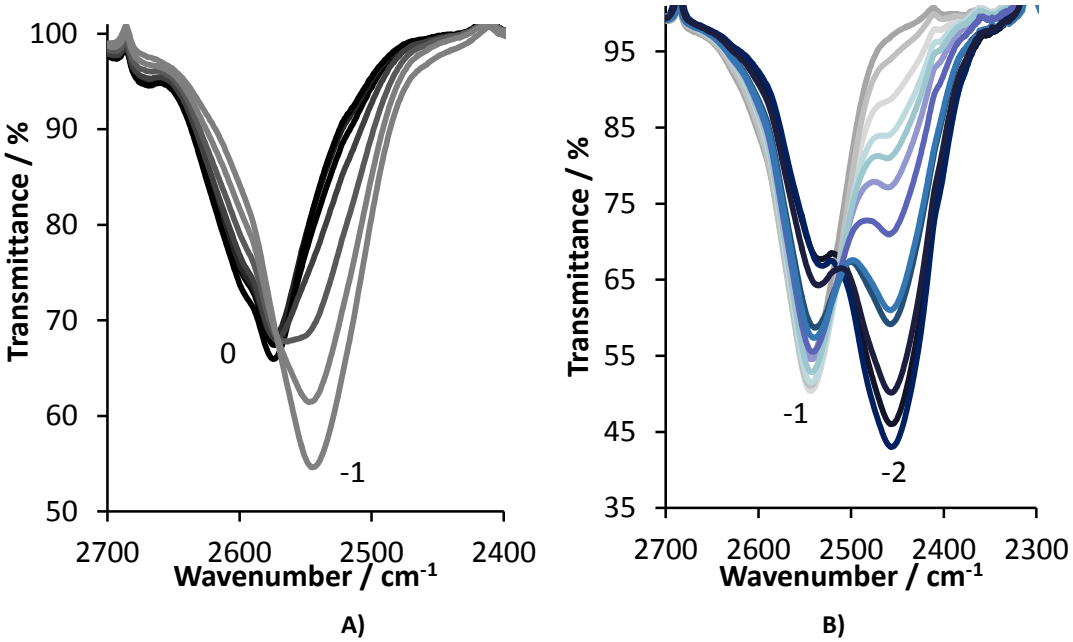

Figure 5–21: IR spectroeletrochemical study of di-naphthyl-ortho-carborane, in 0.1 M NBu4PF6 in DCM. A) reduction from neutral to anion B) reduction of anion to dianion.

For the UV-Vis spectroelectrochemistry studies, again, both the di-naphthyl and di-phenyl compounds produce similar spectra.[3] On reduction from the neutral towards the monoanion, a new band increases in intensity. The radical anion spectrum in Figure 5–22 shows a distinct shape that may be due to the vibrational fine structure of the naphthalene part of the molecule specifically, suggesting that the extra electron may be localised on the naphthalene, not in the cage itself. On further reduction to the dianion, both the bands are seen to reduce in intensity to give a broad band. On reoxidation the neutral band is again recovered.

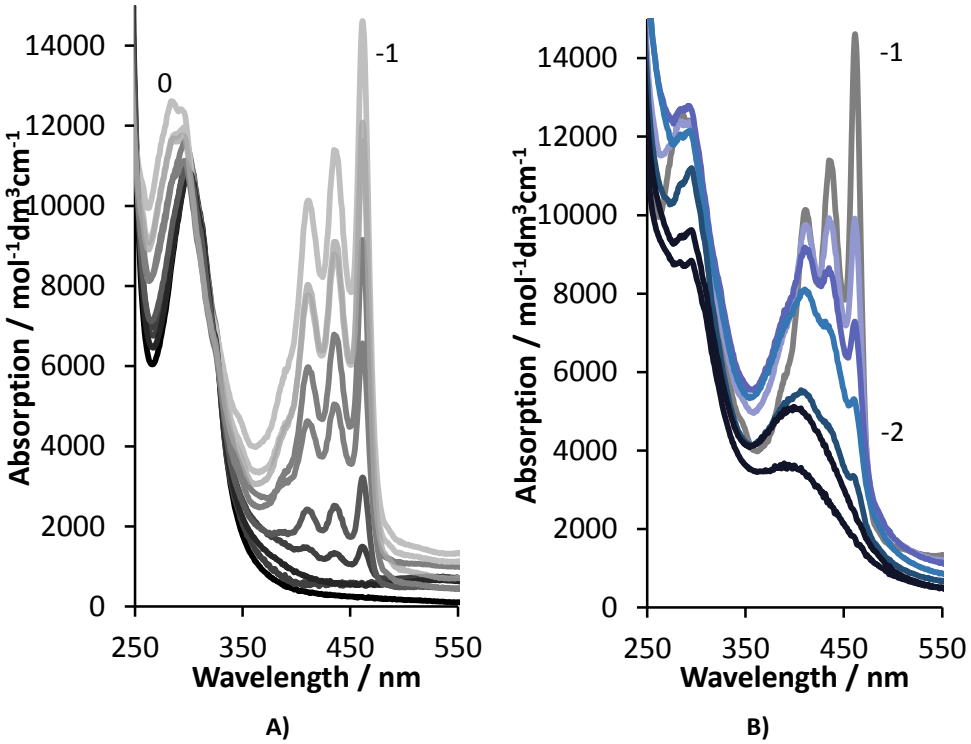

Figure 5–22: UV-Vis spectroelectrochemical study of di-naphthyl-*ortho*-carborane in 0.1 M NBu_4PF_6 in DCM. A) reduction from neutral to anion B) reduction of anion to dianion.

Oxidation state of *ortho* di-naphthyl carborane	IR maxima / cm^{-1}	UV-vis maxima / nm
0	2574, (2595sh)	300
-1	2545	283, 409, 435, 460
-2	2456, (2530)	291, (398)

Table 5–6: IR and UV-vis maxima of different oxidation states of *ortho* di-naphthyl carborane.

5.3.2.2 Ortho mono naphthyl carborane

In the cyclic voltammogram of *ortho* mono naphthyl carborane, unlike for the disubstituted analogue, the radical monoanion was not resolved. As such we would not expect to record the IR and UV-Vis spectra of the radical anion of monosubstituted *ortho* naphthyl carborane. In the UV-Vis spectrum, on reduction the dianion is formed, which has a broad UV-Vis spectrum similar in shape to that observed in the disubstituted analogue. In the IR spectrum, on reduction the BH band shifts by 130 cm^{-1}. Without applying an increased reduction potential, this band diminishes and a band at a shift of 30 cm^{-1} from the original neutral spectrum begins to increase. The large shift in the first band formed on reduction suggests that the dianion is formed first. The formation of the band with a smaller shift from

the neutral spectrum can be assumed to be due to a subsequent structural rearrangement after the initial dianion formation. In both cases the band corresponding to the neutral compound is recovered on reoxidation.

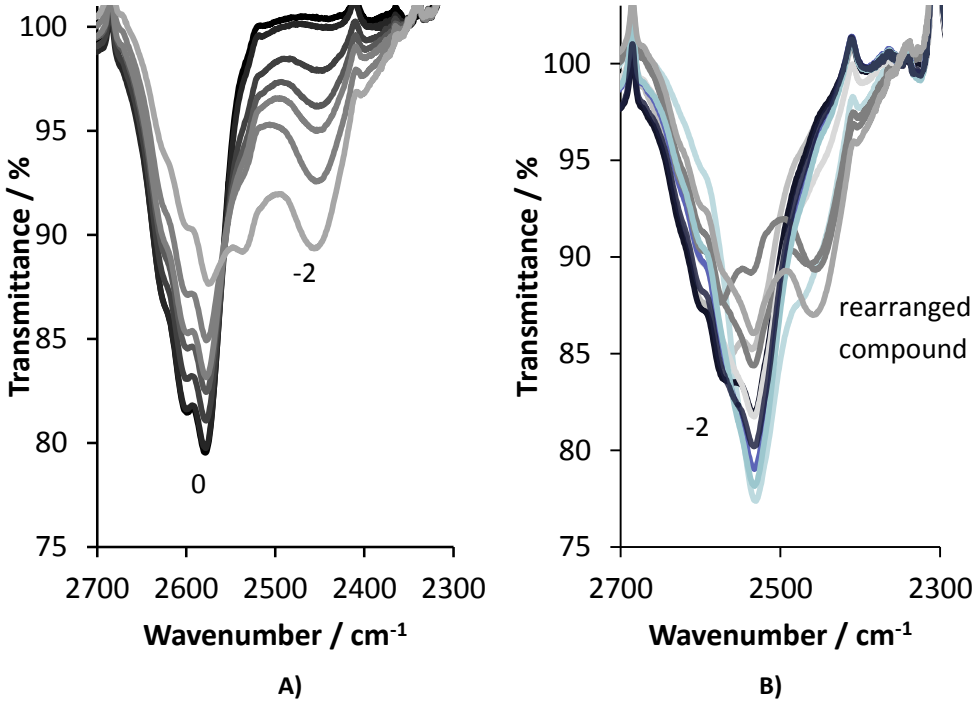

Figure 5–23: IR spectroelectrochemical study of mono-naphthyl-*ortho*-carborane in 0.1 M NBu_4PF_6 in DCM. A) reduction from neutral to a dianion B) conversion of dianion to rearranged compound.

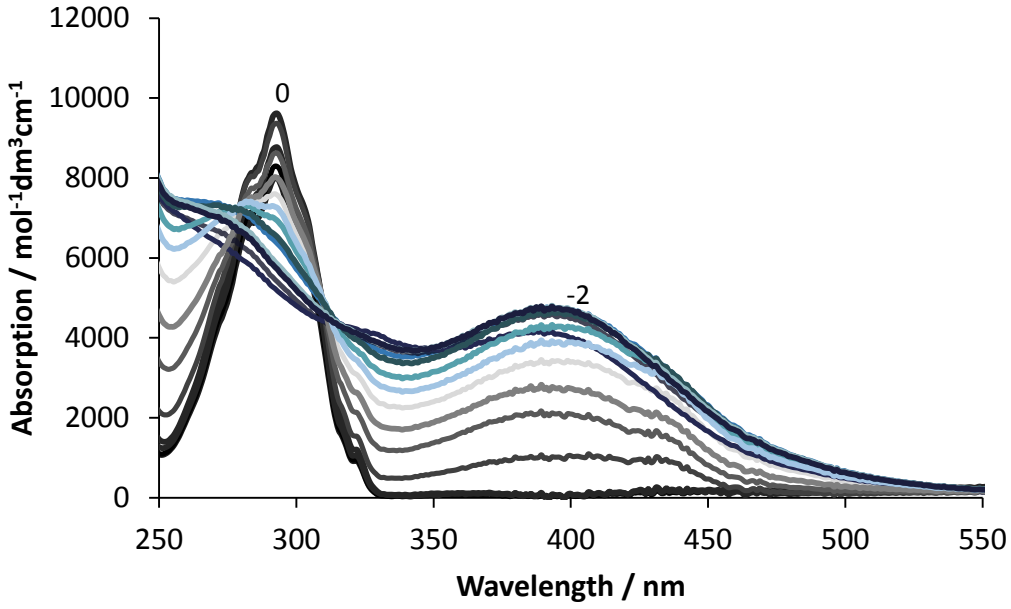

Figure 5–24: UV-Vis spectroelectrochemical study of mono-naphthyl-*ortho*-carborane in 0.1 M NBu_4PF_6 in DCM.

Oxidation state of *ortho* mono naphthyl carborane	IR maxima / cm^{-1}	UV-vis maxima / nm
0	2576, 2600, (2625sh)	291, (300sh, 282sh)
-2	2453, 2530, 2572, (2598sh, 2623sh)	-
Rearranged compound	2530, 2564, 2597, (2622sh)	389

Table 5–7: IR and UV-vis maxima of different oxidation states of *ortho* mono naphthyl carborane.

5.3.3 Calculations

5.3.3.1 Ortho di-naphthyl carborane

We see dramatic changes in the optimised structure of di-naphthyl *ortho* carborane on reducing from the neutral to the anion and then to the dianion. On reduction to the anion the calculated cage C-C bond length increases from 1.928 Å to 2.444 Å. On further reduction to the dianion, the distance increases to 2.940 Å. This opening up of the cage accommodates the addition of electrons.

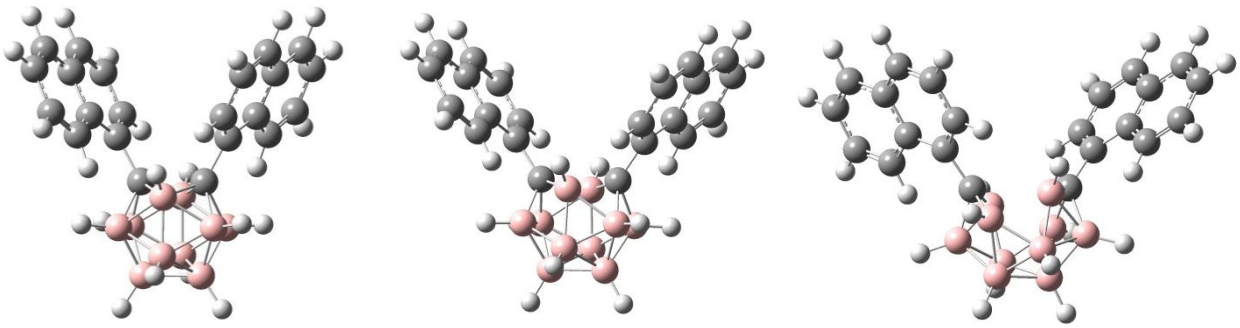

A) **B)** **C)**

Figure 5–25: DFT calculated (B3LYP/6-31G*) optimised geometries for A) neutral B) anion and C) dianion of dinaphthyl *ortho* carborane.

Molecular orbitals calculated for the di-naphthyl *ortho* carborane (B3LYP/6-31G*) monoanion are shown in Figure 5–26. For di-phenyl *ortho* carborane the HOMO-LUMO gap of the neutral molecule is 5.78 eV, greater than for di-naphthyl *ortho* carborane where the gap is much less at 4.01 eV. This is in line with the observation that di-naphthyl *ortho* carborane is more easily reduced than the di-phenyl equivalent. The frontier orbitals are largely based on the naphthalene groups. There is no obvious reason from the calculations as to why a radical anion would be more stable in the case of the di-naphthyl compared with the di-phenyl.

This observed effect therefore may be because the structural change on going from monoanion to dianion is not energetically favourable.

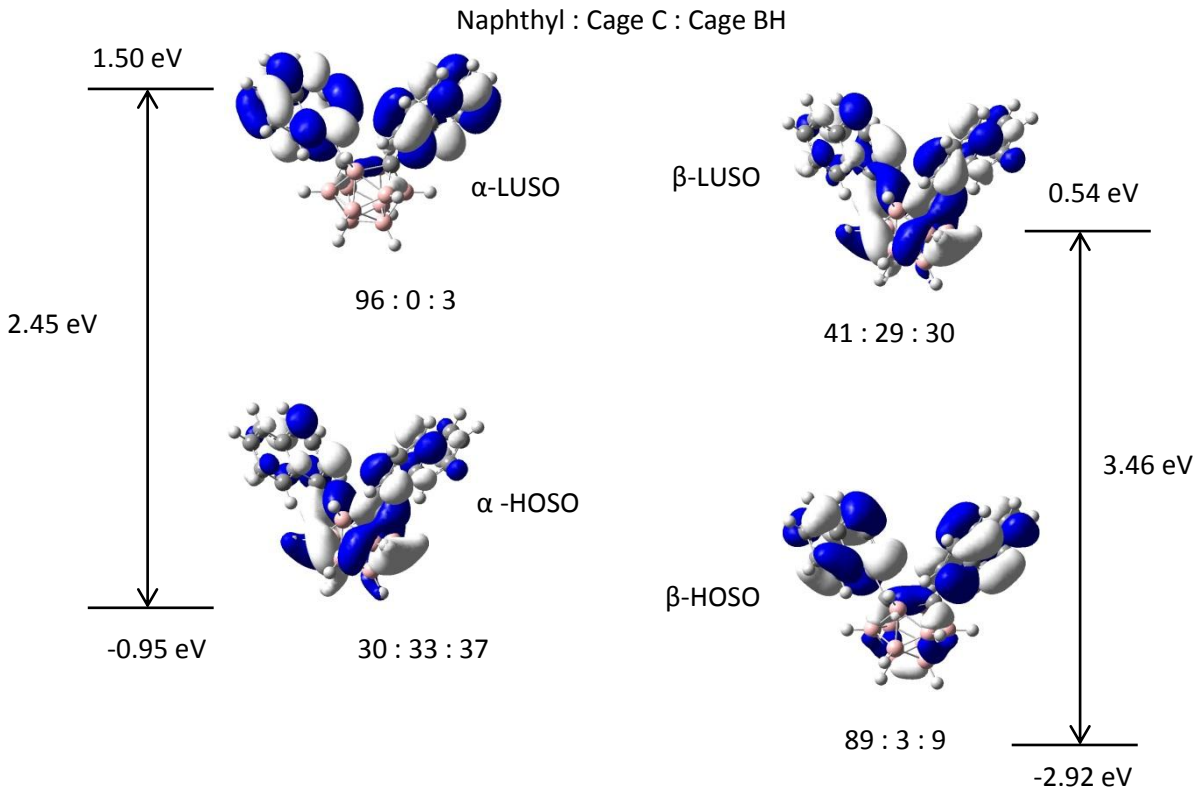

Figure 5–26: Molecular orbitals calculated for a di-naphthyl *ortho* carborane radical monoanion. Ratio of contributions naphthyl: cage C: cage BH.

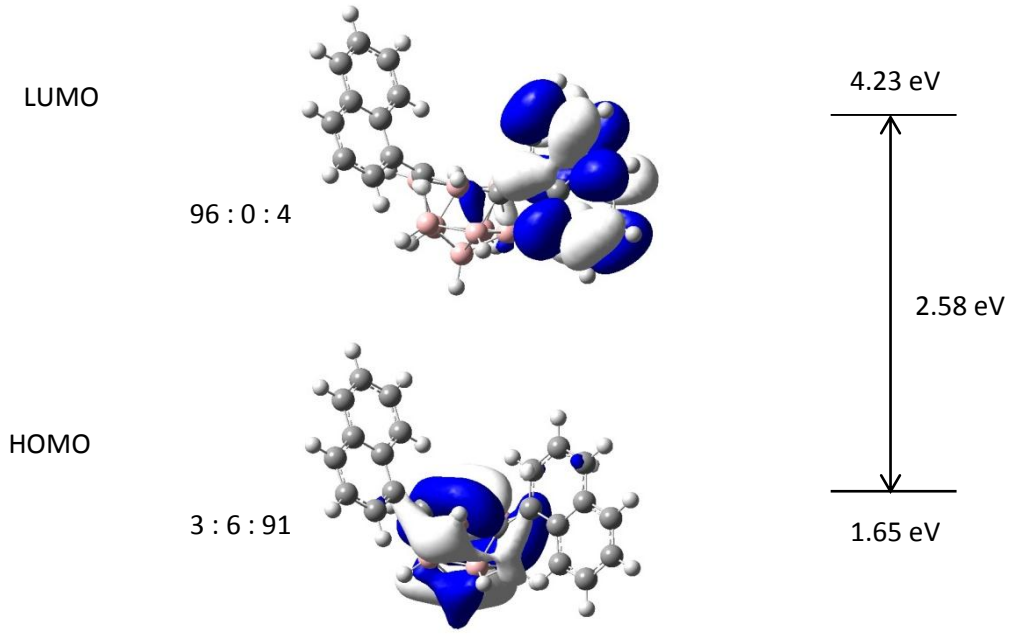

Figure 5–27: Molecular orbitals calculated for a di-naphthyl *ortho* carborane dianion. Ratio of contributions naphthyl : cage C: cage BH.

The IR spectrum was simulated, using DFT computations (B3LYP/6-31G*), for the optimised geometries of the neutral, radical anion and dianion species of di-naphthyl *ortho* carborane. The calculated positions of the BH bands reduce in energy as the carborane cage is reduced. For the neutral species the BH band is calculated to be at 2574 cm^{-1}. For the radical anion the BH band is calculated to be at 2539 cm^{-1}, and on further reduction to the dianion, calculations suggest the band will be further lowered in energy to 2437 cm^{-1}.

The simulated UV-Vis spectrum for the neutral species shows a single band at 208 nm. The radical anion calculated spectrum has bands at 294 and 474 nm and is in good agreement with the observed spectra.

5.3.3.2 Ortho mono naphthyl carborane

Mono naphthyl *ortho* carborane is calculated to undergo an increase in the cage C-C bond length from the neutral and mono anion to the dianion, Figure 5–28. For the neutral, A), the calculated bond length was found to be 1.673 Å. Reduction to the mono anion leads to a small increase in distance, to 1.686 Å. On further reduction to the dianion there is an increase to 2.913 Å.

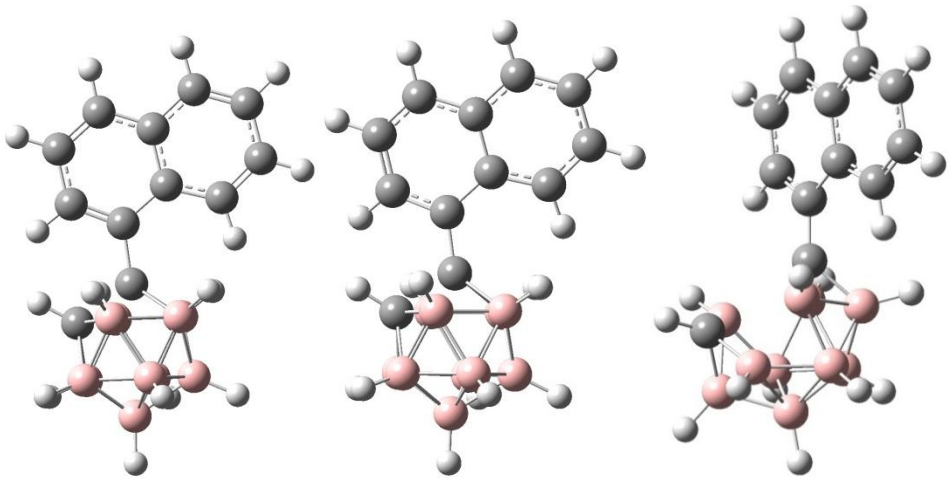

A) **B)** **C)**

Figure 5–28: DFT calculated (B3LYP/6-31G*) optimised geometries for A) neutral B) anion and C) dianion of mono naphthyl *ortho* carborane.

The frontier orbitals of the mono naphthyl anion are based on the naphthyl group predominantly, with a contribution from the carborane cage. The dianion HOMO is based on the carborane cage.

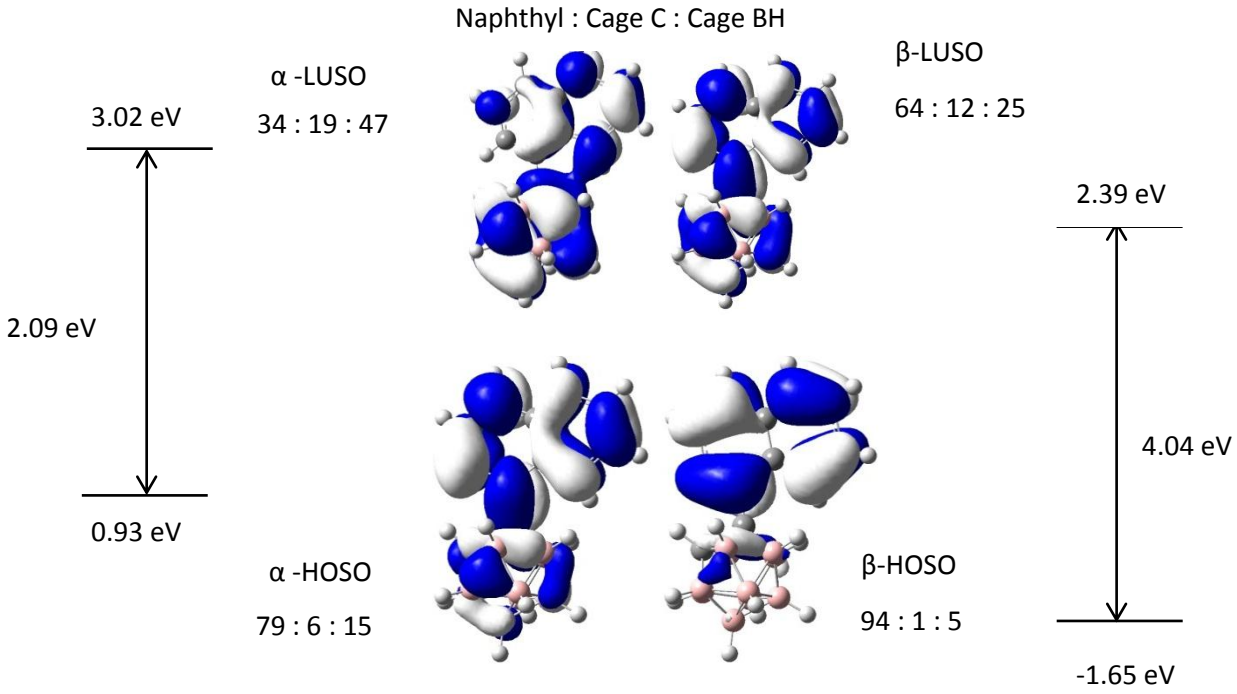

Figure 5–29: Molecular orbitals calculated for a mono naphthyl *ortho* carborane radical monoanion. Ratio of contributions naphthyl: cage C: cage BH.

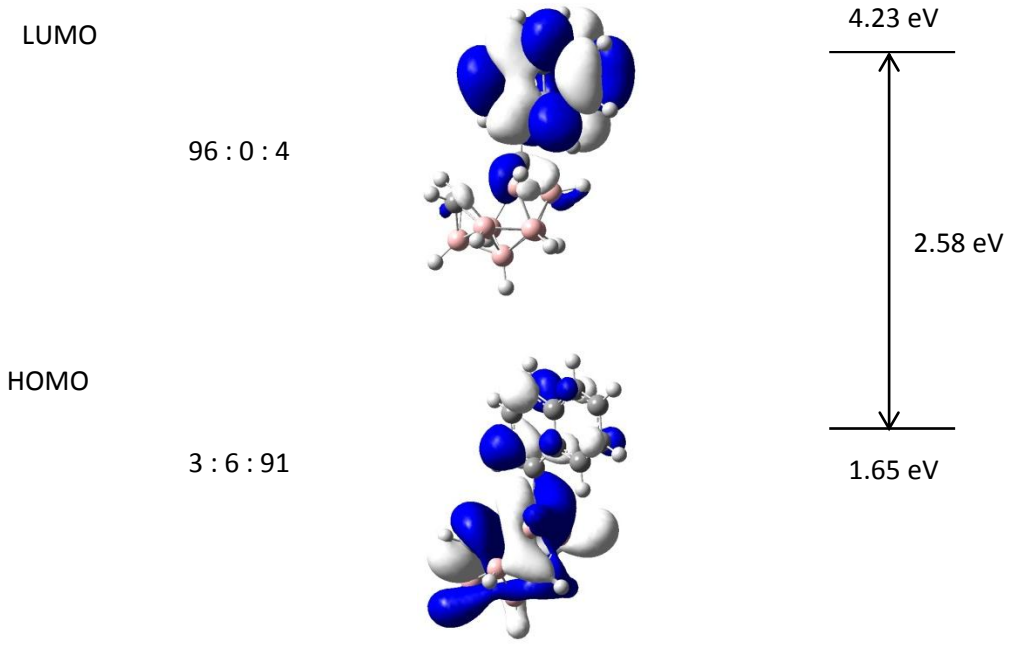

Figure 5–30: Molecular orbitals calculated for a mono naphthyl *ortho* carborane dianion. Ratio of contributions naphthyl: cage C: cage BH.

The IR spectrum was simulated for the optimised geometries of the neutral, radical anion and dianion species of mono-naphthyl *ortho* carborane. The calculated positions of the BH bands reduce in energy as the carborane cage is reduced. For the neutral species the BH band is calculated to be at 2576 cm^{-1}, and on reduction to the lowest energy dianion, calculations suggest the band will be lowered in energy to 2396 cm^{-1}. The two bands that arise on reduction may both be due to different geometries of the dianion. Several other optimised geometries with higher energies have been calculated, with varying cage conformations and different dihedral angles between the cage C-C and naphthyl group. They have been found to display BH IR bands at between 2391 and 2425 cm^{-1}.

The simulated UV-Vis spectrum for the neutral species shows a band at 293 nm, in good agreement with the observed spectrum. The dianion calculated spectrum has a band at 443 nm.

5.4 Carboranyl Triarylamines

The electrochemistry of the carboranyl triarylamines and tritolylamine were investigated and the results are summarised in Table 5–8. In Figure 5–31 the oxidations of these compounds are illustrated alongside that of the internal reference, ferrocene. The *para* disubstituted carboranyl triarylamine was sparingly soluble in the acetonitrile electrolyte solution, leading to the poor quality of the CV shown in Figure 5–31. In all cases a reversible oxidation was observed. The carboranyl triarylamines displayed an $E_{1/2}$(ox) at 0.50 – 0.53 V. Tritolylamine, in contrast, was more easily oxidised with an $E_{1/2}$(ox) of 0.38 V.

o* / *m* / *p	**Mono / Di**	**E(Ox) cathodic V**	**E(Ox) anodic V**	**$E_{1/2}$ (Ox) V**	**Ox p-p mV**	**E(Red) cathodic V**	**E(Red) anodic V**	**$E_{1/2}$ (Red) V**	**Red p-p mV**	**Fc p-p mV**
o	**Mono**	0.51	0.60	0.55	85	-2.18	-1.72	-1.95	457	95
m	**Mono**	0.45	0.56	0.52	105	-	-	-	-	107
m	**Di**	0.47	0.55	0.51	83	-	-	-	-	71
p	**Mono**	0.46	0.55	0.50	88	-	-	-	-	88
p	**Di**	0.47	0.55	0.51	78	-	-	-	-	78
$NTol_3$		0.34	0.43	0.38	88	-	-	-	-	100

Table 5–8: Reduction and oxidation potentials of the carboranyl triarylamines in 0.1 M NBu_4PF_6 in MeCN, 100 mV/s, relative to an internal reference of ferrocene at 0.00 V, using a glassy carbon working electrode.

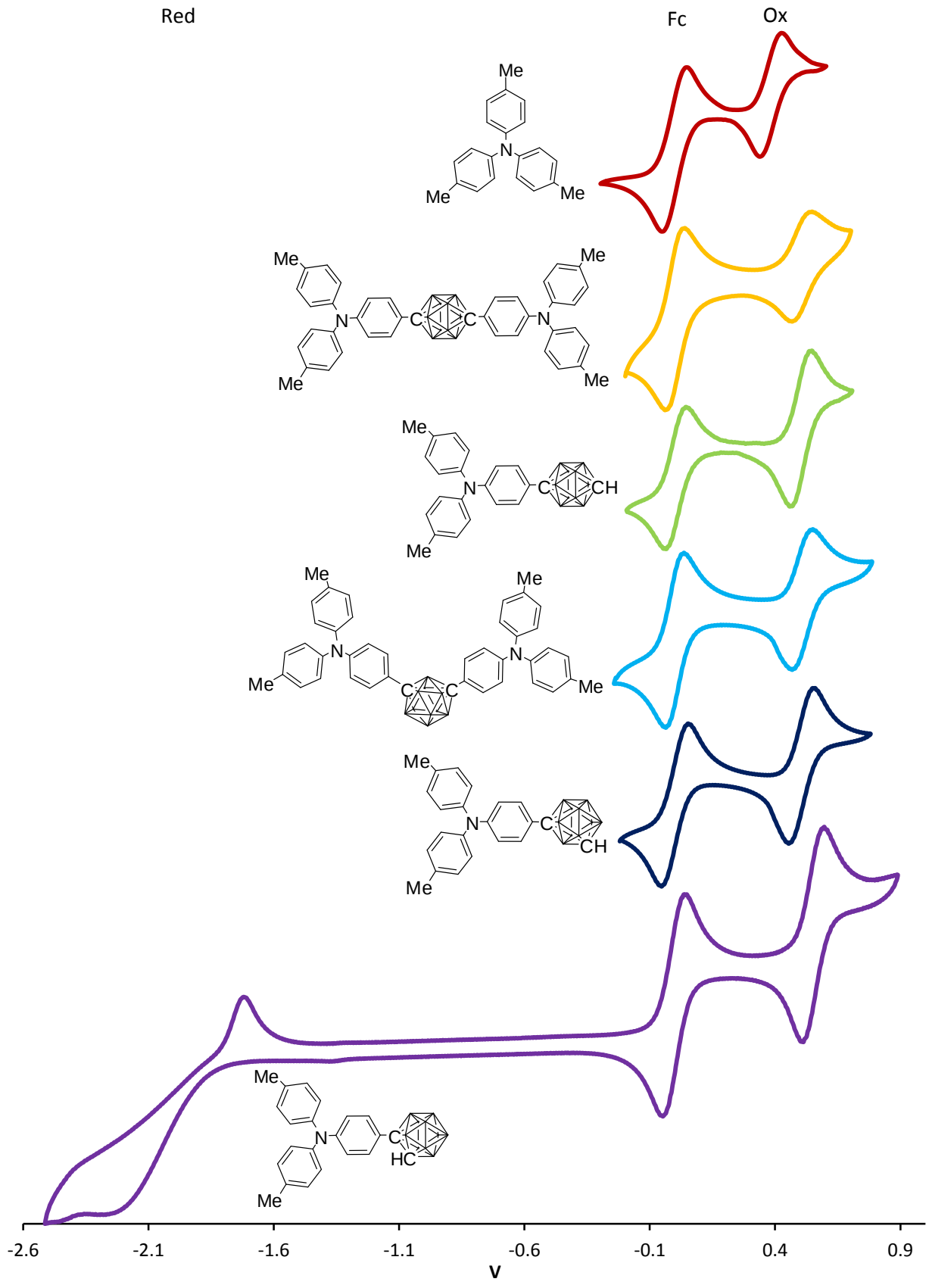

Figure 5–31: Cyclic voltammograms of the carboranyl triarylamines and tritolylamine in 0.1 M NBu_4PF_6 in MeCN, 100 mV/s, relative to an internal reference of ferrocene at 0.00 V, using a glassy carbon working electrode.

Reductions were not observed for the *meta* or *para* carboranyl triarylamines, which is to be expected of *meta* and *para* carboranes. *Ortho* mono substituted carboranyl triarylamine displays an irreversible two electron reduction.

5.4.1 Calculations

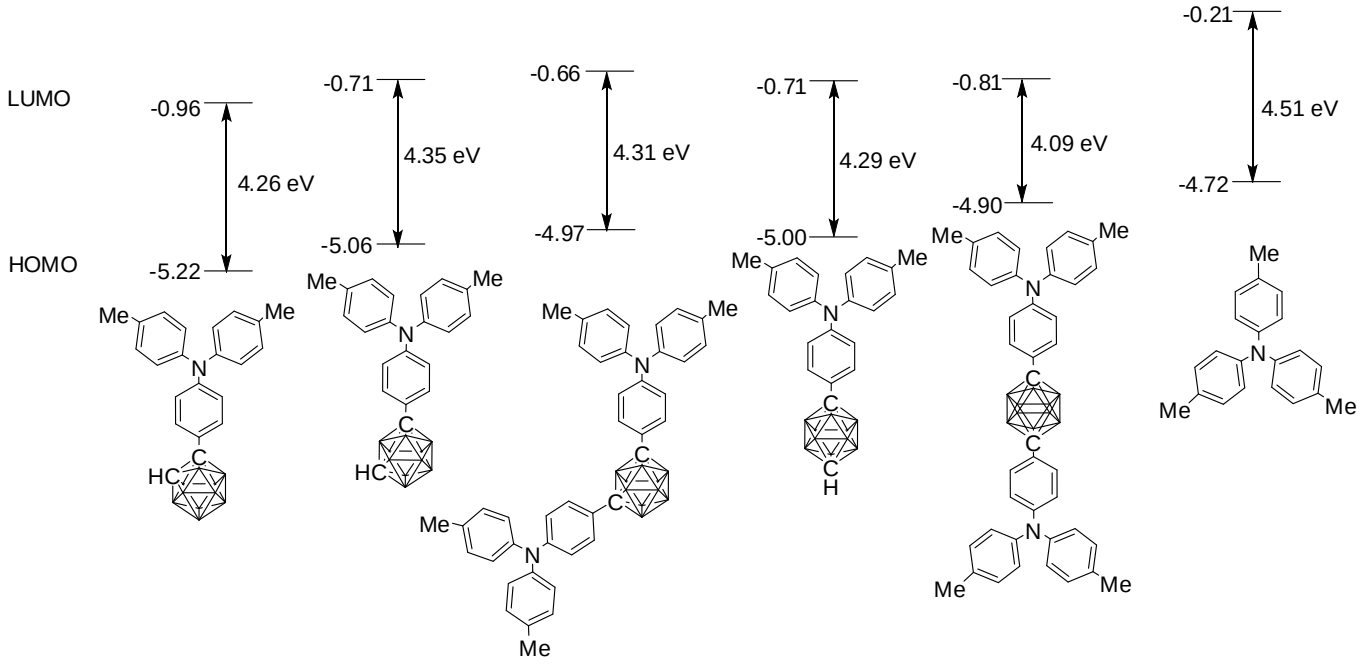

Figure 5–32: DFT (B3LYP/6-31G*) calculated HOMO LUMO energies for the carboranyl triarylamines and tritolylamine.

The carboranyl triarylamines are oxidised at higher energy than tritolylamine. Calculations of the HOMO energies, Figure 5–32, of these molecules are in agreement with this. The HOMO of tritolylamine is higher in energy than that of the carboranyl triarylamines, and as such is able to lose electrons more readily. The electron withdrawing nature of the carborane cage lowers the energy of the LUMO.

The molecular orbitals of the carboranyl triarylamines cations are based primarily on the triarylamine group. For example, the orbitals as shown in Figure 5–33 for the *meta* mono substituted carborane are typical.

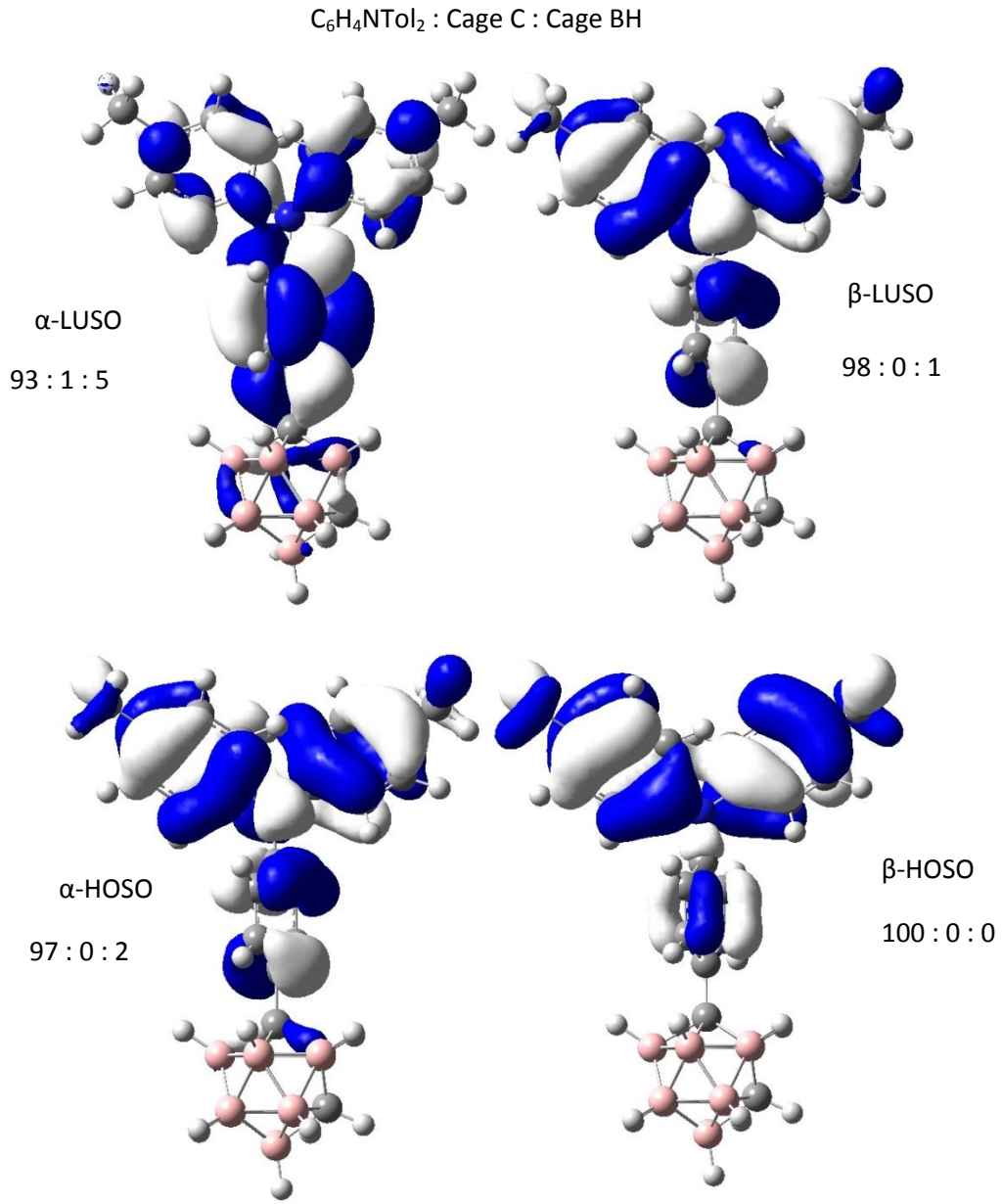

Figure 5–33: DFT (B3LYP/6-31G*) calculated frontier orbitals for the cation of the *meta* mono substituted carboranyl triarylamine.

The *ortho* mono carboranyl triarylamine dianion has an optimised geometry as shown in Figure 5–34. The mono anion has a calculated extended cage C-C bond length of 2.383 Å. The dianion has a cage C-C bond length which is extended further to 2.641 Å. As such, it is to be expected that the HOMO molecular orbital of the dianion is 76 % carborane cage in character, the cage C-C bond elongating to accommodate the additional electrons on the carborane cage.

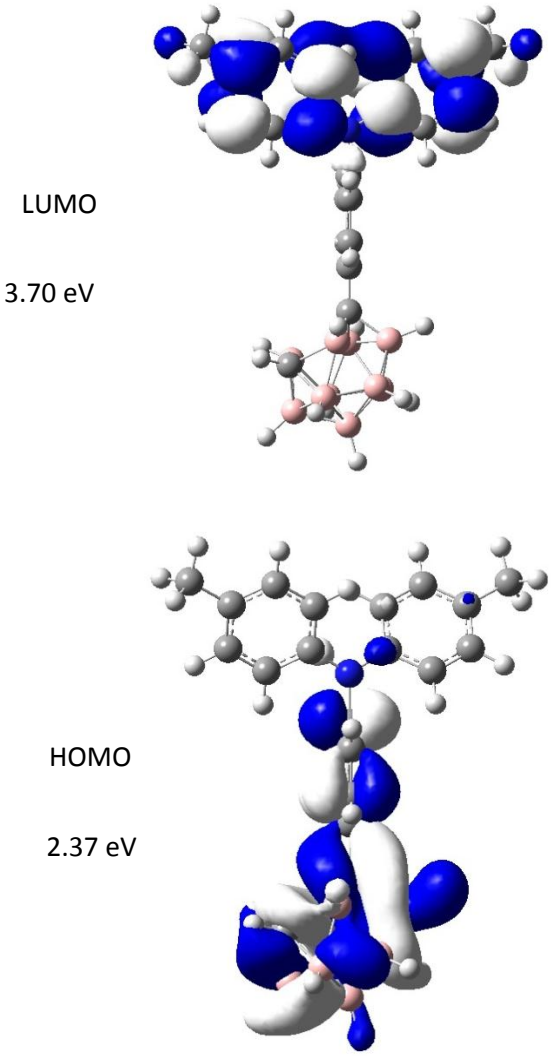

Figure 5–34 : DFT (B3LYP/6-31G*) calculated frontier orbitals for the dianion of the *ortho* mono substituted carboranyl triarylamine.

5.5 Bridged Carboranes

Several molecules have been reported to display electronic communication through a bridging *para* carborane cage as discussed in the literature review, chapter 1.[4,5,6,7,8] Here, we investigated the possibility of electronic communication between two carborane cages through various bridging groups. As the first cage is reduced, the reduction potential required to add electrons to the second cage will be altered if there is communication through a bridging group. In a cyclic voltammogram, if reductions occur close together, then it can be deduced that there is no communication between the two carborane cages, as both cages will accept and lose electrons at the same potential. If there is communication between bridged cages, there will be an increase in the separation of reduction potentials.

Table 5–9 summarises the reduction potentials observed for a variety of bridged carboranes. 1,4-(1'-(4''-^{t}BuC_6H_4)-1',2'-$C_2B_{10}H_{10})_2$-C_6H_4 was sparingly soluble in the acetonitrile electrolyte solution leading to the poor quality of the CV trace in Figure 5–37. 1,4-(1'-C_6H_4NTol_2-1',2'-$C_2B_{10}H_{10})_2C_6F_4$ and 1,4-(1'-C_6H_4NTol_2-1',2'-$C_2B_{10}H_{10})_2$-C_6H_4 were insoluble in the electrolyte solution and so the reduction and oxidation behaviour could not be measured.

1,4-(1'-$C_{10}H_7$-1',2'-$C_2B_{10}H_{10})_2$-C_6F_4 undergoes reduction at the lowest potential of these compounds. All four display two distinct, two electron reversible reductions of the carborane cages. The greatest separation between reductions is seen for 1,4-(1'-$C_{10}H_7$-1',2'-$C_2B_{10}H_{10})_2$-C_6F_4, at 660 mV, indicative of communication between the two cages. 1,4-(1'-(4''-^{t}BuC_6H_4)-1',2'-$C_2B_{10}H_{10})_2$-C_6H_4 and 1,4-(C_6H_5-1',2'-$C_2B_{10}H_{10})_2$-C_4SH_2 also display large separations between reduction potentials. In 4,4'-(1''-C_6H_5-1'',2''-$C_2B_{10}H_{10})_2$-$(C_6H_4)_2$ however the reductions are separated by 190 mV. This separation is comparable in size to that observed in 1,2-$(C_6H_5)_2$-1,2-$C_2B_{10}H_{10}$.

R	X	E(Red_1) cathodic V	E(Red_1) anodic V	$E_{1/2}$ (Red_1) V	Red_1 p-p mV	E(Red_2) cathodic V	E(Red_2) anodic V	$E_{1/2}$ (Red_2) V	Red_2 p-p mV	$\Delta E_{1/2}$ (Red_1-Red_2) mV	E(Ox) V	Fc p-p mV
C_6H_5	4,4'-$(C_6H_4)_2$	-1.63	-1.49	-1.56	134	-1.82	-1.69	-1.75	134	190	-	93
C_6H_5	2,5-C_4SH_2	-1.40	-1.27	-1.34	122	-1.97	-1.88	-1.92	90	580	-	78
4-^{t}BuC_6H_4	1,4-C_6H_4	-1.54	-1.24	-1.39	300	-1.99	-1.87	-1.93	120	540	-	98
$C_{10}H_7$	1,4-C_6F_4	-0.92	-0.86	-0.89	60	-1.60	-1.50	-1.55	100	660	-	78
$C_6H_4NTol_2$	1,4-C_6H_4	-	-	-	-	-	-	-	-	-	-	-
$C_6H_4NTol_2$	1,4-C_6F_4	-	-	-	-	-	-	-	-	-	-	-

Table 5–9: Reduction and oxidation potentials of compounds with bridged *ortho* carboranes, (1-R-1,2-$C_2B_{10}H_{10}$)$_2$X in 0.1 M NBu_4PF_6 in MeCN, 100 mV/s, relative to an internal reference of ferrocene at 0.00 V, using a glassy carbon working electrode.

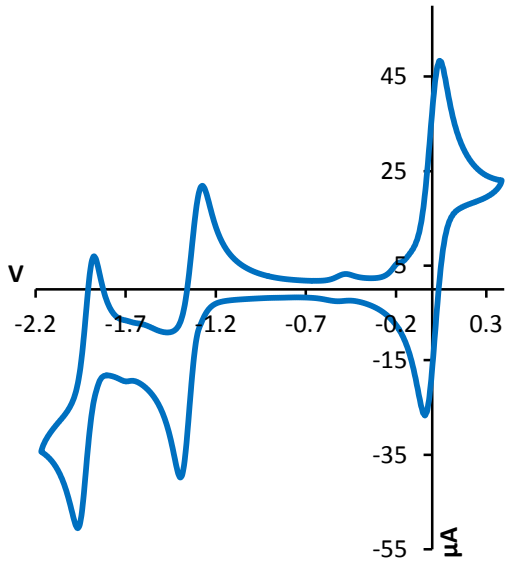

Figure 5–35 : CV of 2,5-(1'-C_6H_5-1',2'-$C_2B_{10}H_{10}$)$_2$-C_4SH_2.[#]

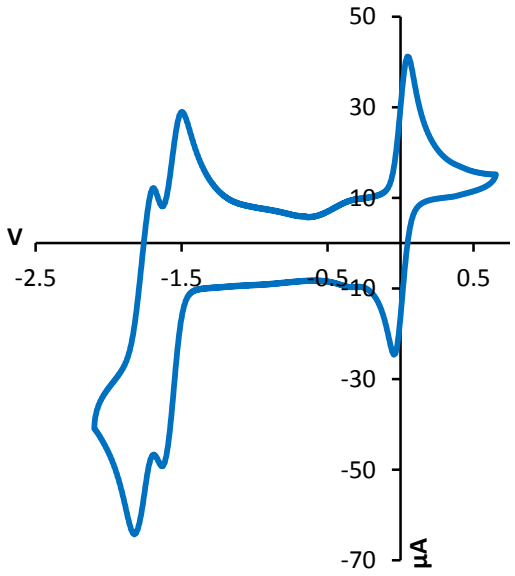

Figure 5–36 : CV of 4,4'-(1''-C_6H_5-1'',2''-$C_2B_{10}H_{10}$)$_2$-(C_6H_4)$_2$.[#]

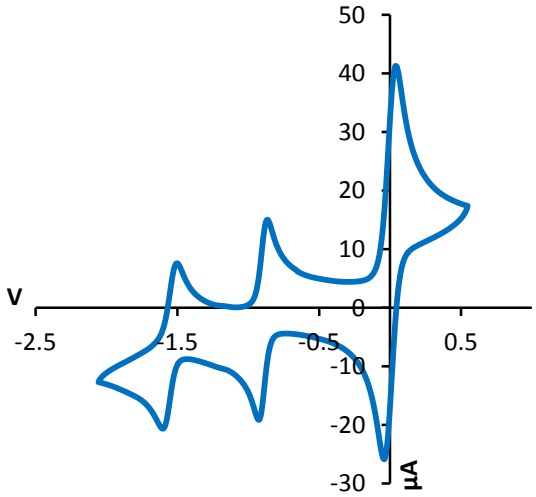

Figure 5–37 : CV of 1,4-(1'-$C_{10}H_7$-1',2'-$C_2B_{10}H_{10}$)$_2$-C_6F_4.[#]

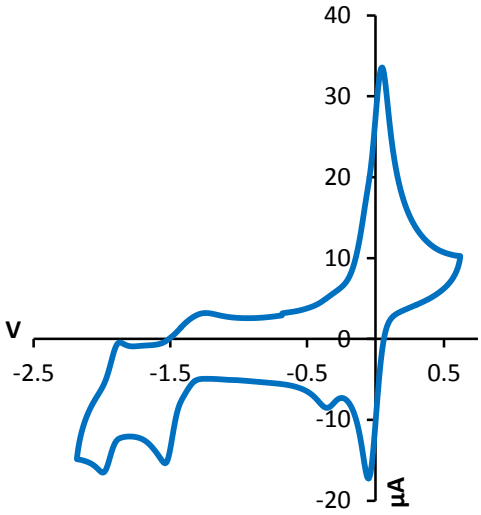

Figure 5–38 : CV of 1,4-(1'-(4''-^{t}BuC_6H_4)-1',2'-$C_2B_{10}H_{10}$)$_2$-C_6H_4.[#]

[#] In 0.1 M NBu4PF6 in MeCN, 100 mV/s, relative to an internal reference of ferrocene at 0.00 V, using a glassy carbon working electrode.

5.5.1 Calculations

The calculated HOMO and LUMO energy levels of these four compounds are shown in Figure 5–39. The molecular orbitals of the frontier orbitals in the dianions of these compounds are shown in Figure 5–40 to Figure 5–43.

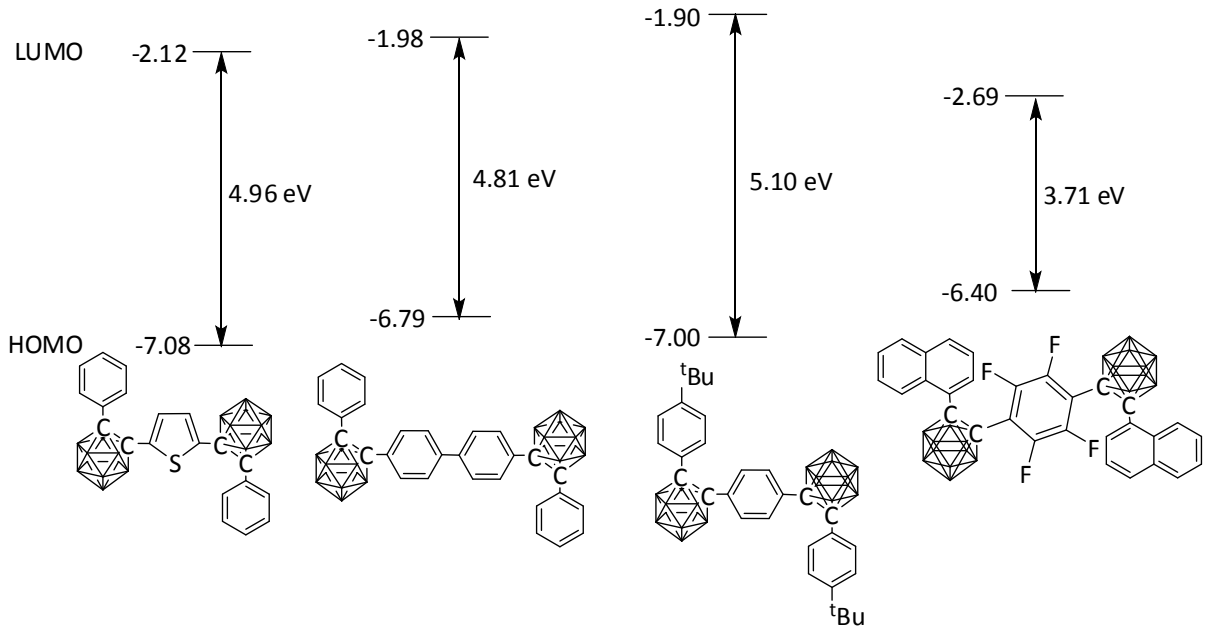

Figure 5–39: DFT (B3LYP/6-31G*) calculated HOMO LUMO energy levels of bridged carboranes.

1,4-(1'-$C_{10}H_7$-1',2'-$C_2B_{10}H_{10}$)$_2$-C_6F_4 is reduced at the lowest potential energy and accordingly is calculated to have the lowest energy LUMO, followed by 2,5-(1'-C_6H_5-1',2'-$C_2B_{10}H_{10}$)$_2$-C_4SH_2 and then 4,4'-(1''-C_6H_5-1'',2''-$C_2B_{10}H_{10}$)$_2$-(C_6H_4)$_2$ and 1,4-(1'-(4''-^{t}BuC_6H_4)-1',2'-$C_2B_{10}H_{10}$)$_2$-C_6H_4. The cage C-C bond lengths are also in line with the observed reduction potentials, Table 5–10. As we have seen before, the larger the cage C-C length, the smaller the reduction potential. This is due to the lesser degree of distortion required to attain the geometry required to accommodate the additional electrons on reduction.

R	X	Calculated C1-C2 / Å	Observed E(red$_1$) cathodic / V	Calculated LUMO energy / eV
C_6H_5	**4,4'-(C_6H_4)$_2$**	1.756 / 1.757	-1.63	-1.98
4-^{t}BuC_6H_4	**1,4-C_6H_4**	1.762 / 1.762	-1.54	-1.90
C_6H_5	**2,5-C_4SH_2**	1.770 / 1.770	-1.40	-2.12
$C_{10}H_7$	**1,4-C_6F_4**	1.845 / 1.849	-0.92	-2.69

Table 5–10 : E(red$_1$) cathodic for bridged carboranes (1-R-1,2-$C_2B_{10}H_{10}$)$_2$X, taken from Table 5–9, compared to DFT(B3LYP/6-31G*) calculated cage C-C lengths and LUMO energy levels.

In all cases the molecular orbitals of the dianions are based predominantly on the carborane cage and the various bridging groups. For each compound, both of the carborane cages display identical cage C-C distances. This is indicative of both cages in each compound undergoing a one electron reduction, forming the dianion. The cage C-C lengths in the tetra-anions of these compounds are greater than those for the dianions and are, again, identical for both cages. This corresponds to each cage accepting a second electron.

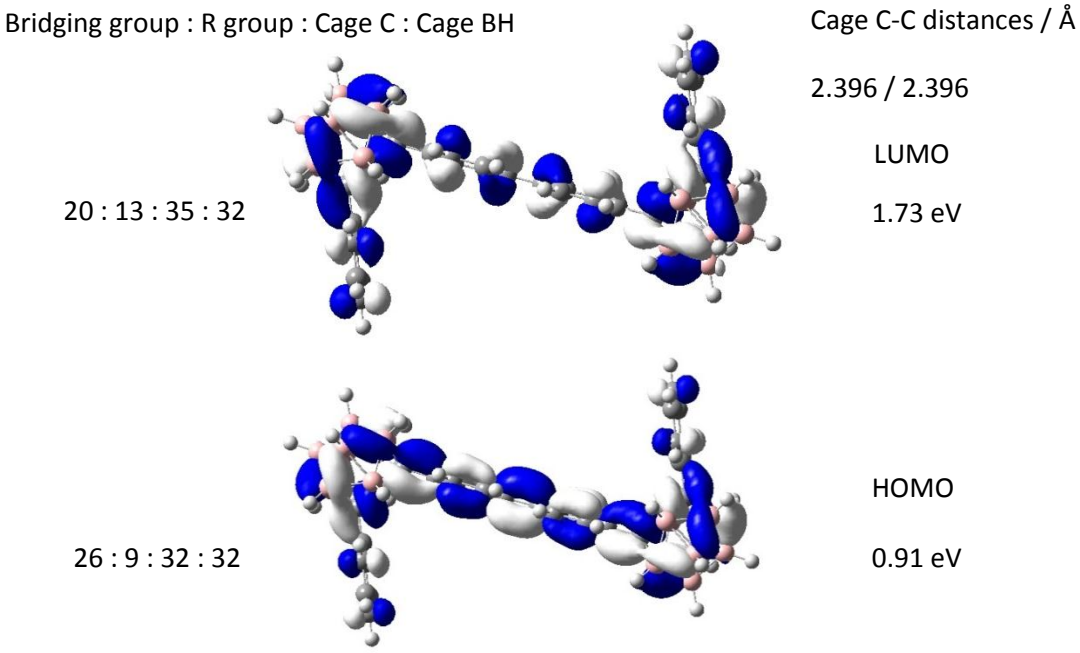

Figure 5–40: DFT (B3LYP/6-31G*) calculated frontier orbitals of the 4,4′-(1′′-C_6H_5-1′′,2′′-$C_2B_{10}H_{10}$)$_2$-(C_6H_4)$_2$ dianion.

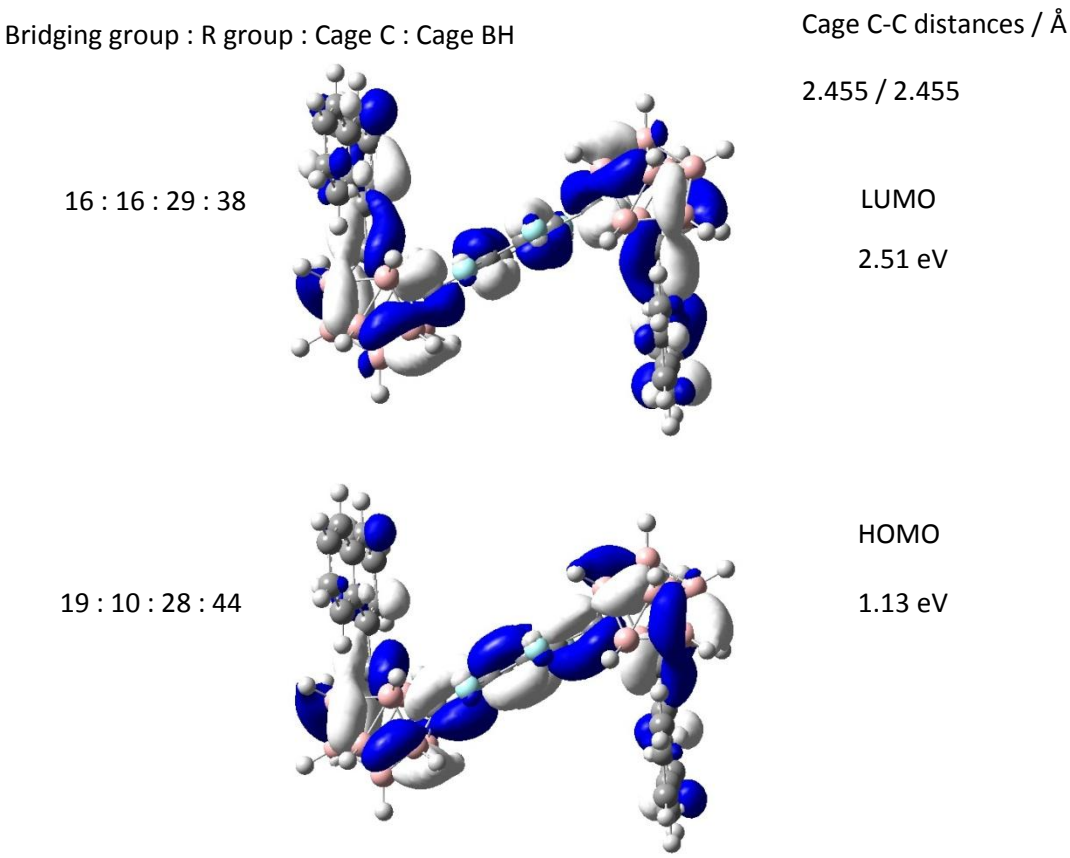

Figure 5–41: DFT (B3LYP/6-31G*) calculated frontier orbitals of the 1,4-(1'-$C_{10}H_7$-1',2'-$C_2B_{10}H_{10}$)$_2$-C_6F_4 dianion.

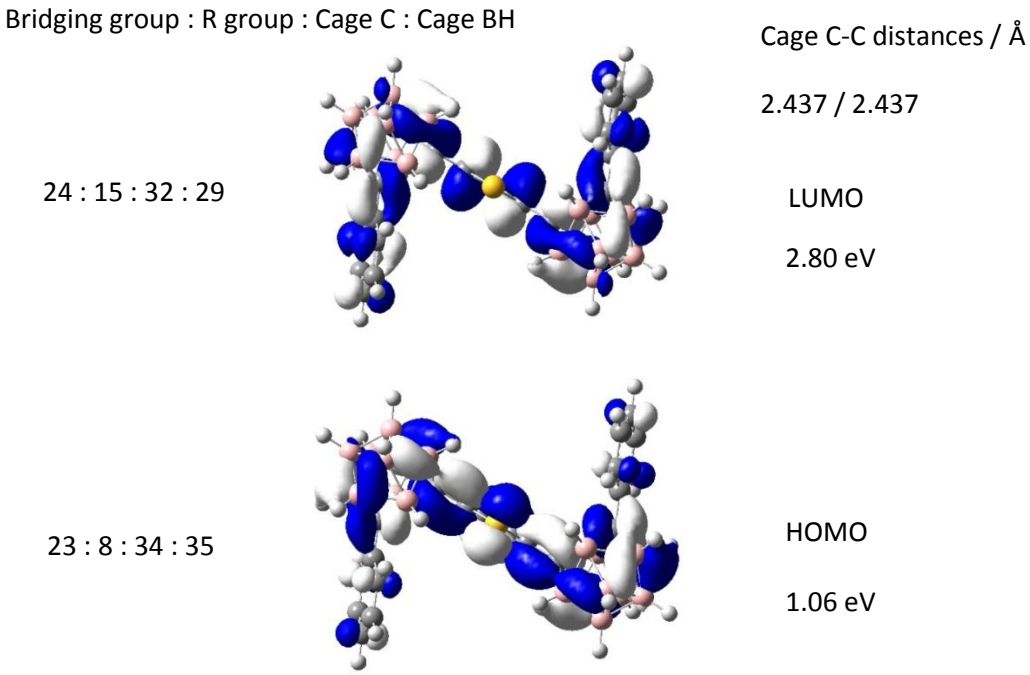

Figure 5–42: DFT (B3LYP/6-31G*) calculated frontier orbitals of the 2,5-(1'-C_6H_5-1',2'-$C_2B_{10}H_{10}$)$_2$-C_4SH_2 dianion.

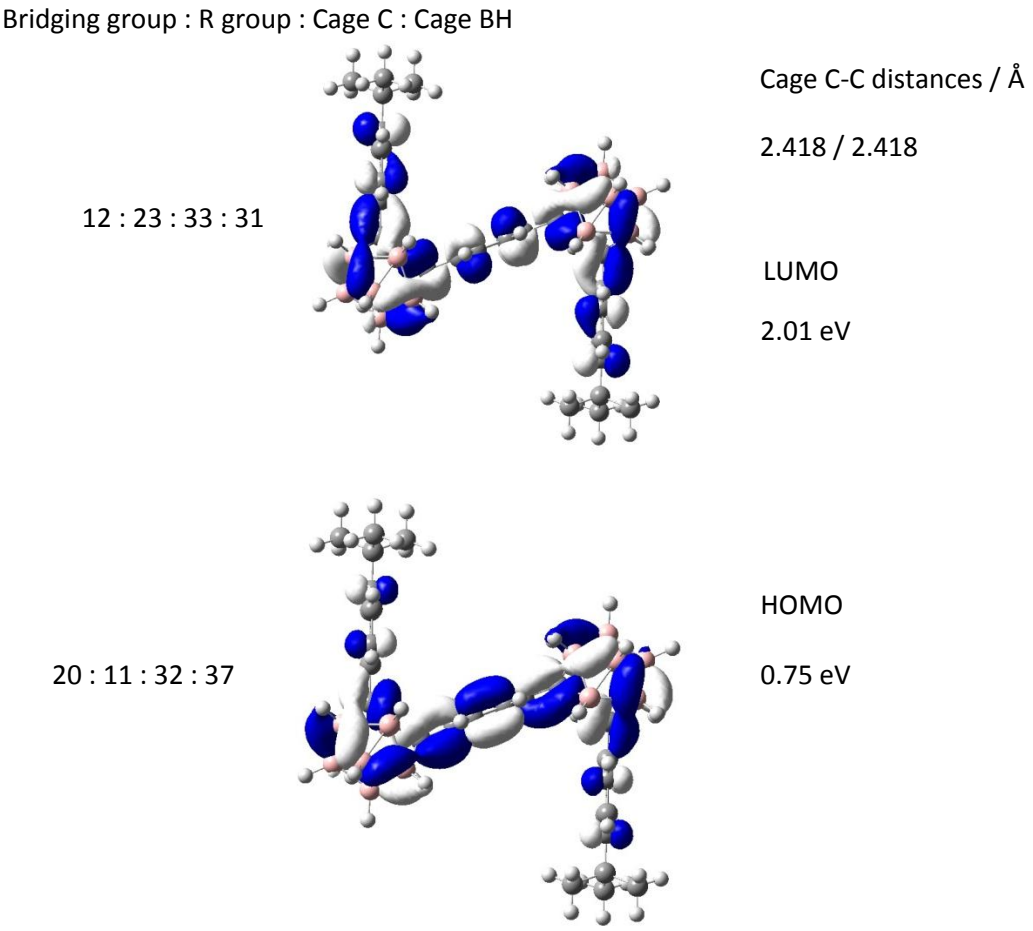

Figure 5–43: DFT (B3LYP/6-31G*) calculated frontier orbitals of the 1,4-(1'-(4''-^{t}BuC$_6$H$_4$)-1',2'-C$_2$B$_{10}$H$_{10}$)$_2$-C$_6$H$_4$ dianion.

5.6 Conclusions

We have investigated the electrochemical properties of the carboranes reported in this thesis along with some simple carboranes. We have seen that *ortho* carborane cages undergo one and two electron reductions. On reduction the carborane cages open up to accommodate the additional electrons. The ease of reduction is seen to correlate to the length of the cage C-C bond which in turn is affected by the steric bulk of the groups at the cage carbons. The *ortho* di-naphthyl carborane is found to form a radical anion on reduction with a 2n + 3 skeletal electron count, as has been reported for *ortho* di-phenyl carborane derivatives. Carborane systems with two cages bridged by different bridging groups are found to display two 2-electron reductions. The large separations between reduction potentials in some examples of the bridged carboranes are indicative of communication between carborane cages.

5.7 Experimental

Electrochemical analyses were carried out using an Autolab PG-STAT 30 potentiostat, with platinum counter and pseudo-reference electrodes and a glassy carbon working electrode. Electrochemistry was carried out in 0.1 M NBu_4PF_6 acetonitrile electrolyte solutions at 100 mV s^{-1}. Ferrocene was used as an internal reference and data are reported against the ferrocene/ferrocenium couple (i.e., $FeCp_2/[FeCp_2]^+$ =0.00 V in MeCN/0.1 M $[NBu_4]PF_6$).

IR and UV-vis-near-IR spectroelectrochemical measurements were made in an OTTLE cell with 0.1 M NBu_4PF_6 electrolyte DCM solutions using a Thermo 6700 FT-IR or a Perkin-Elmer Lambda 900 UV−vis−near-IR spectrophotometer.

Computational work was carried out as described in chapter 2.5.

5.8 References

1. Fox M. A., Nervi C., Crivello A., Batsanov A. S., Howard J. A. K., Wade K. and Low P. J., *J. Solid State Electrochem.*, **2009**, 13, 1483-1495.
2. Alekseyeva E. S., Fox M. A., Howard J. A. K., MacBride J. A. H. and Wade K., *Appl. Organomet. Chem.*, **2003**, 17, 499-508.
3. Fox M. A., Nervi C., Crivello A. and Low P. J., *Chem. Commun*., **2007**, 2372–2374.
4. Fox M. A., Paterson M. A. J., Nervi C., Galeotti F., Puschmann H., Howard J. A. K. and Low P. J., *Chem. Commun.*, **2001**, 1610-1611.
5. Le Guennic B., Costuas K., Halet J-F., Nervi C., Peterson M. A. J., Fox M. A., Roberts R. L., Albesa-Jove D., Puschmann H., Howard J. A. K. and Low P. J., *C. R. Chimie.*, **2005**, 1833-1896.
6. Wedge T. J., Herzog A., Huertas R., Lee M. W., Knobler C. B. and Hawthorne M. F., *Organometallics*, **2004**, 23, 482-489.
7. Fox M. A., Roberts R. L., Baines T. E., Le Guennic B., Halet J. F., Hartl F., Yufit D. S., Albesa-Jove D., Howard J. A. K. and Low P. J., *J. Am. Chem. Soc.*, **2008**, 130, 3566-3578.
8. Brown N. J., Lancashire H. N., Fox M. A., Collison D., Edge R., Yufit D. S., Howard J. A. K., Whiteley M. W. and Low P. J., *Organometallics*, **2011**, 30, 884-894.

6 : Conclusions and Future Work

Ortho mono naphthyl carborane displayed two emission bands, due to two S_1 excited states, with the naphthyl carborane group at a different dihedral angle to the carborane cage, allowed by free rotation around the cage C – naphthyl C bond. In the disubstituted naphthyl analogue steric hindrance between the two naphthyl groups prevents free rotation around the cage C – naphthyl C bond, leading to only one S_1 excited state geometry and one emission band. Mono naphthyl *ortho* carborane could be reacted further, to give a series of compounds of the type oNapCbR, where R could be for example a methyl, ethyl, propyl, *n*-butyl or *tert*-butyl, which would be expected to have varying steric interactions with the naphthyl group. These compounds could have their photophysical properties investigated. A greater steric interaction, which still allows for rotation between the two groups, could be expected to increase the cage C-C bond length and hence may have an influence of the emission properties. The reduction properties of such compounds would also be interesting and could be expected to be reduced at a smaller potential than for the mono naphthyl *ortho* carborane.

Extra photophysical data, such as fluorescence lifetimes and solid state emission properties, about all of the compounds discussed here could be collected with the use of better facilities. Quantum yields of the naphthyl and bridged carboranes may also be collected with a different experimental set up in a different facility.

The mono phenanthrenyl *ortho* carborane has been reported in the literature and found to exhibit fluorescence emission at 517 nm in 1:99 THF:H_2O.[1] This molecule was found to be stable, unlike the similar 9-anthracyl carboranes, reported here. This series of anthracyl carboranes are likely to display interesting emission properties at lower energies than the equivalent naphthyl carboranes. The *meta* and *para* mono and di 9-phenanthrenyl compounds could be synthesised via copper coupling reactions. The *ortho* disubstituted compound could be

synthesised via a rearrangement reaction from the *meta* or *para* di phenanthrenyl carboranes. An alternative method for the synthesis of this molecule would be reacting decaborane with the appropriate alkyne.

A natural progression from naphthyl and phenanthrenyl carboranes would be to investigate the emission properties of the pyrene and perylene substituted carboranes, which could be synthesised via similar routes to the other aryl carboranes. A computational study could be carried out first to ascertain whether these compounds would be stable. The mono substituted *ortho* carboranes may exhibit dual fluorescence, whilst the disubstituted could be expected to emit at lower energies than the equivalent naphthyl carboranes. The presence of the carborane cage may increase the thermal stability of the compounds compared to the aryl starting materials. Whilst the presence of the *ortho* carborane cage is likely to decrease the quantum yields in solution, the *meta* and *para* carborane cages may lead to an increase in quantum yields as compared to the aryl starting materials.

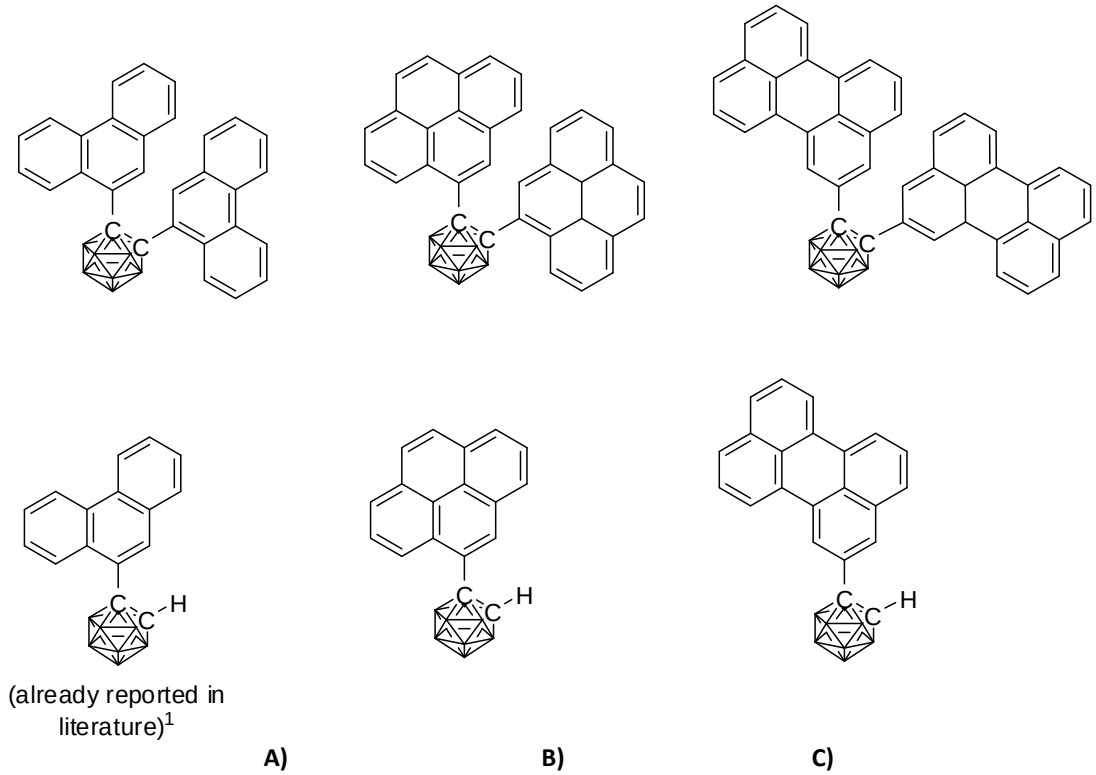

Figure 6–1: *Ortho* carboranes with A) Phenanthrene, B) pyrene and C) perylene groups.

The *ortho* di-substituted phenanthrene, pyrene and perylene substituted compounds could also be investigated by cyclic voltammetry for the presence of a stable radical anion. We would expect that there would be a greater steric strain in these molecules between the aromatic groups and the carborane cage than for the di-naphthyl *ortho* carborane and di-phenyl *ortho* carborane, due to the greater bulkiness of the aryl groups. This greater steric bulk would be expected to lead to an extended carborane cage C-C bond length and hence a more stable radical anion than for the di-naphthyl and di-phenyl carboranes.

Further work on the spectroelectrochemistry of *ortho* mono naphthyl carborane should be done to understand what structural changes occur on reduction. The spectroelectrochemistry of *ortho* mono phenyl carborane should be carried out to compare with the results seen in the naphthyl carborane.

We have reported the synthesis of the *meta* and *para* mono and di substituted carboranyl triarylamines and the *ortho* mono substituted carboranyl triarylamine. Synthesis of the *ortho* di substituted molecule could be carried out by a rearrangement reaction or via a decaborane method, as shown in Figure 6–2. This molecule is likely to display red emission in the solid state and in 1:99 THF:water solution. The electrochemistry of this molecule would also be of interest.

Due to the thermal stability, amorphous character and improved quantum yields observed in the disubstituted carboranyl triarylamines, they could be incorporated into OLED devices and the switch on voltage and the lifetime of such a device tested, to ascertain the suitability of such a compound for applications.

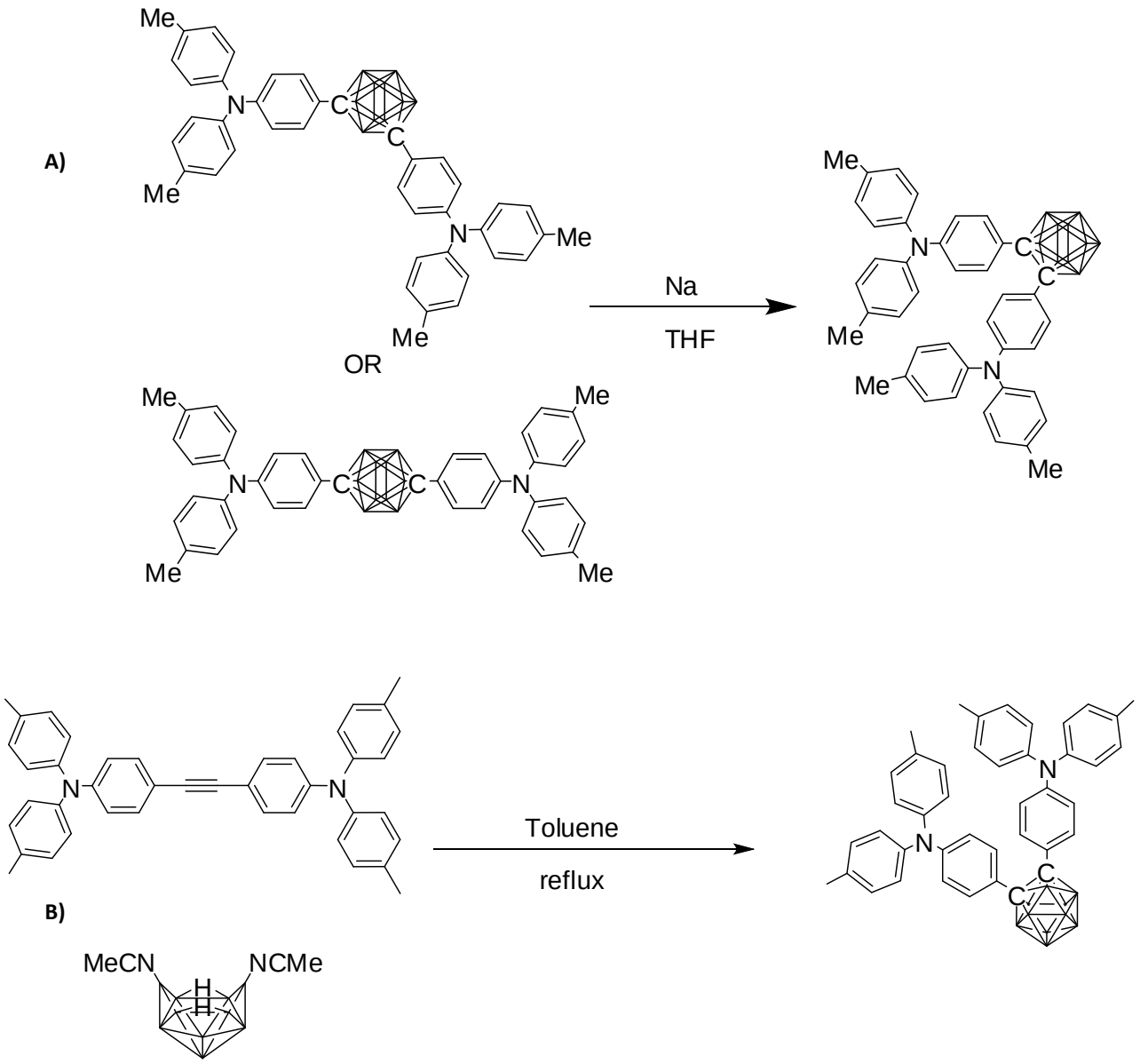

Figure 6–2: Synthetic route to *ortho* disubstituted carboranyl triarylamines using A) rearrangement or B) decaborane methods.

The synthesis of white organic light emitting diodes (WOLEDs) is an area of current research. WOLEDs are sometimes synthesised by combining red, green and blue light emitting compounds in appropriate concentrations to give an emission spectrum covering the whole visible spectrum.[2] We have seen that stable carborane containing compounds with different cage C substituted groups are able to emit over a broad range of wavelengths with varying Stokes shifts, from 2500 cm^{-1} to 18800 cm^{-1}. As such we could investigate the possibility of a WOLED using carborane containing compounds.

We have also seen that bridged carboranes are able to form stable dianions when reduced, with one electron accommodated by each cage, as shown by CV and calculations. These dianions could be isolated and characterised. Crystal structures would be of particular interest as they would reveal the reduced cage conformations. The fluorescence and electrochemical properties of further examples of bridged carboranes could be investigated. For example, bridging groups such as $(C_4SH_2)_2$ and $C_{10}H_6$ are of possible interest. The electrochemical results of carboranes bridged by a $(C_4SH_2)_2$ could be compared with those of the C_4SH_2 bridged compound. Similarly, the electrochemical properties of a compound bridged by a $C_{10}H_6$ group could be compared with those of 1,4-(1'-$C_{10}H_7$-1',2'-$C_2B_{10}H_{10})_2$-C_6F_4.

---

1. Kokado K., Nagai A. and Chujo Y., *Tetrahedron Lett*., **2011**, 52, 293-296.
2. Gather M. C., Köhnen A. and Meerholz K., *Adv. Mater.*, **2011**, 23, 233–248.

7 : Appendix 1: Methods of synthesising C-aryl substituted carboranes.

Table 7–1: C- aryl substituted carboranes, synthesised by the decaborane method.

Product	Reaction	Yield %
1-Ph-1,2-$C_2B_{10}H_{11}$	$B_{10}H_{14}$, MeCN, phenylacetylene, toluene	65-68 [1], 71 [2]
1-Ph-1,2-$C_2B_{10}H_{11}$	$B_{10}H_{14}$, dimethylaniline, phenylacetylene. toluene	88 [3]
1-Ph-1,2-$C_2B_{10}H_{11}$	$B_{10}H_{14}$, MeCN, phenylacetylene, benzene	57 [4]
1-(4'-BrC_6H_4)-1,2-$C_2B_{10}H_{11}$	$B_{10}H_{14}$, MeCN, 4-bromophenylacetylene, benzene	68[5]
1-(2'-Nap)-1,2-$C_2B_{10}H_{11}$	$B_{10}H_{14}$, MeCN, ethynyl 2'-naphthalene, benzene	86[6]
1-(2'-Nap)-1,2-$C_2B_{10}H_{11}$	$B_{10}H_{14}$, Et_2S, ethynyl 2'-naphthalene, toluene	67[6]
1-(1'-Nap)-1,2-$C_2B_{10}H_{11}$	$B_{10}H_{14}$, Et_2S, ethynyl 1'-naphthalene, toluene	30[6]
1-(1'-Nap)-1,2-$C_2B_{10}H_{11}$	$B_{10}H_{14}$, CH_3CN, ethynyl 1'-naphthalene, benzene	52[6]
1-(3'-MeC_6H_4)-1,2-$C_2B_{10}H_{11}$	$B_{10}H_{14}$, MeCN, 3-MeC_6H_4CCH, benzene	not given [7]
1-(4'-MeC_6H_4)-1,2-$C_2B_{10}H_{11}$	$B_{10}H_{12}(NCMe)_2$, 4-MeC_6H_4CCH, toluene	70 [8]
1-(4'-$Me_2NC_6H_4$)-1,2-$C_2B_{10}H_{11}$	$B_{10}H_{14}$, MeCN, 4-$Me_2NC_6H_4CCH$	not given [9]
1-(4'-$CF_3C_6H_4$)-1,2-$C_2B_{10}H_{11}$	$B_{10}H_{14}$, MeCN, 4-$CF_3C_6H_4CCH$	not given [9]
1-(4'-NCC_6H_4)-1,2-$C_2B_{10}H_{11}$	$B_{10}H_{14}$, MeCN, 4-NCC_6H_4CCH, toluene	30 [10]
1-(4'-$MeSC_6H_4$)-1,2-$C_2B_{10}H_{11}$	$B_{10}H_{14}$, MeCN, 4-$MeSC_6H_4CCH$, toluene	58 [10]
1-(4'-$MeOC_6H_4$)-1,2-$C_2B_{10}H_{11}$	$B_{10}H_{14}$, MeCN, 4-$MeOC_6H_4CCH$, toluene	69 [10]
1-(4'-$PhOC_6H_4$)-1,2-$C_2B_{10}H_{11}$	$B_{10}H_{12}(NCMe)_2$, $PhOC_6H_4CCH$, toluene	40 [11]
1-(4'-$COMeC_6H_4$)-1,2-$C_2B_{10}H_{11}$	$B_{10}H_{14}$, MeCN, 4-$COMeC_6H_4CCH$	42[12]
1-Ph-2-Me-1,2-$C_2B_{10}H_{10}$	$B_{10}H_{14}$, Me_2NPh, PhCCMe, toluene	68 [13]
1-PhC≡C-2-Ph-1,2-$C_2B_{10}H_{10}$	$B_{10}H_{14}$, Me_2NPh, PhCCCCPh, toluene	78 [14]
1-PhC≡C-2-Ph-1,2-$C_2B_{10}H_{10}$	$B_{10}H_{12}(NCMe)_2$, PhCCCCPh, toluene	33 [15]
1,2-Ph_2-1,2-$C_2B_{10}H_{10}$	$B_{10}H_{14}$, MeCN, diphenylacetylene, toluene	72 [1]
1,2-Ph $_2$-1,2-$C_2B_{10}H_{10}$	$B_{10}H_{12}(NCMe)_2$, acetylene, aromatic solvent	not given [16]

Table 7-1 cont: C- aryl substituted carboranes, synthesised by the decaborane method.

Product	Reaction	Yield %
1,2-Ph_2-1,2-$C_2B_{10}H_{10}$	$B_{10}H_{14}$, diphenylacetylene, dimethylaniline, toluene	76 [17]
1,2-(2'-$C_4H_3S)_2$-1,2-$C_2B_{10}H_{10}$	$B_{10}H_{14}$, Et_2S, CuI, $Pd(PPh_3)_2$, DBU, $CCSiMe_3$, toluene	not given [18]
1-(4'-OMe-C_6H_4)-2-Ph-1,2-$C_2B_{10}H_{10}$	4-MeO-C_6H_4CCPh, $B_{10}H_{12}(NCMe)_2$, toluene	40 [19]
1-(4'-NMe_2-C_6H_4)-2-Ph-1,2-$C_2B_{10}H_{10}$	4-NMe_2-C_6H_4CCPh, $B_{10}H_{12}(NCMe)_2$, toluene	41 [19]
1-(4'-NH_2-C_6H_4)-2-Ph-1,2-$C_2B_{10}H_{10}$	$H_2NC_6H_4CCPh$, $B_{10}H_{12}(NCMe)_2$, toluene	28 [19]
1-(4'-F-C_6H_4)-2-Ph-1,2-$C_2B_{10}H_{10}$	FC_6H_4CCPh, $B_{10}H_{12}(NCMe)_2$, toluene	47 [19]
1-(2'-Nap)-2-Ph-1,2-$C_2B_{10}H_{10}$	$B_{10}H_{14}$, Et_2S, ethynyl 2'-naphthalene, toluene	65[6]
1-(2'-Nap)-2-Ph-1,2-$C_2B_{10}H_{10}$	$B_{10}H_{14}$, CH_3CN, ethynyl 2'-naphthalene, benzene	42[6]
1-(1'-Nap)-2-Ph-1,2-$C_2B_{10}H_{10}$	$B_{10}H_{14}$, Et_2S, ethynyl 1'-naphthalene, toluene	8[6]
1-(1'-Nap)-2-Ph-1,2-$C_2B_{10}H_{10}$	$B_{10}H_{14}$, CH_3CN, ethynyl 1'-naphthalene, benzene	10[6]
1-(4'-$MeCO_2C_6H_4$)-2-Ph-1,2-$C_2B_{10}H_{10}$	$B_{10}H_{12}(NCMe)_2$, $PhCCC_6H_4CO_2Me$, toluene	37 [11]
1-(3'-$H_2NC_6H_4$)-2-Ph-1,2-$C_2B_{10}H_{10}$	$B_{10}H_{14}$, MeCN, 3-$H_2NC_6H_4CCPh$, benzene	28 [20]
1-(4'-$H_2NC_6H_4$)-2-Ph-1,2-$C_2B_{10}H_{10}$	$B_{10}H_{14}$, MeCN, 4-$H_2NC_6H_4CCPh$, benzene	27 [20]
1,2-(4'-$MeOC_6H_4)_2$-1,2-$C_2B_{10}H_{10}$	$B_{10}H_{14}$, MeCN, $(4\text{-}MeOC_6H_4)_2CC$, benzene	31 [21]
1,2-(4'-$IC_6H_4)_2$-1,2-$C_2B_{10}H_{10}$	$B_{10}H_{12}(SMe_2)_2$, $(4\text{-}IC_6H_4)_2CC$, toluene	58 [22]
1,2-(4'-$MeC_6H_4)_2$-1,2-$C_2B_{10}H_{10}$	$B_{10}H_{14}$, Me_2NPh, $(4\text{-}MeC_6H_4)_2CC$	80 [14]
1,2-(4'-$PhOC_6H_4)_2$-1,2-$C_2B_{10}H_{10}$	$B_{10}H_{12}(SEt_2)_2$, $(4\text{-}PhOC_6H_4)_2CC$, toluene	65 [11]
1-(4'-$PhOC_6H_4$)-2-(4'-$MeCO_2C_6H_4$)-1,2-$C_2B_{10}H_{10}$	$B_{10}H_{12}(NCMe)_2$, $PhOC_6H_4CCC_6H_4CO_2Me$, toluene	22 [11]
1-(4'-$PhOC_6H_4$)-2-(4'-MeC_6H_4)-1,2-$C_2B_{10}H_{10}$	$B_{10}H_{12}(NCMe)_2$, $PhOC_6H_4CCC_6H_4Me$, toluene	23 [11]
1-(4'-$PhOC_6H_4$)-2-(4'-BrC_6H_4)-1,2-$C_2B_{10}H_{10}$	$B_{10}H_{12}(NCMe)_2$, $PhOC_6H_4CCC_6H_4Br$, toluene	34 [11]
1,2-(4'-$C_6H_4(NC_{12}H_8))_2$-1,2-$C_2B_{10}H_{10}$	$B_{10}H_{14}$, *N*,*N*-dimethylaniline, 1,2-bis(4-(*N*-carbazolyl)phenyl)acetylene, toluene	68[23]

Table 7–2: C- aryl substituted carboranes, synthesised by a copper-catalysed coupling method.

Product	Reaction	Yield %
1-Ph-1,2-$C_2B_{10}H_{11}$	1-Li-1,2-$C_2B_{10}H_{11}$, C_6H_5MgBr in THF $CuCl_2$	20-25[24]
1-Ph-1,2-$C_2B_{10}H_{11}$	1-Li-1,2-$C_2B_{10}H_{11}$, CuCl in THF, C_6H_5I in DMF	30-35[24]
1-Ph-1,2-$C_2B_{10}H_{11}$	*o*Cb, BuLi, CuCl/I, $C_6H_5N_2BF_4$	67[25]
1-(2'-Me-C_6H_4)-1,2-$C_2B_{10}H_{11}$	*o*Cb, BuLi, CuCl/I, o-$C_6H_4CH_3N_2BF_4$	50[25]
1-(1'-Nap)-1,2-$C_2B_{10}H_{11}$	*o*Cb , BuLi, CuCl, pyridine, 1'-iodonaphthalene in DME	84[6]
1-(3'-NO_2-C_6H_4)-1,2-$C_2B_{10}H_{11}$	*o*Cb , BuLi, CuCl, pyridine,3-iodonitrobenzene in DME	37[26]
1-(4'-NO_2-C_6H_4)-1,2-$C_2B_{10}H_{11}$	*o*Cb , BuLi, CuCl, pyridine , 4-iodonitrobenzene in DME	42[26]
1-(3'-MeC_6H_4)-1,2-$C_2B_{10}H_{11}$	*o*Cb, BuLi, CuCl/I, 3-$C_6H_4CH_3N_2BF_4$	59[25]
1-(4'-MeC_6H_4)-1,2-$C_2B_{10}H_{11}$	*o*Cb, BuLi , CuCl/I, 4-$C_6H_4CH_3N_2BF_4$	68[25]
1-(2'-OMeC_6H_4)-1,2-$C_2B_{10}H_{11}$	*o*Cb, BuLi, CuCl/I, 2-$C_6H_4OCH_3N_2BF_4$	52[25]
1-(3'-OMeC_6H_4)-1,2-$C_2B_{10}H_{11}$	*o*Cb, BuLi, CuCl/I, 3-$C_6H_4OCH_3N_2BF_4$	55[25]
1-(4'-OMeC_6H_4)-1,2-$C_2B_{10}H_{11}$	*o*Cb, BuLi, CuCl/I, 4-$C_6H_4OCH_3N_2BF_4$	61[25]
1-(3'-FC_6H_4)-1,2-$C_2B_{10}H_{11}$	*o*Cb, BuLi, CuCl/I, 3-C_6H_4F N_2BF_4	63[25]
1-(4'-FC_6H_4)-1,2-$C_2B_{10}H_{11}$	*o*Cb, BuLi, CuCl/I, 4-C_6H_4F N_2BF_4	65[25]
1-(3'-ClC_6H_4)-1,2-$C_2B_{10}H_{11}$	*o*Cb, BuLi, CuCl/I, 3-C_6H_4Cl N_2BF_4	66[25]
1-(4'-ClC_6H_4)-1,2-$C_2B_{10}H_{11}$	*o*Cb, BuLi, CuCl/I, 4-C_6H_4Cl N_2BF_4	68[25]
1-(3'-BrC_6H_4)-1,2-$C_2B_{10}H_{11}$	*o*Cb, BuLi, CuCl/I, 3-C_6H_4Br N_2BF_4	62[25]
1-(4'-BrC_6H_4)-1,2-$C_2B_{10}H_{11}$	*o*Cb, BuLi, CuCl/I, 4-C_6H_4Br N_2BF_4	66[25]
1-(4'-IC_6H_4)-1,2-$C_2B_{10}H_{11}$	*o*Cb, BuLi, CuCl/I, 4-C_6H_4I N_2BF_4	53[25]
1-(4'-$NO_2C_6H_4$)-1,2-$C_2B_{10}H_{11}$	*o*Cb, BuLi, CuCl/I, 4-$C_6H_4NO_2N_2BF_4$	49[25]
1-(C_6H_4($NC_{12}H_8$))-1,2-$C_2B_{10}H_{11}$	*o*Cb, BuLi, CuCl, pyridine, 9-(4-bromophenyl)carbazole in DME	23[23]
1-Ph-1,7-$C_2B_{10}H_{11}$	*m*Cb, BuLi, CuCl, pyridine, iodobenzene in DME	45[26]
1-Ph-1,7-$C_2B_{10}H_{11}$	*m*Cb, potassium ^{t}butoxide, CuCl, Py, iodobenzene in DME	36[26]
1-Ph-1,7-$C_2B_{10}H_{11}$	*m*Cb, potassium ^{t}butoxide, CuCl, Py, iodobenzene in DME	57[26]

Table 7-2 cont: C- aryl substituted carboranes, synthesised by a copper-catalysed coupling method.

Product	Reaction	Yield %
1-Ph-1,7-$C_2B_{10}H_{11}$	1-Li-1,7-$C_2B_{10}H_{11}$, CuCl in THF, C_6H_5I in DMF	30-35[24]
1-Ph-1,7-$C_2B_{10}H_{11}$	*m*Cb, BuLi , CuCl/I, $C_6H_5N_2BF_4$	65[25]
1-Ph-1,7-$C_2B_{10}H_{11}$	1-Li-1,7-$C_2B_{10}H_{11}$,C_6H_5MgBr, $CuCl_2$ in THF	20-25[24]
1-(2'-NC_5H_4)-1,7-$C_2B_{10}H_{11}$	*m*Cb, BuLi, CuCl, pyridine, 2-BrC_5H_4N in DME	57 [27]
1-(4'-NO_2-C_6H_4)-1,7-$C_2B_{10}H_{11}$	*m*Cb, BuLi, CuCl, pyridine, 4-iodonitrobenxene in DME	43[26]
1-(4'-$C_6H_5OC_6H_4$)-1,7-$C_2B_{10}H_{11}$	*m*Cb, BuLi, CuCl, pyridine, 4-iodopolyether in DME	89[26]
1-(4'-$C_6H_5OC_6H_4$)-1,7-$C_2B_{10}H_{11}$	*m*Cb, BuLi, CuCl, pyridine, 4-iodopolyether in DME	8[26]
1-(3'-I-C_6H_4)-1,7-$C_2B_{10}H_{11}$	*m*Cb, BuLi, CuCl, pyridine, 0.5 mol proportion 1,3-diiodobenzene in DME	22[26]
1-(4'-Br-C_6H_4)-1,7-$C_2B_{10}H_{11}$	*m*Cb, BuLi, CuCl, pyridine, 1-I-4-Br-C_6H_4 in DME	40[12]
1-(2'-MeC_6H_4)-1,7-$C_2B_{10}H_{11}$	*m*Cb, BuLi, CuCl/I, 2-$C_6H_4CH_3N_2BF_4$	52[25]
1-(3'-MeC_6H_4)-1,7-$C_2B_{10}H_{11}$	*m*Cb, BuLi, CuCl/I, 3-$C_6H_4CH_3N_2BF_4$	50[25]
1-(4'-MeC_6H_4)-1,7-$C_2B_{10}H_{11}$	*m*Cb, BuLi, CuCl/I, 4-$C_6H_4CH_3N_2BF_4$	64[25]
1-(2'-OMeC_6H_4)-1,7-$C_2B_{10}H_{11}$	*m*Cb, BuLi, CuCl/I, 2-$C_6H_4OCH_3N_2BF_4$	50[25]
1-(3'-OMeC_6H_4)-1,7-$C_2B_{10}H_{11}$	*m*Cb, BuLi, CuCl/I, 3-$C_6H_4OCH_3N_2BF_4$	55[25]
1-(4'-OMeC_6H_4)-1,7-$C_2B_{10}H_{11}$	*m*Cb, BuLi, CuCl/I, 4-$C_6H_4OCH_3N_2BF_4$	63[25]
1-(3'-FC_6H_4)-1,7-$C_2B_{10}H_{11}$	*m*Cb, BuLi, CuCl/I, 3-C_6H_4F N_2BF_4	61[25]
1-(4'-FC_6H_4)-1,7-$C_2B_{10}H_{11}$	*m*Cb, BuLi, CuCl/I, 4-C_6H_4F N_2BF_4	63[25]
1-(3'-ClC_6H_4)-1,7-$C_2B_{10}H_{11}$	*m*Cb, BuLi, CuCl/I, 3-C_6H_4Cl N_2BF_4	67[25]
1-(4'-ClC_6H_4)-1,7-$C_2B_{10}H_{11}$	*m*Cb, BuLi, CuCl/I, 4-C_6H_4Cl N_2BF_4	70[25]
1-(3'-BrC_6H_4)-1,7-$C_2B_{10}H_{11}$	*m*Cb, BuLi, CuCl/I, 3-C_6H_4Br N_2BF_4	65[25]
1-(4'-BrC_6H_4)-1,7-$C_2B_{10}H_{11}$	*m*Cb, BuLi, CuCl/I, 4-C_6H_4Br N_2BF_4	68[25]
1-(4'-IC_6H_4)-1,7-$C_2B_{10}H_{11}$	*m*Cb, BuLi, CuCl/I, 4-C_6H_4I N_2BF_4	51[25]
1-(4'-$NO_2C_6H_4$)-1,7-$C_2B_{10}H_{11}$	*m*Cb, BuLi, CuCl/I, 4-$C_6H_4NO_2N_2BF_4$	47[25]
1,7-Ph_2-1,7-$C_2B_{10}H_{10}$	*m*Cb, potassium ^{t}butoxide, CuCl, Py, iodobenzene in DME	40[26]
1,7-Ph_2-1,7-$C_2B_{10}H_{10}$	*m*Cb, BuLi, CuCl, pyridine, iodobenzene in DME	32[26]
1,7-Ph_2-1,7-$C_2B_{10}H_{10}$	*m*Cb, potassium ^{t}butoxide, CuCl, Py, iodobenzene in DME	18[26]

Table 7-2 cont: C- aryl substituted carboranes, synthesised by a copper-catalysed coupling method.

Product	Reaction	Yield %
1,7-(3'-Cl-C_6H_4)$_2$-1,7-$C_2B_{10}H_{10}$	*m*Cb, BuLi, CuCl, pyridine, 3-chloroiodobenzene in DME	68[26]
1,7-(4'-FC_6H_4)$_2$-1,7-$C_2B_{10}H_{10}$	*m*Cb, BuLi, CuCl, pyridine, 4-FC_6H_4I in DME	62 [28]
1,7-(4'-FC_6H_4)$_2$-1,7-$C_2B_{10}H_{10}$	*m*Cb, 4-FC_6H_4I, CuCl, pyridine in DME	62 [29]
1,7-(4'-CH_3-C_6H_4)$_2$-1,7-$C_2B_{10}H_{10}$	*m*Cb, BuLi, CuCl, pyridine, 4-iodotoluene in DME	62[26]
1,7-(4'-Cl-C_6H_4)$_2$-1,7-$C_2B_{10}H_{10}$	*m*Cb, BuLi, CuCl, pyridine, 4-chloroiodobenzene in DME	80[26]
1,7-(4'-NO_2-C_6H_4)$_2$-1,7-$C_2B_{10}H_{10}$	*m*Cb, BuLi, CuCl, pyridine, 4-iodonitrobenxene in DME	34[26]
1,7-(4'-Br-C_6H_4)$_2$-1,7-$C_2B_{10}H_{10}$	*m*Cb, BuLi, CuCl, pyridine, 4-bromoiodobenzene in DME	65[26]
1,7-(4'-$C_6H_5OC_6H_4$)$_2$-1,7-$C_2B_{10}H_{10}$	*m*Cb, BuLi, CuCl, pyridine, 4-iodopolyether in DME	75[26]
1,7-(3'-I-C_6H_4)$_2$-1,7-$C_2B_{10}H_{10}$	*m*Cb, BuLi, CuCl, pyridine, 1 mol proportion 1,3-diiodobenzene in DME	5[26]
1,7-(2'-C_4H_3S)$_2$-1,7-$C_2B_{10}H_{10}$	1,7-Li_2-1,7-$C_2B_{10}H_{10}$, CuI, C_4H_4S, pyridine, DME	not given [18]
1,7-(3'-I-C_6H_4)$_2$-1,7-$C_2B_{10}H_{10}$	*m*Cb, BuLi, CuCl, pyridine, 2 mol proportion 1,3-diiodobenzene in DME	14[26]
1,7-(C_6H_4($NC_{12}H_8$))$_2$-1,7-$C_2B_{10}H_{10}$	*m*Cb, BuLi, CuCl, pyridine, 9-(4-bromophenyl)carbazole in DME	31[23]
1-Ph-1,12-$C_2B_{10}H_{11}$	*p*Cb, BuLi, CuCl, pyridine, iodobenzene	52 [30]
1-Ph-1,12-$C_2B_{10}H_{11}$	1-Li-1,12-$C_2B_{10}H_{11}$, CuCl in THF, C_6H_5I in DMF	30-35[24]
1-Ph-1,12-$C_2B_{10}H_{11}$	1-Li-1,12-$C_2B_{10}H_{11}$,C_6H_5MgBr, $CuCl_2$ in THF	20-25[24]
1-(4'-ClC_6H_4)-1,12-$C_2B_{10}H_{11}$	*p*Cb, BuLi, CuCl, pyridine, 4-ClC_6H_4I in DME	not given[31]
1-(4'-MeOC_6H_4)-1,12-$C_2B_{10}H_{11}$	*p*Cb, BuLi, CuCl, pyridine, 4-MeOC_6H_4I in DME	60 [32]
1-(3'-MeOC_6H_4)-1,12-$C_2B_{10}H_{11}$	*p*Cb, BuLi, CuCl, pyridine, 3-MeOC_6H_4I in DME	61[33]
1-(4'-$C_6H_5OC_6H_4$)-1,12-$C_2B_{10}H_{11}$	*p*Cb, BuLi, CuCl, pyridine, 4-iodophenylether in DME	25[26]
1-(4'-OMe-C_6H_4)-1,12-$C_2B_{10}H_{11}$	*p*Cb, BuLi, CuCl, pyridine, 4-iodoanisole	79 [30]
1-(4'-NO_2-C_6H_4)-1,12-C2$B_{10}H_{11}$	*p*Cb, BuLi, CuCl, pyridine, 1-iodo-4-nitrobenzene	43 [30]
1-(4'-NMe_2-C_6H_4)-1,12-$C_2B_{10}H_{11}$	*p*Cb, BuLi, CuCl, pyridine, 1-(dimethylamino)-4-iodobenzene	82 [30]
1-(4'-CF_3-C_6H_4)-1,12-$C_2B_{10}H_{11}$	*p*Cb, BuLi, CuCl, pyridine, 1-iodo-4-trifluoromethylbenzene	50 [30]
1-(4'-Br-C_6H_4)-1,12-$C_2B_{10}H_{11}$	*p*Cb, BuLi, CuCl, pyridine, 1-I-4-Br-C_6H_4 in DME	35[12]
1,12-Ph_2-1,12-$C_2B_{10}H_{10}$	*p*Cb, BuLi, CuCl, pyridine, iodobenzene	18 [30]
1,12-(4'-CF_3-C_6H_4)$_2$-1,12-$C_2B_{10}H_{10}$	*p*Cb, BuLi, CuCl, pyridine, 1-iodo-4-trifluoromethylbenzene	9 [30]

Table 7-2 cont: C- aryl substituted carboranes, synthesised by a copper-catalysed coupling method.

Product	Reaction	Yield %
1,12-(4'-Me-C_6H_4)$_2$-1,12-$C_2B_{10}H_{10}$	*p*Cb, BuLi, CuCl, pyridine, iodotoluene	84 [30]
1,12-(4'-NMe_2-C_6H_4)$_2$-1,12-$C_2B_{10}H_{10}$	*p*Cb, BuLi, CuCl, pyridine, 1-(dimethylamino)-4-iodobenzene	0.8 [30]
1,12-(4'-NO_2-C_6H_4)$_2$-1,12-$C_2B_{10}H_{10}$	*p*Cb, BuLi, CuCl, pyridine, 1-iodo-4-nitrobenzene	38 [30]
1,12-(4'-OMe-C_6H_4)$_2$-1,12-$C_2B_{10}H_{10}$	*p*Cb, BuLi, CuCl, pyridine, 4-iodoanisole	7 [30]
1,12-(4'-$C_6H_5OC_6H_4$)$_2$-1,12-$C_2B_{10}H_{10}$	*p*Cb, BuLi, CuCl, pyridine, 4-iodophenylether in DME	~20[26]
1,12-(4'-$PhOC_6H_4$)$_2$-1,12-$C_2B_{10}H_{10}$	*p*Cb, BuLi, CuCl, pyridine, 4-$PhOC_6H_4I$ in DME	78 [34]
1-(4'-$O_2NC_6H_4$)-12-(4'-$MeOC_6H_4$)-1,12-$C_2B_{10}H_{10}$	1-(4-$MeOC_6H_4$)-1,12-$C_2B_{10}H_{11}$, BuLi, CuCl, pyridine, 4-$O_2NC_6H_4I$ in DME	71 [30]
1-(3',5'-$(F_3C)_2C_6H_4$)-12-(4'-$MeOC_6H_4$)-1,12-$C_2B_{10}H_{10}$	1-(4-$MeOC_6H_4$)-1,12-$C_2B_{10}H_{11}$, BuLi, CuCl, pyridine, 3,5-$(F_3C)_2C_6H_4I$ in DME	96 [30]
1-(4-$O_2NC_6H_4$)-12-(4'-$Me_2NC_6H_4$)-1,12-$C_2B_{10}H_{10}$	1-(4-$Me_2NC_6H_4$)-1,12-$C_2B_{10}H_{11}$, BuLi, CuCl, pyridine, 4-$O_2NC_6H_4I$ in DME	69 [30]
1,12-($C_{25}BrH_{32}$)$_2$-1,12-$C_2B_{10}H_{10}$	*p*Cb, BuLi, CuCl, pyridine, $C_{25}H_{32}IBr$ in DME	10[35]
1,12-($C_6H_4(NC_{12}H_8)$)$_2$-1,12-$C_2B_{10}H_{10}$	*p*Cb, BuLi, CuCl, pyridine, 9-(4-bromophenyl)carbazole in DME	36[23]

Table 7–3: Alternative methods for forming C- aryl substituted carboranes.

Product	Reaction	Yield %
1-(4'-BrC_6F_4)-2-Me-1,2-$C_2B_{10}H_{10}$	1-Me-1,2-$C_2B_{10}H_{11}$, BuLi in Et_2O, C_6F_5Br	81 [36]
1-(4'-BrC_6F_4)-2-^{t}Bu-1,2-$C_2B_{10}H_{10}$	1-^{t}Bu-1,2-$C_2B_{10}H_{11}$, BuLi in Et_2O, C_6F_5Br	49 [36]
1-(1'-Nap)-2-(4'-NO_2-C_6H_5)-1,2-$C_2B_{10}H_{11}$	1-Nap-1,2-$C_2B_{10}H_{11}$, KO^{t}Bu, 1-F-4-NO_2-C_6H_4	90[6]
1-(2',3'-$Cl_2C_6H_3$)-2-Me-1,2-$C_2B_{10}H_{10}$	1-Me-1,2-$C_2B_{10}H_{11}$, BuLi in Et_2O, (o-$C_6H_4Cl_2$)$Cr(CO)_3$, I_2	not given[37]
1-(4'-BrC_6F_4)-2-Ph-1,2-$C_2B_{10}H_{10}$	1-Ph-1,2-$C_2B_{10}H_{11}$, BuLi in Et_2O, C_6F_5Br	85 [36]
1-(4'-$NO_2C_6H_4$)-2-Ph-1,2-$C_2B_{10}H_{10}$	1-Ph-1,2-$C_2B_{10}H_{11}$, 1-F-4-NO_2-C_6H_4, NaH in DMF	76 [38]
(1-(4'-C_6H_4)-1,2-$C_2B_{10}H_{11})_2$ SO_2	$SO_2(C_6H_4$-4-Cl$)_2$, 1,2-$C_2B_{10}H_{12}$, BuLi in cyclohexane	56 [39]
(1-(4'-C_6H_4)-2-CH_2-1,2-$C_2B_{10}H_{11})_2$ SO_2	$SO_2(C_6H_4$-4-Cl$)_2$, 1-CH_2-1,2-$C_2B_{10}H_{11}$, BuLi in cyclohexane	67 [39]
(1-(4'-C_6H_4)-2-Ph-1,2-$C_2B_{10}H_{11})_2$ SO_2	$SO_2(C_6H_4$-4-Cl$)_2$, 1-C_6H_5-1,2-$C_2B_{10}H_{11}$, BuLi in cyclohexane	49 [39]
1,4-(1'-Ph-1',2'-$C_2B_{10}H_{10})_2C_6F_4$	1-Ph-2-Li-1,2-$C_2B_{10}H_{10}$, C_6F_6	65 [40,41]
1,4-(1'-Me-1',2'-$C_2B_{10}H_{10})_2C_6F_4$	1-Me-2-Li-1,2-$C_2B_{10}H_{10}$, C_6F_6	60 [40,41]
1,4-(1'-closo-2'-Ph-1',2'0$C_2B_{10}H_{10})_2C_6F_4$	1-Ph-1,2-$C_2B_{10}H_{11}$, BuLi in Et_2O, C_6F_6	69 [42]
1-F_5C_6-7-Ph-1,7-$C_2B_{10}H_{10}$	1-Ph-1,7-$C_2B_{10}H_{11}$, BuLi, C_6F_6 in Et_20	19 [43]
1-Ph-1,12-$C_2B_{10}H_{11}$	*p*Cb, BuLi, CuCl, PhI, $(Ph_3P)_2PdCl_2$, NMP	68 [44]
1-PhCCC_6H_4I-1,12-$C_2B_{10}H_{11}$	*p*Cb, BuLi, CuI, I$C_6H_4CCC_6H_4$I, $(Ph_3P)_2PdCl_2$, NMP, THF	6 [45]
1-C_6F_5-12-Ph-1,12-$C_2B_{10}H_{10}$	1-Ph-1,12-$C_2B_{10}H_{11}$, BuLi, C_6F_6 in Et_2O	52 [43]

Table 7–4: C- aryl substituted carboranes, synthesised by rearrangement reactions.

Product	Reaction	Yield %
1-Ph-1,2-$C_2B_{10}H_{11}$	1-Ph-1,7-$C_2B_{10}H_{11}$, Na, $C_{10}H_8$ in THF	not given[46]
1,2-Ph_2-1,2-$C_2B_{10}H_{10}$	1,7-Ph_2-1,7-$C_2B_{10}H_{10}$, Na, $C_{10}H_8$ in THF	93 [47]
1,2-Ph_2-1,2-$C_2B_{10}H_{10}$	1,7-Ph_2-1,7-$C_2B_{10}H_{10}$, Na, $C_{10}H_8$ in THF	not given[46]
1,2-Ph_2-1,2-$C_2B_{10}H_{10}$	1,12-Ph_2-1,12-$C_2B_{10}H_{10}$, Na in THF	not given[48]
1-Ph-1,7-$C_2B_{10}H_{11}$	1-Ph-1,2-$C_2B_{10}H_{10}$ Δ 415-420 °C under argon	58[49]
1-Ph-1,7-$C_2B_{10}H_{11}$	1-Ph-1,2-$C_2B_{10}H_{10}$ Δ 420 °C under vacuum	69[50]
1,7-Ph_2-1,7-$C_2B_{10}H_{10}$	1,2-Ph_2-1,2-$C_2B_{10}H_{10}$ Δ 415-425 °C under argon	54 [47]

Table 7–5: Synthesis of C-heteroaryl substituted carboranes.

Product	Reaction	Yield %
1-(2'-NC_5H_4)-1,2-$C_2B_{10}H_{11}$	$B_{10}H_{12}(SEt_2)_2$, 2-NC_5H_4CCH, toluene	28 [26]
1-(4'-Br-2'-NC_5H_4)-1,2-$C_2B_{10}H_{11}$	$B_{10}H_{12}(SEt_2)_2$, 4-Br-2-NC_5H_4CCH, toluene	32 [51]
1-(2'-SC_4H_3)-1,2-$C_2B_{10}H_{11}$	$B_{10}H_{14}$, MeCN, 2-ethynylthiophene, toluene	52 [52]
1-(2'-SC_4H_3)-1,2-$C_2B_{10}H_{11}$	$B_{10}H_{14}$, Et_2S, 2-ethynylthiophene, toluene	53 [53]
1-(3'-$C_2H_4S_2CC_6H_4$)-1,2-$C_2B_{10}H_{11}$	$B_{10}H_{14}$, MeCN, 3-$C_2H_4S_2CC_6H_4CCH$, toluene	57 [54]
1-(2'-NC_5H_4)-1,2-$C_2B_{10}H_{11}$	$B_{10}H_{12}(SEt_2)_2$, 2-NC_5H_4CCH, toluene	28 [26]
1-(4'-Br-2'-NC_5H_4)-1,2-$C_2B_{10}H_{11}$	$B_{10}H_{12}(SEt_2)_2$, 4-Br-2-NC_5H_4CCH, toluene	32 [51]
1-(2'-SC_4H_3)-1,2-$C_2B_{10}H_{11}$	$B_{10}H_{14}$, MeCN, 2-ethynylthiophene, toluene	52 [52]
1-(2'-SC_4H_3)-1,2-$C_2B_{10}H_{11}$	$B_{10}H_{14}$, Et_2S, 2-ethynylthiophene, toluene	53 [53]
1,2-(2'-$C_4H_3S)_2$-1,2-$C_2B_{10}H_{10}$	$B_{10}H_{14}$, Et_2S, CuI, $Pd(PPh_3)_2$, DBU, $HCCSiMe_3$, toluene	not given [18]
1-(2'-NC_5H_4)-1,7-$C_2B_{10}H_{11}$	*m*Cb, BuLi, CuCl, pyridine, 2-BrC_5H_4N, DME	57 [27]
1,7-(2'-$C_4H_3S)_2$-1,7-$C_2B_{10}H_{10}$	1,7-Li_2-1,7-$C_2B_{10}H_{10}$, CuI, C_4H_4S, pyridine, DME	not given [18]
1,12-(2'-$C_4H_3S)_2$-1,12-$C_2B_{10}H_{10}$	1,12-Li_2-1,12-$C_2B_{10}H_{10}$, CuI, C_4H_4S, pyridine, DME	not given [18]
1-(OTBS)-12-(2'-C_5H_4N)-1,12-$C_2B_{10}H_{10}$	1-(OTBS)-1,12-$C_2B_{10}H_{10}$, BuLi, CuCl, pyridine, 2-bromopyridine	52 [55]
1-(OTBS)-12-(3'-C_5H_4N)-1,12-$C_2B_{10}H_{10}$	1-(OTBS)-1,12-$C_2B_{10}H_{10}$, BuLi, CuCl, pyridine, 3-bromopyridine	58 [55]
1-(OTBS)-12-(4'-C_5H_4N)-1,12-$C_2B_{10}H_{10}$	1-(OTBS)-1,12-$C_2B_{10}H_{10}$, BuLi, CuCl, pyridine, 4-bromopyridine	65 [55]
1,12-(2'-$NC_5H_4)_2$-1,12-$C_2B_{10}H_{10}$	*p*Cb, BuLi, CuCl, pyridine, 2-BrC_5H_4N, DME	67 [27]

1. Stanko V. I., Kopylov V. V. and Klimova A. I., *J. Gen. Chem. USSR*, **1965**, 35, 1437.
2. Wilbur D. S., Chyan M. K., Hamlin D. K., Kegley B. B., Risler R., Pathare P. M., Quinn J., Vessella R. L., Foulon C., Zalutsky M., Wedge T. J. and Hawthorne M.F., *Bioconjugate Chemistry*, **2004**, 15, 203-223.
3. Zakharkin L. I., Bregadze V. I. and Yu O. O., *J. Organomet. Chem.*, **1966**, 6, 228.
4. Brain P. T., Cowie J., Donohoe D. J., Hnyk D., Rankin D. W. H., Reed D., Reid B. D., Robertson H. E., Welch A. J., Hofmann M. and Schleyer P. V. R., *Inorg. Chem.*, **1996**, 35, 1701-1708.
5. Hawthorne M. F., Young D. C., Garrett P. M., Owen D. A., Schwerin S. G., Tebbe F. N. and Wegner P. A., *J. Am. Chem. Soc.*, **1968**, 90, 862.
6. Ohta K., Goto T. and Endo Y., *Inorg. Chem.*, **2005**, 44, 8569-8573.
7. Endo Y., Iijima T., Yaguchi K., Kawachi E., Inoue N., Kagechika H., Kubo A. and Itai A., *Bioorg. Med. Chem. Lett.*, **2001**, 11, 1307-1311.
8. Wyzlic I. M., Tjarks W., Soloway A. H., Perkins D. J., Burgos M. and Oreilly K. P., *Inorg. Chem.*, **1996**, 35, 4541-4547.
9. Endo Y. and Taoda Y., *Tetrahedron Lett.*, **2001**, 42, 6327-6331.
10. Murphy D. M., Mingos D. M. P. and Forward J. M., *J. Mat. Chem.*, **1993**, 3, 67-76.
11. Brown D. A., Colquhoun H. M., Daniels J. A., MacBride J. A. H., Stephenson I. R. and Wade K., *J. Mat. Chem.*, **1992**, 2, 793-804.
12. Dash B. P., Satapathy R., Gaillard E. R., Norten K. M., Maguire J. A., Chug N. and Hosmane N. S., *Inorg. Chem.*, **2011**, 50, 5485-5493.
13. McGrath T. D. and Welch A. J., *Acta. Crystallogr. C*, **1995**, 51, 646-649.
14. Murphy D. M., Mingos D. M. P, Haggitt J. L., Powell H. R., Westcott S. A., Marder T. B., Taylor N. J. and Kanis D. R., *J. Mat. Chem.*, **1993**, 3, 139-148.
15. Clegg W., Coult R., Fox M. A., Gill W. R., MacBride J. A. H. and Wade K., *Polyhedron*, **1993**, 12, 2711-2717.
16. Fein M. M., Cohen M. S., Mayes N., Schwartz N. and Bobinski J., *Inorg. Chem.*, **1963**, 2, 1111-1115.
17. Zakharkin L. I. and Kalinin V. N., *Bull. Acad. Sci. USSR*, **1966**, 549-551.
18. Hao E., Fabre B., Fronczek F. R. and Vicente M. G. H., *Chem. Commun.*, **2007**, 4387-4389.
19. Fox M. A., Nervi C., Crivello A., Batsanov A. S., Howard J. A. K., Wade K. and Low P. J., *J. Solid. State Electrochem.*, **2009**, 13, 1483-1495.
20. Endo Y., Songkram C., Yamasaki R., Tanatani A., Kagechika H., Takaishi K. and Yamaguchi K., *J. Organomet. Chem.*, **2002**, 657, 48-58.
21. Endo Y., Yoshimi T., Iijima T. and Yamakoshi Y., *Bioorg. Med. Chem. Lett.*, **1999**, 9, 3387-3392.
22. Fox M. A., Howard J. A. K., MacBride J. A. H., Mackinnon A. and Wade K., *Journal of Organometallic Chemistry*, **2003**, 680, 155-164.
23. Wee K-R., Han W-S., Cho D. W., Kwon S., Pac C. and Kang S. O., *Angew. Chem. Int. Ed.*, **2012**, 51, 2677-2680.
24. Zakharkin L. I. and Kovredov A. I., *Bull. Acad. Sci. USSR Div. Chem. Sci.*, **1974**, 710.
25. Kovradov A. I., Shaujumbekova Z. S., Kazantsev V. A. and Zakharkin L. I., *J. Gen. Chem. USSR.*,**1986**, 56, 2045.
26. Coult R., Fox M. A., Gill W. R., Herbertson P. L., MacBride J. A. H. and Wade K., *J. Organomet. Chem.*, **1993**, 462, 19-29.

27. Gill W. R., Herbertson P. L., MacBride J. A. H. and Wade K., *J. Organomet. Chem.*, **1996**, 507, 249-255.
28. King A. S., Ferguson G., Britten J. F. and Valliant J. F., *Inorg. Chem.*, **2004**, 43, 3507-3513.
29. Fox M. A. and Wade K., *Polyhedron*, **1997**, 16, 2517-2525.
30. Fox M. A., MacBride J. A. H., Peace R. J. and Wade K., *J. Chem. Soc. Dalton Trans.*, **1998**, 401-411.
31. Colquhoun H. M., Herbertson P. L., Wade K., Baxter I. and Williams D. J., *Macromolecules*, **1998**, 31, 1694-1696.
32. Yamamoto K. and Endo Y., *Bioorg. Med. Chem. Lett.*, **2001**, 11, 2389-2392.
33. Endo Y., Iijima T., Yamakoshi Y., Kubo A. and Itai A., *Bioorg. Med. Chem. Lett.*, **1999**, 9, 3313-3318.
34. Colquhoun H. M., Lewis D. F., Herbertson P. L. and Wade K., *Polymer*, **1997**, 38, 4539-4546.
35. Peterson J. J., Simon Y. C., Coughlin B. E. and Carter K. R., *Chem. Commun.*, **2009**, 4950-4952.
36. Thomas R. L. and Welch A. J., *Polyhedron*, **1999**, 18, 1961-1968.
37. Henly T. J., Knobler C. B. and Hawthorne M. F., *Organometallics*, **1992**, 11, 2313-2316.
38. Ohta K., Goto T. and Endo Y., *Tetrahedron Lett.*, **2005**, 46, 483-485.
39. Vyakaranam K., Rana G. and Ratanasuwan A., *Organometallics*, **2002**, 21, 3905-3912.
40. Zakharkin L. I. and Lebedev V. N., *Bull. Acad. Sci. USSR Div. Chem. Sci.*, **1970**, 914.
41. Zakharkin L. I. and Lebedev V. N., *Bull. Acad. Sci. USSR Div. Chem. Sci.*, **1972**, 2273-2275
42. Thomas Rh. Ll. and Welch A. J., *Acta Crystallogr. C*, **1996**, 52, 1689-1691.
43. Batsanov A. S., Fox M. A., Howard J. A. K. and Wade K., *J. Organomet. Chem.*, **2000**, 597, 157-163.
44. Schoberl U., Magnera T. F., Harrison R. M., Fleischer F., Pflug J. L., Schwab P. F. H., Meng X. S., Lipiak D., Noll B. C., Allured V. S., Rudalevige T., Lee S. and Michl J., *J. Am. Chem. Soc.*, **1997**, 119, 3907-3917.
45. Harrison R. M., Brotin T., Noll B. C. and Michl J., *Organometallics*, **1997**, 16, 3401-3412.
46. Zakharkin L. I., Kalinin V. N. and Podvisotskaya L. S., *Bull. Acad. Sci. USSR Div. Chem. Sci.*, **1966**, 1444.
47. Zakharkin L. I., Kalinin V. N. and Podvisotskaya L. S., *Bull. Acad. Sci. USSR*, **1967**, 2212-2217.
48. Zlatogorsky S., Ellis D., Rosair G. M. and Welch A. J., *Chem. Commun.*, **2007**, 2178-2180.
49. Zakharkin L. I. and Kalinin V. N., *Bull. Acad. Sci. USSR*, **1965**, 2173.
50. Hawthorne M. F., Young D. C., Garrett P. M., Owen D. A., Schwerin S. G., Tebbe F. N. and Wegner P. A., *J. Am. Chem. Soc.*, **1968**, 90, 862.
51. Alekseyeva E. A., Batsanov A. S., Boyd L. A., Fox M. A., Hibbert T. G., Howard J. A. K., MacBride J. A. H., Mackinnon A. and Wade K., *Dalton Trans.*, **2003**, 475-482.
52. Yan Y. K., Mingos D. M. P., Kurmoo M., Li W. S., Scowen I. J., McPartlin M., Coomber A. T. and Friend R. H., *J. Chem. Soc. Dalton Trans.*, **1995**, 2851-2860.
53. Fabre B, Hao E., LeJeune Z. M., Amuhaya E. K., Barriere F., Garno J. C. and Vicente M. G. H., *Applied Materials and Interfaces*, **2010**, 691-702.

54. Frixa C., Mahon M. F., Thompson A. S. and Threadgill M. D., *Org. Biomol. Chem.*, **2003**, 1, 306-317.
55. Ohta K., Goto T., Fijii S., Suzuki T., Ohta S. and Endo Y., *Bioorg. Med. Chem.*, **2008**, 16, 8022-8028.

8 : Appendix 2: Photophysical data reported for carboranes in the literature.

Table 8-1: Photophysical data of ortho carborane containing compounds in the literature.

Compound	Solvent	Abs max / nm	ε / $mol^{-1}cm^{-1}$	Em max / nm	Stokes Shift / cm^{-1}	Quantum Yield ϕ_F	Lifetime / ns	Reference
1,2-$((C_6H_4)CC(C_6H_4)OCH_2(C_2O))_2$-1,2-$C_2B_{10}H_{10}$	1:99 THF:H_2O	310	-	551	14100	0.19	-	1
1,2$((C_6H_4)CC(3',5'-(CF_3)_2-C_6H_3))_2$-1,2-$C_2B_{10}H_{10}$	THF	292, 312	66400	-	-	-	-	2
	1:99 THF:H_2O	-	-	452	9930	0.20	-	2
1,2-$((C_6H_4)CC(4'-(CF_3)-C_6H_4))_2$-1,2-$C_2B_{10}H_{10}$	THF	294, 314	64300	-	-	-	-	2
	1:99 THF:H_2O	-	-	473	10700	0.10	-	2
1,2-$((C_6H_4)CC(C_6H_5))_2$-1,2-$C_2B_{10}H_{10}$	THF	294, 311	56200	-	-	-	-	2
	1:99 THF:H_2O	-	-	491	11800	0.27	-	2
	1:99 THF:H_2O	318	-	486	10900	0.27	-	3
1,2-$((C_6H_4)CC(4'-(CH_3)-C_6H_4))_2$-1,2-$C_2B_{10}H_{10}$	THF	300, 316	63800	-	-	-	-	2
	1:99 THF:H_2O	-	-	504	11800	0.31	-	2
1,2-$((C_6H_4)CC(4'-(OMe)-C_6H_4))_2$-1,2-$C_2B_{10}H_{10}$	THF	310	58800	-	-	-	-	2
	1:99 THF:H_2O	-	-	533	13500	0.31	-	2
1,2-$((C_6H_4)CC(3',4',5'-(OMe)_3-C_6H_2))_2$-1,2-$C_2B_{10}H_{10}$	THF	315	44100	-	-	-	-	2
	1:99 THF:H_2O	-	-	583	14600	0.03	-	2
1,2-$((C_6H_4)CC(4'-(NMe_2)-C_6H_2))_2$-1,2-$C_2B_{10}H_{10}$	THF	356	61900	-	-	-	-	2
	1:99 THF:H_2O	-	-	662	13000	0.003	-	2
1-$(C_{14}H_9)$-1,2-$C_2B_{10}H_{11}$	1:99 THF:H_2O	315	-	517	12400	0.24	-	3
(1-(C_6H_4)-2-$((C_6H_4)CC(3,6-(OC_8H_{17})_2-C_6H_2)CC)$-1,2-$C_2B_{10}H_{10})_n$	1:99 THF:H_2O	-	-	559	-	-	-	4
(1-(C_6H_4)-2-$((C_6H_4)CC(3',6'-(OC_{16}H_{33})_2-C_6H_2)CC)$-1,2-$C_2B_{10}H_{10})_n$	1:99 THF:H_2O	-	-	550	-	-	-	4
(1-(C_6H_4)-2-$((C_6H_4)CC(C_{16}NH_{15})CC)$ -1,2-$C_2B_{10}H_{10})_n$	1:99 THF:H_2O	-	-	583	-	-	-	4

Table 8-1 cont: Photophysical data of *ortho* carborane containing compounds in the literature.

Compound	Solvent	Abs max / nm	ε / $mol^{-1}cm^{-1}$	Em max / nm	Stokes Shift / cm^{-1}	Quantum Yield ϕ_F	Lifetime / ns	Reference
$(1\text{-}(C_6H_4)2\text{-}((C_6H_4)CC(3'\text{-}(C_8F_{17})\text{-}6'\text{-}(CF_3)\text{-}C_6H_2)CC)\text{-}1,2\text{-}C_2B_{10}H_{10})_n$	THF	-	-	405	-	<0.0002	-	4
	1:99 THF:H_2O	-	-	485	-	0.12	-	4
$1\text{-}((2',5'\text{-}(OC_8H_{17})_2\text{-}C_6H_2)CC)_n(C_6H_5)\text{-}(2\text{-}(2',5'\text{-}(OC_8H_{17})\text{-}1,2\text{-}C_2B_{10}H_{10})_mCC(C_6H_5)$	1:99 THF:H_2O	-	-	529-568	-	-	-	5
$(CC(3',5'\text{-}(OC_{12}H_{25})\text{-}C_6H_2)CC(C_6H_4)\text{-}(1,2\text{-}(C_4H(C_6H_4))\text{-}1,2\text{-}C_2B_{10}H_{10})_n$	THF	312, 375	42370	411, 430	2340, 3410	0.51	-	6
$(CC(3'\text{-}(C_8F_{17})\text{-}5'\text{-}(CF_3)\text{-}C_6H_2)CC(C_6H_4)\text{-}(1,2\text{-}(C_4H(C_6H_4))\text{-}1,2\text{-}C_2B_{10}H_{10})_n$	THF	353, 368	47080	383, 410	1060, 2780	0.40	-	6
$(1\text{-}(C_6H_4)\text{-}2\text{-}((C_6H_4)CC(C_{20}H_{10}(OC_8H_{17})_2)\text{-}1,2\text{-}C_2B_{10}H_{10})_n$	THF	241, 283, 338	47000	-	-	-	-	7
	1:99 THF:H_2O	-	-	566	11900	0.05	-	7
$1\text{-}(C_{13}H_7(C_6H_{13})_2)\text{-}2\text{-}((C_{13}H_7(C_6H_{13})_2)_2(1'\text{-}(C_{13}H_7(C_6H_{13})_2)\text{-}1',2'\text{-}C_2B_{10}H_{10})\text{-}1,2\text{-}C_2B_{10}H_{10}$	$CHCl_3$	-	-	415,565	-	-	-	8
$(C_6H_4)((CH_2O(C_6H_2(1\text{-}CH_2\text{-}2\text{-}(C_6H_5)\text{-}1,2\text{-}C_2B_{10}H_{10})_2)_2$	THF	320	124	373	4440	-	-	9
	Acetone	329	123	374	3660	-	-	9
$1',2',3',4',5',6'\text{-}((C_6H_4)CH_2\text{-}1\text{-}CH_3\text{-}1,2\text{-}C_2B_{10}H_{10})_6C_6$	DCM	230,254	-	344	10300	-	-	10
$1',3',5'\text{-}((C_6H_4)(C_6H_4)CH_2\text{-}1\text{-}CH_3\text{-}1,2\text{-}C_2B_{10}H_{10})_3\text{-}C_6H_3$	DCM	290	-	360	6710	0.33	-	11
$1',3',5'\text{-}((C_6H_4)(C_6H_4)(C_6H_4)CH_2\text{-}1\text{-}CH_3\text{-}1,2\text{-}C_2B_{10}H_{10})_3\text{-}C_6H_3$	DCM	307	-	360,380	4800, 6260	0.86	-	11
$1',3',5'\text{-}((C_6H_4)(C_6H_4)(CH_2\text{-}1\text{-}CH_3\text{-}1,2\text{-}C_2B_{10}H_{10})_2)_3\text{-}C_6H_3$	DCM	294	-	370	6990	0.46	-	11
$1',3',5'\text{-}((C_6H_4)\text{-}1,2\text{-}C_2B_{10}H_{11})_3$	DCM	269	-	355	9010	0.024	-	12
$1',3',5'\text{-}((C_6H_4)_2\text{-}1,2\text{-}C_2B_{10}H_{11})_3$	DCM	298	-	361	5860	0.007	-	12

Table 8-1 cont: Photophysical data of *ortho* carborane containing compounds in the literature.

Compound	Solvent	Abs max / nm	ε / $mol^{-1}cm^{-1}$	Em max / nm	Stokes Shift / cm^{-1}	Quantum Yield ϕ_F	Lifetime / ns	Reference
$(1,2\text{-}(C_{13}H_6R_2)_2\text{-}1,2\text{-}C_2B_{10}H_{10})_n$	Solid state	-	-	530	-	-	-	13
$1\text{-}(C_6H_5)\text{-}2/3\text{-}(C_5NH_2(Tol)C_5NH_4(PtCl))\text{-}1,2\text{-}C_2B_{10}H_{10}$	DCM	420-430	-	-	-	-	-	14
	77K 2-MeTHF	-	-	532	-	-	-	14
$1\text{-}(CH_3)\text{-}2/3\text{-}(C_5NH_2(4'\text{-}Br\text{-}C_6H_4)C_5NH_4(PtCl))\text{-}1,2\text{-}C_2B_{10}H_{10}$	DCM	420-430	-	-	-	-	-	14
	77K 2-MeTHF	-	-	532	-	-	-	14
$1\text{-}(CH_3)\text{-}2\text{-}(C(C_6H_5)NH(C_{22}H_{11}))\text{-}1,2\text{-}C_2B_{10}H_{10}$	THF	316	32800	453	9570	-	-	15
$1\text{-}(CH_3)\text{-}2\text{-}(C(C_6H_5)NH(C_{26}H_{15}))\text{-}1,2\text{-}C_2B_{10}H_{10}$	THF	314	35700	449	9580	-	-	15
$(C_6H_4)((CH_2O(C_6H_3(1\text{-}CH_2\text{-}2\text{-}(C_6H_5)\text{-}1,2\text{-}C_2B_{10}H_{10})_2)_2$	THF	-	-	369	-	-	-	16
$(C_6H_4)((CH_2O(C_6H_3(1\text{-}CH_2\text{-}2\text{-}(CH_3)\text{-}1,2\text{-}C_2B_{10}H_{10})_2)_2$	THF	-	-	333	-	-	-	16
$1',3'\text{-}(1\text{-}(C_6H_5)\text{-}2\text{-}CH_2\text{-}1,2\text{-}C_2B_{10}H_{10})_2(C_6H_4)$	THF	-	-	371	61 nm	-	-	16
$1',3'\text{-}(1\text{-}(C_6H_5)\text{-}2\text{-}CH_2\text{-}1,2\text{-}C_2B_{10}H_{10})_2(C_5NH_3)$	THF	-	-	343	33 nm	-	-	16
$1\text{-}(C_6H_5)\text{-}2\text{-}(CH_2(C_6H_4)CHCH_2)\text{-}1,2\text{-}C_2B_{10}H_{10}$	MeCN	254	-	409	14900	0.004	-	17
$1\text{-}(CH_3)\text{-}2\text{-}(CH_2(C_6H_4)CHCH_2)\text{-}1,2\text{-}C_2B_{10}H_{10}$	MeCN	254	-	312	7320	0.19	-	17
$1\text{-}(CH_2(C_6H_4)CHCH_2)\text{-}1,2\text{-}C_2B_{10}H_{11}$	MeCN	254	-	312	7320	0.40	-	17
$1,2\text{-}(CH_2(C_6H_4)CHCH_2)_2\text{-}1,2\text{-}C_2B_{10}H_{10}$	MeCN	254	-	312	7320	0.052	-	17
$1\text{-}(B(NEt_2)(C_6H_4))\text{-}1,2\text{-}C_2B_{10}H_{11}$	Cyclohexane	285, 288, 294	11410, 11080, 3910	311, 596	1960, 15700	<0.01	-	18
	DCM	287, 295	9350, 9970	720	19000	<0.01	-	18
$1\text{-}(B(NEt_2)(C_6H_4))\text{-}1,2\text{-}C_2B_{10}H_{11}$	Solid state	291, 297	-	561	16100	0.51	-	18
$1\text{-}(CH_3)\text{-}2\text{-}(B(NEt_2)(C_6H_4))\text{-}1,2\text{-}C_2B_{10}H_{10}$	Cyclohexane	289, 296	12060, 11760	574	16500	0.08	-	18
	DCM	291, 296	15100, 14900	692	19800	0.03	-	18

Table 8-1 cont: Photophysical data of *ortho* carborane containing compounds in the literature.

Compound	Solvent	Abs max / nm	ε / $mol^{-1}cm^{-1}$	Em max / nm	Stokes Shift / cm^{-1}	Quantum Yield ϕ_F	Lifetime / ns	Reference
1-(CH_3)-2-($B(NEt_2)(C_6H_4)$)-1,2-$C_2B_{10}H_{10}$	Solid state	292	-	573	16500	0.65	-	18
1-(C_6H_5)-2-($B(NEt_2)(C_6H_4)$)-1,2-$C_2B_{10}H_{10}$	Cyclohexane	295	11760	615	18100	0.06	-	18
1-(C_6H_5)-2-($B(NEt_2)(C_6H_4)$)-1,2-$C_2B_{10}H_{10}$	DCM	296	13500	757	21300	0.01	-	18
	Solid state	297	-	613	15100	0.30	-	18
1-^{t}Bu-2-($B(NEt_2)(C_6H_4)$)-1,2-$C_2B_{10}H_{10}$	Cyclohexane	291, 296	13400, 13620	587	17400	0.32	-	18
	DCM	296	11190	713	20300	0.03	-	18
	Solid state	293	-	611	16200	0.42	-	18
1-($SiMe_3$)-2-($B(NEt_2)(C_6H_4)$)-1,2-$C_2B_{10}H_{10}$	Cyclohexane	290, 296	15400, 15000	602	18100	0.18	-	18
	DCM	291, 296	11740, 11770	726	20900	0.02	-	18
	Solid state	289	-	631	20300	0.30	-	18
1-($B(NPh_2)(C_6H_4)$)-1,2-$C_2B_{10}H_{11}$	Cyclohexane	283, 289	9740, 11430	302, 346	1850, 6600	0.01	-	18
	DCM	284, 290	7850, 8600	417	11200	<0.01	-	18
	Solid state	286, 292	-	-	-	-	-	18
1-(CH_3)-2-($B(NPh_2)(C_6H_4)$)-1,2-$C_2B_{10}H_{10}$	Cyclohexane	285, 292	8020, 8310	345,534	5540, 15900	<0.01	-	18
	DCM	286, 292	12380, 12520	646	19200	<0.01	-	18
	Solid state	288,294	-	523	15300	0.25	-	18
(1,2-($C_{13}R_2H_6$)$_2$-1,2-$C_2B_{10}H_{10}$)$_n$	$CHCl_3$	384	-	569	8470	-	-	19
	Solid state	-	-	563	-	-	-	19
	Electroluminescence	-	-	570	-	-	-	19
(1-($C_{13}R_2H_6$)-2-(($C_{13}R_2H_6$)(C_4SH_2))-1,2-$C_2B_{10}H_{10}$)$_n$	$CHCl_3$	441	-	602	6060	-	-	19

Table 8-1 cont: Photophysical data of *ortho* carborane containing compounds in the literature.

Compound	Solvent	Abs max / nm	ε / $mol^{-1}cm^{-1}$	Em max / nm	Stokes Shift / cm^{-1}	Quantum Yield ϕ_F	Lifetime / ns	Reference
$(1\text{-}(C_{13}R_2H_6)\text{-}2\text{-}((C_{13}R_2H_6)(C_4SH_2))\text{-}1,2\text{-}C_2B_{10}H_{10})_n$	Solid state	-	-	570	-	-	-	19
	Electroluminescence	-	-	620	-	-	-	19
$1,2\text{-}((C_6H_4)(C_{12}NH_8))_2\text{-}1,2\text{-}C_2B_{10}H_{10}$	Toluene	293, 325, 338	-	360,410, 531	1810, 5200, 10800	0.06	2.83	20
$1,2\text{-}((C_6H_4)_2(C_{12}NH_8))_2\text{-}1,2\text{-}C_2B_{10}H_{10}$	Toluene	291, 326, 338	-	365, 583	2190, 12400	0.05	3.41	20
$1\text{-}((C_6H_4)(C_{12}NH_8))\text{-}1,2\text{-}C_2B_{10}H_{11}$	Toluene	293, 324, 338	-	350, 360, 595	1010, 1810, 12800	0.04	1.28	20
$1,2\text{-}(Au(PPh_3))_2\text{-}1,2\text{-}C_2B_{10}H_{10}$	Solid state RT	-	-	368, 500	-	-	-	21
	Solid state 77 K	-	-	399, 500	-	-	-	21
$1,2\text{-}(Au(PMe_3))_2\text{-}1,2\text{-}C_2B_{10}H_{10}$	Solid state RT	-	-	391, 500	-	-	-	21
	Solid state 77 K	-	-	403, 516	-	-	-	21

Table 8-2: Photophysical data of *meta* and *para* carborane containing compounds in the literature.

Compound	Solvent	Abs max / nm	ε / $mol^{-1}cm^{-1}$	Em max / nm	Stokes Shift / cm^{-1}	Quantum Yield ϕ_F	Lifetime / ns	Reference
$(1\text{-}((C_6H_4)CC)\text{-}7\text{-}((C_6H_4)CC(3',5'\text{-}(OC_8H_{17})_2\text{-}C_6H_2)\text{-}1,7\text{-}C_2B_{10}H_{10})_n$	$CHCl_3$	314, 378	36000	415	2360	0.25	-	22
$(1\text{-}((C_6H_4)CC)\text{-}7\text{-}((C_6H_4)CC(3',5'\text{-}(OC_{16}H_{33})_2\text{-}C_6H_2)\text{-}1,7\text{-}C_2B_{10}H_{10})_n$	$CHCl_3$	314, 378	22000	415	2360	0.25	-	22
$(1\text{-}((C_6H_4)CC)\text{-}7\text{-}((C_6H_4)CC(C_{13}H_6(C_6H_{13})_2)\text{-}1,7\text{-}C_2B_{10}H_{10})_n$	$CHCl_3$	319, 362	69000	386, 410	1720, 3230	0.11	-	22
$(1\text{-}((C_6H_4)CC)\text{-}7\text{-}((C_6H_4)CC(3',5'\text{-}(CF_3)_2\text{-}C_6H_2)\text{-}1,7\text{-}C_2B_{10}H_{10})_n$	$CHCl_3$	345, 366	56400	409	2870	0.22	-	22
$(1\text{-}(C_6H_4)\text{-}7\text{-}((C_6H_4)CC(C_{20}H_{10}(OC_8H_{17})_2)\text{-}1,7\text{-}C_2B_{10}H_{10})_n$	THF	239, 292, 335	58100	388	4080	0.50	-	7
$1',3',5'\text{-}((C_6H_4)\text{-}1,7\text{-}C_2B_{10}H_{11})_3$	DCM	267	-	353	9125	0.25	-	12
$1',3',5'\text{-}((C_6H_4)_2\text{-}1,7\text{-}C_2B_{10}H_{11})_3$	DCM	297	-	361	5970	0.47	-	12
$9\text{-}(CH_2(C_{17}N_2H_{13}))\text{-}1,7\text{-}C_2B_{10}H_{12}$	$CHCl_3$	298	-	380	7240	0.14	-	23
	$CHCl_3$	293	-	369	7030	0.21	-	23
$9\text{-}(CH_2(C_{17}N_2H_{13})ZnCl_2)\text{-}1,7\text{-}C_2B_{10}H_{12}$	$CHCl_3$	336	-	385	3790	0.86	-	23
	$CHCl_3$	315	-	383	5640	0.87	-	23
$1,7\text{-}((C_6H_4)(C_{12}NH_8))_2\text{-}1,7\text{-}C_2B_{10}H_{10}$	Toluene	293, 308, 339	-	349, 361	845, 1800	0.31	6.26	20
$1,7\text{-}(Au(PPh_3))_2\text{-}1,7\text{-}C_2B_{10}H_{10}$	Solid state RT	-	-	394, 527	-	-	-	21
	Solid state 77 K	-	-	396, 513	-	-	-	21
$(1,12\text{-}(C_{13}H_6(C_6H_{13})_2)_2\text{-}1,12\text{-}C_2B_{10}H_{10})_n$	$CHCl_3$	-	-	400	-	-	-	24
$1\text{-}(CHCH(C_6H_4)CC(C_6H_4)CHCH(4'\text{-}NPh_2\text{-}C_6H_4)\text{-}1,12\text{-}C_2B_{10}H_{11}$	DCM	395	9.9	496	5160	0.58	-	25

Table 8-2 cont: Photophysical data of *meta* and *para* carborane containing compounds in the literature.

Compound	Solvent	Abs max / nm	ε / $mol^{-1}cm^{-1}$	Em max / nm	Stokes Shift / cm^{-1}	Quantum Yield ϕ_F	Lifetime / ns	Reference
1-(CHCH(C_6H_4)CC(C_6H_4)CHCH(3',4',5'-($C_{12}H_{25}O$)-C_6H_4)-1,12-$C_2B_{10}H_{11}$	DCM	363	12.2	458	5710	0.59	-	25
1-(CHCH(C_6H_4)CC(C_6H_4)CHCH(3',4',5'-($O(CH_2CH_2O)_3CH_3$)-C_6H_4)-1,12-$C_2B_{10}H_{11}$	DCM	360	10.7	438	4950	0.69	-	25
	H_2O	346	7.2	467	7490	0.24	-	25
1-(CC(C_6H_4)CC(C_6H_4)($C_{17}H_{22}BN_2$)-12-(CC(C_6H_4)CC(C_6H_4)($C_{43}H_{48}N_4BO_4$)-1,12-$C_2B_{10}H_{10}$	Dioxane	525,694	65200, 81100	728	1670	0.30	3.3	26
1-(η^5-$CpFe(CO)_2$)-1,12-$C_2B_{10}H_{11}$	DCM	252, 364	5890, 590	704	13300	-	-	27
Hg(1-(η^5-$CpFe(CO)_2$)-1,12-$C_2B_{10}H_{11}$)$_2$	DCM	266, 365	10790, 1180	728	13700	-	-	27
1,12-(η^5-$CpFe(CO)_2$)$_2$-1,12-$C_2B_{10}H_{10}$	DCM	272, 364	38020, 3760	762	14300	-	-	27
1',3',5'-((C_6H_4)-1,12-$C_2B_{10}H_{11}$)$_3$	DCM	267	-	353	9130	0.24	-	12
1',3',5'-((C_6H_4)$_2$-1,12-$C_2B_{10}H_{11}$)$_3$	DCM	297	-	361	5970	0.36	-	12
1,12-((C_6H_4)($C_{12}NH_8$))$_2$-1,12-$C_2B_{10}H_{10}$	Toluene	293, 310, 339	-	350, 362	927, 1950	0.33	6.37	20
1,12-($Au(PPh_3)$)$_2$-1,12-$C_2B_{10}H_{10}$	Solid state RT	-	-	367, 506	-	-	-	21
	Solid state 77K	-	-	389, 555	-	-	-	21

1. Kokado K., Nagai A and Chujo Y., *Macromolecules*, **2010**, 43, 6463-6468.
2. Kokado K. and Chujo Y., *J. Org. Chem.*, **2011**, 76, 316-319.
3. Kokado K., Nagai A and Chujo Y., *Tetrahedron Lett.*, **2011**, 52, 293-296.
4. Kokado K. and Chujo Y., *Macromolecules*, **2009**, 42, 1418-1420.
5. Kokado K. and Chujo Y., *Polymer Journal*, **2010**, 42, 363-367.
6. Kokado K., Tominaga M. and Chujo Y., *Macromol. Rapid Commun.*, **2010**, 31, 1389-1394.
7. Kokado K., Tokoro Y. and Chujo Y., *Macromolecules*, **2009**, 42, 9238-9242.
8. Peterson J. J., Werre M., Simon Y. C., Coughlin E. B. and Carter K. R., *Macromolecules*, **2009**, 42, 8594-8598.
9. Lerouge F., Vinas C., Teixidor F., Nunez R., Abreu A., Xochitiotzi E., Santillan R. and Farfan N., *Dalton Trans.*, **2007**, 1898-1903.
10. Dash B. P., Satapathy R., Maguire J. A. and Hosmane N. S., *Chem. Commun.*, **2009**, 3267-3269.
11. Dash B. P., Satapathy R., Gailliard E. R., Maguire J. A. and Hosmane N. S., *J. Am. Chem. Soc.*, **2010**, 132, 6578-6587.
12. Dash B. P., Satapathy R., Gailliard E. R., Norten K. M., Maguire J. A., Chug N. and Hosmane N. S., *Inorg. Chem.*, **2011**, 50, 5485-5493.
13. Peterson J. J., Davis A. R., Were A. R., Coughlin E. B. and Carter K. R., *Appl. Mater. Interfaces*, **2011**, 3, 1796-1799.
14. Prokhorov A. M., Slepukhin P. A., Rusinov V. L., Kalinin V. N. and Kozhevnikov D. N., *Chem. Commun.*, **2011**, 47, 7713-7715.
15. Pieters G., Gaucher A., Prim D., Besson T., Giner T., Planas J. G., Teixidor F., Vinas C., Light M. E. and Hursthause M. B., *Chem. Commun.*, **2011**, 47, 7725-7727.
16. Lerouge F., Ferrer-Ugalde A., Vinas C., Teixidor F., Sillanpaa R., Abreu A., Xochitiotzi E., Farfan N., Santillan R. and Nunez R., *Dalton Trans.*, **2011**, 41, 7541-7550.
17. Ferrer-Ugalde A., Juárez-Pérez E. J., Teixidor F., Viñas C., Sillanpää R., Pérez-Inestrosa E. and Núñez R., *Chem. Eur. J.*, **2012**, 18, 544-553.
18. Weber L., Kahlert J., Brockhinke R., Böhling L., Brockhinke A., Stammler H-G., Neumann B., Harder R. A. and Fox M. A., *Chem. Eur. J.*, **2012**, 18, 8347-8357.
19. Davis A. R., Peterson J. J. and Carter K. R., *ACS Macro. Lett.*, **2012**, 1, 469-472.
20. Wee K-R, Han W-S, Cho D. W., Kwon S., Pac C. and Kang S. O., *Angew. Chem. Int. Ed.*, **2012**, 51, 2677-2680.
21. Crespo O., Gimeno M. C., Laguna A., Ospino I., Aullon G. and Oliva J. M., *Dalton Trans.*, **2009**, 3807-3813.
22. Kokado K., Tokoro Y. and Chujo Y., *Macromolecules*, **2009**, 42, 2925-2930.
23. Prokhorov A. M., Slepukhin P. A., Rusinov V. L., Kalinin V. N. and Kozhevnikov D. N., *Tetrahedron Lett.*, **2008**, 49, 3785-3789.
24. Peterson J. J., Simon Y. C., Coughlin B. E. and Carter K. R., *Chem. Commun.*, **2009**, 4950-4952.
25. Nicoud J. F., Bolze F., Sun X. H., Hayek A. and Baldeck P., *Inorg. Chem.*, **2011**, 50, 4272-4278.
26. Ziessel R., Ulrich D., Oliver J. H., Bura T. and Sutter A., *Chem. Commun.*, **2010**, 46, 7978-7980.
27. Bitner T. W., Wedge T. J., Hawthorne M. F. and Zink J. I., *Inorg. Chem.*, **2001**, 40, 5428-5433.

9 : Appendix 3: X-ray crystallography data

1,2-(1'-$C_{10}H_7$)$_2$-1,2-$C_2B_{10}H_{10}$

Identification code	08srv442
Empirical formula	$C_{22}H_{24}B_{10}$
Formula weight	396.51
Temperature/K	120(2)
Crystal system	Monoclinic
Space group	P21/c
a/Å, b/Å, c/Å	12.2349(7), 13.9531(8), 13.6822(8)
α/°, β/°, γ/°	90.00, 116.467(10), 90.00
Volume/Å^3	2090.9(2)
Z	4
ρ_{calc}/mg mm^{-3}	1.260
m/mm^{-1}	0.064
F(000)	824
Crystal size/mm^3	0.4 × 0.1 × 0.08
Theta range for data collection	1.86 to 27.49°
Index ranges	-15 ≤ h ≤ 15, -18 ≤ k ≤ 18, -17 ≤ l ≤ 17
Reflections collected	21082
Independent reflections	4797[R(int) = 0.0830]
Data/restraints/parameters	4797/0/385
Goodness-of-fit on F^2	1.071
Final R indexes [I>2σ (I)]	R1 = 0.0562, wR2 = 0.1238
Final R indexes [all data]	R1 = 0.1034, wR2 = 0.1400
Largest diff. peak/hole / e Å^{-3}	0.229/-0.241

1-(1'-$C_{10}H_7$)-1,2-$C_2B_{10}H_{11}$

Identification code	10srv030
Empirical formula	$C_{12}H_{18}B_{10}$
Formula weight	270.36
Temperature/K	153
Crystal system	Orthorhombic
Space group	Pna21
a/Å, b/Å, c/Å	27.800(2), 6.9089(5), 7.8271(7)
α/°, β/°, γ/°	90.00, 90.00, 90.00
Volume/Å^3	1503.3(2)
Z	4
ρ_{calc}/mg mm^{-3}	1.195
m/mm^{-1}	0.057
F(000)	560
Crystal size/mm^3	0.34 × 0.12 × 0.08
Theta range for data collection	1.46 to 27.99°
Index ranges	-33 ≤ h ≤ 36, -9 ≤ k ≤ 8, -10 ≤ l ≤ 10
Reflections collected	10899
Independent reflections	1942[R(int) = 0.0898]
Data/restraints/parameters	1942/1/271
Goodness-of-fit on F^2	1.044
Final R indexes [I>2σ (I)]	R1 = 0.0420, wR2 = 0.0584
Final R indexes [all data]	R1 = 0.0888, wR2 = 0.0662
Largest diff. peak/hole / e Å^{-3}	0.187/-0.183

1-(1'-$C_{10}H_7$)-1,7-$C_2B_{10}H_{11}$

Identification code	10srv003
Empirical formula	$C_{12}H_{18}B_{10}$
Formula weight	270.36
Temperature/K	120.0
Crystal system	Orthorhombic
Space group	Pna21
a/Å, b/Å, c/Å	26.1610(6), 7.1572(2), 7.8465(2)
α/°, β/°, γ/°	90.00, 90.00, 90.00
Volume/Å^3	1469.17(6)
Z	4
ρ_{calc}/mg mm^{-3}	1.222
m/mm^{-1}	0.059
F(000)	560
Crystal size/mm^3	0.32 × 0.32 × 0.06
Theta range for data collection	1.56 to 30.50°
Index ranges	-37 ≤ h ≤ 37, -10 ≤ k ≤ 10, -11 ≤ l ≤ 11
Reflections collected	18661
Independent reflections	2393[R(int) = 0.0360]
Data/restraints/parameters	2393/1/271
Goodness-of-fit on F^2	1.059
Final R indexes [I>2σ (I)]	R1 = 0.0351, wR2 = 0.0900
Final R indexes [all data]	R1 = 0.0390, wR2 = 0.0934
Largest diff. peak/hole / e Å^{-3}	0.334/-0.158

1-(1'-$C_{10}H_7$)-1,12-$C_2B_{10}H_{11}$

Identification code	10srv002
Empirical formula	$C_{12}B_{10}H_{18}$
Formula weight	270.36
Temperature/K	120.0
Crystal system	Monoclinic
Space group	P21/n
a/Å, b/Å, c/Å	13.2718(3), 16.6794(4), 13.6379(3)
α/°, β/°, γ/°	90.00, 93.92(2), 90.00
Volume/Å^3	3011.89(12)
Z	8
ρ_{calc}/mg mm^{-3}	1.192
m/mm^{-1}	0.057
F(000)	1120
Crystal size/mm^3	0.48 × 0.16 × 0.16
Theta range for data collection	1.93 to 30.00°
Index ranges	-18 ≤ h ≤ 18, -23 ≤ k ≤ 23, -19 ≤ l ≤ 19
Reflections collected	38674
Independent reflections	8778[R(int) = 0.0550]
Data/restraints/parameters	8778/0/541
Goodness-of-fit on F^2	1.003
Final R indexes [I>2σ (I)]	R1 = 0.0475, wR2 = 0.1222
Final R indexes [all data]	R1 = 0.0698, wR2 = 0.1318
Largest diff. peak/hole / e Å^{-3}	0.558/-0.216

4-$IC_6H_4NTol_2$

Identification code	11srv014
Empirical formula	$C_{20}H_{18}IN$
Formula weight	399.25
Temperature / K	120.15
Crystal system	monoclinic
Space group	C2/c
a / Å, b / Å, c / Å	8.0170(2), 11.9111(3), 17.6805(5)
α/°, β/°, γ/°	90.00, 99.288(10), 90.00
Volume / $Å^3$	1666.20(8)
Z	4
ρ_{calc} / mg mm^{-3}	1.592
μ / mm^{-1}	1.918
F(000)	792
Crystal size / mm^3	0.38 × 0.22 × 0.16
2Θ range for data collection	4.66 to 59°
Index ranges	-11 ≤ h ≤ 11, -16 ≤ k ≤ 16, -24 ≤ l ≤ 24
Reflections collected	9213
Independent reflections	2312[R(int) = 0.0247]
Data/restraints/parameters	2312/1/98
Goodness-of-fit on F^2	1.167
Final R indexes [I>2σ (I)]	R_1 = 0.0359, wR_2 = 0.0965
Final R indexes [all data]	R_1 = 0.0369, wR_2 = 0.0970
Largest diff. peak/hole / e $Å^{-3}$	0.722/-0.860

1-(4'-$C_6H_4NTol_2$)-1,7-$C_2B_{10}H_{11}$

Identification code	11srv012
Empirical formula	$C_{22}H_{29}B_{10}N$
Formula weight	415.56
Temperature / K	120.15
Crystal system	triclinic
Space group	P-1
a / Å, b / Å, c / Å	7.3897(2), 11.1210(3), 14.4704(4)
α/°, β/°, γ/°	87.123(10), 83.937(10), 88.535(10)
Volume / $Å^3$	1180.80(6)
Z	2
ρ_{calc} / mg mm^{-3}	1.169
μ / mm^{-1}	0.060
F(000)	436
Crystal size / mm^3	0.38 × 0.14 × 0.02
2Θ range for data collection	2.84 to 58.98°
Index ranges	-10 ≤ h ≤ 10, -15 ≤ k ≤ 14, -20 ≤ l ≤ 20
Reflections collected	13203
Independent reflections	6530[R(int) = 0.0309]
Data/restraints/parameters	6530/0/414
Goodness-of-fit on F^2	1.034
Final R indexes [I>2σ (I)]	R_1 = 0.0517, wR_2 = 0.1293
Final R indexes [all data]	R_1 = 0.0820, wR_2 = 0.1463
Largest diff. peak/hole / e $Å^{-3}$	0.359/-0.244

1-(4'-$C_6H_4NTol_2$)-1,12-$C_2B_{10}H_{11}$

Identification code	11srv182
Empirical formula	$C_{22}H_{29}B_{10}N$
Formula weight	415.56
Temperature/K	120
Crystal system	triclinic
Space group	P-1
a / Å, b / Å, c / Å	9.9427(4), 14.0156(6), 18.4454(7)
α/°, β/°, γ/°	89.4290(10), 83.1170(10), 71.5410(10)
Volume/Å^3	2419.53(17)
Z	4
ρ_{calc} /mg mm^{-3}	1.141
m/mm^{-1}	0.059
F(000)	872
Crystal size/mm^3	0.3 × 0.24 × 0.14
2Θ range for data collection	3.06 to 58°
Index ranges	-13 ≤ h ≤ 13, -19 ≤ k ≤ 19, -25 ≤ l ≤ 25
Reflections collected	25753
Independent reflections	12752[R(int) = 0.0357]
Data/restraints/parameters	12752/0/827
Goodness-of-fit on F^2	1.038
Final R indexes [I>=2σ (I)]	R_1 = 0.0523, wR_2 = 0.1269
Final R indexes [all data]	R_1 = 0.0914, wR_2 = 0.1457
Largest diff. peak/hole / e Å^{-3}	0.302/-0.271

4,4'-(1''-C_6H_5-1'',2''-$C_2B_{10}H_{10}$)$_2$-1,1'-(C_6H_4)$_2$

Identification code	10srv139
Empirical formula	$C_{28}H_{38}B_{20}$
Formula weight	590.78
Temperature / K	153
Crystal system	Triclinic
Space group	P-1
a / Å, b / Å, c / Å	10.9133(3), 16.4785(4), 21.1216(5)
α/°, β/°, γ/°	106.462(10), 101.886(10), 105.656(10)
Volume / Å^3	3339.45(15)
Z	4
ρ_{calc} / mg mm^{-3}	1.175
μ / mm^{-1}	0.057
F(000)	1224
Crystal size / mm^3	0.52 × 0.36 × 0.06
Theta range for data collection	1.40 to 29.00°
Index ranges	-14 ≤ h ≤ 14, -22 ≤ k ≤ 22, -28 ≤ l ≤ 28
Reflections collected	39636
Independent reflections	17680[R(int) = 0.0641]
Data/restraints/parameters	17680/0/1149
Goodness-of-fit on F^2	0.946
Final R indexes [I>2σ (I)]	R1 = 0.0527, wR2 = 0.1199
Final R indexes [all data]	R1 = 0.0904, wR2 = 0.1331
Largest diff. peak/hole / e Å^{-3}	0.390/-0.226

2,5-(1'-C_6H_5-1',2'-$C_2B_{10}H_{10}$)$_2$-C_4SH_2

Identification code	10srv122
Empirical formula	$C_{20}H_{32}B_{20}S$
Formula weight	520.72
Temperature / K	120
Crystal system	Monoclinic
Space group	C2/c
a/Å, b/Å, c/Å	22.7261(7), 6.8441(2), 19.2116(6)
α/°, β/°, γ/°	90.00, 107.196(10), 90.00
Volume/Å^3	2854.59(15)
Z	4
ρ_{calc}/mg mm^{-3}	1.212
μ/mm^{-1}	0.128
F(000)	1072
Crystal size/mm^3	0.38 × 0.12 × 0.1
Theta range for data collection	1.88 to 29.50°
Index ranges	-31 ≤ h ≤ 31, -9 ≤ k ≤ 9, -26 ≤ l ≤ 26
Reflections collected	17259
Independent reflections	3991[R(int) = 0.0582]
Data/restraints/parameters	3991/0/250
Goodness-of-fit on F^2	1.038
Final R indexes [I>2σ (I)]	R1 = 0.0498, wR2 = 0.1322
Final R indexes [all data]	R1 = 0.0661, wR2 = 0.1431
Largest diff. peak/hole /e Å^{-3}	0.863/-0.312

1,4-(1'-(4''-^{t}Bu-C_6H_4)-1',2'-$C_2B_{10}H_{10}$)$_2$-C_6H_4

Identification code	10srv183
Empirical formula	$C_{30}H_{50}B_{20}$ x CH_2Cl_2
Formula weight	711.83
Temperature / K	120.1500
Crystal system	monoclinic
Space group	C2/c
a / Å, b / Å, c / Å	22.2320(10), 12.80180(10), 15.3177(8)
α/°, β/°, γ/°	90.00, 106.82(3), 90.00
Volume / Å^3	4173.1(3)
Z	4
ρ_{calc} / mg mm^{-3}	1.133
μ / mm^{-1}	0.180
F(000)	1488
Crystal size / mm^3	0.2000 × 0.2000 × 0.2000
Theta range for data collection	1.3928 to 61.0138°
Index ranges	-27 ≤ h ≤ 27, -15 ≤ k ≤ 15, -18 ≤ l ≤ 18
Reflections collected	6576
Independent reflections	4102[R(int) = 0.2360]
Data/restraints/parameters	4102/0/243
Goodness-of-fit on F^2	1.036
Final R indexes [I>2σ (I)]	R_1 = 0.0895, wR_2 = 0.1862
Final R indexes [all data]	R_1 = 0.1399, wR_2 = 0.2103
Largest diff. peak/hole / e Å^{-3}	0.334/-0.285

1,4-(1'-(1''-$C_{10}H_7$)-1',2'-$C_2B_{10}H_{10}$)$_2$-C_6F_4

Identification code	10srv205
Empirical formula	$C_{30}H_{34}B_{20}F_4$
Formula weight	686.77
Temperature / K	100.00
Crystal system	triclinic
Space group	P-1
a / Å, b / Å, c / Å	12.9462(2), 14.2819(3), 15.1680(3)
α/°, β/°, γ/°	78.564(10), 73.407(10), 81.200(10)
Volume / Å^3	2620.46(9)
Z	3
ρ_{calc} / mg mm^{-3}	1.306
μ / mm-1	0.634
F(000)	1050
Crystal size / mm^3	0.02 × 0.01 × 0.002
Theta range for data collection	3.08 to 105°
Index ranges	-12 ≤ h ≤ 13, -14 ≤ k ≤ 14, -15 ≤ l ≤ 15
Reflections collected	8987
Independent reflections	5418[R(int) = 0.0374]
Data/restraints/parameters	5418/0/926
Goodness-of-fit on F^2	0.994
Final R indexes [I>2σ (I)]	R1 = 0.0537, wR2 = 0.1351
Final R indexes [all data]	R1 = 0.0818, wR2 = 0.1566
Largest diff. peak/hole / e Å^{-3}	0.573/-0.152

1,4-(1'-(4''-$C_6H_4NTol_2$)-1',2'-$C_2B_{10}H_{10}$)$_2$-C_6H_4

Identification code	08srv433
Empirical formula	$C_{50}H_{60}B_{20}N_2$
Formula weight	905.20
Temperature / K	120(2)
Crystal system	Monoclinic
Space group	$P2_1/n$
a / Å, b / Å, c / Å	14.9178(2), 10.84210 (10), 17.0384(2)
α/°, β/°, γ/°	90.00, 110.801(10), 90.00
Volume / Å^3	2576.17(15)
Z	2
ρ_{calc} / mg mm^{-3}	1.167
μ / mm^{-1}	0.061
F(000)	948
Crystal size / mm^3	0.14 x 0.12 x 0.1
Theta range for data collection	1.56 to 29.00°
Index ranges	-20 ≤ h ≤ 20, -14 ≤ k ≤ 14, -23 ≤ l ≤ 23
Reflections collected	35728
Independent reflections	6840[R(int)=0.0406]
Data/restraints/parameters	6840/0/445
Goodness-of-fit on F^2	1.017
Final R indexes [I>2σ (I)]	R1 = 0.0556, wR2 = 0.1503
Final R indexes [all data]	R1 = 0.0787, wR2 = 0.1730
Largest diff. peak/hole / e Å^{-3}	0.390/-0.221

The following conferences and symposia were attended during the period of study:-

Euroboron 5, Heriot Watt University, 2010, poster presentation.

Dalton Summer School, University of Edinburgh, 2010, poster presentation.

Universities of Scotland Inorganic Chemistry (USIC) Conference, Durham University, 2010, poster presentation.

Departmental postgraduate symposium, 2011, poster presentation.

Rennes 2012, Durham University, oral presentation.

Departmental postgraduate symposium, 2012, oral presentation.

CHEMISTRY
A EUROPEAN JOURNAL

FULL PAPER

DOI: 10.1002/chem.201200390

Luminescence Properties of *C*-Diazaborolyl-*ortho*-Carboranes as Donor–Acceptor Systems

Lothar Weber,*[a] Jan Kahlert,[a] Regina Brockhinke,[a] Lena Böhling,[a] Andreas Brockhinke,[a] Hans-Georg Stammler,[a] Beate Neumann,[a] Rachel A. Harder,[b] and Mark A. Fox*[b]

Abstract: Seven derivatives of 1,2-dicarbadodecaborane (*ortho*-carborane, 1,2-$C_2B_{10}H_{12}$) with a 1,3-diethyl- or 1,3-diphenyl-1,3,2-benzodiazaborolyl group on one cage carbon atom were synthesized and structurally characterized. Six of these compounds showed remarkable low-energy fluorescence emissions with large Stokes shifts of 15100–20260 cm^{-1} and quantum yields (Φ_F) of up to 65% in the solid state. The low-energy fluorescence emission, which was assigned to a charge-transfer (CT) transition between the cage and the heterocyclic unit, depended on the orientation (torsion angle, ψ) of the diazaborolyl group with respect to the cage C–C bond. In cyclohexane, two compounds exhibited very weak dual fluorescence emissions with Stokes shifts of 15660–18090 cm^{-1} for the CT bands and 1960–5540 cm^{-1} for the high-energy bands, which were assigned to local transitions within the benzodiazaborole units (local excitation, LE), whereas four compounds showed only CT bands with Φ_F values between 8–32%. Two distinct excited singlet-state (S_1) geometries, denoted S_1(LE) and S_1(CT), were observed computationally for the benzodiazaborolyl-*ortho*-carboranes, the population of which depended on their orientation (ψ). TD-DFT calculations on these excited state geometries were in accord with their CT and LE emissions. These *C*-diazaborolyl-*ortho*-carboranes were viewed as donor–acceptor systems with the diazaborolyl group as the donor and the *ortho*-carboranyl group as the acceptor.

Keywords: carboranes · charge transfer · diazaboroles · donor–acceptor systems · luminescence

Introduction

Organic molecules with extended conjugated π-electron systems and boryl-substituents (BR_2) have attracted considerable interest over the last two decades. Interaction of the empty p-orbital on the three-coordinate boron atom with the LUMO of organic scaffolds leads to a narrowing of the HOMO–LUMO gap, thereby bringing about interesting optical and electronic properties that facilitate their potential use in functional materials.[1] Such compounds exhibit sizable second- and third-order nonlinear optical coefficients,[2,3] large two-photon absorption cross-sections,[4] and can be used as efficient electron-transporting and/or emitting layers in organic light-emitting diodes (OLEDs).[5] Moreover, three-coordinate-boron-containing compounds are effective colorimetric and luminescent sensors for anions such as fluoride[6] and cyanide.[7] The most prominent boron-based substituent is the dimesitylboryl ($BMes_2$) moiety, which provides stabilization to unsaturated boron centers through steric effects of the *ortho*-methyl groups. A number of conjugated molecules with such boryl side-groups have displayed very large Stokes shifts and high quantum yields both in solution and in the solid state, which was attributed to the lack of close packing.[8] The $BMes_2$ group is considered to be a π-acceptor of comparable quality to the familiar nitro[9] and cyano[10] functionalities.

Within the past decade, the chemistry of another class of three-coordinate boron compounds, namely the 1,3,2-diazaboroles, has developed rapidly.[11–16] Some of these compounds have shown strong fluorescence.[17–28] Owing to the facile and inexpensive synthesis of its precursor, the 1,3-diethyl-1,3,2-benzodiazaborolyl group (1,3-Et_2-1,3,2-$N_2BC_6H_4$) is widely used and compounds containing this unit are moderately air-stable.[13,19–24] Previous calculations on 2-arylethynyl-1,3,2-benzodiazaboroles showed a localization of the HOMO on the diazaborole fragment, which led to the suggestion that this group is a π-donor.[22] Cyclic voltammetry studies disclosed that diazaboroles are easily oxidized.[15q,18,20,23] A subsequent study on linear π-conjugated systems with the 1,3-diethyl-1,3,2-benzodiazaborolyl group

[a] Prof. Dr. L. Weber, J. Kahlert, Dr. R. Brockhinke, L. Böhling, Dr. A. Brockhinke, Dr. H.-G. Stammler, B. Neumann
Fakultät für Chemie der Universität Bielefeld
33615 Bielefeld (Germany)
E-mail: lothar.weber@uni-bielefeld.de

[b] R. A. Harder, Dr. M. A. Fox
Department of Chemistry, Durham University
Durham DH1 3 LE (UK)
E-mail: m.a.fox@durham.ac.uk

Supporting information for this article, including a detailed description of the photophysical measurements, additional spectroscopic and photophysical data, detailed synthetic procedures, characterizations, and ^1H NMR, $^1H\{^{11}B\}$ NMR, $^{13}C\{^1H\}$ NMR, and $^{11}B\{^1H\}$ NMR spectra of carboranes **1**–**7**, is available on the WWW under http://dx.doi.org/10.1002/chem.201200390.

as a π-donor at one end and the dimesitylboryl unit as a π-acceptor at the other end revealed that the π-electron-donating strength of the 1,3-diethyl-1,3,2-benzodiazaborolyl function lies between that of the methoxy and dimethylamino groups.[27] To improve their thermal, chemical, and photophysical properties, as well as to enhance our understanding of such push-pull molecules, it is desirable to explore a different acceptor group within these molecules.

With regard to alternative acceptor units, we focused our interest on *closo*-1,2-dicarbadodecaboranes (*ortho*-carboranes). This choice was obvious because our benzodiazaborolyl group is electron-releasing when linked through the B atom[22] and *ortho*-carboranyl cages are electron-withdrawing when attached through cage carbon atoms C1 or C2.[29] Thus, *C*-diazaborolyl-*ortho*-carboranes may be regarded as donor–acceptor (D–A) systems (Figure 1). In fact, during

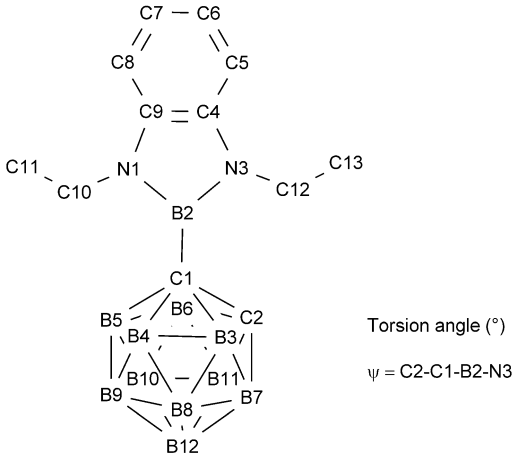

Figure 1. Atom labeling of diethylbenzodiazaborolyl-*ortho*-carborane (**1**); the hydrogen atoms that are attached to the C2, B3–B12, C5–C8, and C10–C13 atoms are omitted for clarity.

our project, a number of articles appeared in which the incorporation of *ortho*-carborane cages into conjugated molecules gave rise to unforeseen low-energy emissions.[30] These emissions were ascribed to CT processes that occurred between the π-system and the carbon atoms of the cluster. Herein, we report our synthetic, structural, photophysical, and computational studies on *C*-diazaborolyl-*ortho*-carboranes, including our discovery of dual fluorescence emissions in solution as well as remarkable low-energy CT fluorescence emissions from the solid- and solution states of such compounds.

Results and Discussion

Syntheses: *C*-diazaborolyl carboranes **1–5** were formed by lithiation of their corresponding *ortho*-carborane, followed by the addition of an equimolar amount of 2-bromo-1,3-diethyl-1,3,2-benzodiazaborole[14] (Scheme 1). After short-path distillation or extraction of the crude product from the reac-

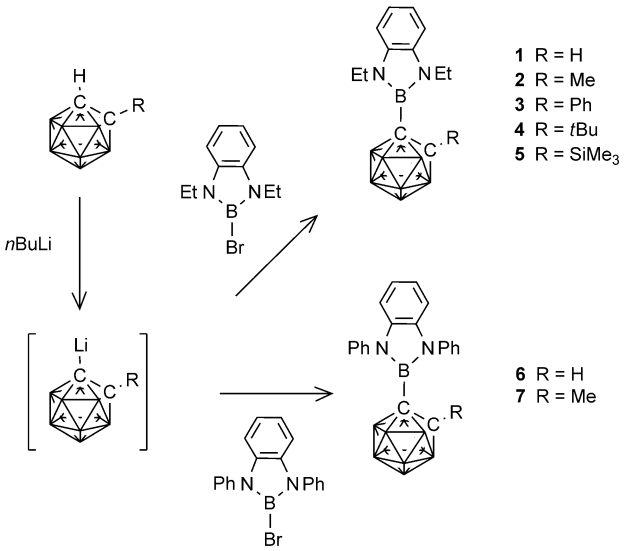

Scheme 1. Synthesis of benzodiazaborolyl-*ortho*-carboranes **1–7**; each unmarked cluster vertex represents BH.

tion residue with toluene, these compounds were purified by crystallization from *n*-hexane/CH_2Cl_2 as colorless or light-yellow solids in 44–82% yield. A similar procedure, with 2-bromo-1,3-diphenyl-1,3,2-benzodiazaborole[24] instead of the diethyl derivative, gave functionalized carboranes **6** and **7** in lower yield (21–24%).

Compounds **1–7** were colorless, oxygen-, and moisture-sensitive solids. They were well-soluble in common polar aprotic solvents and aromatic hydrocarbons and slightly soluble in alkanes. The more stable 1,3-diphenyl-1,3,2-benzodiazaboroles **6** and **7** were stored for days in air without visible deterioration.

In the $^{11}B\{^1H\}$ NMR spectra of compounds **1–7**, the exopolyhedral boron atoms of the benzodiazaborolyl groups gave rise to singlets in the narrow range $\delta = 22.1$–24.0 ppm. Similar chemical shifts were reported for 2-bromo-1,3-diethyl-1,3,2-benzodiazaborole ($\delta = 22.8$ ppm)[14] and 2-bromo-1,3-diphenyl-1,3,2-benzodiazaborole ($\delta = 24.0$ ppm).[24] Thus, the carboranyl groups influenced the NMR shifts of the 3-coordinate boron atoms in the benzodiazaboroles like an inductively electron-withdrawing bromine atom.

In the ^1H NMR spectra of compounds **1** and **3**, the *N*-methylene units gave rise to well-resolved quartets in the range $\delta = 3.57$–4.02 ppm ($^3J = 7$ Hz), whereas, in 1-methyl-*ortho*-carborane **2**, this CH_2 group appeared as a broad and unresolved resonance at $\delta = 3.64$ ppm. In compounds **4** and **5**, which contained bulky *tert*-butyl- and trimethylsilyl groups, respectively, well-resolved signals were observed for the two non-equivalent methylene protons, thereby reflecting the decreased rotational mobility around the B2−C1 bond owing to steric congestion. The cage C2−H protons in compounds **1** and **6** were observed as broad singlets at $\delta =$ 4.00 and 3.02 ppm, respectively. The upfield shift of about 1 ppm pointed to an intramolecular cage CH···π-ring interaction with the *N*-phenyl-substituents in compound **6** and

suggested that conformers that had N3-B2-C1-C2 torsion angles (ψ) of around 0° predominated.

X-ray crystallography: Molecular structures of compounds **1–7** were determined by X-ray diffraction (Figure 2). Selected bond lengths and torsion angles are given in Table 1. The

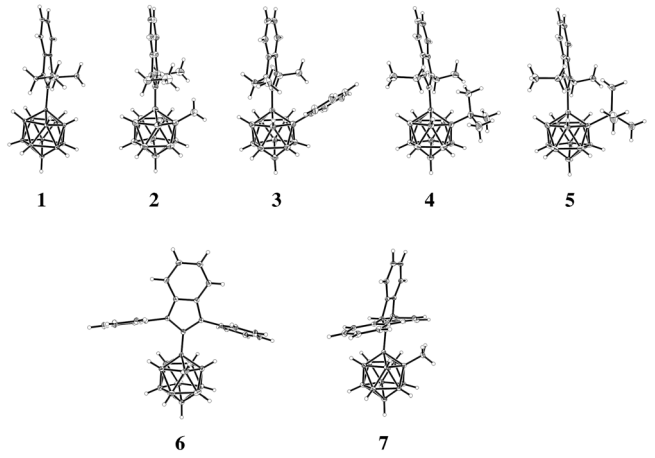

Figure 2. Molecular structures of compounds **1–7** were determined by X-ray crystallography; cage C2–H···π interactions were observed for compounds **1** and **6** with cage C–H···ring-centroid distances of 2.428 and 2.752 Å, respectively.

Table 1. Selected bond lengths [Å] and torsion angles [°] for *ortho*-carboranes **1–7**.

	C1–B2	C1–C2	C2–R	R	Torsion angle C2-C1-B2-N3 [ψ]
1	1.594(2)	1.670(1)	0.94(2)	H	92.4
2[a]	1.605(3)	1.684(2)	1.516(3)	Me	88.8
	1.600(3)	1.687(2)	1.511(3)	Me	89.8
3[b]	1.600(2)	1.730(2)	1.514(2)	Ph	89.3
	1.600(2)	1.720(2)	1.512(2)	Ph	86.6
	1.609(2)	1.701(2)	1.511(2)	Ph	67.5
4	1.606(1)	1.756(1)	1.573(1)	*t*Bu	89.6
5	1.605(1)	1.710(1)	1.931(1)	Me_3Si	83.7
6	1.586(2)	1.670(2)	1.04(2)	H	16.6
7	1.591(2)	1.686(2)	1.513(2)	Me	80.0

[a] Two independent molecules in the asymmetric unit. [b] Three independent molecules in the asymmetric unit.

asymmetric unit of compound **2** contained two independent molecules and that of compound **3** contained three independent molecules.

The bond lengths and angles in the 1,3,2-benzodiazaborolyl units were similar to the corresponding data in other previously reported structures (B–N 1.44 Å, C–N 1.40 Å, C–C 1.40 Å).[18–28] Similarly, the B–C (1.73 Å) and B–B bond lengths (1.77 Å) within the *ortho*-carborane cage were expected for *ortho*-carboranes.[31] The *exo*-cage B–C single-bond lengths were in the range 1.586(2) Å in compound **6** to 1.609(2) Å in one conformer of compound **3**. The C1–C2 cage distances in *ortho*-carboranes are known to be very sensitive towards substituents that are attached onto the cage carbons. In our benzodiazaborolyl-functionalized carboranes, these values were in the range 1.670(2) Å (**1**, R = H; **6**, R = H) to 1.756(1) Å (**4**, R = *t*Bu). Thus, these values were markedly longer than the corresponding distance in the parent 1,2-$C_2B_{10}H_{12}$ (1.62 Å).[32] The remarkable elasticity of the C1–C2 bond in *ortho*-carboranes has been reported previously[33,34] and may have been either due to steric crowding[35] and/or to conjugation with π-donor substituents at the cage carbon atoms.[36]

The torsion angles C2-C1-B2-N3 (ψ) were measured between the extremes of a near perpendicular orientation between a plane that was defined by the atoms B2, C1, C2 and the diazaborolyl plane in compound **1** ($\psi = 92.4°$) and a near co-planar orientation between those planes in compound **6** ($\psi = 16.6°$). These orientations were favored by cage CH π-interactions in the solid state (see the Supporting Information, Figure S29).[37,38] Compound **1** showed an intermolecular π-interaction between the cage CH protons and the *o*-phenylene ring of the benzodiazaborole moiety on a neighboring molecule (CH···ring centroid = 2.428 Å). In contrast, the CH group in compound **6** was involved in an intramolecular π-interaction[37] with an *N*-phenyl ring (CH···*N*-phenyl ring centroid = 2.752 Å).

In the *ortho*-carboranes (compounds **2–5** and **7**), the C2-C1-B2-N3 torsion angles (ψ) were in the range 80–90° (Table 1). These angles were partly due to steric effects between the two substituents at the C1 and C2 positions, as indicated by the hindered rotation around the B2–C1 bond in the NMR data for compounds **2**, **4**, and **5**. Considering the three conformers of compound **3**, decreasing torsion angles at the borolyl units (89.3°, 86.6°, 67.3°) and at the phenyl rings (85.5°, 75.8°, 59.2°) were reflected in successive shortening of the C1–C2 bond (1.730(2) Å, 1.720(2) Å, 1.701(2) Å, respectively). The orientation of the aryl groups with respect to the C1–C2 axis is known to influence the C1–C2 bond lengths.[39] According to the interplanar angles that were enclosed by the *N*-phenyl rings and the diazaborole planes in compounds **6** (75.8°, 76.4°) and **7** (72.2°, 76.5°), no conjugation between these π-systems was expected.

UV/Vis and luminescence spectroscopy

Absorption: The absorption maxima for solutions of compounds **1–7** in cyclohexane ($\lambda = 283–296$ nm) and CH_2Cl_2 ($\lambda = 284–296$ nm) were essentially the same as their respective values in the solid state (286–297 nm; Table 2). For comparison, a solution of 2-*tert*-butyl-1,3-diethyl-1,3,2-benzodiazaborole in cyclohexane gave an intense absorption at $\lambda = 285$ nm.[24] The absence of significant solvatochromism in the absorption maxima pointed to very similar dipole moments in the electronic ground states and the initially formed Franck–Condon excited states of derivatives **1–7**. Thus, it was conceivable that the absorption bands reflected local π–π* transitions within the benzodiazaborole parts of the molecules.

Table 2. Absorption data of compounds **1–7**.[a]

Compound	Absorption λ_{max} [nm] (ε)[a] in cyclohexane	Absorption λ_{max} [nm] (ε)[a] in CH_2Cl_2	Absorption λ_{max} [nm] in the solid state
1	285 (11410), 288 (11080), 294 (13910)	287 (9350), 295 (9970)	291, 297[b]
2	289 (12060), 296 (11760)	291 (15100), 296 (14900)	292
3	295 (11790)	296 (13500)	297
4	291 (13400), 296 (13620)	296 (11190)	293
5	290 (15400), 296 (15000)	291 (11740), 296 (11770)	289
6	283 (9740), 289 (11430)	284 (7850), 290 (8600)	286, 292[b]
7	285 (8020), 292 (8310)	286 (12380), 292 (12520)	288, 294[b]

[a] In L mol^{-1} cm^{-1}. [b] Global maximum of the spectrum.

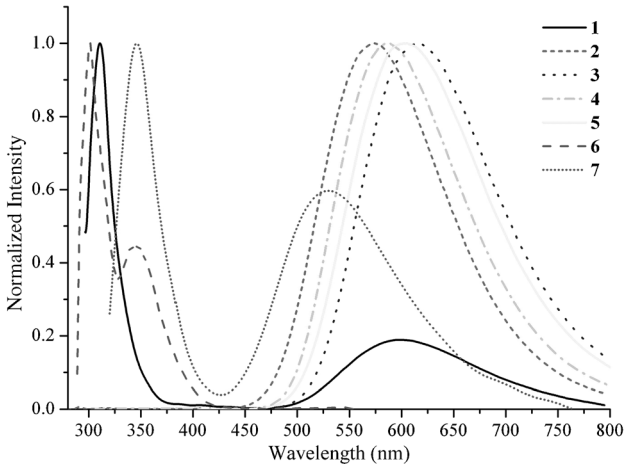

Figure 3. Emission spectra for compounds **1–7** in cyclohexane.

Solution-state emission: Table 3 lists the emission data of all of the *ortho*-carboranes studied herein. Solutions of compounds **1–5** and **7** in cyclohexane showed visible emissions that ranged from green (**7**, 534 nm) to orange (**3**, 615 nm; Figure 3). Large Stokes shifts that ranged from 15660 cm^{-1} (**1**) to 18090 cm^{-1} (**5**) pointed to distinct geometric rearrangements that resulted from relaxation of the initially formed excited state. No visible (low-energy) emission was observed for compound **6**.

The diphenylbenzodiazaborolyl group in compound **7** was less electron releasing than the diethylbenzodiazaborolyl group in compound **2**, which agreed with the blue shift of 40 nm in cyclohexane on going from compounds **2** to **7**.

Because similar low-energy emissions have previously been attributed to aggregation,[30] luminescence spectra of *tert*-butyl-*ortho*-carborane **4** were recorded in cyclohexane at different concentrations. No unusual concentration-dependence on the luminescence intensity was evident (see the Supporting Information, Figure S34), thus ruling out aggregates (and excimers) as sources.

The luminescence spectra of all of the carboranes showed solvatochromism. In the polar solvent CH_2Cl_2, the low-energy emissions for compounds **1–5** and **7** showed maxima between 646 nm (**7**) and 757 nm (**3**), with Stokes shifts in the range 19030 cm^{-1} (**1**) to 21340 cm^{-1} (**3**). These values were red-shifted with respect to the emission maxima in cyclohexane.

According to the Lippert–Mataga equation, the transition dipole moment, that is the difference between the excited- and ground-state dipole moments, could be calculated from the slope of a plot of the Stokes shift versus the orientational polarizability of the solvents (see the Supporting Information, Figure S32). Transition dipole moments of 7.4 D (**5**) to 8.4 D (**1**) were obtained with an Onsager radius of 3.52 Å (Table 3). These results demonstrated that the excited state was more polarized than the ground state and that the low-energy emissions were accompanied by a pronounced intramolecular charge transfer.

In addition to the CT bands, solutions of compounds **1** and **7** in cyclohexane displayed emissions in the UV region (**1**: $\lambda_{max}=311$; **7**: 345 nm). Presumably, a smaller energy barrier to rotation around the B2–C1 bond in these molecules opened a pathway to a different excited state with a geometry that was similar to the ground-state structure in this solvent. Compound **6** had two very weak high-energy emission bands at $\lambda=302$ nm and 346 nm in cyclohexane.

The quantum yields of solutions of compounds **4** (32%) and **5** (18%) in cyclohexane were significantly higher than

Table 3. Emission data of compounds **1–7**.

	Emission λ_{max} [nm] in cyclohexane	Stokes shift [cm^{-1}] in cyclohexane	Φ_F [%] in cyclohexane	Emission λ_{max} [nm] in CH_2Cl_2	Stokes shift [cm^{-1}] in CH_2Cl_2	Φ_F [%] in CH_2Cl_2	Emission λ_{max} [nm] in solid state	Stokes shift [cm^{-1}] in solid state	Φ_F [%] in solid state[e]	Transition dipole moment [D][f]
1	311, 596[a]	1960, 15660	<1	720	19030	<1	561	16060	51	8.4
2	574	16480	8	692	19800	3	573	16520	65	8.1
3	615	18050	6	757	21340	1	613	15100	30	8.3
4	587	17420	32	713	20330	3	611	16160	42	7.6
5	602	18090	18	726	20870	2	631	20260	30	7.4
6	302, 346[b]	1850, 6600	1	417	11170	<1	–[d]	–	–	–
7	345, 534[c]	5540, 15880	<1	646	19200	<1	523	15340	25	8.0

[a] Relative height 1.0:0.2. [b] Relative height 1.0:0.5. [c] Relative height 1.0:0.6. [d] No emission observed. [e] Measured by using the integrating sphere method.[40] [f] Lippert–Mataga method.

those of the other carboranes investigated herein (<1–8%). It is known that intramolecular rotations can effectively quench excitons and that restriction of such rotational motions in turn promotes emission efficiency.[42] Against this background, it was clear that the increased Φ_F values for compounds **4** and **5** were due to the restricted rotation around the B2–C1 bond, which was evident from the ^{1}H NMR spectra (see above). CH_2Cl_2 seemed to favor non-radiative-decay processes because the quantum yields determined in this solvent were much lower for all of the investigated diazaborolyl-*ortho*-carboranes (≤3%).

Solid-state emission: Importantly, the spectroscopically investigated solid layers showed virtually the same emission colors under UV irradiation (Figure 4) as the single crystals that were analyzed by X-ray crystallography (Figure 5). This result suggested that the molecular conformations in the crystals and in the layers were similar. With respect to solutions in cyclohexane, the visible emission maxima of solid samples of *ortho*-carboranes **1**–**5** and **7** were either blue-shifted (**1**: 561 nm; **7**: 523 nm), similar (**2**: 573 nm; **3**: 613 nm), or red-shifted (**4**: 611 nm; **5**: 631 nm), which pointed to different interactions in the solid state. In these compounds, the C1–C2 vector was oriented perpendicular to the plane of the heterocycle, as shown by the C2-C1-B2-N3 torsion angles (ψ = 80.0–92.4°; Table 1). In sharp contrast, no luminescence was detected for solid **6**, where a near coplanar orientation between the diazaborole ring and the C1–C2 bond (ψ = 16.6°) was observed. Based on these results, we concluded that the diazaborolyl orientation played a crucial role in accessing the excited CT state.

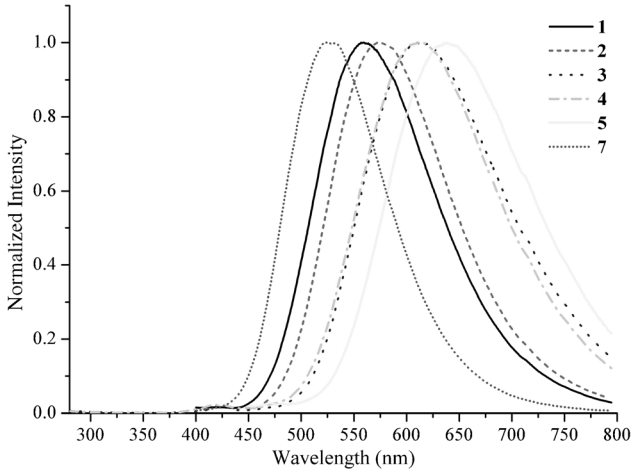

Figure 4. Solid-state emission spectra for compounds **1**–**5** and **7**.

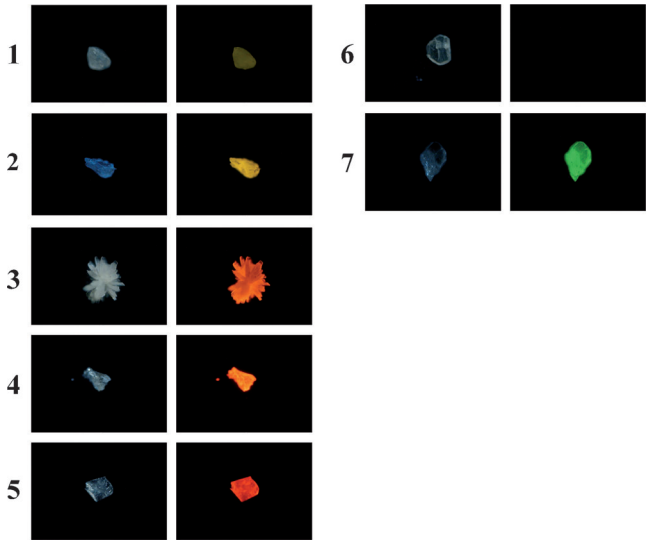

Figure 5. Crystals of compounds **1**–**7**. Left columns: Without UV irradiation. Right columns: Under UV irradiation at 350 nm.

The quantum yields (Φ_F) of solid diazaborolyl-*ortho*-carboranes **1**–**5** and **7** were markedly higher than in solution and ranged from 25% (**7**) to 65% (**2**). Again, this result could be rationalized by the restriction of molecular motion and intermolecular interactions in the solid state. These values are, to the best of our knowledge, the highest reported to date for any solid carborane. To discriminate fluorescence from phosphorescence, the emission lifetime of solid **7** was 5.2 ns, which clearly underlined that the observed long-wave emissions arose from fluorescence processes.

Computational data: The molecular geometries of all seven carboranes (**1**–**7**), as well as the model diazaborolyl-*ortho*-carborane 1-[$C_6H_4(NH)_2B$]-1,2-$C_2B_{10}H_{11}$ (**8**), were optimized at B3LYP/6-31G* with no symmetry constraints (see the Supporting Information, Table S5). The effect of different substituents at the C2 position on the lengths of the B2–C1 and C1–C2 bonds, as observed from X-ray data, were in accord with the trends in the computed bond lengths. These variations were due to the steric effects of the substituents[35] and, for compound **3**, the orientational electronic effect of the phenyl group also played a part.[39] Rotation barriers around the cage–borolyl C–B bond (C1–B2) for compounds **1** and **6** were computed to be 3.5 and 3.8 kcalmol^{-1}, respectively (see the Supporting Information, Figure S42). Computed GIAO-NMR data from these optimized geometries were in excellent agreement with the observed ^{11}B NMR data (see the Supporting Information, Table S6).

The frontier orbitals and orbital energies of boroles, $C_6H_4(NR)_2BH$, where R = H, Et, or Ph, and *ortho*-carborane, are listed in Table 4. The diazaboroles had much higher HOMO energies than the *ortho*-carborane, with a difference

Table 4. Types of frontier orbitals and orbital energies for parent benzodiazaboroles and *ortho*-carborane at B3LYP/6-31G*.

	$C_6H_4(NEt)_2BH$	$C_6H_4(NH)_2BH$	$C_6H_4(NPh)_2BH$	*ortho*-$C_2B_{10}H_{12}$
LUMO energy [eV]	π*(borolyl) −0.23	π*(borolyl) −0.23	π*(phenyl) −0.22	cage* −0.25
HOMO energy [eV]	π(borolyl) −5.37	π(borolyl) −5.49	π(borolyl) −5.54	cage −8.59

of around 3 eV. By contrast, the computed LUMO energies for the benzodiazaboroles and *ortho*-carborane were comparable. Based on these MO calculations, the low-lying unoccupied orbitals would be on the diazaborolyl and cage moieties for benzodiazaborolyl-*ortho*-carboranes, whereas the highest occupied orbitals would be on the borolyl group. The LUMOs in $C_6H_4(NPh)_2BH$ were on the phenyl rings. Thus, three distinct low-lying orbitals were expected in benzodiazaborolyl-*ortho*-carboranes where phenyl groups were present.

Figure 6 shows the important orbitals for model compound **8** at different borolyl orientations ($\psi = 0°$ and 90°) with respect to the cage C–C (C1–C2) bond. As expected, the HOMO and HOMO−1 orbitals were on the diazaborolyl group. Given the similarity between the LUMO energies of diazaborole $C_6H_4(NH)_2BH$ and the *ortho*-carborane (Table 4), the LUMO was the empty p-orbital on the boron atom with substantial orbital contributions from both the C_6H_4 ring and the cage. This type of orbital was denoted as πB* to distinguish it from the other two orbital types: LUMO+1 and LUMO+2 (Figure 6). In the geometry at $\psi = 0°$, LUMO+1 was the C_6H_4 ring antibonding orbital and was described as π*(borolyl) whilst LUMO+2 was the cage antibonding orbital and labeled as cage*. Interestingly, the antibonding orbital energies of the π*(borolyl) and cage* orbitals were reversed for the geometry at $\psi = 90°$.

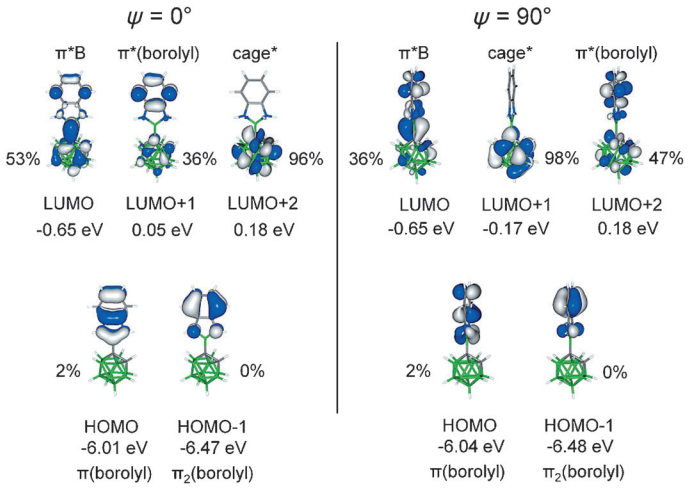

Figure 6. Effect of the orientation of the borolyl moiety at $\psi = 0°$ and $\psi = 90°$ on the nature of the important molecular orbitals in model compound 1-$[C_6H_4(NH)_2B]$-1,2-$C_2B_{10}H_{11}$ (**8**). The amount of cage ($C_2B_{10}H_{11}$) character for each orbital is shown as a percentage. Similar molecular-orbital compositions were found for compounds **1**, **2**, **4**, and **5**.

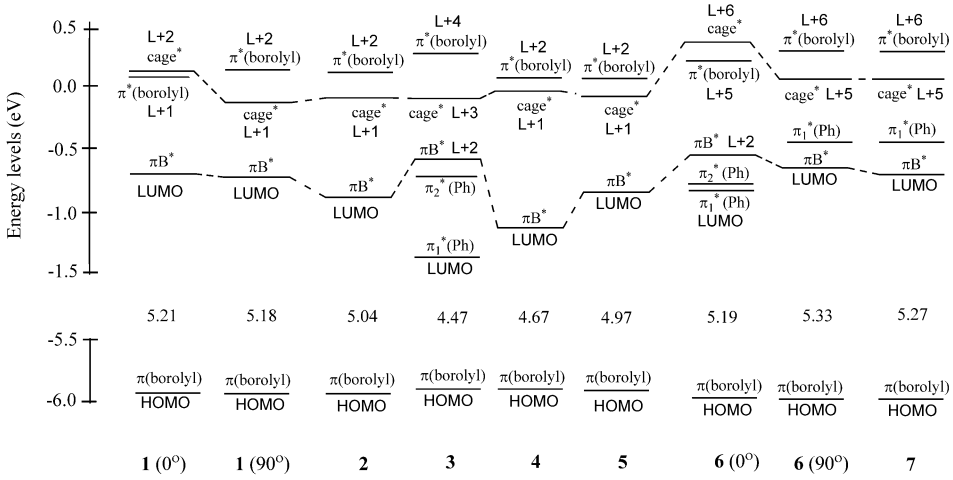

Figure 7. Relative energies of important molecular orbitals in compounds **1**–**7**; the energy values shown between the HOMO and LUMO levels are the HOMO–LUMO energy gaps (in eV).

Selected molecular orbitals and their energies for the optimized geometries of compounds **1**–**7** are listed in Figure 7. The HOMO in each *ortho*-carborane was located on the diazaborolyl group and the HOMO energies were in the narrow range of −5.78 to −5.96 eV. The LUMO in *C*-benzodiazaborolyl-*ortho*-carboranes, wherein no phenyl group(s) existed, was the empty p-orbital on the boron atom, πB*.

For the geometry of compound **6** at $\psi = 0°$, the antibonding orbitals at the phenyl groups, π*(Ph), were LUMO and LUMO+1, and the πB* orbital was LUMO+2 with all three orbital energies close together (see the Supporting Information, Figure S44). Orbitals with similar energy were observed for the geometry of compound **6** at $\psi = 90°$, but the πB* orbital was the LUMO in this case. Figure 7 shows that the LUMO for *ortho*-carboranes with phenyl groups may have either been the πB* orbital or the π*(Ph) orbital. The antibonding cage orbitals, cage*, were substantially higher in energy than the πB* orbitals. Thus, at least for the absorption processes, the clusters in these compounds merely played inductive roles.

The HOMO–LUMO energy gaps (HLGs) for compounds **1**, **2** and **5**–**7** were in the range 4.97–5.33 eV, which were similar to that for the parent diazaboroles (Table 4). Compounds **3** and **4** had HLGs of 4.47 and 4.67 eV, respectively, and a remarkable low-energy LUMO that was located on the phenyl group was found for compound **3** (see the Supporting Information, Figure S43). However, a πB* orbital was the LUMO for compound **4**, which was substantially lower in energy than other πB* orbital energies. According to calculations, the percentage molecular-orbital contribution of the C1–C2 unit to the LUMO was largest in compound **4** (see the Supporting Information, Table S8), which also displayed the largest C1–C2 separation for this series of compounds. As has already been mentioned, one obvious reason for the long C1–C2 bond was steric encumberance. However, it was not unambiguously clear in what way this

bond elongation was exactly related to the low LUMO energy.

TD-DFT calculations on these geometries predicted π-(borolyl) > πB* transitions with high oscillation strengths (f = 0.177–0.328) for all of the compounds investigated (see the Supporting Information, Table S7). Moreover, there were diazaborolyl to phenyl transitions for compounds **3**, **6**, and **7**, which contained one or two phenyl groups, but these had low oscillation strengths. The absorption data for all of the compounds were similar and the transition bands at about 292 nm were assigned as having π(borolyl) > πB* character.

Given the remarkable low-energy emissions observed for the benzodiazaborolyl-*ortho*-carboranes in the solid and solution states, the excited-state geometries of these compounds were examined to gain an insight into these emissions. The geometry of model 1-[$C_6H_4(NH)_2B$]-1,2-$C_2B_{10}H_{11}$ (**8**) was studied in detail. Each starting geometry was optimized at the S_1 excited state with a fixed torsion angle (ψ) at 10° intervals between 0–90°. The C1–C2 bond lengths in these optimized S_1 geometries were remarkably dependent on the orientation with two distinct bond lengths at about 1.6 Å for ψ = 0–30° and about 2.4 Å for ψ = 40–90° (Figure 8). Thus, two distinct S_1 excited-state geometries ('closed' and 'open') existed for compound **8**, depending on the orientation preference.

Table 5 lists the bond lengths for the S_1 excited-state geometries of compounds **1**–**7**. For the disubstituted *ortho*-carboranes, the 'open' S_1 geometries were favored, which was perhaps not surprising given that the steric effects of substituents on both neighboring cage carbon atoms and the orientation of the borolyl moiety would facilitate such geometries. The 'closed' and 'open' S_1 geometries were located for monosubstituted *ortho*-carboranes **1** and **6**, which had different borolyl orientations.

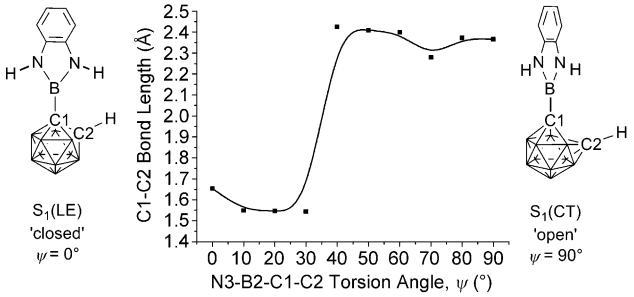

Figure 8. C1–C2 bond lengths of the excited state (S_1) geometries for compound **8** with respect to the orientation of the diazaborolyl group (ψ).

Electronic-structure calculations were carried out on the two S_1 geometries for compound **8** (at the S_0 ground state where the LUMO and HOMO were considered as the highest and second-highest singly occupied orbitals, respectively, at the S_1 excited state). They revealed the LUMO to be πB* for the 'closed' S_1 geometry (ψ = 0°) and an antibonding cage orbital (cage*) for the 'open' S_1 geometry (ψ = 90°; Figure 9). The cage* orbital as the LUMO indicated that the cluster played a vital role in the low-energy CT emission of benzodiazaborolyl-*ortho*-carboranes. MO calculations on all of the open S_1 geometries listed in Table 5 showed their LUMOs to be on the carborane clusters.

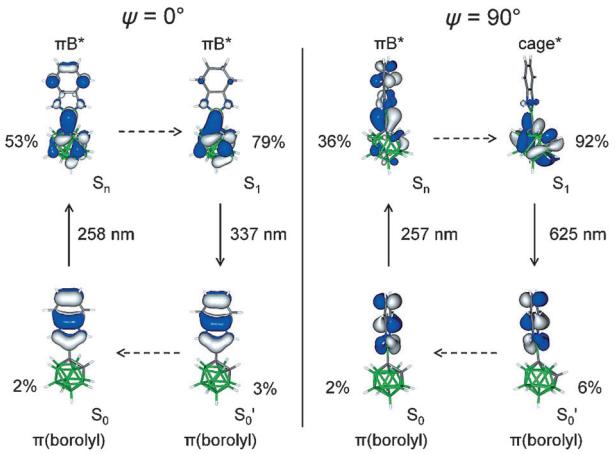

Figure 9. Molecular orbitals involved in the absorption and emission processes for geometries of model compound **8** with ψ = 0° and ψ = 90°.

TD-DFT computations on the S_1 geometries (assuming an S_0 state) for compound **8** predicted a low-energy emission for the 'open' S_1(CT) geometry, whereas a high-energy emis-

Table 5. Comparison of calculated and observed emission (Em) data for solutions of *C*-benzodiazaborolyl-*ortho*-carboranes **1**–**7** in cyclohexane.

	S_1 C1–C2 (calcd) [Å]	S_1 C1–B2 (calcd) [Å]	Em (obs) [eV]	Em $S_0 < S_1$ (calcd) [eV]	Oscillator strength (f)	Major MO contributions[a] [%]	Transition type $S_0 < S_1$
1 (ψ = 0°)	1.699	1.557	3.99	3.39	0.2613	H < L (70)	π(borolyl) < πB*
1 (ψ = 90°)	2.387	1.599	2.08	1.88	0.2100	H < L (71)	π(borolyl) < cage*
2	2.397	1.590	2.16	1.94	0.2121	H < L (71)	π(borolyl) < cage*
3	2.420	1.589	2.02	1.77	0.1725	H < L (71)	π(borolyl) < cage*
4	2.420	1.590	2.11	1.88	0.1839	H < L (71)	π(borolyl) < cage*
5	2.406	1.592	2.06	1.87	0.1879	H < L (71)	π(borolyl) < cage*
6 (ψ = 0°)	1.658	1.575	3.58	2.96	0.0000	H < L (70)	π(borolyl) < phenyl*
6 (ψ = 90°)	2.385	1.581	–	2.03	0.2114	H < L (71)	π(borolyl) < cage*
7	2.397	1.575	2.32	2.07	0.2057	H < L (71)	π(borolyl) < cage*

[a] H < L = HOMO < LUMO.

sion was expected for the 'closed' S_1(LE) geometry (Figure 9). The low-energy emission was characterized as a charge-transfer (CT) transition process where the electron was transferred from the cage to the diazaborolyl group. The high-energy emission was a transition from the πB* orbital with considerable cage character to the π(borolyl) orbital and was more like a borolyl–borolyl transfer (local excitation, LE). The relatively good agreement between the calculated and observed emission data (Table 5) showed that the experimental low-energy emissions from benzodiazaborolyl-*ortho*-carboranes **1**–**5** and **7** arose from electron transfer from the cluster to the diazaborolyl group and were charge-transfer (CT) transitions. The negligible oscillator strength of the HOMO–LUMO transition for the S_1 geometry of compound **6** at $\psi = 0°$ was in agreement with the absence of luminescence in the solid material, where a small value of ψ was measured (Table 5).

Conclusion

Seven derivatives of *ortho*-carborane that contained 1,3,2-diazaborolyl groups were synthesized and structurally characterized. In six of the seven solid-state geometries, the plane of the borolyl group was perpendicular to the C1−C2 axis ($\psi \approx 90°$) and these compounds showed remarkable low-energy fluorescence emissions with large Stokes shifts of 15100–20260 cm^{-1} on excitation in the solid state. In contrast, the solid-state geometry of the borolylcarborane that had a different borolyl orientation ($\psi \approx 0°$) gave no low-energy emission on excitation. The observed CT emissions were assigned to charge-transfer from the cage to the borolyl group, based on the computed S_1 excited-state geometry and TD-DFT data.

Experimental Section

All manipulations were performed under an atmosphere of dry, oxygen-free argon by using Schlenk techniques. All solvents were dried according to standard procedures and freshly distilled prior to use. 2-Bromo-1,3-diethyl-1,3,2-benzodiazaborole,[14] 2-bromo-1,3-diphenyl-1,3,2-benzodiazaborole,[24] 1-phenyl-1,2-dicarbadodecaborane,[42] 1-*tert*-butyl-1,2-dicarbadodecaborane,[43] and 1-trimethylsilyl-1,2-dicarbadodecaborane[43] were prepared according to literature procedures. 1,2-Dicarbadodecaborane and 1-methyl-1,2-dicarbadodecaborane were purchased from commercial sources. NMR spectra were recorded in solution at RT on a Bruker AM Avance DRX500 (^1H, ^{11}B, ^{13}C), a Bruker Avance III 500, or a Bruker Avance 400 spectrometer ($^1H\{^{11}B\}$) with $SiMe_4$ (^1H, ^{13}C) and $BF_3{\cdot}OEt_2$ (^{11}B) as external standards. ^1H NMR and $^{13}C\{^1H\}$ NMR spectra were calibrated by using the solvent signal ($CDCl_3$: 7.24 (^1H), 77.16 (^{13}C); C_6D_6: 7.15 (^1H), 128.06 (^{13}C)). The expected broad ^{13}C NMR peaks owing to the carbon atoms attached to the borole-boron atoms were not detected above the noise levels. MS was performed on a VG Autospec sector field mass spectrometer (Micromass). Absorption was measured with a UV/Vis double-beam spectrometer (Shimadzu UV-2550) by using the solvent as a reference. The setup that was used to acquire excitation–emission spectra (EES) was similar to that used in commercial static fluorimeters. A typical synthetic procedure is described below.

Synthesis of 3: A solution of *n*-butyllithium (1.6 M in *n*-hexane, 3.10 mL, 4.96 mmol) was added dropwise to a chilled (0 °C) solution of 1-phenyl-1,2-dicarbadodecaborane (1.03 g, 4.67 mmol) in Et_2O (30 mL). The mixture was stirred for 1.5 h at ambient temperature, whereupon it was re-cooled to 0 °C. A solution of 2-bromo-1,3-diethyl-1,3,2-benzodiazaborole (1.20 g, 4.74 mmol) in *n*-hexane (15 mL) was added dropwise and the mixture was stirred for 20 h at ambient temperature. Volatile materials were removed in vacuo, the residue was extracted with toluene (2× 20 mL), and the combined extracts were evaporated to dryness. The residue was taken up in a mixture of *n*-hexane (60 mL) and CH_2Cl_2 (4 mL) and the solution was filtered through a frit. Light-yellow crystals of compound **3** were grown from the filtrate at −30 °C (1.48 g, 81 %).

Computational studies: All computations were carried out with the Gaussian09 package.[44] The model geometries from various starting conformers were fully optimized with the B3LYP functional[45] with no symmetry constraints by using the 6–31G* basis set[46] for all atoms. Frequency calculations on these optimized geometries (**1**–**7**) revealed no imaginary frequencies. Partially optimized geometries for compounds **1** and **6** and the model diazaborolyl-*ortho*-carborane 1-$[C_6H_4(NH)_2B]$-1,2-$C_2B_{10}H_{11}$ (**8**) with a constrained dihedral angle ψ were obtained by using OPT(Z-MAT) to determine energy barriers to rotation around the C1−B2 axis. The singlet excited-state geometries (S_1) for compounds **1**–**7** were optimized with C_s symmetry constraints by using TD-DFT calculations at B3LYP/6–31G*. The excited-state geometries for compound **8** were generated from optimization of geometries with a constrained dihedral angle (Figure 7). Computed absorption data were obtained from TD-DFT calculations on S_0 geometries, whereas computed emission data were obtained from the S_1 geometries. The MO diagrams and orbital contributions were generated with the aid of Gabedit[47] and GaussSum[48] packages, respectively. Calculated ^{11}B, ^{13}C, and ^1H NMR chemical shifts that were obtained at the GIAO[49]-B3LYP/6–31G*//B3LYP/6–31G* level on the optimized geometries were referenced to $BF_3{\cdot}OEt_2$ for ^{11}B: $\delta(^{11}B) = 111.7\text{-}\sigma(^{11}B)$ and referenced to TMS for ^{13}C: $\delta(^{13}C) = 189.4\text{-}\sigma(^{13}C)$ and ^1H: $\delta(^1H) = 32.39\text{-}\sigma(^1H)$. Computed NMR values were averaged where possible. This combined observed and computed ^{11}B NMR method has been successfully used elsewhere to determine carborane geometries.[50] Calculations on compound **8** by using the CAM-B3LYP functional,[51] which is more appropriate for push–pull systems and charge-transfer transitions than the B3LYP functional, gave similar results to those described herein with the B3LYP functional.

Crystallographic studies: Single crystals were coated with a layer of hydrocarbon oil and attached onto a glass fiber. Crystallographic data were collected on a Bruker Nonius KappaCCD diffractometer with $Mo_{K\alpha}$ radiation (graphite monochromator, $\lambda = 0.71073$ Å) at 100 K. Crystallographic programs used for structure solution and refinement were from SHELX-97.[52] The structures were solved by direct methods and were refined by using full-matrix least-squares on F^2 of all unique reflections with anisotropic thermal parameters for all non-hydrogen atoms. All hydrogen atoms were refined isotropically for compound **7**. For compounds **1**, **3**, **4**, **5**, and **6** only the hydrogen atoms that were bonded onto the carborane unit were refined isotropically; the other hydrogen atoms were refined by using a riding model with $U(H) = 1.5\ U_{eq}$ for the CH_3 groups and $U(H) = 1.2\ U_{eq}$ for all others. For compound **2**, all hydrogen atoms were refined by using this riding model. Crystallographic data for the compounds are listed in Table 6.

CCDC-847427 (**1**), CCDC-847428 (**2**), CCDC-847429 (**3**), CCDC-847430 (**4**), CCDC-847431 (**5**), CCDC-847432 (**6**), and CCDC-847433 (**7**) contain the supplementary crystallographic data for this paper. These data can be obtained free of charge from The Cambridge Crystallographic Data Centre via www.ccdc.cam.ac.uk/data_request/cif.

Table 6. Crystallographic data for compounds **1–7**.

	1	**2**	**3**	**4**	**5**	**6**	**7**
formula	$C_{12}H_{25}B_{11}N_2$	$C_{13}H_{27}B_{11}N_2$	$C_{18}H_{29}B_{11}N_2$	$C_{16}H_{33}B_{11}N_2$	$C_{15}H_{33}B_{11}N_2Si$	$C_{20}H_{25}B_{11}N_2$	$C_{21}H_{27}B_{11}N_2$
M_w [g mol^{-1}]	316.25	330.28	392.34	372.35	388.43	412.33	426.36
crystal size [mm]	0.30×0.28×0.28	0.30×0.30×0.30	0.30×0.28×0.16	0.30×0.30×0.29	0.30×0.28×0.27	0.30×0.26×0.16	0.30×0.25×0.20
crystal system	orthorhombic	monoclinic	triclinic	monoclinic	monoclinic	monoclinic	monoclinic
space group	$Pca2_1$	Pn	$P\bar{1}$	$P2_1/c$	$P2_1/c$	$P2_1/n$	$P2_1/n$
a [Å]	26.3835(5)	9.3142(2)	10.4270(2)	14.6080(2)	14.6374(2)	11.3961(2)	14.3383(2)
b [Å]	7.19710(10)	19.7814(4)	14.6024(3)	9.21000(10)	9.42080(10)	10.7376(2)	10.6987(2)
c [Å]	9.58160(10)	11.0017(2)	22.8426(5)	16.6760(2)	16.7015(2)	19.5214(3)	15.7020(3)
α [°]	90	90	81.6179(8)	90	90	90	90
β [°]	90	103.5866(12)	82.7703(8)	106.3550(6)	104.8075(7)	101.8520(12)	94.3399(11)
γ [°]	90	90	77.0942(8)	90	90	90	90
V [Å^3]	1819.40(5)	1970.32(7)	3338.19(12)	2152.80(5)	2226.58(5)	2337.84(7)	2401.80(7)
Z	4	4	6	4	4	4	4
ρ_{calcd} [g cm^{-3}]	1.155	1.113	1.171	1.149	1.159	1.171	1.179
μ [mm^{-1}]	0.058	0.056	0.061	0.059	0.110	0.061	0.062
F (000)	664	696	1236	792	824	856	888
θ [°]	2.93–30.00	3.05–27.48	2.92–27.46	3.11–30.00	3.31–30.00	2.98–27.48	3.22–27.49
total reflns	24242	46318	47371	89562	60126	47513	53292
unique reflns	2794	4497	15220	6211	6482	5347	5513
R (int)	0.029	0.045	0.049	0.043	0.031	0.048	0.05
reflns observed [$I>2\sigma(I)$]	2711	3719	11904	5275	5678	4438	4389
parameters	272	475	964	317	307	342	415
GOF	1.014	1.028	1.035	1.019	1.047	1.030	1.038
R_F [$I>2\sigma(I)$]	0.0280	0.0391	0.0534	0.0441	0.0342	0.0546	0.0409
wR_{F2} (all data)	0.0762	0.1114	0.1606	0.1195	0.0990	0.1397	0.1098
$\Delta\rho_{max/min}$ [e Å^{-3}]	0.213/−0.178	0.183/−0.153	0.863/−0.392	0.352/−0.267	0.383/−0.220	0.516/−0.537	0.240/−0.240

[1] a) C. D. Entwistle, T. B. Marder, *Angew. Chem.* **2002**, *114*, 3051–3056; *Angew. Chem. Int. Ed.* **2002**, *41*, 2927–2931; b) C. D. Entwistle, T. B. Marder, *Chem. Mater.* **2004**, *16*, 4574–4585; c) S. Yamaguchi, A. Wakamiya, *Pure Appl. Chem.* **2006**, *78*, 1413–1424; d) F. Jäkle, *Coord. Chem. Rev.* **2006**, *250*, 1107–1121.

[2] a) Z. Yuan, N. J. Taylor, T. B. Marder, I. D. Williams, S. K. Kurtz, L.-T. Cheng, *J. Chem. Soc. Chem. Commun.* **1990**, 1489–1492; b) Z. Yuan, N. J. Taylor, T. B. Marder, I. D. Williams, S. K. Kurtz, L.-T. Cheng, *Organic Materials for Non-linear Optics II*, ed. R. A. Hann, D. Bloor, RSC, Cambridge, **1991**, p. 190; c) M. Lequan, R. M. Lequan, K. Chane-Ching, *J. Mater. Chem.* **1991**, *1*, 997–999; d) M. Lequan, R. M. Lequan, K. Chane-Ching, M. Barzoukas, A. Fort, H. Lahouche, G. Bravic, D. Chasseau, J. Gaultier, *J. Mater. Chem.* **1992**, *2*, 719–725; e) M. Lequan, R. M. Lequan, K. Chane-Ching, A.-C. Callier, M. Barzoukas, A. Fort, *Adv. Mater. Opt. Electron.* **1992**, *1*, 243–248; f) Z. Yuan, N. J. Taylor, Y. Sun, T. B. Marder, I. D. Williams, L.-T. Cheng, *J. Organomet. Chem.* **1993**, *449*, 27–37; g) C. Branger, M. Lequan, R. M. Lequan, M. Barzoukas, A. Fort, *J. Mater. Chem.* **1996**, *6*, 555–558; h) Z. Yuan, N. J. Taylor, R. Ramachandran, T. B. Marder, *Appl. Organomet. Chem.* **1996**, *10*, 305–316; i) Z. Yuan, J. C. Collings, N. J. Taylor, T. B. Marder, C. Jardin, J.-F. Halet, *J. Solid State Chem.* **2000**, *154*, 5–12; j) Y. Liu, X. Xu, F. Zheng, Y. Cui, *Angew. Chem.* **2008**, *120*, 4614–4617; *Angew. Chem. Int. Ed.* **2008**, *47*, 4538–4541.

[3] Z. Yuan, C. D. Entwistle, J. C. Collings, D. Albesa-Jové, A. S. Batsanov, J. A. K. Howard, H. M. Kaiser, D. E. Kaufmann, S.-Y. Poon, W.-Y. Wong, C. Jardin, S. Fatallah, A. Boucekkine, J.-F. Halet, T. B. Marder, *Chem. Eur. J.* **2006**, *12*, 2758–2777.

[4] a) Z.-Q. Liu, Q. Fang, D. Wang, G. Xue, W.-T. Yu, Z.-S. Shao, M.-H. Jiang, *Chem. Commun.* **2002**, 2900–2901; b) Z.-Q. Liu, Q. Fang, D. Wang, D.-X. Cao, G. Xue, W.-T. Yu, H. Lei, *Chem. Eur. J.* **2003**, *9*, 5074–5084; c) D.-X. Cao, Z.-Q. Liu, Q. Fang, G.-B. Xu, G. Xue, G.-Q. Liu, W.-T. Yu, *J. Organomet. Chem.* **2004**, *689*, 2201–2206; d) Z.-Q. Liu, Q. Fang, D.-X. Cao, D. Wang, G.-B. Xu, *Org. Lett.* **2004**, *6*, 2933–2936; e) Z.-Q. Liu, M. Shi, F.-Y. Li, Q. Fang, Z.-H. Chen, T. Yi, C.-H. Huang, *Org. Lett.* **2005**, *7*, 5481–5484; f) M. Charlot, L. Porrès, C. D. Entwistle, A. Beeby, T. B. Marder, M. Blanchard-Desce, *Phys. Chem. Chem. Phys.* **2005**, *7*, 600–606; g) L. Porrès, M. Charlot, C. D. Entwistle, A. Beeby, T. B. Marder, M. Blanchard-Desce, *Proc. SPIE-Int. Soc. Opt. Eng.* **2005**, *92*, 5934–5936; h) D.-X. Cao, Z.-Q. Liu, G.-Z. Li, G.-Q. Liu, G.-H. Zhang, *J. Mol. Struct.* **2008**, *874*, 46–50; i) J. C. Collings, S.-Y. Poon, C. Le Droumaguet, M. Charlot, C. Katan, L.-O. Pålsson, A. Beeby, J. A. Mosely, H. M. Kaiser, D. Kaufmann, W.-Y. Wong, M. Blanchard-Desce, T. B. Marder, *Chem. Eur. J.* **2009**, *15*, 198–208.

[5] a) T. Noda, Y. Shirota, *J. Am. Chem. Soc.* **1998**, *120*, 9714–9715; b) T. Noda, H. Ogawa, Y. Shirota, *Adv. Mater.* **1999**, *11*, 283–285; c) T. Noda, Y. Shirota, *J. Lumin.* **2000**, *87–89*, 1168–1170; d) Y. Shirota, M. Kinoshita, T. Noda, K. Okumuto, T. Ohara, *J. Am. Chem. Soc.* **2000**, *122*, 11021–11022; e) M. Kinoshita, N. Fujii, T. Tsukaki, Y. Shirota, *Synth. Met.* **2001**, *121*, 1571–1572; f) H. Doi, M. Kinoshita, K. Okumoto, Y. Shirota, *Chem. Mater.* **2003**, *15*, 1080–1089; g) W.-L. Jia, D.-R. Bai, T. McCormick, Q.-D. Liu, M. Motala, R.-Y. Wang, C. Seward, Y. Tao, S. Wang, *Chem. Eur. J.* **2004**, *10*, 994–1006; h) W.-L. Jia, D. Feng, D.-R. Bai, Z. H. Lu, S. Wang, G. Vamvounis, *Chem. Mater.* **2005**, *17*, 164–170; i) W.-L. Jia, M. J. Moran, Y.-Y. Yuan, Z. H. Lu, S. Wang, *J. Mater. Chem.* **2005**, *15*, 3326–3333; j) M. Mazzeo, V. Vitale, F. Della Sala, M. Anni, G. Barbarella, L. Favaretto, G. Sotgui, R. Cingolani, G. Gigli, *Adv. Mater.* **2005**, *17*, 34–39; k) W.-Y. Wong, S.-Y. Poon, M.-F. Lin, W.-K. Wong, *Aust. J. Chem.* **2007**, *60*, 915–922; l) G.-J. Zhou, C.-L. Ho, W.-Y. Wong, Q. Wang, D.-G. Ma, L.-X. Wang, Z.-Y. Lin, T. B. Marder, A. Beeby, *Adv. Funct. Mater.* **2008**, *18*, 499–511.

[6] a) S. Yamaguchi, S. Akiyama, K. Tamao, *J. Am. Chem. Soc.* **2001**, *123*, 11372–11375; b) S. Yamaguchi, T. Shirasaka, S. Akiyama, K. Tamao, *J. Am. Chem. Soc.* **2002**, *124*, 8816–8817; c) Y. Kubo, M. Yamamoto, M. Ikeda, M. Takeuchi, S. Shinkai, S. Yamaguchi, *Angew. Chem.* **2003**, *115*, 2082–2086; *Angew. Chem. Int. Ed.* **2003**, *42*, 2036–2040; d) S. Solé, F. P. Gabbaï, *Chem. Commun.* **2004**, 1284–1285; e) M. Melaïmi, F. P. Gabbaï, *J. Am. Chem. Soc.* **2005**, *127*, 9680–9681; f) A. Sundararaman, M. Victor, R. Varughese, F. Jäkle, *J. Am. Chem. Soc.* **2005**, *127*, 13748–13749; g) T. W. Hundall, M. Melaïmi, F. P. Gabbaï, *Org. Lett.* **2006**, *8*, 2747–2749; h) K. Parab, K. Venkatasubbaiah, F. Jäkle, *J. Am. Chem. Soc.* **2006**, *128*, 12879–12885; i) C.-W. Chiu, F. P. Gabbaï, *J. Am. Chem. Soc.* **2006**, *128*, 14248–

14249; j) X.-Y. Liu, D.-R. Bai, S. Wang, *Angew. Chem.* **2006**, *118*, 5601–5604; *Angew. Chem. Int. Ed.* **2006**, *45*, 5475–5478; k) E. Sakuda, A. Funahashi, N. Kitamura, *Inorg. Chem.* **2006**, *45*, 10670–10677; l) D.-R. Bai, X.-Y. Liu, S. Wang, *Chem. Eur. J.* **2007**, *13*, 5713–5723; m) S.-B. Zhao, T. McCormick, S. Wang, *Inorg. Chem.* **2007**, *46*, 10965–10967; n) T. W. Hundall, F. P. Gabbaï, *J. Am. Chem. Soc.* **2007**, *129*, 11978–11986; o) M. H. Lee, T. Agou, J. Kobayashi, T. Kawashima, F. P. Gabbaï, *Chem. Commun.* **2007**, 1133–1135; p) M.-S. Yuan, Z.-Q. Liu, Q. Fang, *J. Org. Chem.* **2007**, *72*, 7915–7922; q) Y. Kim, F. P. Gabbaï, *J. Am. Chem. Soc.* **2009**, *131*, 3363–3369.

[7] Y. Kim, H.-S. Huh, M. H. Lee, I. L. Lenov, H. Zhao, F. P. Gabbaï, *Chem. Eur. J.* **2011**, *17*, 2057–2062.

[8] a) C.-H. Zhao, A. Wakamiya, Y. Inukai, S. Yamaguchi, *J. Am. Chem. Soc.* **2006**, *128*, 15934–15935; b) A. Wakamiya, K. Mori, S. Yamaguchi, *Angew. Chem.* **2007**, *119*, 4351–4354; *Angew. Chem. Int. Ed.* **2007**, *46*, 4273–4276; c) H. Li, K. Sundararaman, K. Venkatasubbaiah, F. Jäkle, *J. Am. Chem. Soc.* **2007**, *129*, 5792–5793; d) M. Elbing, G. C. Bazan, *Angew. Chem.* **2008**, *120*, 846–850; *Angew. Chem. Int. Ed.* **2008**, *47*, 834–838.

[9] M. E. Glogowski, J. L. R. Williams, *J. Organomet. Chem.* **1981**, *218*, 137–146.

[10] A. Schulz, W. Kaim, *Chem. Ber* **1989**, *122*, 1863–1868.

[11] a) L. Weber, *Coord. Chem. Rev.* **2001**, *215*, 39–77; b) L. Weber, *Coord. Chem. Rev.* **2008**, *252*, 1–31.

[12] a) M. Yamashita, K. Nozaki, *J. Synth. Org. Chem. Jpn.* **2010**, *68*, 359–369; b) M. Yamashita, K. Nozaki, *Pure Appl. Chem.* **2008**, *80*, 1187–1194; c) M. Yamashita, K. Nozaki, *Bull. Chem. Soc. Jpn.* **2008**, *81*, 1377–1392.

[13] L. Weber, H. B. Wartig, H.-G. Stammler, B. Neumann, *Organometallics* **2001**, *20*, 5248–5250.

[14] L. Weber, H. B. Wartig, H.-G. Stammler, B. Neumann, *Z. Anorg. Allg. Chem.* **2001**, *627*, 2663–2668.

[15] For selected examples of 1,3,2-diazaboroles, see a) T. Habereder, H. Nöth, *Appl. Organomet. Chem.* **2003**, *17*, 525–538; b) L. Weber, I. Domke, J. Kahlert, H.-G. Stammler, *Eur. J. Inorg. Chem.* **2006**, 3419–3424; c) L. Weber, A. Rausch, H.-G. Stammler, B. Neumann, *Z. Anorg. Allg. Chem.* **2004**, *630*, 2657–2664; d) L. Weber, J. Förster, H.-G. Stammler, B. Neumann, *Eur. J. Inorg. Chem.* **2006**, 5048–5056; e) L. Weber, M. Schnieder, T. C. Maciel, H. B. Wartig, M. Schimmel, R. Boese, D. Bläser, *Organometallics* **2000**, *19*, 5791–5794; f) J. M. Murphy, J. D. Lawrence, K. Kawamura, C. Incarvito, J. F. Hartwig, *J. Am. Chem. Soc.* **2006**, *128*, 13684–13685; g) T. B. Marder, *Science* **2006**, *314*, 69–70; h) Y. Segawa, M. Yamashita, K. Nozaki, *Science* **2006**, *314*, 113–115; i) Y. Segawa, M. Yamashita, K. Nozaki, *Angew. Chem.* **2007**, *119*, 6830–6833; *Angew. Chem. Int. Ed.* **2007**, *46*, 6710–6713; j) T. Kajiwara, T. Terabayashi, M. Yamashita, K. Nozaki, *Angew. Chem.* **2008**, *120*, 6708–6712; *Angew. Chem. Int. Ed.* **2008**, *47*, 6606–6610; k) Y. Segawa, Y. Suzuki, M. Yamashita, K. Nozaki, *J. Am. Chem. Soc.* **2008**, *130*, 16069–16079; l) M. Yamashita, Y. Suzuki, Y. Segawa, K. Nozaki, *Chem. Lett.* **2008**, *37*, 802–803; m) T. Terabayashi, T. Kajiwara, M. Yamashita, K. Nozaki, *J. Am. Chem. Soc.* **2009**, *131*, 14162–14163; n) A. Hinchliffe, F. S. Mair, E. J. L. Mc Innes, R. G. Pritchard, J. E. Warren, *Dalton Trans.* **2008**, 222–233; o) E. Giziroglu, B. Donnadieu, G. Bertrand, *Inorg. Chem.* **2008**, *47*, 9751–9753; p) A. Chrostowska, M. Maciejczyk, A. Dargelos, P. Baylere, L. Weber, V. Werner, D. Eickhoff, H.-G. Stammler, B. Neumann, *Organometallics* **2010**, *29*, 5192–5198; q) L. Weber, I. Domke, W. Greschner, K. Miqueu, A. Chrostowska, P. Baylère, *Organometallics* **2005**, *24*, 5455–5463.

[16] S. Maruyama, Y. Kawanishi, *J. Mater. Chem.* **2002**, *12*, 2245–2249.

[17] Y. Kubo, K. Tsuruzoe, S. Okuyama, R. Nishiyabu, T. Fujihara, *Chem. Commun.* **2010**, *46*, 3604–3606.

[18] L. Weber, I. Domke, C. Schmidt, T. Braun, H.-G. Stammler, B. Neumann, *Dalton Trans.* **2006**, 2127–2132.

[19] L. Weber, A. Penner, I. Domke, H.-G. Stammler, B. Neumann, *Z. Anorg. Allg. Chem.* **2007**, *633*, 563–569.

[20] L. Weber, V. Werner, I. Domke, H.-G. Stammler, B. Neumann, *Dalton Trans.* **2006**, 3777–3784.

[21] L. Weber, V. Werner, M. A. Fox, T. B. Marder, S. Schwedler, A. Brockhinke, H.-G. Stammler, B. Neumann, *Dalton Trans.* **2009**, 1339–1351.

[22] L. Weber, V. Werner, M. A. Fox, T. B. Marder, S. Schwedler, A. Brockhinke, H.-G. Stammler, B. Neumann, *Dalton Trans.* **2009**, 2823–2831.

[23] L. Weber, J. Kahlert, H.-G. Stammler, B. Neumann, *Z. Anorg. Allg. Chem.* **2008**, *634*, 1729–1734.

[24] L. Weber, J. Halama, V. Werner, K. Hanke, L. Böhling, A. Chrostowska, A. Dargelos, M. Maciejczyk, A. L. Raza, H.-G. Stammler, B. Neumann, *Eur. J. Inorg. Chem.* **2010**, 5416–5425.

[25] L. Weber, D. Eickhoff, V. Werner, L. Böhling, S. Schwedler, A. Chrostowska, A. Dargelos, M. Maciejczyk, H.-G. Stammler, B. Neumann, *Dalton Trans.* **2011**, *40*, 4434–4446.

[26] S. Schwedler, D. Eickhoff, R. Brockhinke, D. Cherian, L. Weber, A. Brockhinke, *Phys. Chem. Chem. Phys.* **2011**, *13*, 9301–9310.

[27] L. Weber, J. Halama, L. Böhling, A. Chrostowska, A. Dargelos, H.-G. Stammler, B. Neumann, *Eur. J. Inorg. Chem.* **2011**, 3091–3101.

[28] L. Weber, D. Eickhoff, T. B. Marder, M. A. Fox, P. J. Low, A. D. Dwyer, D. J. Tozer, S. Schwedler, A. Brockhinke, H.-G. Stammler, B. Neumann, *Chem. Eur. J.* **2012**, *18*, 1369–1382.

[29] M. F. Hawthorne, T. E. Berry, P. A. Wegner, *J. Am. Chem. Soc.* **1965**, *87*, 4746–4750.

[30] a) K. Kokado, Y. Chujo, *Macromolecules* **2009**, *42*, 1418–1420; b) J. J. Peterson, M. Werre, Y. C. Simon, E. B. Coughlin, K. R. Carter, *Macromolecules* **2009**, *42*, 8594–8598; c) K. Kokado, Y. Tokoro, Y. Chujo, *Macromolecules* **2009**, *42*, 9238–9242; d) K. Kokado, Y. Chujo, *Polym. J.* **2010**, *42*, 363–367; e) K. Kokado, A. Nagai, Y. Chujo, *Tetrahedron Lett.* **2011**, *52*, 293–296; f) K. Kokado, Y. Chujo, *Dalton Trans.* **2011**, *40*, 1919–1923; g) K. Kokado, Y. Chujo, *J. Org. Chem.* **2011**, *76*, 316–319; h) J. J. Peterson, A. R. Davis, M. Werre, E. B. Coughlin, K. R. Carter, *ACS Appl. Mater. Interfaces* **2011**, *3*, 1796–1799.

[31] A search in the Cambridge structural database (CSD) in July 2011 revealed B–C bond lengths of 1.68–1.79 Å and B–B bond lengths of 1.76–1.82 Å for 544 structurally characterized *ortho*-carboranes.

[32] a) M. G. Davidson, T. G. Hibbert, J. A. K. Howard, A. Mackinnon, K. Wade, *Chem. Commun.* **1996**, 2285–2286; b) A. R. Turner, H. E. Robertson, K. B. Borisenko, D. W. H. Rankin, M. A. Fox, *Dalton Trans.* **2005**, 1310–1318; c) M. J. Hardie, C. L. Raston, *CrystEngComm* **2001**, *3*, 162–164.

[33] a) D. A. Brown, W. Clegg, H. M. Colquhoun, J. A. Daniels, I. R. Stephenson, K. Wade, *J. Chem. Soc. Chem. Commun.* **1987**, 889–891; b) R. Coult, M. A. Fox, W. R. Gill, K. Wade, W. Clegg, *Polyhedron* **1992**, *11*, 2717–2721; c) R. Kivekäs, R. Sillanpää, F. Teixidor, C. Viñas, R. Nuñez, *Acta Crystallogr. Sect. C* **1994**, *50*, 2027–2030; d) R. Kivekäs, R. Sillanpää, F. Teixidor, C. Viñas, R. Nuñez, M. Abad, *Acta Crystallogr. Sect. C* **1995**, *51*, 1864–1868; e) R. Kivekäs, F. Teixidor, C. Viñas, R. Nuñez, *Acta Crystallogr. Sect. C* **1995**, *51*, 1868–1870; f) J. M. Oliva, C. Viñas, *J. Mol. Struct.* **2000**, *556*, 33–42.

[34] a) L. A. Boyd, W. Clegg, R. C. B. Copley, M. G. Davidson, M. A. Fox, T. G. Hibbert, J. A. K. Howard, A. Mackinnon, R. J. Peace, K. Wade, *Dalton Trans.* **2004**, 2786–2799; b) M. A. Fox, J. A. H. MacBride, R. J. Peace, W. Clegg, M. R. J. Elsegood, K. Wade, *Polyhedron* **2009**, *28*, 789–795; c) M. A. Fox, R. J. Peace, W. Clegg, M. R. J. Elsegood, K. Wade, *Polyhedron* **2009**, *28*, 2359–2370.

[35] a) B. W. Hutton, F. MacIntosh, D. Ellis, F. Herisse, S. A. Macgregor, D. McKay, V. Petrie-Armstrong, G. M. Rosair, D. S. Perekalin, H. Tricas, A. J. Welch, *Chem. Commun.* **2008**, 5345–5347; b) R. L. Thomas, A. J. Welch, *Polyhedron* **1999**, *18*, 1961–1968; c) T. D. McGrath, A. J. Welch, *Acta Crystallogr. Sect. C* **1995**, *51*, 654–657.

[36] J. M. Oliva, N. L. Allan, P. v. R. Schleyer, C. Viñas, F. Teixidor, *J. Am. Chem. Soc.* **2005**, *127*, 13538–13547.

[37] M. A. Fox, A. K. Hughes, *Coord. Chem. Rev.* **2004**, *248*, 457–476.

[38] a) R. J. Blanch, M. Williams, G. D. Fallon, M. G. Gardiner, R. Kaddour, C. L. Raston, *Angew. Chem.* **1997**, *109*, 520–522; *Angew. Chem. Int. Ed. Engl.* **1997**, *36*, 504–506; b) M. J. Bayer, A. Herzog, M. Diaz, G. A. Harakas, H. Lee, C. B. Knobler, M. F. Hawthorne,

Chem. Eur. J. **2003**, *9*, 2732–2744; c) M. J. Hardie, C. L. Raston, *Eur. J. Inorg. Chem.* **1999**, 195–200.
[39] a) Z. G. Lewis, A. J. Welch, *Acta Crystallogr. Sect. C* **1939**, *5*, 705–710; b) W. Clegg, R. Coult, M. A. Fox, W. R. Gill, J. A. H. MacBride, K. Wade, *Polyhedron* **1993**, *12*, 2711–2717; c) T. D. McGrath, A. J. Welch, *Acta Crystallogr. Sect. C* **1995**, *51*, 646–649; d) E. S. Alekseyeva, M. A. Fox, J. A. K. Howard, J. A. H. MacBride, K. Wade, *Appl. Organomet. Chem.* **2003**, *17*, 499–508; e) M. Tsuji, *J. Org. Chem.* **2004**, *69*, 4063–4074; f) I. V. Glukhov, M. Y. Antipin, K. A. Lyssenko, *Eur. J. Inorg. Chem.* **2004**, *7*, 1379–1384; g) M. A. Fox, C. Nervi, A. Crivello, A. S. Batsanov, J. A. K. Howard, K. Wade, P. J. Low, *J. Solid State Electrochem.* **2009**, *13*, 1483–1495; h) I. V. Glukhov, K. A. Lyssenko, A. A. Korlyukov, M. Y. Antipin, *Russ. Chem. Bull.* **2005**, *54*, 547–559.
[40] J. C. de Mello, H. F. Wittmann, R. H. Friend, *Adv. Mater.* **1997**, *9*, 230–232.
[41] Y. Hong, J. W. Y. Lam, B. Z. Tang, *Chem. Soc. Rev.* **2011**, *40*, 5361–5388.
[42] L. I. Zakharkin, V. I. Bregadze, O. Y. Okhlobystin, *J. Organomet. Chem.* **1966**, *6*, 228–234.
[43] M. Tsuji, *J. Org. Chem.* **2003**, *68*, 9589–9597.
[44] Gaussian 09, Revision A.02, M. J. Frisch, G. W. Trucks, H. B. Schlegel, G. E. Scuseria, M. A. Robb, J. R. Cheeseman, G. Scalmani, V. Barone, B. Mennucci, G. A. Petersson, H. Nakatsuji, M. Caricato, X. Li, H. P. Hratchian, A. F. Izmaylov, J. Bloino, G. Zheng, J. L. Sonnenberg, M. Hada, M. Ehara, K. Toyota, R. Fukuda, J. Hasegawa, M. Ishida, T. Nakajima, Y. Honda, O. Kitao, H. Nakai, T. Vreven, Jr., J. A. Montgomery, J. E. Peralta, F. Ogliaro, M. Bearpark, J. J. Heyd, E. Brothers, K. N. Kudin, V. N. Staroverov, R. Kobayashi, J. Normand, K. Raghavachari, A. Rendell, J. C. Burant, S. S. Iyengar, J. Tomasi, M. Cossi, N. Rega, J. M. Millam, M. Klene, J. E. Knox, J. B. Cross, V. Bakken, C. Adamo, J. Jaramillo, R. Gomperts, R. E. Stratmann, O. Yazyev, A. J. Austin, R. Cammi, C. Pomelli, J. W. Ochterski, R. L. Martin, K. Morokuma, V. G. Zakrzewski, G. A. Voth, P. Salvador, J. J. Dannenberg, S. Dapprich, A. D. Daniels, O. Farkas, J. B. Foresman, J. V. Ortiz, J. Cioslowski, D. J. Fox, Gaussian, Inc., Wallingford CT, **2009**.
[45] a) A. D. Becke, *J. Chem. Phys.* **1993**, *98*, 5648–5652; b) C. Lee, W. Yang, R. G. Parr, *Phys. Rev. B* **1988**, *37*, 785–789.
[46] a) G. A. Petersson, M. A. Al-Laham, *J. Chem. Phys.* **1991**, *94*, 6081–6090; b) G. A. Petersson, A. Bennett, T. G. Tensfeldt, M. A. Al-Laham, W. A. Shirley, J. Mantzaris, *J. Chem. Phys.* **1988**, *89*, 2193–2218.
[47] A. R. Allouche, *J. Comput. Chem.* **2011**, *32*, 174–182.
[48] N. M. O'Boyle, A. L. Tenderholt, K. M. Langner, *J. Comput. Chem.* **2008**, *29*, 839–845.
[49] a) R. Ditchfield, *Mol. Phys.* **1974**, *27*, 789–807; b) C. M. Rohling, L. C. Allen, R. Ditchfield, *Chem. Phys.* **1984**, *87*, 9–15; c) K. Wolinski, J. F. Hinton, P. Pulay, *J. Am. Chem. Soc.* **1990**, *112*, 8251–8260.
[50] a) M. Bühl, P. v. R. Schleyer, *J. Am. Chem. Soc.* **1992**, *114*, 477–491; b) P. v. R. Schleyer, J. Gauss, M. Bühl, R. Greatrex, M. A. Fox, *J. Chem. Soc. Chem. Commun.* **1993**, 1766–1768; c) C. E. Willans, C. A. Kilner, M. A. Fox, *Chem. Eur. J.* **2010**, *16*, 10644–10648.
[51] T. Yanai, D. P. Tew, N. C. Handy, *Chem. Phys. Lett.* **2004**, *393*, 51–57.
[52] G. M. Sheldrick, *Acta Crystallogr. Sect. A* **2008**, *64*, 112–122.

Received: February 6, 2012
Published online: May 23, 2012

Dalton Transactions

RSC Publishing

PAPER

View Article Online
View Journal

Electrochemical and spectroelectrochemical studies of C-benzodiazaborolyl-*ortho*-carboranes†

Cite this: DOI: 10.1039/c2dt32378h

Lothar Weber,*[a] Jan Kahlert,[a] Lena Böhling,[a] Andreas Brockhinke,[a] Hans-Georg Stammler,[a] Beate Neumann,[a] Rachel A. Harder,[b] Paul J. Low[b] and Mark A. Fox*[b]

Received 8th October 2012,
Accepted 13th November 2012

DOI: 10.1039/c2dt32378h

www.rsc.org/dalton

Fifteen C-diazaborolyl-*ortho*-carboranes, 1-R′-2-R′′-1,2-$C_2B_{10}H_{10}$, where R′ represents the groups 2-(1,3-Et_2-1,3,2-$N_2BC_6H_4$)-, 2-(1,3-Ph_2-1,3,2-$N_2BC_6H_4$)-, 2-(1,3-Ph_2-5,6-Me_2-1,3,2-$N_2BC_6H_2$)-, 2-(1,3-$^{i}Pr_2$-1,3,2-$N_2BC_6H_4$)-, and 2-(1,3,2-$N_2BC_6H_6$)- and where R′′ is H, Me, Ph, ^{t}Bu or $SiMe_3$, were synthesized. Cyclic voltammetry studies of the compounds showed irreversible oxidation waves which are caused by the oxidation of the heterocycle. Those C-diazaborolyl-*ortho*-carboranes with Ph, *t*Bu and $SiMe_3$ substituents at the adjacent C-atom of the cage displayed two one-electron reduction waves reflecting the formation of stable radical monoanions with unusual (2*n* + 3) skeletal electron counts. The geometries of these anions were determined by combinations of infrared, UV-visible spectroelectrochemical and computational studies. Additionally the structures of seven new C-diazaborolyl-*ortho*-carboranes and one new 2-bromo-1,3,2-benzodiazaborole were determined by X-ray crystallography and compared with previously obtained structures.

Introduction

Although numerous carborane clusters have been known for fifty years,[1,2] efforts to understand their unique electronic properties are still continuing. The most widely studied carborane 1,2-$C_2B_{10}H_{12}$, *ortho*-carborane, displays a rich chemistry.[1] Because of the electron deficient character of this icosahedral cage its C–H bonds are activated and thus prone to deprotonation and substitution processes.

As a *closo*-cluster, 1,2-$C_2B_{10}H_{12}$ possesses 26 skeletal electrons, or 2*n* + 2 skeletal electrons according to Wade's electron-counting rules (*n* = number of cluster atoms).[3] This molecule readily accommodates two additional electrons to form a dianion with 28 skeletal electrons (2*n* + 4) and a more open *nido*-structure.[4] Electrochemical studies on the parent *ortho*-carborane revealed an irreversible two-electron reduction which is rationalized by a facile CH-cleavage and the subsequent reaction of the transient anion $C_2B_{10}H_{11}^-$ with a second molecule of 1,2-$C_2B_{10}H_{12}$ to afford the two-cage anion [*closo*-$C_2B_{10}H_{11}$–*nido*-$C_2B_{10}H_{12}$]$^-$.[5,6]

Logically, *ortho*-carboranes with two substituents at the adjacent C-atoms should be electrochemically more robust. Cyclovoltammetric investigations on the 1,2-diphenyl-derivative showed two one-electron reduction waves which are taken as evidence for the occurrence of a stable radical anion.[7] More recently, the geometry of the radical anion was elucidated by means of IR- and UV-spectroelectrochemical, ESR and computational methods (Scheme 1).[8]

According to computations, the additional electron is located at the cage atoms giving rise to an elongated C–C distance of 2.39 Å in comparison to the neutral precursor (1.76 Å). With regard to the many *closo*- and *nido*-carboranes, carborane-based radical anions featuring a 2*n* + 3 electron count are somewhat rare.[8–13] In a more recent report on the photophysics of *ortho*-carboranes with donating arylcarbazolyl substituents it was suggested that the species in their excited

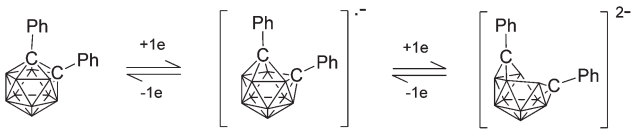

Scheme 1 Two one-electron reductions for 1,2-diphenyl-*ortho*-carborane.

[a]*Fakultät für Chemie der Universität Bielefeld, 33615 Bielefeld, Germany. E-mail: lothar.weber@uni-bielefeld.de*
[b]*Department of Chemistry, Durham University, Durham DH1 3LE, UK. E-mail: m.a.fox@durham.ac.uk*

†Electronic supplementary information (ESI) available: Synthetic procedures and characterisation data for **8**, **9**, **11–15**, **18–21**, **27**, **30** and **31**, figures of NMR spectra for **8–15**, crystallographic data and additional structural data, additional photophysical data including absorption and emission spectra for **8–15**, additional computed structural data, simulated IR spectra for **3–5**. CCDC 894654 (**8**), 894655 (**9**), 894656 (**10**), 894657 (**11**), 894658 (**12**), 894659 (**13**), 894660 (**15**) and 894661 (**19**). For ESI and crystallographic data in CIF or other electronic format see DOI: 10.1039/c2dt32378h

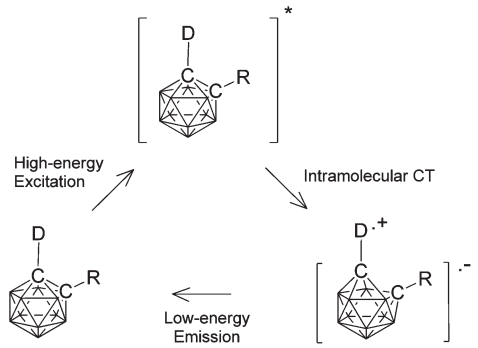

Scheme 2 Excited state geometries for *ortho*-carboranes proposed to explain low-energy emissions observed experimentally. D represents a donor group.

states consist of carbazolyl radical cations and radical cluster anions. This assumption was based on absorption spectroscopy where a transient band at 415 nm with a similar spectral profile to the corresponding radical anion was observed (Scheme 2).[13] There are many reports of unusual low-energy emissions from 1-mono- and 1,2-di-aryl-*ortho*-carboranes which are explained by charge-transfer between the electron-accepting *ortho*-carborane and the electron-donating aryl groups.[14,15]

We recently reported[16] on the synthesis and photophysical behaviour of a number of *ortho*-carboranes (**1–7**, Chart 1) featuring a 1,3-diethyl- or 1,3-diphenyl-1,3,2-benzodiazaborolyl substituent at one cage carbon atom. Apart from **6**, these compounds show remarkable low-energy fluorescence emissions with Stokes shifts of 15 100–20 260 cm^{-1} and quantum yields up to 65% in the solid state. These low-energy emissions are due to a charge transfer between the electron-accepting cage and the electron-donating benzodiazaborolyl unit.

Here we describe the syntheses, structural, photophysical and computational studies for the eight new C-diazaborolyl-carboranes, **8–15** (Chart 1). More importantly, electrochemical and spectroelectrochemical studies disclose carborane radical anions on reductions of some diazaborolyl-*ortho*-carboranes. This study shows that unusual $2n + 3$ carborane radical anions

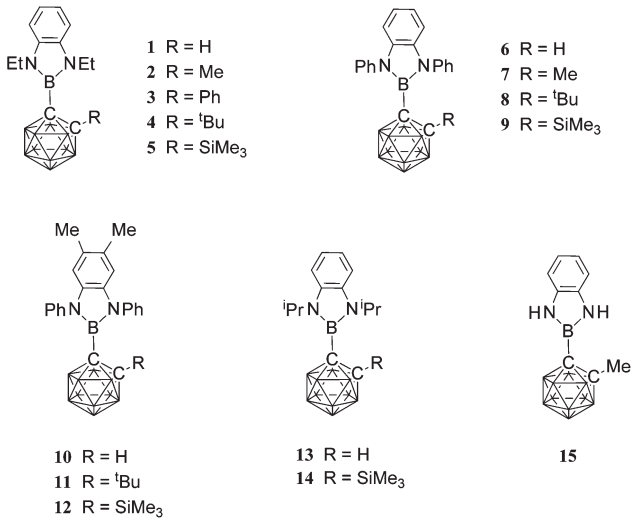

Chart 1

were formed with bulky *tert*-butyl and trimethylsilyl substituents in addition to aryl groups at the adjacent cage carbon.

Syntheses

In our group the 2-bromo-1,3,2-benzodiazaborole 2-Br-1,3-Et_2-1,3,2-$N_2BC_6H_4$ [17] has been frequently used as a precursor for many fluorescent benzodiazaboroles[18–22] including carboranes **1–5** (Chart 1). Analogously, 2-Br-1,3-Ph_2-1,3,2-$N_2BC_6H_4$ (**16**)[19] (Scheme 3) was utilized as a starting material for benzodiazaborole dyes such as **6** and **7**.[16] The protocol for **16** was extended for the preparation of the novel compounds **17–19** having phenyl or mesityl rings at the N-atoms and hydrogen or methyl substituents at the six-membered ring (Scheme 3).

Surprisingly the corresponding reaction of **28**, featuring two *N-tert*-butyl groups, with BBr_3 failed. The $^{11}B\{^1H\}$ NMR spectrum of the reaction mixture was characterized by a broad hump at 25 ppm and a less intense signal at 22 ppm which

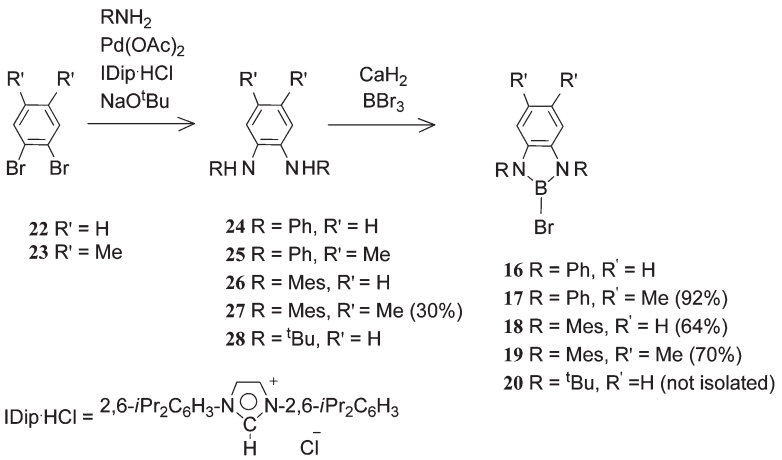

Scheme 3 Syntheses of bromodiazaboroles from 1,2-dibromobenzenes (yields of new compounds in parentheses).

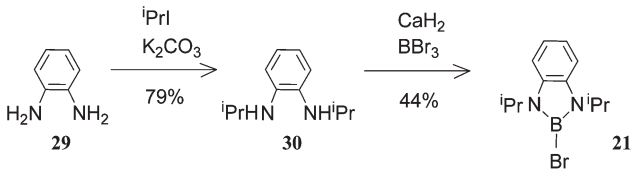

Scheme 4 Synthesis of bromoborole **21**.

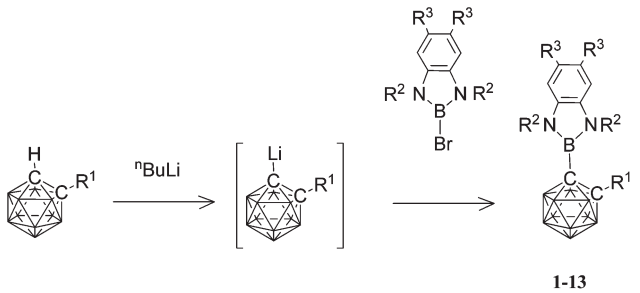

Scheme 5 General route to C-monodiazaborolyl-*ortho*-carboranes, **1–13**.

were presumably due to oligomeric triaminoboranes and 2-bromobenzodiazaboroles (including **20**), respectively. The known cyclic B_3N_3 trimer $(C_6H_4NHBN)_3$ [23] was identified in the reaction mixture by mass spectroscopy.

The synthesis of 2-bromo-1,3-di-*iso*-propylbenzodiazaborole (**21**)[24] required the *N*,*N*′-di-*iso*-propylphenylene diamine (**30**), which, deviating from the literature, was obtained by a facile multigram procedure from 1,2-phenylene diamine (**29**) and 2-iodopropane in the presence of K_2CO_3 (79% yield, Scheme 4).

The standard protocol for C-monodiazaborolyl carboranes is based on the treatment of the lithiated carborane with bromodiazaboroles as depicted in Scheme 5. Thus, the reactions of bromodiazaboroles **16**, **17** and **21** with the corresponding lithiated carborane afforded the carboranes **8–13**.

Attempts to form C-diazaborolylcarboranes with the bromodiazaboroles **18** and **19** containing bulky mesityl groups were not successful. The trimethylsilylcarborane **14** was obtained from lithiation of **13** followed by addition of Me_3SiCl.

Due to the failure of the synthesis of 2-bromobenzodiazaborole **20** a protocol according to Scheme 5 for a C-diazaborolyl carborane with two bulky *tert*-butyl groups at the N-atoms had to be discarded. Thus an alternative route *via* a base assisted cyclocondensation of phenylene diamine **28** with 1-dibromo-2-methyl-*ortho*-carborane **31** was envisaged. Compound **31** resulted from the metalation of 1-methyl-*ortho*-carborane by *n*-butyllithium in toluene and the subsequent addition of BBr_3 to the lithio-carborane at −90 °C. The low temperature during the addition of BBr_3 was crucial to avoid an intractable product mixture. Short path distillation afforded pure **31** as a colourless oil in 67% yield. For further transformations this material was, however, employed *in situ*. Thus, the reaction with **28** afforded diazaborolyl carborane **15** in 25% isolated yield. Obviously the *tert*-butyl groups were liberated

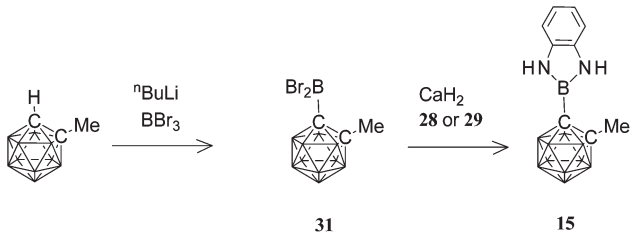

Scheme 6 Synthesis of carborane **15** *via* the dibromoboryl-*ortho*-carborane **31**.

during the cyclocondensation. In keeping with this the yield of **15** can be improved to 46% by reacting **31** with 1,2-phenylene diamine **29** (Scheme 6).

^1H, ^{11}B and ^{13}C NMR spectra for all new carboranes **8–15** are depicted in Fig. S1–S24.† Of interest are the two distinct methyl group resonances observed in the ^1H and ^{13}C NMR spectra of compound **14**, pointing to a restricted rotation of the ^{i}Pr groups due to the silyl group. Similarly, two sets of ^1H and ^{13}C NMR signals for the *ortho*-positions in the *N*-phenyl rings in **8**, **9**, **11** and **12** are indicative of the hindered rotations of the diazaborolyl group and the phenyl groups.

X-ray crystallography

Molecular structures were determined for the 1-diazaborolyl-*ortho*-carboranes, **8–13** and **15** (Fig. 1). Table 1 lists selected bonding parameters for these compounds in comparison to the data previously reported[16] for **1–7** including the torsion angles C2–C1–B2–N3 (ψ) and the aryl–borolyl interplanar angles (ω) as shown in Fig. 2. The carborane C1–C2 bond length increases with more steric bulk of the substituent at C2, in the series **1–13** going from 1.656(1)–1.670(1) Å for H, 1.684(2)–1.686(2) Å for Me, 1.707(2)–1.719(2) Å for $SiMe_3$ and 1.701(2)–1.730(2) Å for Ph to 1.738(3)–1.756(1) Å for ^{t}Bu. Compound **15** with a methyl substituent at C2 has a shorter C1–C2 bond (1.669(1) Å) than the similar carboranes **2** and **7** due to the

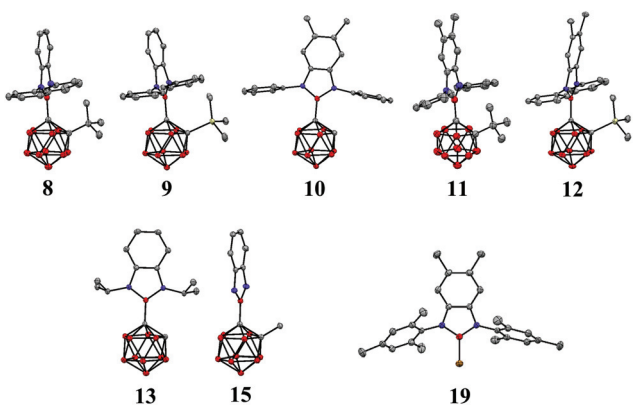

Fig. 1 Molecular structures of compounds **8–13**, **15** and **19**. All hydrogen atoms are omitted for clarity.

Table 1 Selected bond lengths and angles of 1-benzodiazaborolyl-*ortho*-carboranes **1–13** and **15**

	Substituents[a]			Bond lengths [Å]		Angles [°]	
	R^1	R^2	R^3	C1–B2	C1–C2	ψ	ω
1	H	Et	H	1.594(2)	1.670(1)	92.4	—
2	Me	Et	H	1.605(3)	1.684(2)	88.8	—
				1.600(3)	1.687(2)	89.8	
3	Ph	Et	H	1.600(2)	1.730(2)	89.3	—
				1.600(2)	1.720(2)	86.6	
				1.609(2)	1.701(2)	67.5	
4	^{t}Bu	Et	H	1.606(1)	1.756(1)	89.6	—
5	$SiMe_3$	Et	H	1.605(1)	1.710(1)	83.7	—
6	H	Ph	H	1.586(2)	1.670(2)	16.6	75.8/76.4
7	Me	Ph	H	1.591(2)	1.686(2)	80.0	72.2/76.5
8	^{t}Bu	Ph	H	1.595(2)	1.750(2)	82.9	77.2/89.0
9	$SiMe_3$	Ph	H	1.595(2)	1.707(2)	79.6	84.0/83.2
10	H	Ph	Me	1.585(2)	1.656(1)	12.2	67.8/80.2
11	^{t}Bu	Ph	Me	1.597(3)	1.743(3)	87.3	83.2/83.8
				1.595(3)	1.738(3)	85.9	84.1/76.1
12	$SiMe_3$	Ph	Me	1.594(2)	1.719(2)	79.2	64.5/77.8
13	H	^{i}Pr	H	1.604(2)	1.664(1)	12.2	—
15	Me	H	H	1.580(1)	1.669(1)	77.7	—

[a] See Scheme 5.

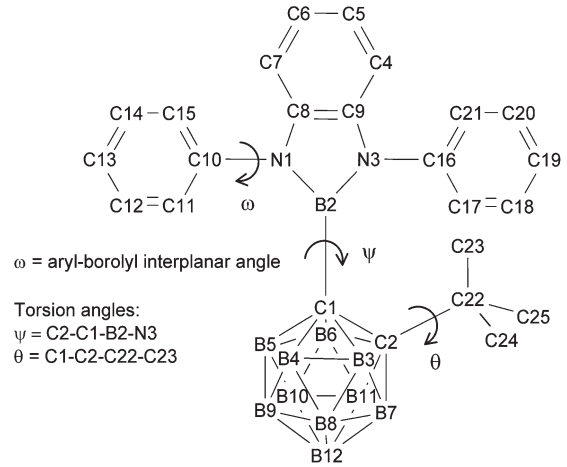

Fig. 2 Atom labelling of 1-(1′,3′-diphenylbenzodiazaborolyl)-2-*tert*-butyl-*ortho*-carborane (**8**) with pertinent torsion angles (ψ, θ) and interplanar angle ω.

lack of substituents at the nitrogen atoms of the diazaborolyl group.

Each of the four compounds **1**, **6**, **10** and **13** has a hydrogen atom attached to C2, which may cause cage disorders in the crystal in the absence of C–H···X interactions.[25] Indeed, there are such C–H···π interactions in **1**, **6** and **10** but not in the di-*iso*-propyl derivative **13**. The latter compound contains two independent molecules in the asymmetric unit, one of which has a disordered cage. The data of the ordered molecule of **13** are listed in Table 1.

In the crystal of compound **4**, the *tert*-butyl group is disordered over two positions with torsion angles C1–C2–C22–C23 (θ, Fig. 2) of 8.9° (conformer **4A** with one methyl group almost co-planar with the C1–C2 bond) and 43.0° (conformer **4B**) with 77 : 23 occupancies.[16] The *tert*-butyl groups in **8** and **11** are not disordered and show torsion angles θ of 17.3° and 21.1°, respectively.

The four independent molecules in the unit cell of bromobenzodiazaborole **19** show mesityl groups which are nearly orthogonally oriented to the plane of the heterocycle with interplanar angles (ω) between 75.2 and 87.5° (Table S1†). These values are similar to the interplanar angles ω observed in the molecular structures for compounds **6–12** as shown in Table 1. The B–Br bond lengths of 1.909(2)–1.915(2) Å in **19** are slightly shorter than the B–Br distance of 1.925(5) Å in the only other structurally characterized bromobenzodiazaborole, 1,4-[1′-(2′-Br-3′-^{i}Pr-1′,3′,2′-$N_2BC_6H_4$)]$_2C_6H_4$.[20]

The bonding parameters within the benzodiazaborole units were similar to those of other previously reported structures.[16,18–21] The carborane C1–borolyl B bond lengths increase from 1.580(1) Å in **15** with NH groups *via* 1.586(2)–1.597(3) Å with NPh substituents to 1.594(2)–1.609(2) Å with *N*-alkyl groups reflecting the increased bulk of the substituents.

Photophysics

Absorption data for the 1-benzodiazaborolyl-*ortho*-carboranes **8–15** in cyclohexane, toluene, chloroform and dichloromethane solutions and also as solids are listed in Table S3† and shown in Fig. S25–S32.† Like for **1–7**,[16] all highest energy absorption maxima were observed in the 288–303 nm region. These absorptions are assigned to local π to π* transitions at the diazaborolyl groups.

Table 2 lists the emission data for **8–15** in cyclohexane and dichloromethane solutions and as solids along with data for **1–7** for comparison. Additional emission data for **8–15** in other solvents are listed in Tables S4–S7† and the respective spectra are shown in Fig. S25–S32.† In cyclohexane solutions, low-energy emissions with maxima between 534 nm (for **7**) and 620 nm (for **14**) were observed for all carboranes except for **6** and **10**. These emissions are assigned to a charge-transfer (CT) from the cluster to the benzodiazaborolyl group. Notably, the emission maxima of 1,3-diphenylbenzodiazaboroles **8** and **9** are blue-shifted by 36–45 nm compared to their 1,3-diethyl- and 5,6-dimethyl-1,3-diphenyl analogues **4**, **5**, **11** and **12**. This underlines that the CT state is better stabilized by the more electron-rich benzodiazaborolyl groups. High-energy emissions between 302 nm and 346 nm were present for **1**, **6**, **7** and **10** and are attributed to local π* to π transitions at the diazaborolyl groups. The quantum yields of the low energy emission (Φ_F) depend on the substituent R^1 (Scheme 5) at carbon C2 of **1–14** with values of 1% or less for R^1 = H, up to 8% for Me, 6% for Ph, 14–45% for $SiMe_3$ and 32–38% for ^{t}Bu. Thus, the new C-diazaborolyl-carboranes confirm the idea that bulky substituents at C2 increase the quantum yields by restriction of intramolecular rotations.

In the more polar solvent dichloromethane, low-energy emissions were detected for all carboranes except **6**, **10** and **15**. The emission maxima in dichloromethane were red-shifted

Table 2 Emission data of **1–15**

	R^1	R^2	R^3	Emission λ_{max} [nm] in cyclohexane	Stokes shift [cm^{-1}] in cyclohexane	Φ_F [%] in cyclohexane	Emission λ_{max} [nm] in DCM	Stokes-shift [cm^{-1}] in DCM	Φ_F[%] in DCM	Emission λ_{max} [nm] in solid state	Stokes shift [cm^{-1}] in solid state	Φ_F[%] in solid state[a]	Transition dipole moment[b] [D]
1	H	Et	H	311, 596	1960, 15 660	<1	720	19 030	<1	561	16 060	51	8.4
2	Me	Et	H	574	16 480	8	692	19 800	3	573	16 520	65	8.1
3	Ph	Et	H	615	18 050	6	757	21 340	1	613	15 100	30	8.3
4	^{t}Bu	Et	H	587	17 420	32	713	20 330	3	611	16 160	42	7.6
5	Me_3Si	Et	H	602	18 090	18	726	20 870	2	631	20 260	30	7.4
6	H	Ph	H	302, 346	1850, 6600	1	417	11 170	<1	—[c]	—	—	—
7	Me	Ph	H	345, 534	5540, 15 880	<1	646	19 200	<1	523	15 340	25	8.0
8	^{t}Bu	Ph	H	548	16 510	38	665	19 560	6	557	17 030	70	7.7
9	Me_3Si	Ph	H	557	16 920	40	669	19 890	3	573	15 620	58	7.6
10	H	Ph	Me	314	1840	<1	317	2010	<1	—[c]	—	—	—
11	^{t}Bu	Ph	Me	584	16 420	33	720	19 680	2	606	16 550	55	8.4
12	Me_3Si	Ph	Me	598	14 120	45	733	20 150	1	621	14 590	27	10.9
13	H	^{i}Pr	H	616	18 560	1	744	21 030	<1	654	17 270	5	6.9
14	Me_3Si	^{i}Pr	H	620	18 320	14	739	20 740	1	627	16 200	58	6.9
15	Me	H	H	551	17 300	<1	—[d]	—	—	595	16 460	33	—[e]

[a] Measured by using an integrating sphere method. [b] From low energy emission data. [c] Not emissive in the solid state. [d] Decomposes in DCM. [e] Not enough data for a Lippert–Mataga plot.

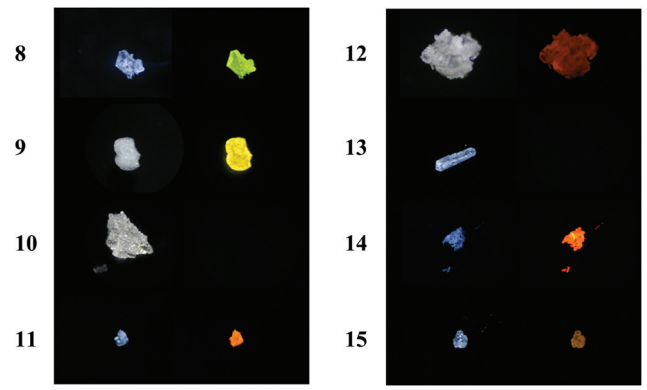

Fig. 3 Left columns: crystals of compounds **8–15** without UV irradiation. Right columns: under UV irradiation at 350 nm.

with respect to those observed in cyclohexane. The transition dipole moments estimated by use of the Lippert–Mataga method with an Onsager radius of 3.52 Å range from 6.9 to 10.9 D reflecting the CT nature of these emissions. The quantum yields were generally much lower in dichloromethane solutions, with the highest value of Φ_F = 6% for **8**, when compared with those in cyclohexane solutions.

Coloured emission can be seen with the naked eye, when crystals of **8**, **9**, **11**, **12**, **14** and **15** are irradiated by UV-light (Fig. 3). Compound **13** gives a faint yellow emission under UV irradiation which was not bright enough to be photographed. The solid state emission data are listed in Table 2 whereby the quantum yields reflect the brightness of the colours in Fig. 3. The relationship between the borolyl orientation described by ψ in the crystals and the low-energy CT emissions previously postulated for **1–7** is reinforced for the new carboranes **8–13** and **15**. The two compounds **6** and **10** which do not emit in the solid state contain the borolyl units in near co-planar orientation with the C1–C2 bond featuring small ψ angles of 16.6° and 12.2°, respectively. Increased ψ angles between 67.5° and 92.4° were found for **1–5**, **7–9**, **11–13** and **15** with Φ_F values between 25 and 70%.

Carborane **13** has one molecule in the asymmetric unit with ψ = 12.2° so it would not be expected to emit in the solid state but the second molecule probably contains conformers with higher ψ angles as the cluster in the latter molecule is disordered. These conformers are presumably responsible for the relatively weak low energy emission with Φ_F = 5% observed in the solid state.

Electrochemistry

Cyclic voltammetry (CV) data on **1–15** with a platinum working electrode in dichloromethane are summarised in Table 3. CV traces for the reduction waves of the disubstituted carboranes **3**, **4** and **5** are depicted in Fig. 4. These poorly resolved CV waves are typical for disubstituted carboranes as shown elsewhere[15,26] including diaryl-*ortho*-carboranes.[8,10–13] CV traces for the phenyl (**3**) and trimethylsilyl (**5**) derivatives show cathodic waves indicating a two-electron reduction and anodic waves corresponding to two one-electron oxidations after reduction. The CV trace for the *tert*-butyl derivative **4**, however, subtly reveals two one-electron waves on reduction rather than one two-electron reduction. The electron transfer rate for the second one-electron reduction is faster than the first one-electron reduction. The slow electron transfer with the first reduction may be related to a considerable geometric rearrangement taking place. Similar CV traces as for **4** and **5** are observed for the other *tert*-butyl and trimethylsilyl derivatives, **8**, **9**, **11**, **12** and **14**, with data listed in Table 3.

Compounds **1**, **2**, **6**, **7**, **10**, **13** and **15** with hydrogen or methyl groups at C2 do not show reduction waves within the

Table 3 Cyclic voltammetry (CV) data for **1–15** with a platinum working electrode in dichloromethane and a scan rate of 100 mV s^{-1}

	R^1	R^2	R^3	E^a (Ox)[a] V	E^c (Red1)[b] V	E^a (Red1) V	$E_{1/2}$ (Red1) V	E^a–E^c (Red1) mV	E^c (Red2) V	E^a (Red2) V	$E_{1/2}$ (Red2) V	E^a–E^c (Red2) mV	$\Delta E_{1/2}$ (Red1–Red2) mV
1	H	Et	H	0.92									
2	Me	Et	H	*1.2*									
3	Ph	Et	H	0.97	−1.92	−1.54	−1.73	380	−1.92	−1.77	−1.85	150	120
4	^{t}Bu	Et	H	1.04	−2.03	−1.57	−1.80	460	−2.03	−1.92	−1.98	110	180
5	Me_3Si	Et	H	1.09	−2.06	−1.50	−1.78	560	−2.06	−1.80	−1.93	260	150
6	H	Ph	H	1.11									
7	Me	Ph	H	*1.2*									
8	^{t}Bu	Ph	H	1.24	−2.26	−1.52	−1.89	740	−2.26	−1.94	−2.10	320	210
9	Me_3Si	Ph	H	1.19	−2.56	−1.51	−2.04	1050	−2.56	−1.91	−2.24	650	200
10	H	Ph	Me	0.89									
11	^{t}Bu	Ph	Me	0.98	−2.27	−1.56	−1.92	710	−2.27	−1.97	−2.12	300	200
12	Me_3Si	Ph	Me	1.13	−2.62	−1.49	−2.06	1130	−2.62	−1.89	−2.26	730	200
13	H	^{i}Pr	H	0.96									
14	Me_3Si	^{i}Pr	H	1.31	−2.29	−1.30	−1.76	990	−2.29	−1.76	−2.03	530	270
15	Me	H	H	1.13									

[a] Irreversible wave, values in italics are from ill-defined waves. [b] No observed reduction waves within the solvent window for **1**, **2**, **6**, **7**, **10**, **13** and **15**.

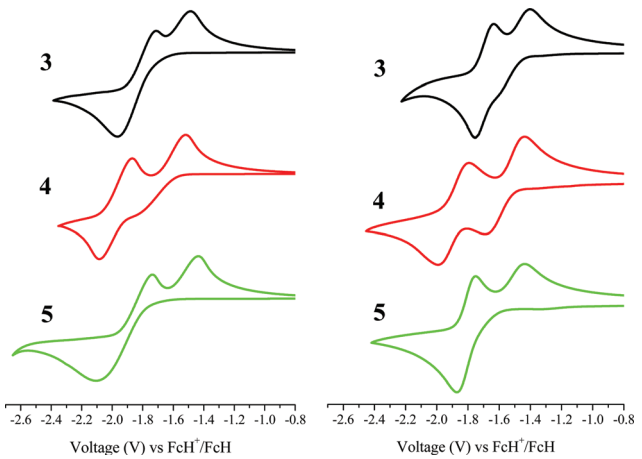

Fig. 4 Cyclic voltammetry traces for reductions of **3**, **4** and **5** in dichloromethane (left) and in acetonitrile (right) solutions.

solvent window of dichloromethane. These derivatives are thus more difficult to reduce than the phenyl, *tert*-butyl and silyl derivatives which may be related to the differences in the C1–C2 bond lengths with 1.656(1)–1.687(2) Å for R^1 = H or Me and 1.701–1.756 Å for R^1 = Ph, ^{t}Bu or $SiMe_3$ from X-ray studies (Table 1).

All the benzodiazaborolyl-*ortho*-carboranes here exhibit irreversible oxidation waves with multiple electron oxidations as may be deduced from the peak current of the waves relative to the reduction waves. These irreversible oxidations take place at the electron-donating diazaborolyl group in agreement with other benzodiazaboroles.[21,27] The anodic wave values E^a(Ox) should be regarded as approximate as these waves are ill-defined.

More defined cyclic voltammetry waves were obtained using a glassy carbon working electrode in acetonitrile as shown in Fig. 4 for **3**, **4** and **5**. The CV of the phenyl derivative **3** shows two one-electron cathodic waves on reduction rather than the one two-electron wave found in dichloromethane. The *tert*-butyl compound **4** shows in CH_3CN clearly defined two one-electron waves whereas the CV of the silyl derivative **5** still displays one two-electron cathodic wave. However, in all compounds the peak–peak separations E^a–E^c are smaller in acetonitrile than in dichloromethane. As the peak–peak separations for the internal ferrocenium–ferrocene couples in both solvents are similar it is obvious that the reduction waves of these carboranes are influenced considerably by the solvent used. CV traces like those for **4** and **5** were observed for the other *tert*-butyl and trimethylsilyl derivatives **8**, **9** and **14** (Table 4). Unfortunately, compounds **11** and **12** were insoluble in acetonitrile.

Reduction waves were also observed in acetonitrile solutions for **1**, **2**, **6**, **7**, **10**, **13** and **15** with hydrogen or methyl groups at C2 *i.e.* R^1 = H or Me (Scheme 5). The cathodic waves occur at reduction potentials E^c of −2.35 to −2.96 V (*vs.* the internal FcH^+–FcH couple), which are more negative than −1.69 to −2.09 V found for the phenyl, butyl and silyl derivatives here. The anodic waves after reductions are at much lower potentials E^a and of lower intensities than the corresponding cathodic waves for compounds with R^1 = H or Me. Similar CV traces have been reported for 1-methyl-*ortho*-carborane and 1,2-dimethyl-*ortho*-carborane where protonation of the formed dianions was postulated.[7] The dianions generated from diazaborolyl-*ortho*-carboranes with R^1 = H or Me are not stable under these electrochemical conditions. The CV traces of the carboranes are thus better defined in acetonitrile than in dichloromethane, but the compounds slowly decompose in acetonitrile.

Differences of 330 and 300 mV between the two one-electron reduction waves for the butyl derivatives **4** and **8** in acetonitrile indicate the radical monoanions to be stable with respect to disproportionation ($K_c \sim 1.2–3.8 \times 10^5$). The phenyl and silyl derivatives have smaller differences of 120 (**3**),

Table 4 Cyclic voltammetry (CV) data for **1–10** and **13–15** with a glassy carbon working electrode in acetonitrile and a scan rate of 100 mV s^{-1}

	R^1	R^2	R^3	E^a (Ox) V[a]	E^c (Red1) V	E^a (Red1) V[b]	$E_{1/2}$ (Red1) V	E^a–E^c (Red1) mV	E^c (Red2) V	E^a (Red2) V[b]	$E_{1/2}$ (Red2) V	E^a–E^c (Red2) mV	$\Delta E_{1/2}$ (Red1–Red2) mV
1	H	Et	H	0.87	−2.81	*−1.50*			−2.81	*−1.80*			
2	Me	Et	H	1.04	−2.35	*−1.50*			−2.35	*−1.76*			
3	Ph	Et	H	0.97	−1.76	−1.39	−1.58	370	−1.76	−1.64	−1.70	120	120
4	^{t}Bu	Et	H	0.98	−1.69	−1.44	−1.56	260	−1.99	−1.79	−1.89	200	330
5	Me_3Si	Et	H	1.02	−1.89	−1.41	−1.65	480	−1.89	−1.75	−1.82	140	170
6	H	Ph	H	1.09	−2.79	*−1.16*							
7	Me	Ph	H	1.12	−2.38	*−1.61*			−2.38	*−1.83*			
8	^{t}Bu	Ph	H	1.15	−1.75	−1.45	−1.60	300	−1.99	−1.82	−1.90	170	300
9	Me_3Si	Ph	H	1.25	−2.09	−1.58	−1.84	510	−2.09	−1.91	−2.00	180	160
10	H	Ph	Me	0.70	−2.88	*−1.67*							
13	H	^{i}Pr	H	0.75	−2.89	*−1.48*							
14	Me_3Si	^{i}Pr	H	1.11	−1.96	−1.30	−1.63	670	−1.96	−1.73	−1.85	230	220
15	Me	H	H	0.96	−2.96	*−1.64*			−2.96	*−1.86*			

[a] Irreversible wave. [b] Values in italics correspond to the anodic wave of the species formed on rearrangement, reaction or decomposition of the initial reduced species.

170 (**5**), 160 (**9**) and 220 (**14**) mV. The reported value for diphenyl-*ortho*-carborane in acetonitrile is 170 mV ($K_c \sim 750$)[8] so the radical anion for the phenyl derivative **3** is less stable but the radical anions for the butyl derivatives are more stable with respect to diphenyl-*ortho*-carborane and to the disproportionation into the dianion and neutral species. It is interesting to note that the electron-donating *tert*-butyl group facilitates radical anion stability more than the more electron-withdrawing phenyl group. It is presumed here that steric effects on the C1–C2 bond length of the carborane are more important for the stabilities of radical anions derived from diazaborolyl-*ortho*-carboranes than electronic effects.

Spectroelectrochemistry

In view of our cyclic voltammetry data, compounds **3**, **4** and **5** were selected for the identification of their stable monoanions and dianions using spectroelectrochemical (and computational) methods. Fig. 5 shows the IR spectra in the region between 1400 and 2800 cm^{-1} and Table 5 lists the band maxima of the ν(BH)-vibrations of the monoanions and dianions on electrochemical reductions of **3**, **4** and **5**. Given the similarities between the IR spectra for the monoanions and the reported IR spectrum of the diphenyl-*ortho*-carborane radical monoanion,[8] these species have closely related cluster geometries with 'free electrons' located in the cages.

The strong bands of the B–H stretching modes are shifted from 2675–2577 cm^{-1} for the neutral species to 2541–2528 cm^{-1} for the monoanions. Further reductions to the dianions led to ν(BH)-bands of 2451–2441 cm^{-1} which are shifted from the B–H bands for the monoanions by 80–100 cm^{-1}. In the case of the phenyl derivative **3**, the band assigned to the aromatic C–C stretch of the phenyl group is not significantly shifted on reduction with values between 1579 and 1589 cm^{-1} but its band intensity increases on going from the neutral species *via* the radical anion to the dianion as shown in Fig. 5.

UV-visible spectra of the colourless compounds **3**, **4** and **5** display bands at 293–298 nm corresponding to local π–π* transitions at the borolyl groups (Fig. 6 and Table 6). Electrochemical reductions of these neutral species gave spectral profiles with several bands observed corresponding to the radical monoanions. Weak lowest-energy bands are found at 433–442 nm along with more intense bands at 345–377 nm. Further reductions gave spectra with broad bands between 300 and 400 nm corresponding to the dianions. The ill-defined spectra of the anions were deconvoluted by Gaussian curve analyses with the lowest energy bands estimated at 382–400 nm.

Geometry and MO computations

Neutral species

The optimised geometries of the neutral species **8–13** and **15** at B3LYP/6-31G* are in good agreement with geometries determined experimentally. Comparison with computed and experimental data reported for **1–7** revealed one unusual difference as shown in Table 7. The reported optimised geometry for **4** has a C1–C2 bond length of 1.820 Å whereas in the optimised geometry for **8** a C1–C2 bond length of 1.765 Å was calculated. The experimentally determined C1–C2 bonds for **4** and **8** are similar at 1.756(1) Å and 1.750(2) Å, respectively (Table 1). Compounds **4** and **8** differ only in the Et and Ph substituents attached to the nitrogens of the borolyl group.

The torsion angles C1–C2–C22–C23 (θ, Fig. 2) were considered to study the influence of the *tert*-butyl group rotation on the geometries for **4** and **8**. Fig. S33† shows the total energies and the C1–C2 bond length with the angle θ constrained at 5 degree intervals for **4** and **8**. Two minima were found for **4** and such conformers *i.e.* **4A** and **4B** were indeed observed in the crystal of **4**. Only one minimum was located for **8** and this conformer was determined by X-ray crystallography. The effect of the *tert*-butyl group on both geometries is intriguing with C1–C2 bond lengths varying from 1.76 to 1.83 Å for **4** and from

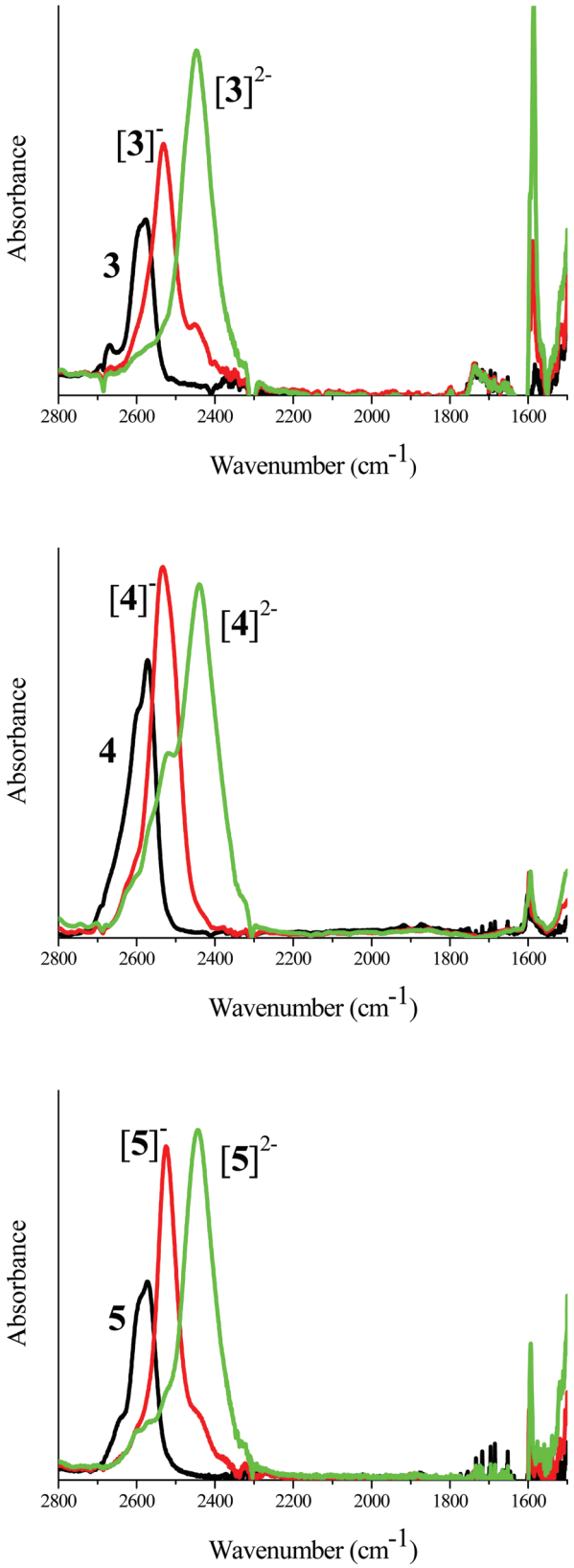

Fig. 5 IR spectra for **3**, **4** and **5** and their mono- and dianions in the region 1400–2800 cm^{-1} in an OTTLE cell (DCM, 0.1 M $^{n}Bu_4NPF_6$).

Table 5 IR data for $[\mathbf{3}]^{n-}$, $[\mathbf{4}]^{n-}$ and $[\mathbf{5}]^{n-}$ (n = 0, −1, −2) in 0.1 M $^{n}Bu_4NPF_6$ DCM solutions

	n	B–H stretch/cm^{-1}	Phenyl ring CC stretch/cm^{-1}
$[\mathbf{3}]^{n-}$	0	2675 (w), 2598 (m), 2580 (m)	1589 (w)
	1	2536 (s)	1579 (m)
	2	2451 (s)	1587 (s)
$[\mathbf{4}]^{n-}$	0	2536 (s), 2602 (m), 2577 (m)	
	1	2541 (s)	
	2	2525 (sh), 2441 (s)	
$[\mathbf{5}]^{n-}$	0	2645 (w), 2595 (m), 2577 (m)	
	1	2528 (s)	
	2	2448 (s)	

1.76 to 1.80 Å for **8** and with low rotation barriers of 0.6 kcal mol^{-1} for **4** and 1.0 kcal mol^{-1} for **8**. These C1–C2 bond length variations of 0.07 and 0.04 Å are larger than those of 0.01–0.03 Å computed for the rotations of a borolyl,[16] phenyl[28] or *tert*-butyl[29] group in C-monosubstituted carboranes. The combined steric congestion and mutual orientations of the *tert*-butyl and diazaborolyl groups influence the C1–C2 distance considerably.

Comparison of the bond lengths for the optimised geometries **4A**, **4B** and the experimental geometry of **4** listed in Table 8 reveals very good agreement between **4B** and **4** for all bonds whereas the agreement between **4A** and **4** is good apart from a significant difference of 0.06 Å found for the C1–C2 bond. Apart from the sensitive C1–C2 bond lengths listed in Table 7, similar bond lengths in the optimised geometry of **4B** are observed in the optimised geometries of the neutral compounds **1–3** and **5–15**.

While C-diazaborolyl-*ortho*-carboranes can be derived from benzodiazaborolyl groups with R^2 = H, Et, ^{i}Pr or Ph (Scheme 5), carboranes with *N*-mesityl or *N*-*tert*-butyl substituents are still elusive. Optimized geometries on these molecules revealed a highly distorted borolyl group for R^2 = ^{t}Bu and a borolyl group with little distortion for R^2 = Mes. This suggests severe steric hindrance in the case of *tert*-butyl groups at nitrogens preventing formation of the C-diazaborolyl-*ortho*-carborane and indeed notable distortions are present in the optimised geometry of the hypothetical bromoborole precursor **20**. The *ortho*-methyl groups in the mesityl groups may obstruct bond formation between the carborane anion and the boron atom of the fused ring system thus inhibiting the synthesis of the C-diazaborolyl-*ortho*-carborane with mesityl groups at nitrogens.

The optimised geometry of the carborane **31** with the BBr_2 group at a cage carbon, which was not structurally characterised, gave calculated ^{11}B GIAO-NMR data in good agreement with observed ^{11}B NMR data where the peak for the three-coordinate boron is at 56.8 ppm. Comparison of the optimised geometry **31** with the optimised geometry for the closely related benzodiazaborolyl carborane **15** reveals very similar C1–C2 and B2–C1 bond lengths for **31** (1.587; 1.679 Å) and **15** (1.581; 1.685 Å). Thus, both Br_2B- and $C_6H_4(NH)_2B$-groups exert similar structural effects on the carborane cluster.

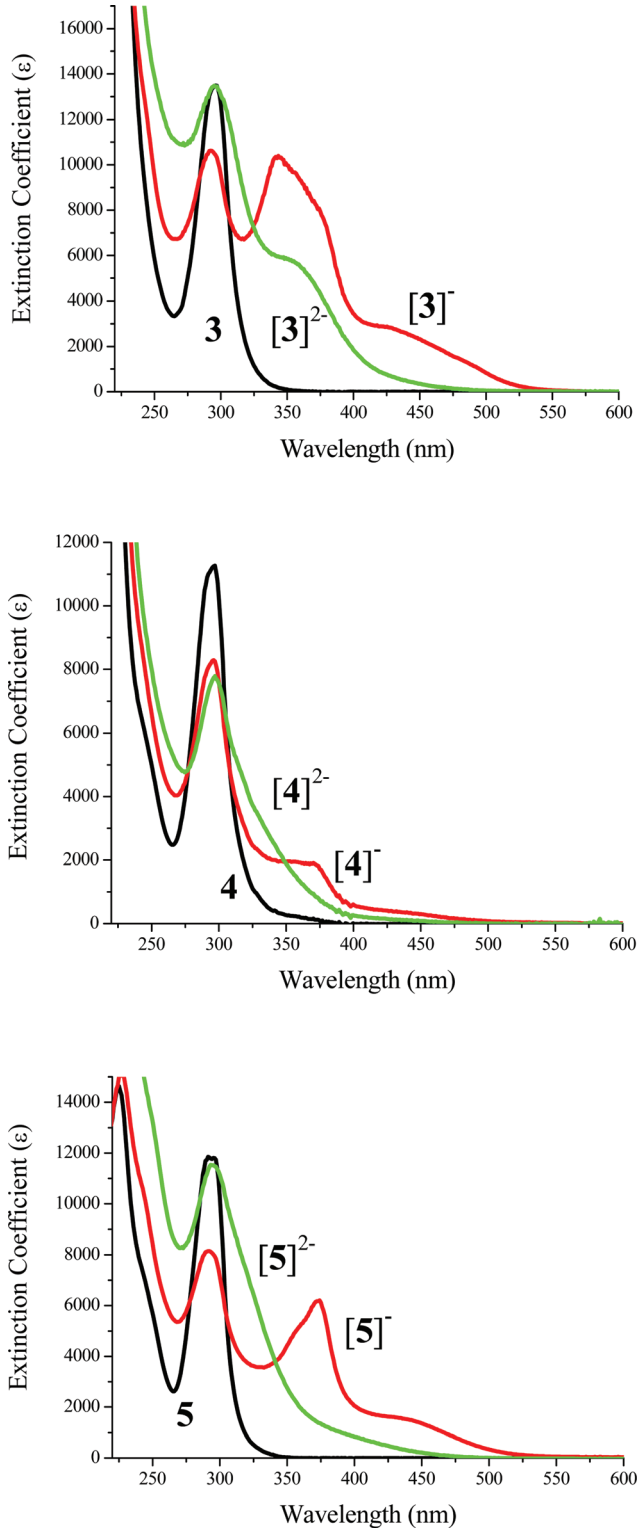

Fig. 6 UV spectra for **3**, **4** and **5** and their mono- and dianion species in an OTTLE cell (DCM, 0.1 M $^{n}Bu_4NPF_6$).

As previously reported[16] for compounds **1–7**, the HOMO is the π(borolyl) orbital whereas the LUMO may be the π*B or a π*(phenyl) orbital. HOMO and LUMO of **4B** are depicted in Fig. 7. Table 7 lists the calculated LUMO and HOMO energies

Table 6 UV-visible data for $[\mathbf{3}]^{n-}$, $[\mathbf{4}]^{n-}$ and $[\mathbf{5}]^{n-}$ (n = 0, −1, −2) in 0.1 M $^{n}Bu_4NPF_6$ DCM solutions

	n	Wavelength/nm (extinction coefficient ε/M^{-1} cm^{-1})
$[\mathbf{3}]^{n}$	0	297 (13 500)
	1	441 (2600), 377 (7700), 362 (9100), 347 (10 200), 295 (10 500)
	2	400 (1200), 375 (3200), 355 (4300), 336 (4700), 318 (6500), 304 (9600), 291 (11 000)
$[\mathbf{4}]^{n}$	0	298 (11 000), 296 (11 300)
	1	433 (400), 372 (1900), 358 (1900), 345 (2000), 297 (8300), 292 (8100)
	2	382 (400), 364 (1000), 345 (1600), 329 (2400), 313 (4000), 298 (7000)
$[\mathbf{5}]^{n}$	0	297 (11 700), 293 (11 800)
	1	442 (1300), 375 (6000), 361 (5300), 297 (7900), 292 (8100)
	2	400 (800), 370 (1200), 350 (2000), 331 (4200), 314 (6500), 300 (8400), 288 (7700)

for **1–15** and compares them with the oxidation and reduction potentials obtained from CV data. Strictly speaking, observed half-wave oxidation and reduction potentials should be used for comparison but such values are not available for most compounds here. Therefore anodic oxidation and cathodic reduction potentials are used here for comparison. The agreement between the experimental oxidation potentials and the HOMO energies is reasonable. The observed reduction potentials, on the other hand, are in poor agreement with the calculated LUMO energies in the sense that there is no obvious trend between the two sets of values. For example, the computed LUMO energies for **2** and **5** are identical but the observed reduction potentials differ by 0.46 V. Here the predicted LUMO energies are thus poor guides for the estimation of the reduction potentials of disubstituted-*ortho*-carboranes. A better correlation between measured reduction potentials and C1–C2 bond lengths (experimental or computed) is shown in Table 7.

The LUMO energy for **4** depends on the two conformers (minima) with −1.12 eV for **4A** and −0.82 eV for **4B**. The cage contributions to the LUMOs are 67% for **4A** and 51% for **4B** and suggest that an increase in the C1–C2 bond results in an increase of the cage contribution to the LUMO. This, in turn, could facilitate the one-electron reduction of the cluster.

Monoanions

The optimised geometry of the monoanion $[\mathbf{4}]^{-}$ is shown here as a representative example for stable monoanion radical anions from **3**, **4**, **5**, **8**, **9**, **11**, **12** and **14** based on their CV data. The C1–C2 bond distances for the eight monoanions range from 2.425 Å $[\mathbf{3}]^{-}$ to 2.445 Å for $[\mathbf{4}]^{-}$ as shown in Table S8.† Selected bond lengths for the monoanion $[\mathbf{4}]^{-}$ are listed in Table 8 using the atom numbering given in Fig. 2. The cluster geometry for $[\mathbf{4}]^{-}$ is clearly more distorted with a C1–C2 bond elongated in comparison to its neutral species **4** whereas the borolyl group in $[\mathbf{4}]^{-}$ resembles the borolyl group in **4**. The 'free electron' is thus located in the cage and the anion $[\mathbf{4}]^{-}$ has a $2n + 3$ skeletal electron count.

Comparison of selected bond lengths between the monoanion $[\mathbf{4}]^{-}$ and the excited state $\mathbf{4}S_1$(CT) geometries shows

Table 7 Selected calculated geometric parameters and comparison between computed and observed MO energies for **1–15**

	R^1		C1–C2 (calc)	LUMO energy obs (V)[a]	LUMO energy calc (eV)	LUMO type	HOMO energy obs (V)[b]	HOMO energy calc (eV)
1	H	ψ = 13.9	1.656	−1.99	−0.66	π*B	−5.67	−5.87
		ψ = 91.8	1.676		−0.71	π*B		−5.89
2	Me		1.714	−2.45	−0.85	π*B	−5.84	−5.89
3	Ph		1.764	−3.04	−1.31	π*(phenyl)	−5.77	−5.78
4	^{t}Bu	**4A** θ = 11.4	1.820	−3.11	−1.12	π*B	−5.78	−5.79
		4B θ = 58.0	1.764		−0.82	π*B		−5.84
5	Me_3Si		1.750	−2.91	−0.85	π*B	−5.82	−5.82
6	H	ψ = 5.5	1.659	−2.01	−0.74	π*(phenyl)	−5.89	−5.93
		ψ = 90.1	1.664		−0.63	π*B		−5.96
7	Me		1.692	−2.42	−0.68	π*B	−5.92	−5.95
8	^{t}Bu	θ = 26.1	1.765	−3.05	−0.77	π*B	−5.95	−5.87
9	Me_3Si		1.729	−2.71	−0.70	π*B	−6.05	−5.91
10	H	ψ = 1.8	1.657	−1.92	−0.70	π*(phenyl)	−5.50	−5.66
		ψ = 89.6	1.665		−0.55	π*B	−5.50	−5.69
11	^{t}Bu	θ = 29.4	1.766	−2.53[c]	−0.71	π*B	−5.78[c]	−5.61
12	Me_3Si		1.730	−2.18[c]	−0.63	π*B	−5.93[c]	−5.64
13	H	ψ = 14.3	1.664	−1.91	−0.66	π*B	−5.55	−5.83
		ψ = 88.8	1.686		−0.73	π*B		−5.85
14	Me_3Si		1.761	−2.84	−0.89	π*B	−5.91	−5.78
15	Me		1.685	−1.84	−0.72	π*B	−5.76	−6.03

[a] Data from Table 4 using E(MO) = $-E^c$(Red1) − 4.8 V with the FcH^+/FcH couple at −4.8 V. [b] Data from Table 4 using E(MO) = $-E^a$(Ox) − 4.8 V. [c] Data from Table 3.

Table 8 Comparison of selected bond lengths (Å) in the experimental geometry for **4** and the optimised geometries **4A**, **4B**, $[4]^-$, **4** S_1(CT) and $[4]^{2-}$

Bond	**4**	**4A**	**4B**	$[4]^-$	**4** S_1 (CT)	$[4]^{2-}$
C1–C2	1.7564(12)	1.820	1.764	2.445	2.420	2.991
C1–B3	1.7318(13)	1.729	1.730	1.759	1.693	2.686
C1–B6	1.7255(13)	1.724	1.726	1.761	1.689	1.555
C1–B4	1.7136(14)	1.699	1.719	1.635	1.636	1.618
C1–B5	1.7155(13)	1.699	1.719	1.635	1.637	1.617
C2–B3	1.7214(14)	1.713	1.729	1.707	1.759	1.527
C2–B6	1.7249(14)	1.720	1.729	1.705	1.762	2.640
C2–B7	1.7224(14)	1.709	1.719	1.641	1.616	1.617
C2–B11	1.7231(14)	1.717	1.721	1.642	1.615	1.616
C1–B2	1.6058(13)	1.610	1.615	1.548	1.589	1.517
C2–C22	1.5726(13)	1.581	1.585	1.550	1.540	1.540
N1–B2	1.4411(12)	1.446	1.450	1.462	1.470	1.481
N3–B2	1.4387(12)	1.448	1.447	1.462	1.474	1.476
N1–C9	1.3992(11)	1.401	1.401	1.391	1.374	1.382
N3–C8	1.3985(11)	1.400	1.401	1.391	1.371	1.395
C8–C9	1.4013(13)	1.408	1.408	1.418	1.442	1.428
C4–C9	1.3929(12)	1.396	1.396	1.394	1.402	1.394
C7–C8	1.3951(13)	1.396	1.396	1.394	1.399	1.395
C4–C5	1.3963(14)	1.397	1.397	1.402	1.388	1.407
C6–C7	1.3956(14)	1.397	1.397	1.402	1.390	1.407
C5–C6	1.3916(15)	1.399	1.399	1.396	1.419	1.394

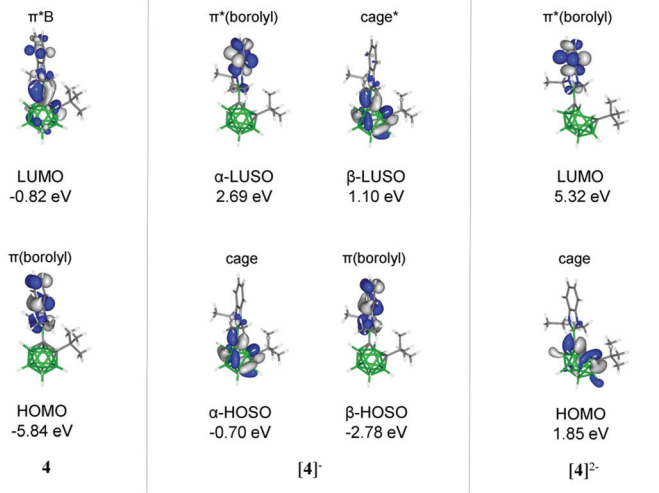

Fig. 7 Selected molecular orbitals for **4**, $[4]^-$ and $[4]^{2-}$.

similarities in the cluster geometries (Table 8). The C1–C2 distances are similar at 2.45 Å for $[4]^-$ and 2.42 Å for the excited state $4S_1$(CT). The borolyl group inevitably acts as a 'donor' in the monoanion and as an 'acceptor' in the excited state thus closer examination of the clusters reveals essentially identical geometries whereby the 'donor' group at the carbon atom lengthens the B3/6-C bond *i.e.* B3/6-C1 of 1.76 Å for $[4]^-$ and B3/6-C2 of 1.76 Å for $4S_1$(CT). Thus data on carborane monoanion radicals could be related to the excited state geometries of such carboranes which are responsible for the low-energy emissions observed here and elsewhere.

The 'free' electron in the monoanion radical is located in the cage based on open-shell electronic structure calculations where the highest singly occupied orbital SOMO (the highest occupied spin orbital α-HOSO) represents the 'free' electron for the monoanion $[4]^-$ in Fig. 7. The α-HOSO, which is considered as the singly occupied molecular orbital SOMO, for $[4]^-$ has 87% cage character and thus 36% more than the LUMO of the neutral species **4B**. It seems likely that addition of an electron to the neutral species goes initially to the π*B orbital and the C1–C2 bond then elongates to accommodate the 'free' electron into the cage. This geometrical rearrangement may be the cause of the slow electron transfer process observed in the CV data for **4**. This process also applies to

other carboranes, **5**, **8**, **9**, **11**, **12** and **14**, with ^{t}Bu or Me_3Si groups. A different situation is given for **3** where the LUMO is located at the phenyl group. In this case, the electron initially goes to the π*(phenyl) orbital on reduction followed by rearrangement of the cage. This route is also likely in diphenyl-*ortho*-carborane (Fig. 1) where slow electron transfer is also evident for the first reduction wave by detailed CV studies.[8]

Dianion species

At least six different geometries for the *nido*-12-vertex carboranes are described.[30] According to quantum chemical calculations, the most stable geometries of the dianions **3**, **4**, **5**, **8**, **9**, **11**, **12** and **14** have C–C separations ranging from 2.944 Å $[9]^{2-}$ to 2.991 Å for $[4]^{2-}$ (Table S8†). They are similar to experimentally determined C–C distances in *nido*-12-vertex carboranes (Table S9†).[31] Moreover calculated distances C1···B3 and C2···B6 (2.582–2.686 Å) are well comparable to experimentally obtained data (2.485–2.743 Å). Pertinent computed bond lengths for $[4]^{2-}$, which was selected as a representative for the dianions here, are collected in Table 8. The bonding parameters within the diazaborolyl fragments of $[4]^{-}$ and $[4]^{2-}$ are similar, whereas changes in the cluster are obvious. Thus, distances C1–B3 and C2–B6 are elongated by 0.93 Å and the bond length C1–C2 increased by 0.55 Å. Obviously the second electron upon reduction of $[4]^{-}$ to $[4]^{2-}$ is accommodated in the cluster. The HOMO of dianion $[4]^{2-}$ has 90% cage character, whereas the LUMO is located at the C_6H_4-part of the benzodiazaborolyl substituent (Fig. 7). From the similar geometries of $[4]^{2-}$ and $[4]^{-}$ and the natures of the HOMO in $[4]^{2-}$ and the SOMO in $[4]^{-}$ one might expect a rapid electron transfer between the two species, which is underlined by the CV data presented earlier.

Infrared and UV-visible computations

Selected data obtained by TD-DFT calculations for **3**, **4** and **5** and their anions and the corresponding experimental infrared- and UV-visible-data are listed in Table 9. In all cases excellent agreement between observed and computed IR-frequencies reflects the substantial shifts of the B–H stretching modes on sequential one-electron reduction (for simulated IR spectra of **3–5** and their anions see Fig. S35†).

TD-DFT data on the nine species are also in broad agreement with the observed low-energy bands. The relevant orbitals discussed here are shown in Fig. 7 for $[4]^{n-}$ (n = 0, −1, −2) where similar orbitals are found for $[3]^{n-}$ and $[5]^{n-}$ analogues. In the neutral species, the strong bands observed at 4.19 eV correspond to HOMO > LUMO transitions (π(borolyl) > πB*) as reported elsewhere for **3–5**.[16] The weak lowest energy bands observed for the three monoanionic radicals are assigned to α-HOSO > α-LUSO transitions which are largely cage to π* (borolyl) and thus charge-transfer in nature. Higher energy bands at 3.0–3.3 eV in the UV spectra of the monoanions are assigned to π(borolyl) > cage* transitions (β-HOSO > β-LUSO). The lowest energy bands observed for the dianions are assigned to HOMO > LUMO transitions (cage > π*(borolyl)).

Given the excellent agreements between observed and computed spectroscopic data for the monoanions and dianions of **3–5**, the optimised geometries for these anions are likely to be found experimentally. These anion geometries are also present for reduced carboranes **8**, **9**, **11**, **12** and **14** as these compounds gave CV data similar to **4** and **5**.

Conclusions

The family of C-benzodiazaborolyl-*ortho*-carboranes has been expanded by three new benzodiazaborolyl groups. While most derivatives were synthesized using the standard bromoborole–lithiocarborane synthetic route, two alternative protocols to new C-benzodiazaborolyl-*ortho*-carboranes were developed. Low-energy fluorescence emissions were observed in the solution- and solid-state for seven of the eight new compounds with Stokes shifts between 14 100 and 21 000 cm^{-1} and quantum yields up to 70%.

Table 9 Comparison of observed IR and UV-visible data with calculated frequency and TD-DFT data for $[3]^{n-}$, $[4]^{n-}$ and $[5]^{n-}$ (n = 0, −1, −2)

	Obs (cm^{-1})	Calc (cm^{-1})	Vibration type	Obs (eV)	Calc (eV)	Osc. str.[a]	Major orbital contributions (%)	Transition type
3	2580	2580	B–H stretch	4.19	4.68	0.2099	HOMO > LUMO + 2 (68)	π(borolyl) > πB*
	1589	1572	CC ring stretch					
$[3]^{-}$	2536	2525	B–H stretch	2.81	2.74	0.0434	α-HOSO > α-LUSO (87)	Cage > π *(borolyl)
	1579	1573	CC ring stretch	3.29	2.99	0.0794	β-HOSO > β-LUSO (84)	π(borolyl) > cage*
$[3]^{2-}$	2451	2420	B–H stretch	3.10	3.08	0.0892	HOMO > LUMO (70)	Cage > π*(borolyl)
	1587	1564	CC ring stretch					
4A	2577	2580	B–H stretch	4.19	4.15	0.2586	HOMO > LUMO (70)	π(borolyl) > πB*
4B	2577	2580	B–H stretch	4.19	4.49	0.3009	HOMO > LUMO (67)	π(borolyl) > πB*
$[4]^{-}$	2541	2508	B–H stretch	2.87	2.82	0.0453	α-HOSO > α-LUSO (97)	Cage > π*(borolyl)
				3.34	3.21	0.1488	β-HOSO > β-LUSO (95)	π (borolyl) > cage*
$[4]^{2-}$	2441	2412	B–H stretch	3.25	3.00	0.0809	HOMO > LUMO (70)	Cage > π*(borolyl)
5	2580	2580	B–H stretch	4.19	4.44	0.2726	HOMO > LUMO (69)	π(borolyl) > πB*
$[5]^{-}$	2528	2509	B–H stretch	2.81	2.86	0.0338	α-HOSO > α-LUSO (95)	Cage > π*(borolyl)
				3.31	3.16	0.1602	β-HOSO > β-LUSO (95)	π(borolyl) > cage*
$[5]^{2-}$	2448	2412	B–H stretch	3.10	3.12	0.0871	HOMO > LUMO (70)	Cage > π*(borolyl)

[a] Oscillation strength.

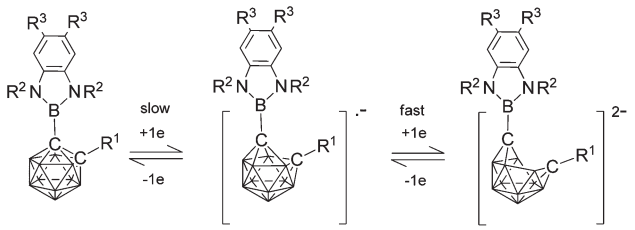

Fig. 8 Postulated geometries of the anions obtained by reduction of carboranes with R^1 = Ph, ^{t}Bu and $SiMe_3$.

All fifteen C-diazaborolyl-carboranes examined by CV studies reveal oxidation and reduction waves in acetonitrile solutions. While oxidations are centered at the electron-donating benzodiazaborolyl groups, the reductions occur at the electron-withdrawing carborane clusters. For the C-diazaborolyl-*ortho*-carboranes with a phenyl, *tert*-butyl or trimethylsilyl substituent at the second carbon (R^1 in Fig. 8), the reduction waves showed evidence of stable monoanionic radicals and dianions. The stabilities of these anions were supported by infrared and UV-visible spectroelectrochemical methods. The anions were cleanly transferred to their neutral precursors by oxidation.

The geometries of the radical anions with $2n + 3$ skeletal electron counts and the dianions (*nido*, $2n + 4$ skeletal electron count) were determined by computations (Fig. 8). The computed frequencies of the B–H stretching vibrations and TD-DFT data from these optimised geometries were in very good agreement with the spectroelectrochemical data indicating that such geometries may also be formed experimentally.

Based on the electronic structure calculations of the three geometries in Fig. 8, the first reduction process involves adding an electron to the boron atom with the empty p-orbital followed by rearrangement of the cluster which allows the formation of the stable radical anion. The cluster rearrangement is likely to be responsible for the slow electron transfer reflected by the CV traces for the first reduction process. This slow electron transfer process is strongly dependent on the solvent which is perhaps not surprising given that negative charge is transferred from the borolyl group to the cage during the rearrangement process. The second reduction step is a straightforward addition of the second electron to the carborane radical anion resulting in a fast electron transfer as inferred from the CV studies.

For C-diazaborolyl-*ortho*-carboranes with hydrogen or methyl groups at the adjacent cage carbon, the measured reduction potentials here demonstrate that they are considerably more difficult to reduce in comparison to those with phenyl, *tert*-butyl and trimethylsilyl groups. This is strongly related to the C1–C2 bond distances where experimental values are 1.656(1)–1.686(2) Å for R^1 = H, Me and 1.701(2)–1.756(1) Å for R^1 = Ph, ^{t}Bu, $SiMe_3$. The C1–C2 separations in neutral *ortho*-carboranes are thus important parameters for the stabilization of 12-vertex geometries with $2n + 3$ skeletal electron counts.

The similarities in the optimised cluster geometries of the monoanions here and the charge transfer (CT) singlet excited states of their neutral species suggest a close relationship between the monoanion and the S_1(CT) state in these diazaborolylcarboranes. Low-energy emissions were observed for C-benzodiazaborolyl-*ortho*-carboranes with R^1 = Ph, ^{t}Bu, $SiMe_3$ which are also those with long C1–C2 bond distances and with the stable $2n + 3$ monoanions.

Experimental

General

All manipulations were performed under an atmosphere of dry oxygen-free argon using Schlenk techniques. All solvents were dried by standard methods and freshly distilled prior to use. The compounds 2-bromo-1,3-diethyl-1,3,2-benzodiazaborole,[17] 2-bromo-1,3-diphenyl-1,3,2-benzodiazaborole (**16**),[19] 4,5-dimethyl-*N*,*N*′-diphenyl-*ortho*-phenylenediamine (**25**),[32] *N*,*N*′-dimesityl-*ortho*-phenylenediamine (**26**),[33] *N*,*N*′-di-*tert*-butyl-*ortho*-phenylenediamine(**28**),[34] 1-*tert*-butyl-1,2-dicarbadodecaborane[35] and 1-trimethylsilyl-1,2-dicarbadodecaborane[35] were prepared as described in the literature. Compounds **22**, **23**, **29**, 1,2-dicarbadodecaborane and 1-methyl-1,2-dicarbadodecaborane were purchased commercially. NMR spectra were recorded from solutions at room temperature on a Bruker Avance III 300, a Bruker AM Avance DRX500 (^{1}H, ^{11}B, ^{13}C), a Bruker Avance III 500 and a Bruker Avance 400 spectrometer (^{1}H{^{11}B}) with $SiMe_4$ (^{1}H, ^{13}C) and $BF_3{\cdot}OEt_2$ (^{11}B) as external standards. ^{1}H- and ^{13}C{^{1}H} NMR spectra were calibrated on the solvent signal [$CDCl_3$: 7.24 (^{1}H), 77.16 (^{13}C); C_6D_6: 7.15 (^{1}H), 128.06 (^{13}C)]. The expected broad ^{13}C peaks corresponding to the carbon atoms attached to the borole-boron atoms were not detected above the noise levels. Mass spectra were recorded with a VG Autospec sector field mass spectrometer (Micromass). See ESI† for further spectroscopic data, ^{1}H, ^{13}C{^{1}H} and ^{11}B{^{1}H} NMR spectra of carboranes **8–15** and detailed synthetic procedures. Typical procedures for the syntheses of C-benzodiazaborolyl-*ortho*-carboranes and 2-bromo-1,3,2-benzodiazaboroles are described below.

Synthesis of 2-(1′,2′-dicarbadodecaboran-1′-yl)-1,3-diphenyl-5,6-dimethyl-1,3,2-benzodiazaborole (**10**). *n*-Butyllithium (1.6 M in *n*-hexane, 4.00 mL, 6.40 mmol) was added to a chilled (0 °C) solution of *ortho*-carborane (0.87 g, 6.03 mmol) in diethyl ether (10 mL). After stirring for 1.5 h at room temperature a solution of 2-bromo-1,3-diphenyl-5,6-dimethyl-1,3,2-benzodiazaborole **17**, (2.28 g, 6.05 mmol) in toluene (11 mL) was added dropwise at 0 °C. After stirring for 19 h at room temperature the solvent was removed *in vacuo*. The residue was extracted with hot toluene (5 × 10 mL) and the combined extracts were evaporated to dryness. The remaining solid was crystallized from dichloromethane (27 mL) and washed with *n*-hexane (8 mL). Product **10** was obtained as a colourless solid. Yield: 1.87 g (70%). Found: C, 59.77; H, 6.63; N, 6.33%; $C_{22}H_{29}B_{11}N_2$ requires C, 60.00; H, 6.64; N, 6.36%; ^{1}H-NMR ($CDCl_3$): δ [ppm] = 0.9–3.0 (m, br, 10 H, BH), 2.15 (s, 6 H, CCH_3), 2.99 (s, br,

1 H, cage C*H*), 6.30 (s, 2 H, H4,7), 7.30 (m, 4 H, H_{ortho}), 7.51 (m, 6 H, H_{meta}, H_{para}); $^{13}C\{^1H\}$-NMR ($CDCl_3$): δ [ppm] = 19.9 (s, CCH_3), 58.3 (s, cage*C*H), 111.8 (s, C4,7), 128.6 (s, C_{para}), 129.5 (s, C_{ortho}), 129.6 (s, C5,6), 129.9 (s, C_{meta}), 136.1 (s, C8,9), 139.0 (s, C_{ipso}); $^{11}B\{^1H\}$-NMR ($CDCl_3$): δ [ppm] = −12.8 (s), −11.0 (s), −7.9 (s), −2.2 (s), 0.2 (s) (polyhedral boron atoms), 23.2 (s, exo-polyhedral boron atom); MS (EI): m/z = 440.4 (M^+, 100%), 425.3 (M^+ − Me, 10%).

Synthesis of 2-bromo-1,3-diphenyl-5,6-dimethyl-1,3,2-benzodiazaborole (**17**). A solution of 4,5-dimethyl-*N*,*N*′-diphenyl-*o*-phenylenediamine (**25**) (5.58 g, 19.35 mmol) in chloroform (60 mL) was dripped to a mixture of calcium hydride (3.26 g, 77.45 mmol), boron tribromide (2.20 mL, 5.81 g, 23.21 mmol) and chloroform (60 mL). After stirring for 21 h at ambient temperature the mixture was filtered and the filter-cake was washed with chloroform (30 mL). The combined filtrates were freed from volatiles and the residue was purified by short-path distillation (5×10^{-2} mbar) using a flame. Product **17** was obtained as a colourless solid. Yield: 6.68 g (92%). ^{1}H-NMR ($CDCl_3$): δ [ppm] = 2.26 (s, 6 H, $C_6H_2(CH_3)_2$), 6.89 (s, 2 H, H4,7), 7.39 (tt, $^3J_{HH}$ = 7.3 Hz, $^4J_{HH}$ = 1.2 Hz, 2 H, H_{para}), 7.45 (dd, $^3J_{HH}$ = 8.4 Hz, $^4J_{HH}$ = 1.2 Hz, 4 H, H_{ortho}), 7.52 (m, 4 H, H_{meta}); $^{13}C\{^1H\}$-NMR ($CDCl_3$): δ [ppm] = 20.0 (s, $C_6H_2(CH_3)_2$), 111.6 (s, C4,7), 126.7 (s, C_{para}), 127.3 (s, C_{ortho}), 128.9 (s, C5,6), 129.4 (s, C_{meta}), 135.2 (s, C8,9), 139.3 (s, C_{ipso}); $^{11}B\{^1H\}$-NMR ($CDCl_3$): δ [ppm] = 23.6 (s); MS (EI): m/z = 375.9 (M^+, 100%), 360.9 (M^+ − Me, 38%).

Photophysics

All experiments in solution were performed in quartz cuvettes of 10 × 10 mm (Hellma type 111-QS, suprasil, optical precision). Cyclohexane was used as received from commercial sources (p. a. quality), the other solvents were dried by standard methods prior to use. Sample concentrations varied from 20 to 70 μM according to their optical density. Solid samples were prepared by vacuum sublimation on quartz plates (35 × 10 × 1 mm) using standard Schlenk equipment and conditions.

Absorption spectra were taken with a UV/VIS double-beam spectrometer (Shimadzu UV-2550), using the solvent as a reference. The setup used to acquire excitation–emission spectra (EES) was similar to that employed in commercial static fluorimeters. The output of a continuous Xe-lamp (75 W, LOT Oriel) was wavelength-separated by a first monochromator (Spectra Pro ARC-175, 1800 l·mm^{-1} grating, Blaze 250 nm) and then used to irradiate a sample. The fluorescence was collected by mirror optics at right angles and imaged on the entrance slit of a second spectrometer while compensating astigmatism at the same time. The signal was detected by a back-thinned CCD camera (RoperScientific, 1024\256 pixels) in the exit plane of the spectrometer. The resulting images were spatially and spectrally resolved. As the next step, one averaged fluorescence spectrum was calculated from the raw images and stored in the computer. This process was repeated for different excitation wavelengths. The result is a two-dimensional fluorescence pattern with the *y*-axis corresponding to the excitation, and the *x*-axis to the emission wavelength. The time to acquire a complete EES is typically less than 15 min. Post-processing of the EES includes subtraction of the dark current background, conversion of pixel to wavelength scales, and multiplication with a reference file to take the varying lamp intensity as well as grating and detection efficiency into account. The quantum yields were determined against POPOP (*p*-bis-5-phenyl-oxazolyl(2)-benzene) (Φ = 0.93) as the standard.

The solid-state fluorescence was measured by addition of an integrating sphere (Labsphere, coated with Spectralon, Ø 12.5 cm) to the existing experimental setup. At the exit slit of the first monochromator the exciting light was transferred into a quartz fiber (LOT Oriel, LLB592). It passed a condenser lens and illuminated a 1 cm^2 area on the sample in the centre of the sphere. The emission and exciting light was imaged by a second quartz fiber on the entrance slit of the detection monochromator. The optics for correction of astigmatism was passed by the light on this way.

Post-processing of the spectra was done as described above. The experimental determination and calculation of quantum yields was performed according to the method described by de Mello *et al.*[36] Stokes shifts were calculated from excitation and emission maxima, which were extracted from spectra that were converted from wavelength to wavenumbers beforehand.

X-ray crystallography

Single crystals were coated with a layer of hydrocarbon oil and attached to a glass fiber. Crystallographic data were collected with Nonius Kappa CCD and Bruker KAPPA APEX II diffractometers with Mo-K_α radiation (graphite monochromator, λ = 0.71073 Å) and a Bruker AXS X8 Prospector Ultra with APEX II with Cu-K_α radiation (graphite monochromator, λ = 1.54178 Å) at 100 K. Crystallographic programs used for structure solution and refinement were from SHELX-97.[37] The structures were solved by direct methods and were refined by using full-matrix least squares on F^2 of all unique reflections with anisotropic thermal parameters for all non-hydrogen atoms. All hydrogen atoms, except those of a disordered methyl group, were refined isotropically for **15**. For **8–13** only the hydrogen atoms bonded to (non-disordered) carborane units were refined isotropically, the other hydrogen atoms were refined using a riding model with U(H) = 1.5 U_{eq} for CH_3 groups and U(H) = 1.2 U_{eq} for all others. For **19** all hydrogen atoms were refined using this riding model. Crystallographic data for the compounds are listed in Table S2.† CCDC-894654 (**8**), CCDC-894655 (**9**), CCDC-894656 (**10**), CCDC-894657 (**11**), CCDC-894658 (**12**), CCDC-894659 (**13**), CCDC-894660 (**15**) and CCDC-894661 (**19**) contain the supplementary crystallographic data for this paper.

Cyclic voltammetry

Electrochemical measurements (Autolab PG-STAT 30) were carried out using dry dichloromethane or acetonitrile solutions containing 0.1 M NBu_4PF_6 electrolyte in a standard three-electrode cell using platinum (1 mm diameter disc) or glassy carbon (2 mm) working electrodes with platinum wires as counter and reference electrodes. Potentials are reported

using an internal ferrocenium–ferrocene couple (FcH^+/FcH = 0.0 V) as a reference. All electrochemical experiments were carried out in a glove box at ambient temperature.

Spectroelectrochemistry

Spectroelectrochemical experiments were performed at room temperature in an airtight optically transparent thin-layer electrochemical (OTTLE) cell equipped with Pt minigrid working and counter electrodes (32 wires cm^{-1}), an Ag wire pseudo-reference electrode and CaF_2 windows for a 200 μm path-length solvent compartment.[38] The cell was positioned in the sample compartment of a Nicolet Avatar 6700 FT-IR spectrometer or a Perkin-Elmer Lambda-900 spectrophotometer. An initial potential was applied such that no electrochemical work was done. The applied potential was then increased in a small (50–100 mV) step and the system allowed to reach equilibrium, as determined by both the decrease in current flowing through the cell and the reproducibility of spectra *vs.* time, before further increase in applied potential. When complete electrolysis had been achieved (as determined by the relative changes in the spectroscopic profile), the chemical reversibility was determined by back oxidation using a similar sequence of controlled potential steps. The controlled-potential electrolyses were carried out using an Autolab PG-STAT 30 potentiostat.

Computations

DFT calculations were performed with the Gaussian03 and 09 programs,[39] at the B3LYP/6-31G* level[40] of theory. Geometry optimizations were performed without any symmetry constraints, and frequency calculations on the resulting optimized geometries showed no imaginary frequencies. The computed frequencies were scaled by 0.95 for comparison with observed IR data.[41] Electronic transitions were calculated by the time-dependent DFT (TD-DFT[42]) method. The MO contributions were generated using the GaussSum package[43] and plotted using the GabEdit[44] package. Calculated ^{11}B chemical shifts for **31** were carried out on the optimised geometry of **31** using the GIAO[45]-NMR method and referenced to $BF_3{\cdot}OEt_2$ with $\delta(^{11}B) = 111.7 - \sigma(^{11}B)$. Calculated GIAO ^{11}B-NMR for **31**: δ [ppm] = −11.7 (B4,5), −11.4 (B3,6), −10.7 (B7,11), −9.5 (B8,10), −5.7 (B9), 1.5 (B12), 68.7 (exopolyhedral boron atom).

References

1 R. N. Grimes, *Carboranes*, Academic Press (Elsevier), New York, 2nd edn, 2011.
2 For other reviews on carboranes; see (*a*) B. P. Dash, R. Satapathy, J. A. Maguire and N. S. Hosmane, *New J. Chem.*, 2011, **35**, 1955–1972; (*b*) I. B. Sivaev and V. V. Bregadze, *Eur. J. Inorg. Chem.*, 2009, 1433–1450; (*c*) F. Issa, M. Kassiou and L. M. Rendina, *Chem. Rev.*, 2011, **111**, 5701–5722; (*d*) M. Scholz and E. Hey-Hawkins, *Chem. Rev.*, 2011, **111**, 7035–7062; (*e*) J. F. Valliant, K. J. Guenther, A. S. King, P. Morel, P. Schaffer, O. O. Sogbein and K. A. Stephenson, *Coord. Chem. Rev.*, 2002, **232**, 173–230; (*f*) V. N. Kalinin and V. A. Ol'shevskaya, *Russ. Chem. Bull.*, 2008, **57**, 815–836; (*g*) A. F. Armstrong and J. F. Valliant, *Dalton Trans.*, 2007, 4240–4251; (*h*) V. I. Bregadze, *Chem. Rev.*, 1992, **92**, 209–223; (*i*) L. A. Leites, *Chem. Rev.*, 1992, **92**, 279–323; (*j*) T. J. Wedge and M. F. Hawthorne, *Coord. Chem. Rev.*, 2003, **240**, 111–128.
3 (*a*) K. Wade, *Chem. Commun.*, 1971, 792; (*b*) K. Wade, *Adv. Inorg. Chem. Radiochem.*, 1976, **18**, 1.
4 (*a*) L. I. Zakharkin, *Pure Appl. Chem.*, 1972, **29**, 513–526; (*b*) J. H. Morris, H. J. Gysling and D. Reed, *Chem. Rev.*, 1985, **85**, 51–76.
5 (*a*) A. V. Bukhtiarov, V. N. Golyshin, A. V. Lebedev, Y. G. Kudryavtsev, I. A. Rodnikov, L. I. Zakharkin and O. V. Kuz'min, *Dokl. Akad. Nauk SSSR*, 1989, **304**, 879–882. (Russian; English translation 1989, 45–48); (*b*) A. V. Lebedev, A. V. Buchtiarov, N. N. Golyshin, Y. G. Kudryatsev, I. Y. Lovchinovsky and L. N. Rozhkov, *Metalloorganischeskaya Khim.*, 1991, **4**, 426–432. (Russian; English version, *Organomet. Chem. USSR*, 1991, **4**, 205–208); (*c*) A. V. Lebedev, A. V. Bukhtiarov, Y. G. Kudryavtsev and I. N. Rozhkov, *Metalloorganischeskaya Khim.*, 1991, **4**, 433–438 (Russian; English version *Organomet. Chem. USSR*, 1991, **4**, 208–212); (*d*) F. Teixidor, J. Pedrajas and C. Viñas, *Inorg. Chem.*, 1995, **34**, 1726–1729.
6 (*a*) C. E. Willans, C. A. Kilner and M. A. Fox, *Chem.–Eur. J.*, 2010, **16**, 10644–10648; (*b*) A. R. Popescu, A. D. Musteti, A. Ferrer-Ugalde, C. Viñas, R. Núñez and F. Teixidor, *Chem.–Eur. J.*, 2012, **18**, 3174–3184.
7 (*a*) M. V. Yarosh, T. V. Baranova, V. L. Shirokii, A. A. Érdman and N. A. Maier, *Élektrokhimiya*, 1993, **29**, 921–922 (Russian; English version *Russ. J. Electrochem.* 1993, **29**, 789–790); (*b*) M. V. Yarosh, T. V. Baranova, V. L. Shirokii, A. A. Érdman and N. A. Maier, *Élektrokhimiya*, 1994, **30**, 406–408 (Russian; English version *Russ. J. Electrochem.* 1994, **30**, 366–368).
8 M. A. Fox, C. Nervi, A. Crivello and P. J. Low, *Chem. Commun.*, 2007, 2372–2374.
9 (*a*) G. D. Mercer, J. Lang, R. Reed and F. R. Scholer, *Inorg. Chem.*, 1975, **14**, 761–763; (*b*) N. S. Hosmane, H. Zhang, J. A. Maguire, Y. Wang, T. Demissie, T. J. Colacot, M. B. Ezhova, K.-J. Lu, D. Zhu, T. G. Gray, S. C. Helfert, S. N. Hosmane, J. D. Collins, F. Baumann, W. Kaim and W. N. Lipscomb, *Organometallics*, 2000, **19**, 497–508; (*c*) X. Fu, H.-S. Chan and Z. Xie, *J. Am. Chem. Soc.*, 2007, **129**, 8964–8965.
10 K. Hosoi, S. Inagi, T. Kubo and T. Fuchigami, *Chem. Commun.*, 2011, **47**, 8632–8634.
11 M. A. Fox, C. Nervi, A. Crivello, A. S. Batsanov, J. A. K. Howard, K. Wade and P. J. Low, *J. Solid State Electrochem.*, 2009, **13**, 1483–1495.
12 H. Tricas, M. Colon, D. Ellis, S. A. Macgregor, D. McKay, G. M. Rosair, A. J. Welch, I. V. Glukhov, F. Rossi, F. Laschi and P. Zanello, *Dalton Trans.*, 2011, **40**, 4200–4211.
13 K.-R. Wee, W.-S. Han, D. W. Cho, S. Kwon, C. Pac and S. O. Kang, *Angew. Chem., Int. Ed.*, 2012, **51**, 2677–2680.

14 (*a*) K. Kokado and Y. Chujo, *Macromolecules*, 2009, **42**, 1418–1420; (*b*) J. J. Peterson, M. Werre, Y. C. Simon, E. B. Coughlin and K. R. Carter, *Macromolecules*, 2009, **42**, 8594–8598; (*c*) K. Kokado, Y. Tokoro and Y. Chujo, *Macromolecules*, 2009, **42**, 9238–9242; (*d*) K. Kokado and Y. Chujo, *Polym. J.*, 2010, **42**, 363–367; (*e*) K. Kokado, A. Nagai and Y. Chujo, *Tetrahedron Lett.*, 2011, **52**, 293–296; (*f*) K. Kokado and Y. Chujo, *Dalton Trans.*, 2011, **40**, 1919–1923; (*g*) K. Kokado and Y. Chujo, *J. Org. Chem.*, 2011, **76**, 316–319; (*h*) J. J. Peterson, A. R. Davis, M. Werre, E. B. Coughlin and K. R. Carter, *ACS Appl. Mater. Interfaces*, 2011, **3**, 1796–1799; (*i*) A. R. Davis, J. J. Peterson and K. R. Carter, *ACS Macro Lett.*, 2012, **1**, 469–472.

15 A. Ferrer-Ugalde, E. J. Juárez-Pérez, F. Teixidor, C. Viñas, R. Sillanpää, E. Pérez-Inestrosa and R. Núñez, *Chem.–Eur. J.*, 2012, **18**, 544–553.

16 L. Weber, J. Kahlert, R. Brockhinke, L. Böhling, A. Brockhinke, H.-G. Stammler, B. Neumann, R. A. Harder and M. A. Fox, *Chem.–Eur. J.*, 2012, **18**, 8347–8357.

17 L. Weber, H. B. Wartig, H.-G. Stammler and B. Neumann, *Z. Anorg. Allg. Chem.*, 2001, **627**, 2663–2668.

18 (*a*) L. Weber, D. Eickhoff, T. B. Marder, M. A. Fox, P. J. Low, A. D. Dwyer, D. J. Tozer, S. Schwedler, A. Brockhinke, H.-G. Stammler and B. Neumann, *Chem.–Eur. J.*, 2012, **18**, 1369–1382; (*b*) L. Weber, V. Werner, M. A. Fox, T. B. Marder, S. Schwedler, A. Brockhinke, H.-G. Stammler and B. Neumann, *Dalton Trans.*, 2009, 1339–1351; (*c*) L. Weber, V. Werner, M. A. Fox, T. B. Marder, S. Schwedler, A. Brockhinke, H.-G. Stammler and B. Neumann, *Dalton Trans.*, 2009, 2823–2831; (*d*) L. Weber, D. Eickhoff, V. Werner, L. Böhling, S. Schwedler, A. Chrostowska, A. Dargelos, M. Maciejczyk, H.-G. Stammler and B. Neumann, *Dalton Trans.*, 2011, **40**, 4434–4446.

19 L. Weber, J. Halama, V. Werner, K. Hanke, L. Böhling, A. Chrostowska, A. Dargelos, M. Maciejczyk, A. L. Raza, H.-G. Stammler and B. Neumann, *Eur. J. Inorg. Chem.*, 2010, 5416–5425.

20 L. Weber, D. Eickhoff, J. Kahlert, L. Böhling, A. Brockhinke, H.-G. Stammler, B. Neumann and M. A. Fox, *Dalton Trans.*, 2012, **41**, 10328–10346.

21 (*a*) L. Weber, V. Werner, I. Domke, H.-G. Stammler and B. Neumann, *Dalton Trans.*, 2006, 3777–3784; (*b*) L. Weber, A. Penner, I. Domke, H.-G. Stammler and B. Neumann, *Z. Anorg. Allg. Chem.*, 2007, **633**, 563–569.

22 (*a*) S. Schwedler, D. Eickhoff, R. Brockhinke, D. Cherian, L. Weber and A. Brockhinke, *Phys. Chem. Chem. Phys.*, 2011, **13**, 9301–9310; (*b*) L. Weber, J. Halama, L. Böhling, A. Chrostowska, A. Dargelos, H.-G. Stammler and B. Neumann, *Eur. J. Inorg. Chem.*, 2011, 3091–3101.

23 R. Goetze and H. Nöth, *Chem. Ber.*, 1976, **109**, 3247–3249.

24 (*a*) T. Habereder and H. Nöth, *Appl. Organomet. Chem.*, 2003, **17**, 525–538; (*b*) H. R. Morales, M. Pérez-Juárez, L. Cuéllar, L. Mendoza, H. Fernandez and R. Contreras, *Synth. Commun.*, 1984, **14**, 1213–1220.

25 M. A. Fox and A. K. Hughes, *Coord. Chem. Rev.*, 2004, **248**, 457–476.

26 K. M. Lee, J. O. Huh, T. Kim, Y. Do and M. H. Lee, *Dalton Trans.*, 2011, **40**, 11758–11764.

27 S. Maruyama and Y. Kawanishi, *J. Mater. Chem.*, 2002, **12**, 2245–2249.

28 E. S. Alekseyeva, M. A. Fox, J. A. K. Howard, J. A. H. MacBride and K. Wade, *Appl. Organomet. Chem.*, 2003, **17**, 499–508.

29 M. Tsuji, *J. Org. Chem.*, 2004, **69**, 4063–4074.

30 M. A. Fox, in *Comprehensive Organometallic Chemistry III*, ed. R. H. Crabtree and D. M. P. Mingos, Elsevier, Oxford, 2007, vol 3, pp. 49–112.

31 (*a*) T. L. Venable, R. B. Maynard and R. N. Grimes, *J. Am. Chem. Soc.*, 1984, **106**, 6187–6193; (*b*) J. T. Spencer, M. R. Pourian, R. J. Butcher, E. Sinn and R. N. Grimes, *Organometallics*, 1987, **6**, 335–343; (*c*) N. S. Hosmane, T. J. Colacot, H. Zhang, J. Yang, J. A. Maguire, Y. Wang, M. B. Ezhova, A. Franken, T. Demissie, K.-J. Lu, D. Zhu, J. L. C. Thomas, J. D. Collins, T. G. Gray, S. N. Hosmane and W. N. Lipscomb, *Organometallics*, 1998, **17**, 5294–5309; (*d*) G. Zi, H.-W. Li and Z. Xie, *Organometallics*, 2002, **21**, 5415–5427; (*e*) L. Deng, M.-S. Cheung, H.-S. Chen and Z. Xie, *Organometallics*, 2005, **24**, 6244–6249; (*f*) J. P. H. Charmant, M. F. Haddow, R. Mistry, N. C. Norman, A. G. Orpen and P. G. Pringle, *Dalton Trans.*, 2008, 1409–1411.

32 T. Wenderski, K. M. Light, D. Ogrin, S. G. Bott and C. J. Harlan, *Tetrahedron Lett.*, 2004, **45**, 6851–6853.

33 J. V. Dickschat, S. Urban, T. Pape, F. Glorius and F. E. Hahn, *Dalton Trans.*, 2010, **39**, 11519–11521.

34 D. M. Khramov and C. W. Bielawski, *J. Org. Chem.*, 2007, **72**, 9407–9417.

35 M. Tsuji, *J. Org. Chem.*, 2003, **68**, 9589–9597.

36 J. C. de Mello, H. F. Wittmann and R. H. Friend, *Adv. Mater.*, 1997, **9**, 230–232.

37 G. M. Sheldrick, *Acta Crystallogr., Sect A: Fundam. Crystallogr.*, 2008, **64**, 112–122.

38 M. Krejčík, M. Daněk and F. Hartl, *J. Electroanal. Chem.*, 1991, **317**, 179–187.

39 (*a*) M. J. Frisch, G. W. Trucks, H. B. Schlegel, G. E. Scuseria, M. A. Robb, J. R. Cheeseman, J. A. Montgomery Jr., T. Vreven, K. N. Kudin, J. C. Burant, J. M. Millam, S. S. Iyengar, J. Tomasi, V. Barone, B. Mennucci, M. Cossi, G. Scalmani, N. Rega, G. A. Petersson, H. Nakatsuji, M. Hada, M. Ehara, K. Toyota, R. Fukuda, J. Hasegawa, M. Ishida, T. Nakajima, Y. Honda, O. Kitao, H. Nakai, M. Klene, X. Li, J. E. Knox, H. P. Hratchian, J. B. Cross, V. Bakken, C. Adamo, J. Jaramillo, R. Gomperts, R. E. Stratmann, O. Yazyev, A. J. Austin, R. Cammi, C. Pomelli, J. W. Ochterski, P. Y. Ayala, K. Morokuma, G. A. Voth, P. Salvador, J. J. Dannenberg, V. G. Zakrzewski, S. Dapprich, A. D. Daniels, M. C. Strain, O. Farkas, D. K. Malick, A. D. Rabuck, K. Raghavachari, J. B. Foresman, J. V. Ortiz, Q. Cui, A. G. Baboul, S. Clifford, J. Cioslowski, B. B. Stefanov, G. Liu, A. Liashenko,

P. Piskorz, I. Komaromi, R. L. Martin, D. J. Fox, T. Keith, M. A. Al-Laham, C. Y. Peng, A. Nanayakkara, M. Challacombe, P. M. W. Gill, B. Johnson, W. Chen, M. W. Wong, C. Gonzalez and J. A. Pople, *GAUSSIAN 03 (Revision E.01)*, Gaussian, Inc., Wallingford CT, 2004; (*b*) M. J. Frisch, G. W. Trucks, H. B. Schlegel, G. E. Scuseria, M. A. Robb, J. R. Cheeseman, G. Scalmani, V. Barone, B. Mennucci, G. A. Petersson, H. Nakatsuji, M. Caricato, X. Li, H. P. Hratchian, A. F. Izmaylov, J. Bloino, G. Zheng, J. L. Sonnenberg, M. Hada, M. Ehara, K. Toyota, R. Fukuda, J. Hasegawa, M. Ishida, T. Nakajima, Y. Honda, O. Kitao, H. Nakai, T. Vreven Jr., J. A. Montgomery, J. E. Peralta, F. Ogliaro, M. Bearpark, J. J. Heyd, E. Brothers, K. N. Kudin, V. N. Staroverov, R. Kobayashi, J. Normand, K. Raghavachari, A. Rendell, J. C. Burant, S. S. Iyengar, J. Tomasi, M. Cossi, N. Rega, J. M. Millam, M. Klene, J. E. Knox, J. B. Cross, V. Bakken, C. Adamo, J. Jaramillo, R. Gomperts, R. E. Stratmann, O. Yazyev, A. J. Austin, R. Cammi, C. Pomelli, J. W. Ochterski, R. L. Martin, K. Morokuma, V. G. Zakrzewski, G. A. Voth, P. Salvador, J. J. Dannenberg, S. Dapprich, A. D. Daniels, O. Farkas, J. B. Foresman, J. V. Ortiz, J. Cioslowski and D. J. Fox, *GAUSSIAN 09 (Revision A.02)*, Gaussian, Inc., Wallingford CT, 2009.

40 (*a*) A. D. Becke, *J. Chem. Phys.*, 1993, **98**, 5648–5652; (*b*) C. Lee, W. Yang and R. G. Parr, *Phys. Rev. B: Condens. Matter*, 1988, **37**, 785–789; (*c*) G. A. Petersson and M. A. Al-Laham, *J. Chem. Phys.*, 1991, **94**, 6081–6090; (*d*) G. A. Petersson, A. Bennett, T. G. Tensfeldt, M. A. Al-Laham, W. A. Shirley and J. Mantzaris, *J. Chem. Phys.*, 1988, **89**, 2193–2218.

41 J. P. Merrick, D. Moran and L. Radom, *J. Phys. Chem. A*, 2007, **111**, 11683–11700.

42 E. Runge and E. K. U. Gross, *Phys. Rev. Lett.*, 1984, **52**, 997–1000.

43 N. M. O'Boyle, A. L. Tenderholt and K. M. Langner, *J. Comput. Chem.*, 2008, **29**, 839–845.

44 A. R. Allouche, *J. Comput. Chem.*, 2011, **32**, 174–182.

45 (*a*) R. Ditchfield, *Mol. Phys.*, 1974, **27**, 789–807; (*b*) C. M. Rohling, L. C. Allen and R. Ditchfield, *Chem. Phys.*, 1984, **87**, 9–15; (*c*) K. Wolinski, J. F. Hinton and P. Pulay, *J. Am. Chem. Soc.*, 1990, **112**, 8251–8260.